

**Simultaneous production of carbon nanotubes and
hydrogen gas from the thermal treatment of waste
plastics**

Jonathan Christopher Acomb

Submitted in accordance with the requirements for the degree of
Doctor of Philosophy

The University of Leeds

School of Chemical and Process Engineering

July 2015

The candidate confirms that the work submitted is his own, except work which has formed part of jointly-authored publications has been included. The contribution of the candidate and the other authors to this work has been explicitly indicated overleaf. The candidate confirms that appropriate credit has been given within the thesis where reference has been made to the work of others.

a) Investigation of WEEE plastics in Chapter 4 is based on the published paper [1]; Investigation of different steam injection rates and different plastic types in Chapter 5 is based on published paper [2]; Investigation of different catalyst metals and calcination temperatures in Chapter 6 is based on published paper [3]; Investigation of different catalyst temperatures and the ratio of feedstock to catalyst in Chapter 7 is based on published paper [4].

b) Published papers

[1] J.C. Acomb, M.A. Nahil, and P.T. Williams, Thermal processing of plastics from waste electrical and electronic equipment for hydrogen production. *Journal of Analytical and Applied Pyrolysis*, 103, (2013), 320-327.

[2] J.C. Acomb, C. Wu, and P.T. Williams, Control of steam input to the pyrolysis-gasification of waste plastics for improved production of hydrogen or carbon nanotubes. *Applied Catalysis B: Environmental*, 147, (2014), 571-584.

[3] J.C. Acomb, C. Wu, and P.T. Williams, Effect of growth temperature and feedstock:catalyst ratio on the production of carbon nanotubes and hydrogen from the pyrolysis of waste plastics, *Journal of Analytical and Applied Pyrolysis*, 113, (2015), 231-238

[4] J.C. Acomb, C. Wu and P.T. Williams, The use of different metal catalysts for the simultaneous production of carbon nanotubes and hydrogen from pyrolysis of plastic feedstocks, *Applied Catalysis B: Environmental*, 180, (2016), 497-510

- c) The candidate (J.C. Acomb) performed the experimental and analytical work and prepared the initial draft of the published papers along with supporting materials including tables and figures, and carried out the calculation and summarisation of the results and developed the discussion part.

- d) The co-authors, Prof. P. T. Williams, C. Wu and M. A. Nahil supervised and supported the research work, proof read the drafts and made suggestions and corrections to the draft papers.

This copy has been supplied on the understanding that it is copyright material and that no quotation from the thesis may be published without proper acknowledgement.

The right of Jonathan Acomb to be identified as Author of this work has been asserted by him in accordance with the Copyright, Designs and Patents Act 1988.

© 2015 The University of Leeds and Jonathan Acomb

Acknowledgements

My thanks and gratitude goes to the Engineering and Physical Science Research Council for my funding and scholarship, without which I would not have been able to undertake this research.

I would like to extend special thanks to both my supervisors Paul Williams and Chunfei Wu for the invaluable help, guidance and support they offered me throughout my studies. I genuinely could not have asked for better supervisors.

Special thanks are also extended to Jude Onwudili for his help analytical support, and Mohamad Anas Nahil for his encouragement, support and guidance throughout my studies which were of great help. Special thanks also to Ed Woodhouse for his help with technical support in the re-design and modification of my reactor.

I would also like to thank my colleagues and friends within my research group including Amal, Chika, Eyup, Juniza, Paula, Ramzi, Yeshui and the rest. Your friendship and support has meant a lot to me and you have made my PhD studies a pleasure. Many thanks also to the rest of the office including Jo, Holly and the rest of the DTC for their friendship and making me feel welcome.

Thanks are also given to my family and friends both here in Leeds and elsewhere, who have made my life during my studies so amazing.

And of course, immense thanks, gratitude and all the love in the world to my amazing partner Fern, without whom I'm sure I would not have been able to achieve this.

Abstract

In this work a two-stage reaction system was used for the simultaneous production of carbon nanotubes (CNTs) and hydrogen gas from plastic feedstocks. Initial pyrolysis was undertaken in the first stage heated at 600 °C, before the evolved gases were passed to a second stage where a catalyst was held. Carbon deposition builds up on the surface of the catalyst, whilst hydrogen and other gases are then collected downstream. A series of analytical techniques were used to characterise the carbon deposition on the catalysts, as well as any oils or gases produced.

Initially, a two stage pyrolysis-gasification process was undertaken with plastics from waste electrical and electronic equipment for investigation into hydrogen production. The introduction of a nickel catalyst led to increased hydrogen production, with small amounts of CNTs observed in the carbon deposits on the catalyst surface. In order to increase the yield of CNTs, different plastics including polyethylene, polypropylene and polystyrene were investigated. The rate of steam injection into the two stage pyrolysis-gasification process was also investigated, and proved significant to obtaining high yields of CNTs and hydrogen. All of the plastics produced CNTs, with the largest yield obtained from the pyrolysis gasification of polystyrene at a steam injection rate of 0.25 g h⁻¹. Additionally, the use of different catalysts was investigated, with iron, nickel, cobalt and copper catalysts all tested. CNTs were produced on the iron, nickel and cobalt catalysts, with the iron catalyst producing the largest yield. The calcination temperature and metal loading on the nickel catalyst was also studied, with catalyst support interactions of intermediate strength and a higher metal loading producing larger CNT yields. Finally, investigations into the temperature of the second stage where the catalyst was held were undertaken, along with using different ratios of catalyst: plastic sample. These too proved important in achieving large yields of both CNTs and hydrogen.

Table of Contents

Acknowledgements.....	iii
Abstract	iv
1 Introduction.....	xvi
1.1 Waste production and types	1
1.2 Plastic Wastes.....	4
1.2.1 Domestic Waste Plastics.....	5
1.2.2 Waste Electrical and Electronic Equipment (WEEE) plastics	7
1.3 Waste management of plastics	8
1.3.1 Landfilling.....	9
1.3.2 Incineration and energy recovery.....	10
1.3.3 Recycling	12
1.3.4 Chemical recycling.....	14
1.4 Aims and objectives of the research.....	15
2 Literature review.....	19
2.1 Thermal treatment of plastics	19
2.1.1 Pyrolysis and gasification processes	19
2.1.2 Liquid products from thermal treatments.....	20
2.1.3 Solid products from thermal treatments	22
2.1.4 Gas products from thermal treatments.....	23
2.2 Hydrogen production	24
2.2.1 Uses and rationale	25
2.2.2 Production from steam reforming.....	25
2.2.3 Production from thermal treatment.....	26
2.2.4 Production from thermal treatment of plastics.	28
2.2.5 The use of catalysts for hydrogen production .	32
2.2.6 Other effects on hydrogen production.....	42
2.3 Carbon nanotube production	44
2.3.1 Carbon nanotube properties	44
2.3.2 Methods of carbon nanotube production.....	46

2.3.3	Purification of carbon nanotubes.....	47
2.3.4	Uses for carbon nanotubes.....	49
2.3.5	Carbon nanotube identification and metrology	52
2.3.6	Carbon nanotube production mechanisms.....	53
2.3.7	Catalysis in carbon nanotube production	57
2.3.8	Effect of reaction temperature.....	67
2.3.9	Super growth and the effect of steam	70
2.3.10	Simultaneous production of hydrogen and carbon nanotubes	72
2.3.11	Carbon Nanotube Production from Plastics ..	73
3	Materials and methods	93
3.1	Materials.....	93
3.1.1	Plastics samples used.....	93
3.1.2	Catalysts prepared	94
3.2	Experimental reactors	95
3.3	Analytical techniques.....	100
3.3.1	Gas Analysis	100
3.3.2	Gas Chromatography/Mass Spectrometry	104
3.3.3	Thermo gravimetric analysis	104
3.3.4	Scanning Electron Microscopy.....	107
3.3.5	Transmission Electron Microscopy and TEM- EDX	107
3.3.6	Raman Spectroscopy.....	108
3.3.7	X-Ray Diffraction.....	109
4	Pyrolysis-gasification of WEEE plastics for the production of hydrogen.....	111
4.1	Gas yield	111
4.2	Hydrogen production	113
4.3	Characterisation of oils	116
4.4	Characterisation of coke on Ni/Al ₂ O ₃ catalyst.....	121
4.4.1	SEM analysis	121

4.4.2	TEM analysis	123
4.4.3	Temperature programmed oxidation.....	125
4.5	Conclusions.....	127
5	Effect of steam injection rate and plastic type on production of hydrogen and carbon nanotubes ..	130
5.1	Hydrogen production	130
5.1.1	Effect of steam injection	130
5.1.2	Effect of plastic type	131
5.1.3	Study of catalyst.....	136
5.2	Carbon deposits	137
5.2.1	Low Density Polyethylene	137
5.2.2	Polypropylene	143
5.2.3	Polystyrene	148
5.3	Discussion.....	153
5.3.1	Production of hydrogen	153
5.3.2	Effect of steam on carbon deposition.....	154
5.3.3	Effect of plastic type on carbon deposition....	156
5.4	Conclusions.....	158
6	Investigation into the effect of catalyst type on the production of hydrogen and carbon nanotubes ..	161
6.1	Influence of catalyst metal.....	161
6.1.1	Characterisation of fresh catalysts	161
6.1.2	Mass balance and hydrogen production	168
6.1.3	Carbon nanotube production.....	170
6.1.4	Discussion.....	178
6.2	Effect of calcination temperature	179
6.2.1	Characterisation of fresh catalysts	179
6.2.2	Mass balance and hydrogen production	181
6.2.3	Carbon nanotube production.....	182
6.2.4	Discussion.....	184
6.3	Effect of metal loading.....	185

6.4	Conclusions.....	188
7	Effect of temperature and sample:catalyst ratio on production of hydrogen and carbon nanotubes ..	192
7.1	Effect of temperature.....	192
7.1.1	Mass balance and hydrogen production	192
7.1.2	Carbon nanotube production.....	194
7.2	Effect of feedstock:catalyst ratio	198
7.2.1	Mass balance and hydrogen production	198
7.2.2	Carbon nanotube production.....	199
7.3	Conclusion.....	202
8	Conclusions and future work	206
8.1	Conclusions.....	206
8.1.1	Pyrolysis-gasification of WEEE plastics	206
8.1.2	Effect of steam injection rate and plastic type on production of carbon nanotubes and hydrogen	207
8.1.3	Effect of the catalyst on the production of carbon nanotubes and hydrogen.....	209
8.1.4	Effect of temperature and feedstock:catalyst ratio	210
8.2	Future work	211
8.2.1	Production of carbon nanotubes	211
8.2.2	Purification	212
8.2.3	Uses for carbon nanotubes produced	212

List of figures

Figure 1.1 UK waste generation by sector (2012) [2].....	1
Figure 1.2 Waste management in the EU by treatment type (2013) [3].....	2
Figure 1.3 Waste management in the UK by treatment type (2013) [3].....	2
Figure 1.4 Composition of municipal waste in England (2009) [5]... 3	
Figure 1.5 Global and European plastics production [7].....	4
Figure 1.6 European demand for different plastic types (2013) [7]..	5
Figure 1.7 Composition of UK domestic waste plastic (2008) [9]	6
Figure 1.8 Repeating unit of PET plastic [11]	7
Figure 1.9 Plastics waste management in the EU [15, 16]	9
Figure 1.10 Potential recyclability of waste by material [22]	12
Figure 1.11 Resin identification coding.....	13
Figure 1.12 Products from pyrolysis and gasification [23]	14
Figure 2.1 Uses for liquid products from pyrolysis [4].....	20
Figure 2.2 Alignment of hexagonal lattice within CNTs [81]	46
Figure 2.3 Tip growth mechanism for carbon nanotube formation [132]	55
Figure 2.4 Base growth mechanism for carbon nanotube formation [134]	56
Figure 3.1 Schematic diagram of pyrolysis-gasification reactor	96
Figure 3.2 Original reactor setup used for chapters 4 and 5	97
Figure 3.3 Modified reactor setup used for chapters 6 and 7	98
Figure 3.4 GC standard gas chromatogram alkanes.....	101
Figure 3.5 GC standard gas chromatogram alkenes.....	101
Figure 3.6 GC standard gas chromatogram permanent gases ...	102
Figure 3.7 GC standard gas chromatogram carbon dioxide.....	102

Figure 3.8 (a) Temperature programmed oxidation plot, (b) Derivative of temperature programmed oxidation	105
Figure 3.9 Typical EDX spectrum obtained from a catalyst.....	108
Figure 3.10 A typical Raman spectrum of catalyst carbon deposits.....	109
Figure 3.11 A typical XRD plot of a fresh catalyst	109
Figure 4.1 Gas compositions from the pyrolysis-gasification of WEEE, HIPS and ABS	113
Figure 4.2 GC-MS total ion chromatograms of oils obtained from WEEE pyrolysis-gasification using (a) no steam, no catalyst, (b) steam, no catalyst, (c) steam and 5 wt% Ni (d) steam and 10 wt% Ni.....	120
Figure 4.3 SEM images of carbon deposition on used catalyst from pyrolysis gasification of (a) WEEE using 5 wt% Ni, (b) WEEE using 10 wt% Ni, (c) HIPS using 5 wt% Ni, (d) HIPS 10 wt% Ni, (e) ABS using 5 wt% Ni and (f) ABS using 10 wt% Ni	122
Figure 4.4 TEM images of carbon deposition on used catalyst from pyrolysis gasification of (a) WEEE using 5 wt% Ni, (b) WEEE using 10 wt% Ni, (c) HIPS using 5 wt% Ni, (d) HIPS 10 wt% Ni, (e) ABS using 5 wt% Ni and (f) ABS using 10 wt% Ni	124
Figure 4.5 TEM images of CNTs produced from the pyrolysis-gasification of (a) WEEE, (b) HIPS.....	125
Figure 4.6 (a) Temperature programmed oxidation results from carbon deposits on catalysts used in pyrolysis-gasification of plastics, (b) Derivateive plot of 5wt % Ni catalysts used and (c) Derivative plot of 10 wt% Ni catalysts used.....	126
Figure 5.1 XRD analysis of (a) fresh Ni Al ₂ O ₃ catalyst, (b) used Ni Al ₂ O ₃ catalyst with 0 steam injection and (c) used Al ₂ O ₃ catalyst with 4.74 g h ⁻¹ steam injection.....	137
Figure 5.2 SEM images of carbon deposits obtained from LDPE at steam flow rates of (a) 0 g h ⁻¹ , (b) 0.25 g h ⁻¹ , (c) 1.90 g h ⁻¹ and (d) 4.74 g h ⁻¹	138
Figure 5.3 TEM images of carbon deposits obtained from LDPE at steam flow rates of (a-b) 0 g h ⁻¹ (c-d) 0.25 g h ⁻¹ , (e-f) 1.90 g h ⁻¹ and (g-h) 4.74 g h ⁻¹	139

Figure 5.4 Effect of steam on carbon deposition from LDPE: (a) Temperature programmed oxidation, (b) Derivative plot of TPO.	141
Figure 5.5 Raman spectrums for carbon deposits from LDPE with (a) 0 steam injection, (b) 0.25 g h ⁻¹ steam injection, (c) 1.90 g h ⁻¹ steam injection and (d) 4.74 g h ⁻¹ steam injection	143
Figure 5.6 SEM images of carbon deposits obtained from PP at steam flow rates of (a) 0 g h ⁻¹ , (b) 0.25 g h ⁻¹ , (c) 1.90 g h ⁻¹ and (d) 4.74 g h ⁻¹	144
Figure 5.7 TEM images of carbon deposits from PP (a-b) 0 steam, (c-d) 0.25 g h ⁻¹ steam, (e-f) 1.90 g h ⁻¹ steam and (g-h) 4.74 g h ⁻¹ steam	145
Figure 5.8 Effect of steam on carbon deposition from PP: (a) Temperature programmed oxidation, (b) Derivative plot of TPO.	146
Figure 5.9 Raman spectrums for carbon deposits from PP with (a) 0 steam injection, (b) 0.25 g h ⁻¹ steam injection, (c) 1.90 g h ⁻¹ steam injection and (d) 4.74 g h ⁻¹ steam injection.....	148
Figure 5.10 SEM images of carbon deposits obtained from PS at steam flow rates of (a) 0 g h ⁻¹ , (b) 0.25 g h ⁻¹ , (c) 1.90 g h ⁻¹ and (d) 4.74 g h ⁻¹	149
Figure 5.11 TEM images of carbon deposits from PS (a-b) 0 steam, (c-d) 0.25 g h ⁻¹ steam, (e-f) 1.90 g h ⁻¹ steam and (g-h) 4.74 g h ⁻¹ steam	150
Figure 5.12 Effect of steam on carbon deposition from PS: (a) Temperature programmed oxidation, (b) Derivative plot of TPO	151
Figure 5.13 Raman spectrums for carbon deposits from PS with (a) 0 steam injection, (b) 0.25 g h ⁻¹ steam injection, (c) 1.90 g h ⁻¹ steam injection and (d) 4.74 g h ⁻¹ steam injection.....	153
Figure 6.1 SEM images of fresh catalysts used for the two stage pyrolysis of LDPE. Ni/Al ₂ O ₃ , (b) Fe/Al ₂ O ₃ , (c) Co/Al ₂ O ₃ and (d) Cu/Al ₂ O ₃	162
Figure 6.2 TEM images of fresh catalysts used for the two stage pyrolysis of LDPE. Ni/Al ₂ O ₃ , (b) Fe/Al ₂ O ₃ , (c) Co/Al ₂ O ₃ and (d) Cu/Al ₂ O ₃	163
Figure 6.3 EDX spectrums of TEM image of nickel catalyst shown in Figure 6.2(a): (a) Area A1, (b) Point 1, (c) Point 2.....	163

Figure 6.4 EDX spectrums of TEM image of iron catalyst shown in shown in Figure 6.2(b): (a) Area A1, (b) Point 1, (c) Point 2.....	164
Figure 6.5 EDX spectrums of TEM image of cobalt catalyst shown in shown in Figure 6.2(c): (a) Area A1, (b) Point 1, (c) Point 2....	164
Figure 6.6 EDX spectrums of TEM image of copper catalyst shown in shown in Figure 6.2(d): (a) Area A1, (b) Point 1, (c) Point 2....	164
Figure 6.7 XRD investigation of the fresh catalysts used in two stage pyrolysis of LDPE	165
Figure 6.8 Investigation of the fresh catalysts used for the two stage pyrolysis of LDPE by temperature programmed reduction	166
Figure 6.9 Scanning electron microscopy of the carbon deposits on the used catalysts from the two stage pyrolysis of LDPE: (a) Ni/Al ₂ O ₃ , (b) Fe/Al ₂ O ₃ , (c) Co/Al ₂ O ₃ and (d) Cu/Al ₂ O ₃	171
Figure 6.10 Transmission electron microscopy of the carbon deposits on the used catalysts from the two stage pyrolysis of LDPE: (a) Ni/Al ₂ O ₃ , (b) Fe/Al ₂ O ₃ , (c) Co/Al ₂ O ₃ and (d) Cu/Al ₂ O ₃ .	173
Figure 6.11 XRD of the used catalysts from the two stage pyrolysis of LDPE.....	174
Figure 6.12 Temperature programmed oxidation investigation of the used catalysts from the two stage pyrolysis of LDPE: (a) Derivative TPO plot and (b) Amount of different carbon types deposited on the catalysts	175
Figure 6.13 Investigation of the used catalysts from the two stage pyrolysis of LDPE by Raman spectroscopy: Ni/Al ₂ O ₃ , (b) Fe/Al ₂ O ₃ , (c) Co/Al ₂ O ₃ and (d) Cu/Al ₂ O ₃	178
Figure 6.14 Analysis of the fresh Nickel500 catalyst used for the two stage pyrolysis of LDPE: (a) TEM image, (b) XRD and (c) TPR.....	179
Figure 6.15 EDX spectrums of TEM image of Nickel500 catalyst shown in shown in figure 6.14(a): (a) Area A1, (b) Point 1, (c) Point 2	179
Figure 6.16 Analysis of the used Nickel500 catalyst from the two stage pyrolysis of LDPE (a) SEM, (b) Raman spectroscopy and (c) TEM.....	182

Figure 6.17 The effect of calcination temperature on the yield of CNTs from the two stage pyrolysis of LDPE: (a) Derivative TPO graph from used catalysts and (b) Amount of different carbon types deposited on the catalysts.....	183
Figure 6.18 Derivative TPO plot for 5 wt% metal catalysts used for the two stage pyrolysis of LDPE.....	185
Figure 7.1 Effect of growth temperature on (a) mass balance, (b) gas composition and (c) hydrogen conversion from two stage pyrolysis of LDPE	192
Figure 7.2 Scanning electron microscopy and transmission electron microscopy images of carbon deposition on catalyst at experimental temperature of 700 °C (a) and (d), 800 °C (b) and (e) and 900 °C (c) and (f).....	194
Figure 7.3 Raman spectra of carbon deposits obtained from experimental temperatures of (a) 700 °C, (b) 800 °C and (c) 900 °C	195
Figure 7.4 Temperature oxidation results showing effect of temperature; (a) derivative plot and (b) amount of carbon deposition and conversion of plastic to CNTs	197
Figure 7.5 Effect of sample:catalyst ratio on (a) mass balance, (b) gas composition and (c) hydrogen conversion from the two stage pyrolysis of LDPE at 800 °C	199
Figure 7.6 SEM images showing effect of amount of LDPE used at 800 °C. (a) 0.5g, (b) 0.75g, (c) 1.0g and (d) 1.25g	200
Figure 7.7 TEM images showing effect of amount of LDPE used at 800 °C. (a) 0.5g, (b) 0.75g, (c) 1.0g and (d) 1.25g	200
Figure 7.8 Temperature oxidation results showing effect of amount of LDPE used at 800 °C; (a) derivative plot and (b) amount of carbon deposition and conversion of plastic to CNTs.....	201

List of tables

Table 1.1 Calorific values of fossil fuels and plastics [19].....	11
Table 2.1 Mechanical properties of CNTs compared to steel [79].	45
Table 3.1 Elemental composition and maximum H ₂ yield from plastic samples used	94
Table 3.2 Elemental composition, maximum H ₂ yield, and proximate analysis of WEEE plastic samples used	94
Table 3.3 Repetition of research results reactor 1.....	99
Table 3.4 Repetition of research results reactor 2.....	99
Table 4.1 Product yield from pyrolysis-gasification of plastics.....	112
Table 4.2 Hydrogen production and conversion from the pyrolysis-gasification of WEEE, HIPS and ABS	115
Table 4.3 GC-MS identified species in WEEE, HIPS and ABS pyrolysis	117
Table 4.4 GC-MS results showing the effect of catalyst on WEEE oils.....	119
Table 5.1 Mass balance, gas composition and hydrogen yield from the pyrolysis-gasification of LDPE	132
Table 5.2 Mass balance, gas composition and hydrogen yield from the pyrolysis-gasification of PP	133
Table 5.3 Mass balance, gas composition and hydrogen yield from the pyrolysis-gasification of PS	135
Table 5.4 Production of filamentous and amorphous carbons obtained from LDPE	142
Table 5.5 Production of filamentous and amorphous carbons obtained from PP	147
Table 5.6 Production of filamentous and amorphous carbons obtained from PS	152
Table 6.1 Effect of catalyst metal on mass balance, gas composition and hydrogen conversion from the two stage pyrolysis of LDPE.....	170

Table 6.2 Effect of calcination temperature of nickel catalysts on mass balance, gas composition and hydrogen conversion from the two stage pyrolysis of LDPE.....	181
Table 6.3 Effect of metal loading on the production of hydrogen and CNTs from the two stage pyrolysis of LDPE	187

Nomenclature

CNTs - Carbon nanotubes

MWCNTs - Multiwalled carbon nanotubes

TEM - Transmission electron microscopy

SEM - Scanning electron microscopy

TPO - Temperature programmed oxidation

TPR - Temperature programmed reduction

XRD - X ray diffraction

LDPE - Low density polyethylene

PP - Polypropylene

PS - Polystyrene

WEEE - Waste electronic and electrical equipment

1 Introduction

1.1 Waste production and types

The management of waste is an important challenge for all societies and cultures throughout the world. Waste is thought of as items which “*people no longer have any use for, which they either intend to get rid of or they have already discarded*” [1], and so encompass a wide range of activities and products. As such waste is produced in domestic, commercial and industrial activities, with the nature of the waste produced varying from sector to sector. The distribution of waste production by sector in the UK for 2012 is shown in figure 1.1 [2].

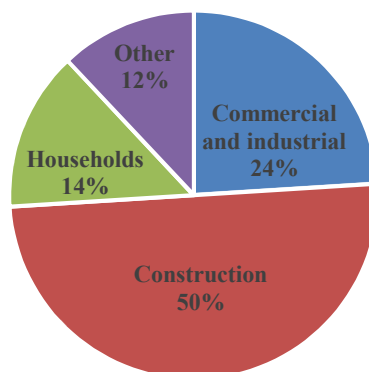


Figure 1.1 UK waste generation by sector (2012) [2]

Whilst the largest proportion is taken up by the construction sector, the majority of this waste is either recycled or recovered [2]. Municipal waste from households however is still largely disposed of in landfills [3], which is a major concern, since landfilling is unsustainable and damaging to the environment. Figures 1.2 and 1.3 [3] show the waste management techniques used for municipal waste from the EU and UK respectively. Whilst the amount of waste sent to landfilling has dropped significantly since 1995, it still makes up the largest proportion, 35% for the UK and 31% in the EU in 2013.

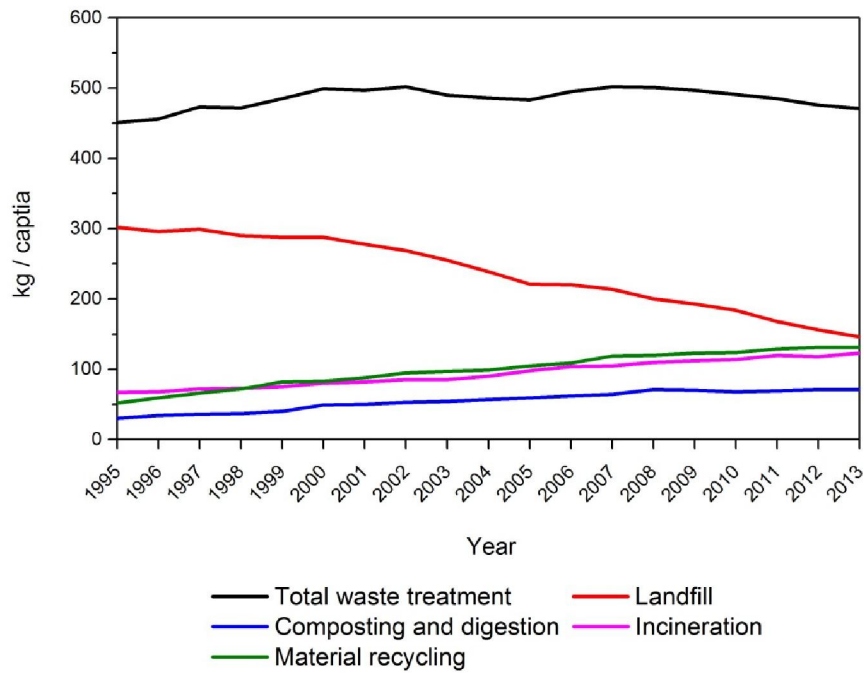


Figure 1.2 Waste management in the EU by treatment type (2013)
[3]

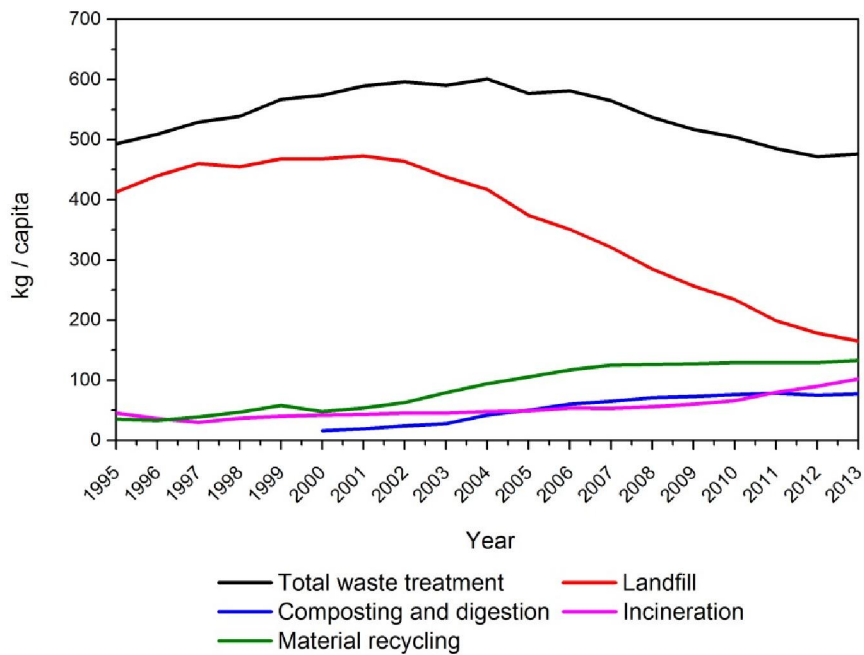


Figure 1.3 Waste management in the UK by treatment type (2013)
[3]

Municipal waste is defined as 'waste from households, as well as other waste which, because of its nature or composition, is similar to waste from household' [4] Figure 1.4 shows the typical composition of a municipal waste sample from England [5]. The largest proportions are made up of biodegradable organic materials such as paper, food waste and garden waste whilst smaller proportions of plastics, glass and other substances are present.

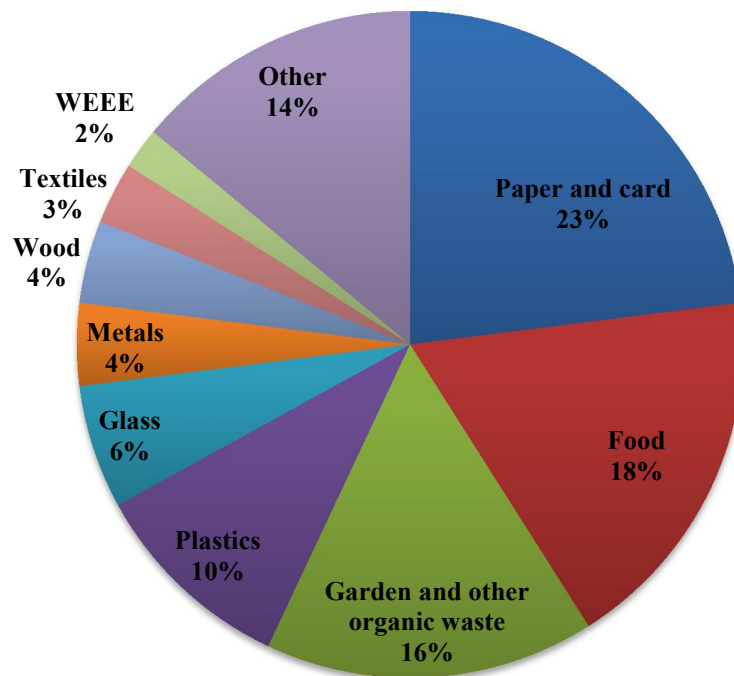


Figure 1.4 Composition of municipal waste in England (2009) [5]

Whilst many of the materials present in municipal waste are easily recovered or recycled, such as paper and glass, plastics are currently much more difficult to recycle. This is a result of high contamination rates as well as the wide range of plastic types that exist complicating their sorting and separation [6]. This makes plastic a particularly important stream of waste as alternative waste management techniques are required to prevent unsustainable landfilling practices.

1.2 Plastic Wastes

Plastics are a key material in modern day life, and are used in a great number of applications. This is as a result of their desirable properties such as their low reactivity, low cost and ability to modify their properties by copolymerisation. However as they are difficult to chemically or biologically degrade their disposal has been a major environmental issue.

Demand for plastics across the globe is high as they can be used in number of different industries such as packaging, construction, automotive, agriculture and electrical [7]. Figure 1.5 shows production of plastics for the world and Europe [7], and reveals that global production has increased exponentially since 1950, and continues to increase rapidly. With such a large production of plastics, suitable waste management techniques will become imperative.

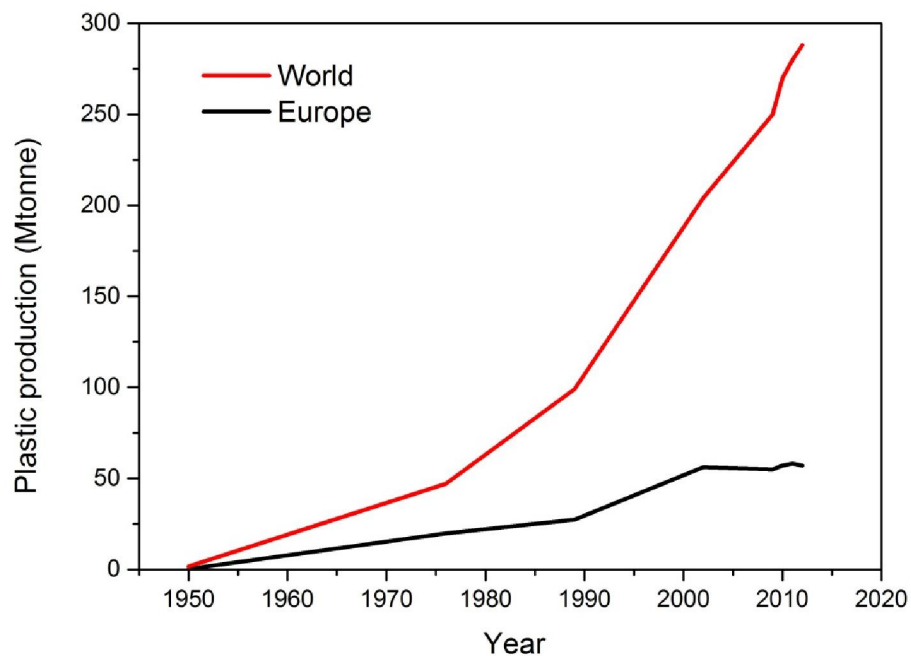


Figure 1.5 Global and European plastics production [7]

Plastics are a wide ranging group of materials that encompass a number of different polymeric materials made from different resins.

European demand for the different plastic materials is shown in figure 1.6 [7]. A large proportion is taken up by polyolefins such as high and low density polyethylene (PE-HD and PE-LD) and polypropylene (PP), with polypropylene making up the largest proportion. Other plastics with significant demands include polyethylene terephthalate (PET), polyvinyl chloride (PVC), polystyrene (PS) and polyurethane (PUR).

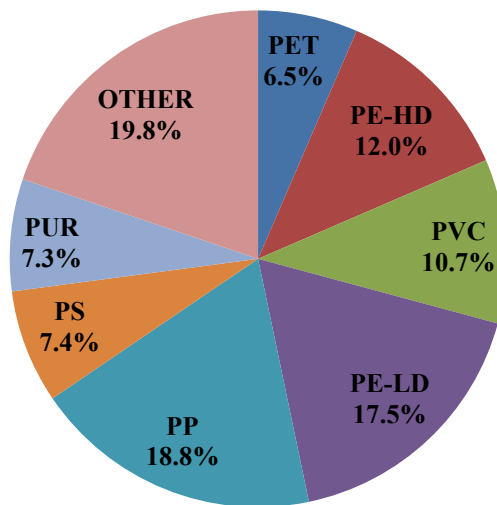


Figure 1.6 European demand for different plastic types (2013) [7]

1.2.1 Domestic Waste Plastics

Significant proportions of plastic wastes are generated from domestic sources. Whilst plastics make up roughly 10 wt% of the municipal waste generated in the UK, in terms of volume percent the figure is much larger, with the value for plastics in Western Europe as high as 20 vol% [8]. This presents a significant environmental and social challenge.

Figure 1.7 shows that domestic plastic waste, excluding bottles, is largely comprised of just five different polymers [9]. Polypropylene (PP) and Polyethylene, both flexible and rigid, make up the largest proportion whilst smaller amounts of Polyethylene Terephthalate (PET), Polyvinyl Chloride (PVC) and Polystyrene (PS) are also present. The sample also contained a significant amount of

contamination, showing why this is a problem in plastics waste management.

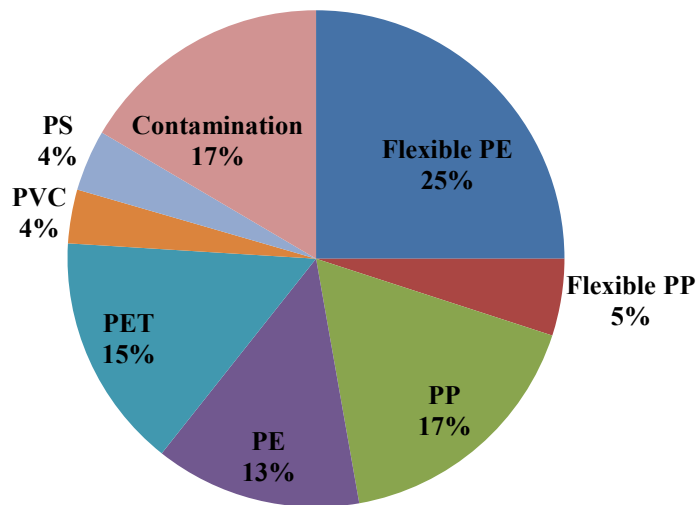


Figure 1.7 Composition of UK domestic waste plastic (2008) [9]

Polyethylene is the highest volume polymer in the world, and can either come in low density (LDPE) or high density (HDPE). It is formed by ethylene polymerisation reactions, and has a repeat structure of $(-\text{CH}_2)_x$. The difference between the two types stems from the structural properties, mainly as a result of branching and linearity. HDPE has much less branching and more linear chains than LDPE and as a result can become well aligned and crystalline which results in a higher strength. Among its properties are high toughness, ductility, excellent chemical resistance, low water vapour permeability, and low water absorption [10].

Structurally polypropylene (PP) is similar to PE except that a methyl group is substituted in place of a hydrogen atom. It is formed by the polymerisation of propylene, and as a result of its methyl group different isomers can be produced such as isotactic and syndiotactic forms, which have different properties. PP is less resistant to degradation such as high temperature oxidation than PE, but has a better environmental stress cracking resistance [10].

Polyethylene Terephthalate (PET) is a far more complex polymer than PE or PP. It is a polyester and has a structure as shown in

figure 1.8 [11]. It is formed in a two-step ester interchange process, and has many uses in blow moulding to form plastic bottles.

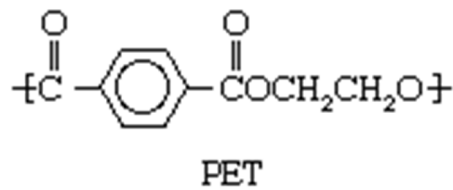


Figure 1.8 Repeating unit of PET plastic [11]

Polyvinyl chloride (PVC) is produced from the polymerisation of a vinyl chloride monomer giving it the repeating unit $-(CH_2-CHCl)_x-$. It is often used in electrics and cabling as it is self-extinguishing and has good fire resistance. This is because HCl is released and air is then restricted from reaching the flame as a result of HCl having a higher density than air. It reacts with UV light, releasing HCl and so UV stabilisers are often added to prevent this occurring.

Unmodified PVC is rigid and is stronger and stiffer than PP and PE, however it can be plasticized by addition of other species to make it more flexible [10].

Whilst not making up a large proportion of domestic waste, polystyrene (PS) is still one of the most commonly used polymers, and is formed from styrene by addition polymerisation. Among its properties are transparency, low density, high modulus and brittleness, as a result of its benzene side group [10].

1.2.2 Waste Electrical and Electronic Equipment (WEEE) plastics

The electronics industry makes up 5.5% of plastics in Europe [7] and so produces a large amount of waste. However with the implementation of the Waste Electrical and Electronic Equipment Directive (2006) it is now a legal imperative to reduce the amount of electrical equipment that is sent to landfill. This gives rise to a significant source of waste plastic that needs to be recycled or reused. As a result of the short lifetime and shelf life of electronics equipment, the amount of WEEE plastics is likely to rise and become an important stream of waste. Plastics that are often used

in electronics equipment include high impact polystyrene [12] and acrylonitrile butadiene styrene [10].

High impact polystyrene (HIPS) is a variant of PS. Due to polystyrenes brittle nature, its usefulness in a number of applications is limited and so to improve its strength it is often blended with a soft phase such as polybutadiene to form HIPS. A copolymer consisting of the polystyrene and polybutadiene is formed where the chains of polybutadiene are grafted onto the PS backbone giving the polymer a more 2D than 1D structure [12]. The addition of a rubber to the polymer leads to a higher impact strength. Various methods are available for the production of HIPS, where the feedstocks can either be simply blended together or the polybutadiene rubber dissolved in the styrene monomer which is then polymerised [13]. HIPS finds uses in a number of industries as a result of its high rigidity and ease of colouring. In addition to their use in electronics they also find use in toys, packaging and bottles. When used in electronics, flame retardants are often added due to the high temperatures these appliances can reach [12].

Another plastic frequently used in electronics applications is Acrylonitrile Butadiene Styrene (ABS) which is another copolymer based around polystyrene. As the name implies the three monomers that make up ABS are Acrylonitrile, Butadiene and Styrene which are added in different quantities depending on the desired properties of the polymer. Acrylonitrile gives the plastic good heat resistance, chemical resistance and strength, whilst butadiene gives it high impact strength and toughness and finally the styrene gives it rigidity and ease of processing [10]. Production is often carried out by graft polymerisation of styrene and acrylonitrile onto a polybutadiene latex and then blending with styrene-acrylonitrile latex [10].

1.3 Waste management of plastics

In order to limit the damage to human health and the environment waste treatment and disposal of plastics is required. There are many different options for waste disposal, with some more sustainable than others.

1.3.1 Landfilling

The largest practice undertaken in the UK and many other European countries is still landfilling of waste [7], as it is a comparatively cheap method of waste disposal and many types of waste are suitable for landfilling [14]. Figure 1.9 shows the waste management of plastics carried out in the EU [15, 16], and shows that whilst landfilling is reducing it still makes up the largest proportion with 38.1%. In the UK the amount sent to landfill is even higher at a value of 66% [7]. This shows that the practice of sending plastics to landfill is still a widely carried out practice.

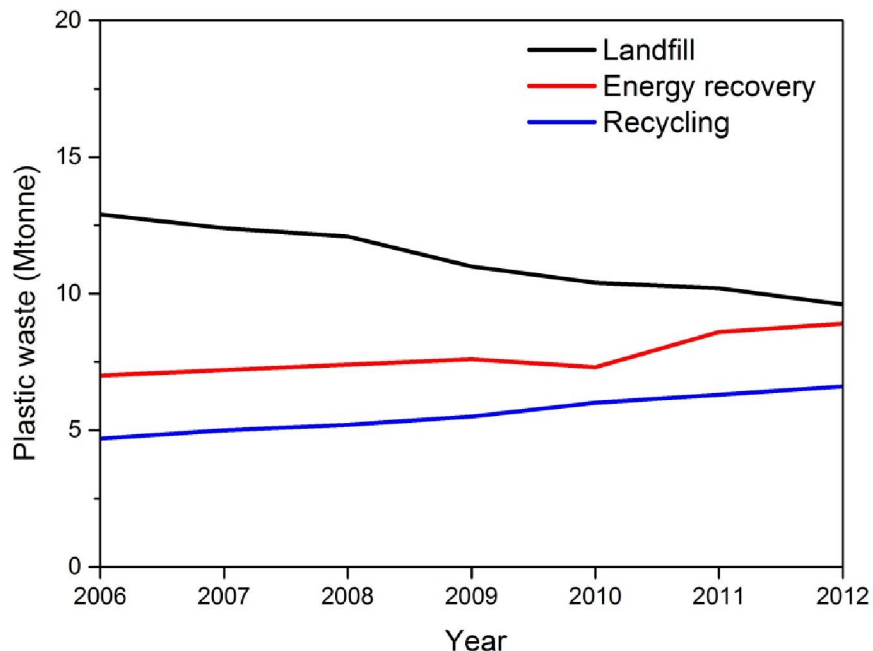


Figure 1.9 Plastics waste management in the EU [15, 16]

Landfilling involves the controlled and managed practice of disposing of waste into a hole in the ground. As such it does not make reuse of the materials that are landfilled. As plastics are finite resources which depend on fossil fuels this poses problems, as there is no recovery of the chemical energy left available in the plastics. Likewise, there is a limit on the suitable location of landfill sites meaning alternative methods of disposal will be required. Landfilling waste also poses detrimental effects on the environment

by the production of leachate and landfill gas. Leachate consists of water which has passed through the waste and collected suspended solids and soluble components from the waste, as well as any water that is produced from the waste itself. Whilst it will vary depending on the nature of waste disposed of, leachate has been found to contain a series of different pollutants including dissolved organic materials, inorganic macrocomponents, heavy metals and components not degraded by organisms in the environment [17]. As a result of these pollutants leachate has been found to be toxic as well as possibly mutagenic and carcinogenic [17]. The other by-product of landfilling waste is landfill gas, which again varies in quantity and composition depending on the waste deposited. It is produced from the breakdown of biodegradable wastes and consists of hydrogen and CO₂ in its early stages and CO₂ and methane as it progresses further [14]. As methane and CO₂ are both known greenhouse gases, their release will have a detrimental effect on the environment via global climate change. Methane is the largest constituent in landfill gas and its concentrations can become high enough to be explosive, posing dangers to local communities and environments [14]. Whilst plastics are largely not biodegradable, contaminants within the waste plastic such as paper labelling could degrade if they are not separated effectively.

Recently incentives have been introduced to limit the amount of waste sent to landfill such as the EC Waste Landfill Directive (1999). Its overall aim is to '*prevent or reduce as far as possible negative effects on the environment*' from the landfilling of waste [4]. One way that aims to discourage the amount of waste landfilled implemented by the UK was to introduce a landfill tax on materials sent to landfill based on a rate per tonne of waste.

1.3.2 Incineration and energy recovery

An alternative to waste disposal in landfill is incineration, where the waste is combusted in air. The proportion of waste incinerated on the whole is significantly smaller than that of waste that is landfilled, often as a result of negative public opinions [14]. The negative opinions stem from fears over the amount of pollutants that are released into the air, though these emissions are controlled by the

EC Waste Incineration Directive (2000). The release of pollutants such as HF, HCl, NO_x, SO₂, CO, VOCs as well as dioxins and furans are given off in varying amounts depending on the nature of the waste during incineration [18]. Whilst these are harmful to human health, they are heavily controlled by the current legislation to minimise the health risks. A small amount of solid waste is still produced in the form of ash and still requires management, usually landfilling, however the amount is significantly less than if the waste were landfilled, typically 10% of its previous volume [14]. Another disadvantage to the incineration of waste is the high capital investment costs that are required to set up the incinerator. Although combustion of waste produces CO₂, no methane, a more potent greenhouse gas is produced. In most instances energy recovery can be performed where steam is produced from the heat from incineration, which can then be used for electricity production, hot water for heating or combined heat and power. This is not only more energy efficient but also helps to make the practice of incineration more cost effective. Plastics are carbonaceous in nature and chemically similar to the fossil fuels they are produced from, and so large amounts of energy can be recovered from their incineration. Table 1.1 [19] shows the calorific values for typical fossil fuels as well as plastics and waste, and shows the comparable calorific values that plastics have.

Table 1.1 Calorific values of fossil fuels and plastics [19]

Fuel	Calorific Value (MJ/kg)
Gasoline	46
Fuel Oil	43
Coal	30
Polyethylene	43
Mixed plastics	30 - 40
Municipal solid waste	10

1.3.3 Recycling

Recycling of waste leads to the production of a new product or material that can be used again in either a similar or new purpose. Whilst plastic recycling is on the increase, plastics tend to have a low level of recycling, as was shown in figure 1.9. This is because contamination of plastics can make recycling more difficult [20]. Post-consumer plastics in particular suffer from contamination [21], meaning recycling often faces challenges. The amount of plastics that can be recycled therefore depends on the amount recoverable. Based on this contamination the amount potentially recyclable for different materials, including plastics, is shown in figure 1.10 [22]. However this is not the full story as it is not technically or economically feasible to recycle all of the uncontaminated material [14].

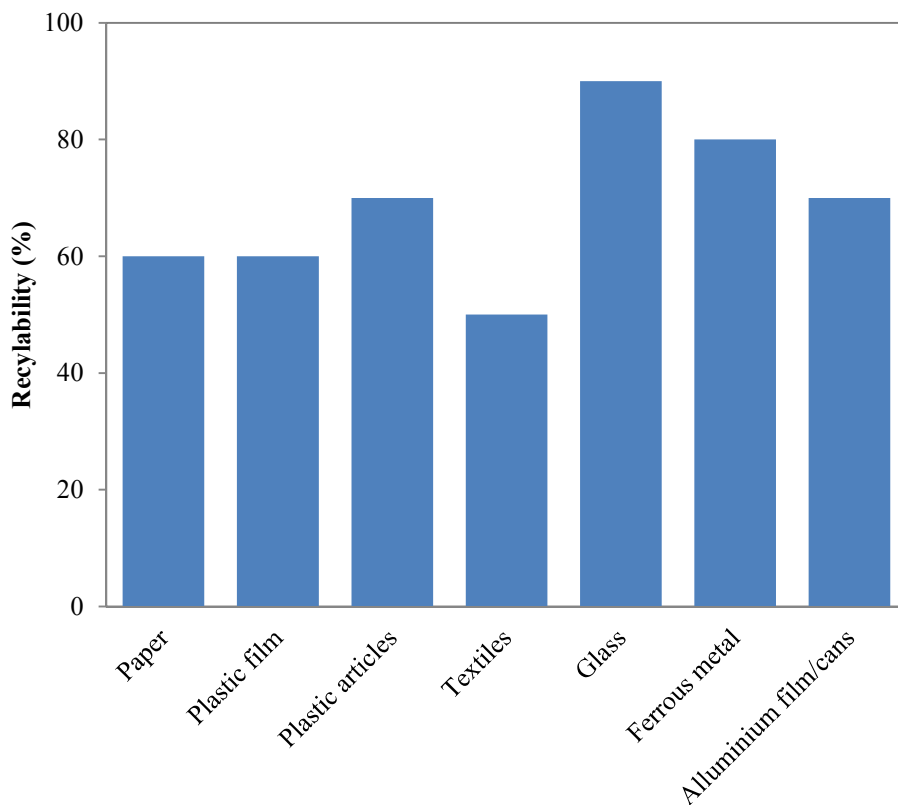


Figure 1.10 Potential recyclability of waste by material [22]

As there are many different types of plastics produced from different resins, separation into the different types is required. To aid this, a classification system for different plastics was introduced by the plastics industry in 1988 called the Resin Identification Coding. This is shown in figure 1.11 and uses numbers 1 to 7 for the different plastic types to ensure that plastics can be segregated. Where mixtures of plastics are recycled together, the different plastics separate out, and cause weaknesses within the plastic structure [21].








	Polyethylene Terephthalate (PET) Polyester Fibres, soda and water bottles
	High Density Polyethylene (HDPE) Bottles, grocery bags, liquid and laundry detergent
	Polyvinyl Chloride (PVC) Clear films, pipe, non-food bottles, blister packs
	Low Density Polyethylene (LDPE) Plastic bags, 6-pack rings, various containers and containers lids
	Polypropylene (PP) Yogurt and deli containers, dishware, auto parts, cosmetic bottles
	Polystyrene (PS) Styrofoam, packing, take-out plates and containers
	Other resins Acrylic, styrene, fiberglass, mixed

Figure 1.11 Resin identification coding

Plastics are most commonly recycled via open loop recycling where they are converted into products different from their original use, however closed loop recycling such as bottle to bottle recycling is being developed [6]. Plastics can be recycled by re-extrusion, mechanical recycling or chemical recycling [20]. Re-extrusion is where the used plastics are reintroduced into the extrusion process used in plastics production. It is suitable for the recycling of scrap plastics into similar products, but a major drawback is that it is only suitable for semi-clean scrap plastics [20]. Mechanical recycling involves reusing plastics recovered by mechanical means such as melting, shredding, granulation. Stages to separate the different types of plastics and washing are also required before the final

product is prepared. Mechanical recycling however is only suitable for single monomer plastics such as PE, PP and PS, as it becomes harder to recycle the plastics as they become more complex [20]. A number of products are produced from mechanically recycled plastics such as fibres in carpets, bottles and apparel [20].

1.3.4 Chemical recycling

Chemical recycling is different to mechanical or re-extrusion processes as the plastics are broken down chemically into either new chemicals for industry or back into monomers.

Depolymerisation of plastics can be done via hydrolysis or glycolysis processes, and is often used for PET [21].

An increasingly desirable form of chemical recycling is thermal treatment via the processes of pyrolysis and gasification. Pyrolysis is a thermal process by which products are broken down into smaller molecules in an inert or oxygen lean environment [14].

Pyrolysis of waste has the benefit of producing valuable products such as oils, fuel gases and solid carbons [14], whilst preventing waste from going to landfill. As shown in figure 1.12 [23], pyrolysis produces gases such as CO and H₂, liquids such as naphtha, tars and phenols and solid char. The oils and gases obtained can be used for fuel applications [24, 25]. The char produced also has the possibility to be upgraded into activated carbons [26]. Other high quality solid products can also be yielded by pyrolysis such as carbon nanostructures such as carbon nanotubes [27]. Because plastic is carbonaceous in its nature, pyrolysis is viable for the production of a gaseous fuel [28].

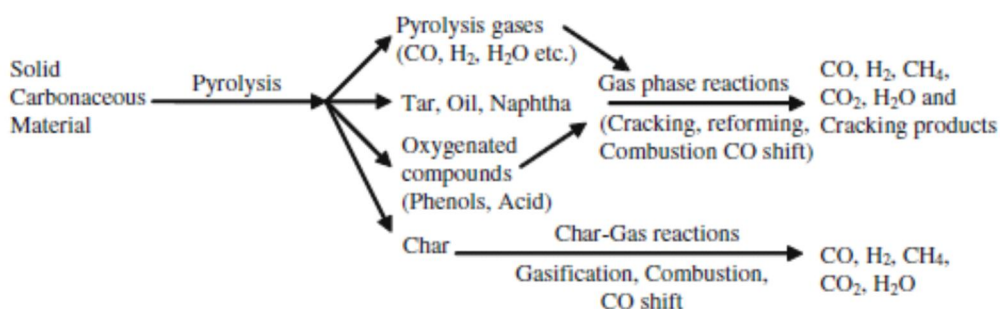


Figure 1.12 Products from pyrolysis and gasification [23]

Gasification differs from pyrolysis since a gasifying agent is used to increase the yield of gases obtained, often at the expense of the oil yield. Gasification agents include a source of oxygen in the form of steam, pure oxygen or air [14]. As the majority of the products obtained are gases, they often find uses in energy applications since hydrogen, syngas and hydrocarbon gases are the major yields. Other products such as tars and ash are still produced [14]. Gases that are produced from gasification include CO, H₂, CH₄, CO₂ and H₂O as shown by figure 1.12 [23].

1.4 Aims and objectives of the research

Management of waste plastics is a serious challenge for modern society, with alternatives required for the unsustainable practice of landfilling. Thermal treatments offer a desirable alternative, as waste products can be converted into more valuable products. The aims of this research project are to convert waste plastics into more valuable products via the thermal treatments of pyrolysis and gasification. In particular, the desired products of the thermal treatments are hydrogen gas and carbon nanotubes (CNTs) with the aim to simultaneously produce the two.

In this research the two stage catalytic thermal treatment of plastics will be carried out with the following objectives:

- The effect of a nickel catalyst on the investigation of pyrolysis-gasification of real world waste plastics for the production of hydrogen. This is to determine whether nickel catalysts can be used to increase the yield of hydrogen from the thermal treatment of plastics.
- The effect of the varying the steam injection rate on the production of hydrogen and carbon nanotubes from pyrolysis-gasification of different plastics. This is to determine the effect steam injection has on the production of hydrogen and carbon nanotubes simultaneously, and

whether certain steam injection rates favour the production of one product over the other.

- The effect of using different plastic types on the production of hydrogen and carbon nanotubes from pyrolysis-gasification of different plastics. This is to determine whether different plastics produce more hydrogen and carbon nanotubes than others, and to investigate why this is the case.
- The effect of using different transition metal catalysts, metal loadings and calcination temperatures on the production of carbon nanotubes and hydrogen from the two stage thermal treatment of plastics. This is to determine the most suitable catalyst for the simultaneous production of carbon nanotubes and hydrogen, and to investigate what makes it an effective catalyst.
- The effect of process conditions such as the temperature of the catalytic reactor and the sample:catalyst ratio on the production of hydrogen and carbon nanotubes. This is to determine the conditions for optimum production of hydrogen and carbon nanotubes.

References

1. *Environmental statistics and accounts in Europe*, 2010, Euro Stat: European Commission
2. DEFRA, *UK Statistics on Waste – 2010 to 2012*, 2015.
3. *Municipal waste generation and treatment, by type of treatment method*. 2014; Available from: <http://ec.europa.eu/eurostat>.
4. EC, *Council Directive 1999/31/EC of 26th April 1999 on the landfill of waste*, in *Official Journal of European Communities* 1999: Brussels, Belgium.
5. DEFRA, *Municipal Waste Composition: A Review of Municipal Waste Component Analyses*, 2009, Department for Environment, Food and Rural Affairs
6. WRAP, *Realising the value of recovered plastics*, in *Market Situation Report - Autumn 2007* 2007, Waste and Resources Action Programme

7. *Plastics - the facts 2013: An analysis of European latest plastics production, demand and waste data 2013*, Plastics Europe.
8. ACRR, *Good practices guide on waste plastics recycling: A guide by and for local and regional authorities*, J.-P. Hannequart, Editor 2004, ACRR, APME, ECVM, EuPR, EUPC.
9. Foster, S., *Domestic Mixed Plastic Packaging: Waste Management Options*, 2008, WRAP.
10. Baker, A.M.M. and J. Mead, *Thermoplastics*, in *Handbook of plastics, elastomers, and composites*, C.A. Harper, Editor 2002, McGraw-Hill.
11. Britannica, E. *Polyethylene terephthalate (PET or PETE)*. August 2012].
12. Fink, J.K., *Handbook of Engineering and Speciality Thermoplastics*. Vol. Volume 1: Polyolefins and Styrenics. 2010: Scrivener Publishing.
13. MAUL, J., et al., *Polystyrene and Styrene Copolymers*, in *Ullmann's Encyclopedia of Industrial Chemistry* 2007, Wiley-VCH.
14. Williams, P.T., *Waste Treatment and Disposal*. Second Edition ed 2005: John Wiley and Sons.
15. *Plastics - the Facts 2011: An analysis of European plastics production, demand and recovery for 2010, 2011*, Plastics Europe.
16. *Plastics – the Facts 2014/2015: An analysis of European plastics production, demand and waste data 2015*, Plastics Europe.
17. Kjeldsen, P., et al., *Present and Long-Term Composition of MSW Landfill Leachate: A Review*. *Critical Reviews in Environmental Science and Technology*, 2002. **32**(4): p. 297-336.
18. Commission, E., *Integrated Pollution Prevention and Control. Draft reference document on the best available techniques for waste incineration*, 2006, European Commission: Brussels, Belgium.
19. Scott, G., *'Green' polymers*. *Polymer Degradation and Stability*, 2000. **68**: p. 1-7.
20. Al-Salem, S.M., P. Lettieri, and J. Baeyens, *Recycling and recovery routes of plastic solid waste (PSW): a review*. *Waste Manag*, 2009. **29**(10): p. 2625-43.
21. Merrington, A., *Recycling of plastics*, in *Applied plastics engineering handbook*, M. Kutz, Editor 2011, William Andrew. p. 177-192.
22. *Waste Management Paper 28: Recycling*, 1991, Departments of the Environment and Transport.
23. Ahmed, I. and A.K. Gupta, *Syngas yield during pyrolysis and steam gasification of paper*. *Applied Energy*, 2009. **86**(9): p. 1813-1821.

24. Demirbas, A., *Pyrolysis of municipal plastic wastes for recovery of gasoline-range hydrocarbons*. Journal of Analytical and Applied Pyrolysis, 2004. **72**(1): p. 97-102.
25. Koderu, Y. and Y. Ishihara, *Novel Process for Recycling Waste Plastics To Fuel Gas Using a Moving-Bed Reactor*. Energy & Fuels, 2006. **20**: p. 155-158.
26. Esfandiari, A., T. Kaghazchi, and M. Soleimani, *Preparation and evaluation of activated carbons obtained by physical activation of polyethyleneterephthalate (PET) wastes*. Journal of the Taiwan Institute of Chemical Engineers, 2012.
27. Mishra, N., et al., *Pyrolysis of waste polypropylene for the synthesis of carbon nanotubes*. Journal of Analytical and Applied Pyrolysis, 2012. **94**: p. 91-98.
28. Buah, W., A. Cunliffe, and P. Williams, *Characterization of Products from the Pyrolysis of Municipal Solid Waste*. Process Safety and Environmental Protection, 2007. **85**(5): p. 450-457.

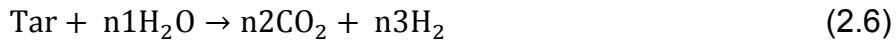
2 Literature review

2.1 Thermal treatment of plastics

2.1.1 Pyrolysis and gasification processes

Thermal treatments such as pyrolysis and gasification are used to convert a range of materials into more valuable products. Waste plastics are difficult to recycle as a result of the different plastic types and contamination, and so thermal treatments offer a desirable alternative. Pyrolysis involves making use of an inert atmosphere, such as nitrogen or argon that allows the feedstock to break down in the absence of oxygen. The feedstock breaks down to form smaller molecules such as gases, liquids and solids. The process is endothermic as it takes energy to break down the bonds within the hydrocarbon structure. Whilst there is no consensus on the mechanism for pyrolysis, studies by Kruse et al and Faravelli et al suggest that plastics breakdown to form smaller gaseous and liquid products by a series of complex free radical reactions [1, 2]. They described the initiation of radicals, propagation reactions and finally termination of the reactive radical groups. Faravelli [2] describes the initiation reactions in polymers as breaking a carbon-carbon bond to form radicals. Propagation of the radicals then continue the reactions before termination of the reaction occurs by either recombination of two radical species into one chemical or disproportionation, where two products are formed. Various different radical reactions that occur have an influence on the products that are obtained, with intramolecular hydrogen transfers influencing the production of smaller products [1].

Gasification is a specific type of thermal treatment which aims to produce larger yields of gases than oils or solids. Rather than just the inert atmosphere used in pyrolysis, gasifying agents are used to help breakdown the hydrocarbons into smaller gas molecules. Gasifying agents are typically oxidising, such as carbon dioxide, water or small amounts of oxygen. He et al describe the gasification of plastics in two steps, by thermochemical decomposition and then by the reaction of gases with the volatile products obtained [3]. Thermal decomposition results in the production of tar, char and volatiles, whilst the second set of reactions yield gaseous products. When PE is gasified the following reactions occur, as displayed in reactions 2.1 to 2.6 [3].



2.1.2 Liquid products from thermal treatments

Liquid hydrocarbons are used for a wide variety of purposes, from chemicals production to transport fuels. Figure 2.1 shows the range of applications that can be used for the liquid products from the thermal treatment by fast pyrolysis [4].

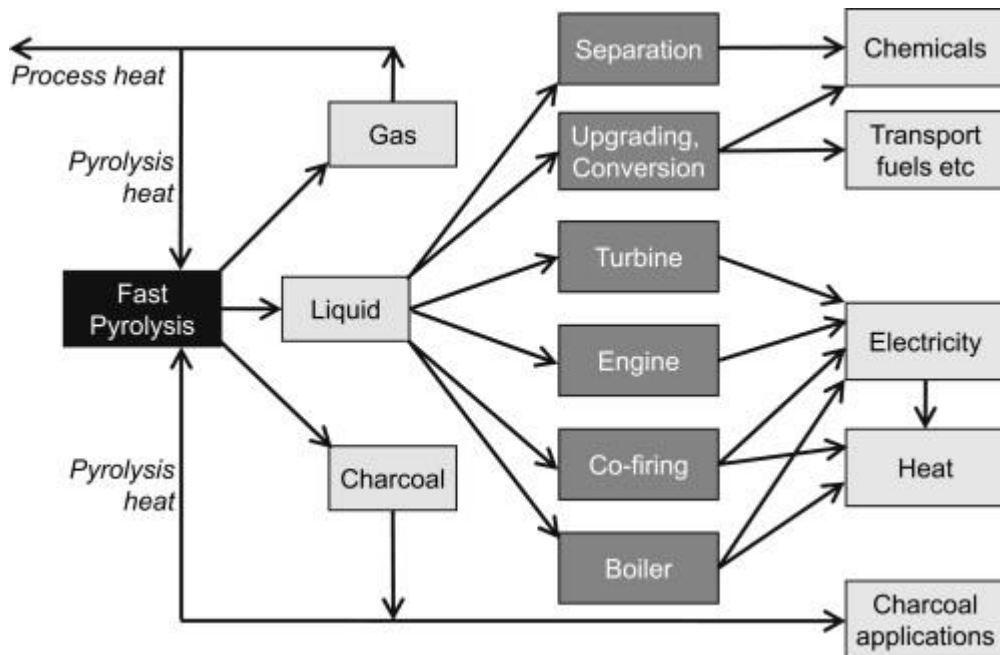


Figure 2.1 Uses for liquid products from pyrolysis [4]

Use of hydrocarbons as fuels is of great importance to modern society, with petroleum products refined to diesel and gasoline to power automobiles. However, there are concerns with the long term sustainability of these fuels as a result of finite resources and greenhouse gas emissions, and so alternatives are required. As a result, the EU has implemented Directive 2009/28/EC, which states that 10 percent of all transport fuels must come

from renewable sources. This has led to an increase in the production and consumption of bioethanol [5]. As liquid hydrocarbons are produced during pyrolysis of plastics, this opens up the possibility of using them for industrial uses such as transport fuels or high quality oils.

Pyrolysis of plastics is often undertaken to obtain high value liquid products. For example, the pyrolysis of waste electrical and electronic equipment (WEEE) plastics was undertaken by Hall and Williams using samples of WEEE from fridge waste, cathode ray tube waste (CRT) and mixed WEEE [6]. A fixed bed reactor was used with a temperature of 600 °C. Liquid yields were high with the CRT giving 83.9 wt% oil, which was mainly composed of aromatic compounds such as styrene, benzenebutanenitrile, ethylbenzene, α -methylstyrene, 1,3-diphenylpropane and toluene. The content of halogens in the oils was found to be low, and so use as a fuel for industrial or commercial means could be possible.

Other wastes are also suitable, as Lopez et al [7] investigated the catalytic pyrolysis of three samples of packaging waste containing plastics. A temperature of 440 °C was used in a nitrogen atmosphere using a ZSM-5 zeolite catalyst. The plastic film rich sample produced 41.5 wt% oils, with large amounts of styrene, xylene, toluene and ethyl-benzene which could be used for industrial purposes.

Siddiqui et al used a wide range of plastics for the production of valuable hydrocarbon oils [8]. PS, LDPE, HDPE, PP and PET were all used, as well as various mixtures of the plastic samples. Pyrolysis temperatures of 430-440 °C were employed with a hydro processing catalyst. Important hydrocarbon compounds were obtained in the liquid products from the pyrolysis of the various plastic mixtures. This demonstrates that a wide range of plastics are suitable feedstocks for the generation of liquid products, and that mixtures of plastics can be used, meaning separation of the different plastic types would not be needed.

The production of oils that can be used in gasoline fuels was investigated by Demirbas by the pyrolysis of waste plastics from landfill [9]. Pyrolysis was undertaken in a steel tube at temperatures between 650 and 875 K, and used PE, PP and PS as well as a mixture of all three plastics. PE and PP yielded more gases, and the oils contained more olefins and paraffins which are less suitable for use in gasoline, whilst PS gave more aromatics such as styrene. This demonstrated how different plastics can be used to produce oils that can be used as a fuel. It is suggested in the study that fractional distillation should be used to separate out the valuable gasoline range oils.

Sharma et al made use of HDPE from waste plastic bags to produce diesel range hydrocarbon products by pyrolysis [10]. A two stage process was used with temperatures of 420 and 440 °C without a catalyst. The oils made up 74 wt% of the pyrolysis mass balance, and after a distillation process and addition of antioxidants was within all petro diesel fuel standards except density. The centane number and lubricity were in fact more suitable than current petroleum diesel fuels.

The oils produced from pyrolysis of plastics have also been directly tested, with Devaraj et al [11] and Mani et al [12] making use of waste plastic pyrolysis oils in a diesel engine. The waste plastic pyrolysis oil was used successfully in the diesel engine, without the need for engine modifications.

Pyrolysis can also be undertaken to obtain oils from waste plastics that can then be used to produce new plastics in a form of recycling. Achilias et al [13] detail a process where model and waste polystyrene were pyrolysed in a fixed bed reactor for 17 minutes at 510 °C. Liquid yields were over 90 wt% for the model PS and an expanded PS waste, whilst the yield for a PS waste was 77 wt%. Styrene monomer and dimer contents obtained in the oils were 77.9 wt%, 65.2 wt% and 79 wt% for the model PS, waste PS and expanded PS waste respectively, and when a BaO catalyst was used on the model PS the yield was increased to 88 wt%. This meant that when the pyrolysis oils were polymerised a PS plastic was obtained, however the presence of other compounds in the oils led to the plastic having a lower molecular weight and glass transition temperature.

2.1.3 Solid products from thermal treatments

Solid products are also produced during thermal treatments. These include waxes, solid residues such as ashes and chars, and solid carbons which are a result of coke formation. Waxes are formed from the longer chains of hydrocarbons which have not broken down enough to be oils or gases. Ashes and solid residues result from non-carbonaceous products in the feedstocks which cannot be broken down into gases or oils, and so are often impurities or metals. Carbon formation often occurs on the catalyst surface as the hydrocarbon gases decompose and deposit solid carbons. Such materials are usually considered unwanted by products, or in the case of carbon deposition direct obstacles to the production of the more valuable oils and gases. However, in recent years, analysis of carbon deposits have been

used to produce valuable forms of carbon such as activated carbons and nanocarbon materials.

The production of activated carbons from the thermal treatment of polyethylene terephthalate (PET) was demonstrated by Esfandiari et al [14]. Pyrolysis of PET was conducted to produce a char by heating the plastic under nitrogen flow in a tube furnace. The char was subsequently upgraded to activated carbons by heating in the presence of carbon dioxide. An optimum process with a yield of activated carbons of 12.32 wt% was obtained with a surface area of 790.31 m²/g.

The potential to produce carbon nanotubes (CNTs) from the pyrolysis of plastics was demonstrated by Kukovitsky et al [15]. Generating CNTs from waste plastics holds the benefit of simultaneously dealing with waste management problems, and also providing a cheap and abundant feedstock for CNT production. Kukovitsky et al used granular polyethylene (PE) which was pyrolysed with a nickel catalyst at temperatures of 420 – 450 °C. Carbon fibres were produced with some CNTs also obtained in the carbon deposits. CNTs are valuable products which have a large number of potential uses and so their production from waste streams such as plastics is of particular interest. Subsequent studies have since gone on to increase the yield of CNTs produced, as will be discussed in later sections of the literature review.

2.1.4 Gas products from thermal treatments

Hydrocarbon gases high in calorific value are produced during thermal treatment of plastic as the hydrocarbon chains are broken down into smaller molecules such as C₁-C₄ hydrocarbons, CO and H₂. As a result, the gases obtained are typically used as fuel gases. A typical example of this is where Koderia and Ishihara [16] used a catalytic pyrolysis process in a moving bed reactor to produce valuable gas products from waste plastics. PP pellets were mixed with sand and a silica alumina catalyst and fed into the reactor by a screw conveyor in a nitrogen atmosphere at temperatures between 500 and 700 °C. Catalytic breakdown of the plastic led to the production of gas and liquid products. Employing higher temperatures led to a gas yield of 94 wt% when the catalyst was used, with the catalyst also increasing the yields of the desired C₄ and C₅ hydrocarbons.

Gasification uses oxidation agents to increase the yield of gases produced during thermal treatments. Tsuji et al used a two stage reactor to first

pyrolyse and subsequently gasify PE [17]. Large gas yields of 82 wt% were obtained when the temperature of the second stage was held at 800 °C. A subsequent study by Tsuji et al compared the two stage gasification of PE with PP and PS [18]. The gas yields obtained were 80 wt%, 74 wt%, and 6.2 wt% for PE, PP and PS respectively at a second stage gasification temperature of 800 °C. This showed that PS produced a much smaller gas yield, as PS was unable to breakdown into gases at this temperature.

Among the gases produced during thermal treatment, hydrogen is of particular interest as it is considered an important future fuel, since its combustion gives off only water. Steam gasification procedures can be utilised to produce valuable gas products such as a syngas [3], or hydrogen [19]. He et al conducted catalytic steam gasification of waste PE in a fixed bed reactor and produced a gas stream which was 64.35 vol% carbon monoxide and hydrogen [3]. A temperature of 900 °C and use of a nickel alumina catalyst was found to yield the highest syngas yield.

Wu and Williams likewise used a catalytic steam reforming process to produce a hydrogen rich gas stream from the gasification of polypropylene [19]. A two-step pyrolysis-gasification process was employed, using a pyrolysis temperature of 500 °C and a gasification temperature of 800 °C. The gasification agent used was steam, which was injected at rate of 4.74 gh⁻¹ and Ni-Al and Ni-Mg-Al catalysts obtained the best results with potential hydrogen productions above 60%.

These studies demonstrated the possibility of producing valuable gas products such as hydrogen from thermal treatment of plastics. As hydrogen is considered an important product and future fuel, subsequent sections of the literature review will investigate its production from plastics further.

2.2 Hydrogen production

Hydrogen gas has been identified as a useful and valuable product of thermal treatments. Production from thermal treatment of waste plastics, which are often difficult to recycle by other means, has also been demonstrated. This makes hydrogen an important and viable product of thermal treatment of residual wastes.

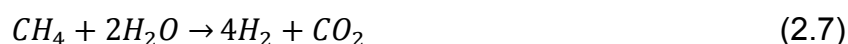
2.2.1 Uses and rationale

Due to hydrogen's status as a potential energy fuel for the future, there is a great deal of interest in its production. Whilst current production still depends on fossil fuels and emits carbon dioxide, other methods of production are available which could make it a truly green fuel.

Hydrogen gas is used in a wide range of industrial applications including petroleum refining and the production of chemicals, dyes, pharmaceuticals and cosmetics [20]. The largest current uses of hydrogen are refining crude oil and the production of ammonia, and use the majority of the 45 million tonnes produced annually [20]. As a fuel source hydrogen is considered important for the future as its combustion gives off only water. As no carbon dioxide is produced the effect on our environment in terms of global warming is substantially smaller than fossil fuels. Air pollution from hydrogen is also favourable, with no volatile organic compounds, carbon monoxide or hydrocarbons resulting from incomplete combustion, and no nitrogen or sulphur oxides formed from impurities, as is the case with fossil fuels. As these products contribute to air pollution and environmental damage, the fact they are not produced from hydrogen is of great benefit.

2.2.2 Production from steam reforming

Whilst other methods such as electrolysis of water are available, the vast majority of hydrogen, around 96%, is currently produced from the reforming of fossil fuels [20]. However, this is dependent on the finite supply of fossil fuels. Carbon dioxide is also released during reforming, making the process damaging to the environment via global climate change. Natural gas is the largest fossil fuel source for hydrogen production by steam reforming. The process is carried out in two steps, where CO and hydrogen are first produced, and the yield of hydrogen then increased further via the water gas shift reaction, producing CO₂. The overall reaction for the process can be thought of as follows:



Steam reforming is an efficient, cheap and proven technology for producing hydrogen, however in the long run a more sustainable low carbon method will be needed. One option which could be applied to make steam reforming

more sustainable is capture and storage of the carbon dioxide given off during the process. As it is normally separated out from the hydrogen by pressure swing adsorption, no additional energy would be required to obtain the carbon dioxide ready for capture.

Steam reforming involves the reaction of natural gas or liquids such as naphtha. Typical conditions are at temperatures of around 800 – 900 °C in the presence of a catalyst [20]. In steam reforming nickel catalysts are commonly used, but face challenges due to the environment and temperatures involved [21]. These are the activity of the catalyst, carbon deposition, sulphur poisoning and sintering [21]. Steam reforming bears similarities to thermal treatments, particularly gasification, as similar chemicals and reactions are present and similar catalysts are used. As a result the problems faced in steam reforming often occur in hydrogen production by thermal treatments, and are of direct interest.

2.2.3 Production from thermal treatment

It has been shown earlier that hydrogen can be produced from thermal treatments such as pyrolysis and gasification. Carbonaceous materials break down to form hydrogen via reactions 2.1 – 2.6. This section will look in more detail at hydrogen production from thermal treatments, and what feedstocks can be utilised.

2.2.3.1 Biomass

Biomass gasification is a desirable means of producing hydrogen as it can be considered carbon neutral since any carbon dioxide emissions are counteracted by carbon dioxide absorbed during the plants growth. Biomass is chemically similar to plastics, with lignin and cellulose being polymeric in nature. As a result, similar reactions take place during thermal treatment, and similar catalysts can be used, so studying hydrogen production from biomass can give a good idea on behaviour on production from plastics. The nature of the biomass feedstock however provides challenges for the production of hydrogen by thermal treatment. The compounds that are present in biomass are more complex than the methane, oils or gases which are typically used in steam reforming, and this leads to complication such as the build-up of tars and coke [22]. This is a problem as the build-up of coke block pipes and tubes within the reactor as well as filters and deactivate the

catalyst [23]. Biomass also naturally contains sulphur and chlorine which can lead to poisoning of the catalyst [21, 24, 25], thereby reducing its activity.

Despite these challenges the production of hydrogen from the thermal treatment of biomass is well researched, with a large number of recent research papers on the subject [26-32]. A specific example of biomass gasification for the production of hydrogen was shown by Demirbas who used a wide variety of biomass samples to produce hydrogen by two different means [27]. Beech wood, olive waste, wheat straw and corncob samples were investigated for their potential to produce hydrogen by pyrolysis and steam gasification at temperatures between 775 and 1125 K. All the samples used produced hydrogen yields of 30% or higher for pyrolysis and gasification on a dry ash free basis. The type of sample used had an effect on the hydrogen yield with wheat straw producing the highest yield of 55% from gasification, whilst the olive waste produced the lowest yield. Gasification was found to produce higher yields of hydrogen than pyrolysis for all the samples used, with a maximum yield from the pyrolysis of wheat straw being 46%, compared with the 55% yield obtained from gasification. It was found that the temperature and amount of steam used also had an effect on the hydrogen yield. This study showed that a wide range of biomass feedstocks can be used for hydrogen production via pyrolysis and gasification. Whilst gasification gave highest yield, it was noted that pyrolysis may be a more economical solution as it has the potential to produce co-products.

2.2.3.2 Waste

The hydrocarbon nature of a number of waste streams makes them suitable for thermal treatment. As a result thermal treatment is also used to produce hydrogen from a range of waste products, since it offers an alternative to unsustainable landfilling practices. Research studies have covered a wide variety of waste types. Ahmed and Gupta used paper as a feed material for the production of syngas using pyrolysis and steam gasification at temperatures between 600 °C and 1000 °C [33]. As was seen with biomass in the study by Demirbas, gasification gave significantly higher yields of hydrogen compared with pyrolysis, with the highest yield for gasification of paper achieved at 900 °C. Ahmed and Gupta also used food waste as a source of syngas via pyrolysis and steam gasification [34]. Temperatures of 800 °C and 900 °C were used and again it was found that gasification

produced the largest yield of hydrogen, with temperature not having as a large impact.

Mixed waste samples can also be used to produce hydrogen with a number of studies using either municipal solid waste or refuse derived fuel [3, 35-38]. For example, He et al [36] used municipal solid waste samples from China to produce hydrogen via steam gasification with a dolomite catalyst.

Temperatures between 750 °C and 950 °C were used, with the highest potential hydrogen yields obtained at 900 °C. These studies show hydrogen can be produced via pyrolysis and gasification from a series of feedstocks, and that mixtures of wastes are also suitable.

Whilst a large number of different wastes can be used to produce hydrogen via thermal treatments, this study will concentrate on waste plastics as they make up a significant proportion of municipal waste and are often difficult to recycle by other means. The following section will concentrate on waste plastics as a feedstock.

2.2.4 Production from thermal treatment of plastics

It has been briefly discussed earlier that hydrogen can be produced from waste plastics via thermal treatment however this section will go into further detail, discussing a series of factors which effect production. Plastics encompass a wide range of materials, and waste plastics can also contain additives and contaminants, so products obtained from pyrolysis and gasification will vary depending on the nature of the plastic used.

2.2.4.1 Comparison of pyrolysis and gasification of plastics

Hydrogen is produced in the gas stream from both pyrolysis and gasification, with studies using biomass and waste by Ahmed and Gupta, and Demirbas showing that gasification produces the largest yields [27, 33, 34]. This is because gasification can produce extra hydrogen by either steam reforming reactions or by water-gas-shift reactions as a result of the steam present. As plastics are similar in their chemical nature, the same should be true. Ahmed and Gupta investigated the use of polystyrene for hydrogen production from both pyrolysis and gasification [39]. The gasifying agent used was steam and no catalyst was used. The temperature proved to be an important factor in hydrogen yield from gasification, with higher temperatures giving higher yields. Straight pyrolysis actually gave a higher yield of hydrogen at 700 °C

and 800 °C. It was suggested that this was because at these temperatures gasification to produce condensable hydrocarbons was favoured. Once the temperature was increased to 900 °C however, gasification produced a significantly larger yield of hydrogen, and produced the highest yield of all the experiments of around 3 g for the 18 g of polystyrene used.

Wu and Williams found similar results with un-catalysed pyrolysis and gasification of polypropylene [19]. Two stage pyrolysis using sand and temperatures of 500 °C for pyrolysis and 800 °C for gasification obtained a higher potential hydrogen production than when steam was added, and it was again concluded that the addition of steam led to the production of more C₂–C₄ hydrocarbons in favour of hydrogen. However, once a catalyst was added, gasification produced significantly higher yields of hydrogen.

He et al investigated the pyrolysis and gasification of PE at 900 °C in a fixed bed reactor [3]. It was found that compared to pyrolysis, gasification with steam produced a larger amount of hydrogen in the gas stream, as steam participated in gas phase reactions and gasified tars and gases to produce larger yields of hydrogen and carbon monoxide. This is comparable to the work of Ahmed and Gupta who likewise found hydrogen production from gasification was higher at a temperature of 900 °C [39].

Overall, gasification of plastics can be used produce large yields of hydrogen. Temperatures of around 800 °C and 900 °C prove most suitable for production by gasification.

2.2.4.2 Use of different plastics for hydrogen production

Thermal treatments have been used to produce hydrogen from a series of different plastics. Polyethylene is a common feedstock in plastics gasification. In their study of gasification of PE, He et al demonstrated hydrogen production from waste PE using steam gasification with a nickel catalyst [3]. Large hydrogen yields were obtained at a temperature of 900 °C with hydrogen making up 35.98 vol% of the gas produced. The waste plastic was recovered from municipal solid waste, with the elemental analysis showing signs of sulphur contamination, which could lead to poisoning of the nickel catalysts.

Erkiaga et al also used HDPE to produce hydrogen using a conical spouted bed reactor [40]. Temperatures of 850 – 900 °C were used along with an alumina catalyst, and hydrogen contents of the gas stream above 60 vol%

were achieved. These studies demonstrate that polyethylene can be used as a feedstock to produce hydrogen via thermal treatments.

Polypropylene is another plastic which has been used to produce hydrogen via thermal treatments. PP has been used as a feedstock to produce large amounts of hydrogen using a two stage process and with various nickel catalysts [19, 41]. Gasification temperatures of 800 °C were used, and with various catalysts the hydrogen content of the gas stream was up to 75.5 vol% and up to 57.7 wt% of the maximum hydrogen production obtainable was achieved.

Czernik and French also made use of a nickel based catalyst for hydrogen production from polypropylene and obtained 80% of the theoretical maximum yield for hydrogen [42]. A two stage process was employed using a steam fluidised bed reactor and a commercial nickel catalyst.

Park et al also used PP to produce hydrogen via a two stage gasification process using a ruthenium catalyst [43]. Varying the pyrolysis, reforming temperatures and catalyst:sample ratio to obtain the optimum conditions, hydrogen contents of the gas of up to 72.0 vol% and hydrogen yields up to 182.7 mmol/g sample were achieved. These studies show that PP is a suitable feedstock for producing large yields of hydrogen via thermal treatment.

Studies have also compared the use of different plastics for their ability to produce hydrogen via thermal treatments. PP, PS, HDPE and a waste plastic sample have been investigated for their ability to produce hydrogen via a two stage gasification process [44]. A Ni-Mg-Al catalyst was used with temperatures of 800 °C and 850 °C. Of the plastics investigated HDPE produced the largest hydrogen yield at 850 °C, 0.303 g/g plastic, followed by PP, 0.241 g/g plastic and finally PS, 0.196 g/g plastic. It was suggested that the pyrolysis products from HDPE, which contained large amounts of alkenes and alkanes, were easier to steam reform and so produced large yields of hydrogen, whilst production from gasification of PS was low as it needed higher temperatures to breakdown PS further.

Tsuji et al found similar results when producing hydrogen from the steam reforming of pyrolysis oils from waste plastics, using PE and PS [45]. Nickel alumina catalysts were used and they obtained hydrogen contents in the gas of 72 vol% and 68 vol% for PE and PS respectively. The lower yield of PS in this study is in agreement with the results obtained by others [44], and

indicates PS is a less suitable feedstock than other plastics for production of hydrogen.

Unlike other studies, Namioka et al used a ruthenium catalyst and demonstrated the potential to produce hydrogen from both PS and PP [46]. A similar two stage pyrolysis-gasification process was used using steam, and reforming temperatures of 853 – 953 K. Similar results were found with more PP converted to gases than was the case with PS at temperatures of 903 and 953 K.

Friengfung investigated the gasification of various plastics, but used a combination of steam and oxygen as gasification agents [47]. A temperature of 1123 K was used with a nickel-dolomite catalyst, testing PS, HDPE, LDPE and PP. Once again PE based plastics proved to be most suitable for the production of hydrogen. HDPE produced the largest yield in mmol/ g sample, followed by PP, LDPE and finally PS again proving the least effective for hydrogen production. The poor performance of PS was again attributed to its aromatic nature, which is stable and so unresponsive to thermal cracking.

Wilk and Hofbauer also investigated different plastics in a dual fluidized bed gasifier using steam [48]. At temperatures between 852 °C and 855 °C PE produced a larger amount of hydrogen in its gas stream compared to PP, consistent with other studies which found PE produces higher yields of hydrogen.

As well as individual plastics, mixtures of plastics and mixed waste plastics have also been investigated for hydrogen production. A mixed waste plastic sample has been investigated in a two stage pyrolysis gasification process with a Ni-Mg-Al catalyst [49]. Large hydrogen yields were obtained, with 0.258 g/g sample at 800 °C using steam gasification, with hydrogen making up more than 65 vol% of the gas stream.

Mixed plastics have also been gasified via air gasification; however hydrogen yields are much lower than for steam gasification. Kaewpengkrow et al used air gasification to obtain hydrogen in a syngas from the gasification of plastic waste [50]. Hydrogen and carbon monoxide contents of over 25 vol% of the gas stream were obtained with the use of a Ni-Mg-La/Al₂O₃ catalyst.

Likewise other studies by Cho et al and Arena et al undertook air gasification of mixed plastics and achieved lower quantities of hydrogen in their gas streams than was achieved with steam gasification [51-53]. A maximum of 27.96 vol% hydrogen achieved by Cho et al [53] with reaction temperatures

of 899 °C for the catalyst in the top reactor and 819 °C for the fluidised bed in the bottom reactor, making use of activated carbon as a catalyst.

Overall, production of hydrogen from plastics has been demonstrated in a number of studies using a range of different plastic types. PE and PP prove to be the most suitable plastics for hydrogen production, with the aromatic nature of PS proving harder to breakdown. Mixed plastics and plastic wastes have also been used to produce large amounts of hydrogen in gas streams from gasification using either steam as the gasification agent. Air gasification produces lower yields of hydrogen, due to the oxygen reacting with hydrogen species and the lack of production via steam reforming and water gas shift reactions.

2.2.5 The use of catalysts for hydrogen production

In order to increase the yield of the desired product of thermal treatments, catalysts are often used. Catalysts need to have a series of different properties in order to be effective such as high mechanical strength, large pore volume, high thermal stability, good accessibility to the active components for reactants and high surface area. For a catalyst to have all these properties, as well as other possible desired characteristics, it is normally necessary for the catalyst to be comprised of a catalytically active component and a support. The support determines the size and shape of the catalyst and so governs properties such as surface area, mechanical strength and porous structure. Calcination of catalysts is undertaken to thermally breakdown non-oxidic precursors, remove unwanted chemical species such as ligands, hydrogen, carbon or nitrogen, and oxidise support and surface species. Another purpose of calcination is to control the crystallinity and grain size of support and surface oxides.

A number of catalysts can be used for the production of hydrogen including calcined rocks such as dolomite, olivine, clay materials, iron ores, char, fluid catalytic cracking catalysts such as zeolites, alkali-based metals, activated alumina and transition metals [22]. Options such as dolomite, olivine, clays, iron ores and chars are cheap catalysts, widely available and are useful at reducing the build-up of tars, however, they are not as active as other catalyst types such as transition metals [22]. Other options such as zeolites, activated alumina and alkali metal based catalysts often have lower catalytic activity and can suffer from deactivation by coking, with this being particularly problematic with zeolite catalysts [22]. Transition metal catalysts

such as nickel give a far higher catalytic activity than dolomite and can be used to obtain high yields of hydrogen and reduce the build-up of tar completely. As a result, transition metal catalysts are often used for hydrogen production.

2.2.5.1 Transition metal catalysts

Transition metal catalysts are typically used for hydrogen production as they offer a higher catalytic activity than other metals, but are cheaper than other effective metal catalysts such as the noble metals [54]. However transition metal catalysts suffer similar problems to those used in steam reforming such deactivation by sulphur poisoning and coking.

Studies have compared different transition metal catalysts when investigating hydrogen production, in order to determine which obtains the highest yield. Hu et al investigated the steam reforming of acetic acid on Ni, Fe, Co and Cu catalysts on an alumina support [55]. Ni and Co catalysts showed good catalytic activity for the production of hydrogen, and it was suggested this was because these catalysts have reasonable activity for water gas shift and good activity for cleavage of C-C and C-H bonds. Fe gave a lower catalytic activity, and it was suggested that whilst Fe has good activity for promoting water gas shift reactions, it was poor at promoting the breakdown of C-H bonds. Likewise Cu produced a low catalytic activity in the breakdown of acetic acid and so produced a small hydrogen yield. It was suggested that this was because Cu had a poor activity for cracking C-C bonds. The Ni catalyst was thought to be the most suitable catalyst in terms of hydrogen production as it had high activity, and was more stable and produced less coking than the Co catalyst.

Aupretre et al also investigated various transition metals including nickel, iron, zinc and copper, as well as noble metals, on alumina supports for the production of hydrogen from steam reforming of bio ethanol [54]. It was found that nickel and rhodium were the most effective catalysts in terms of the hydrogen yield, with ruthenium, platinum, palladium, copper, zinc and iron not proving as catalytically active. Nickel produced the highest hydrogen yield with $3.1 \text{ g h}^{-1} \text{ g}^{-1}$ catalyst, compared with yields between 0.3 and $0.4 \text{ g h}^{-1} \text{ g}^{-1}$ catalyst for the other transition metals of copper, iron and zinc. It was suggested that this was because nickel and rhodium were more active in terms of steam reforming reactions than the other catalysts. Other catalysts, such as copper, iron and zinc had poor activity for steam reforming but

better activity for water gas shift, which led to an equilibrium being reached for water gas shift reactions and so restricted hydrogen production.

Tomishige et al also investigated noble transition metal catalysts for hydrogen production using a $\text{CeO}_2/\text{SiO}_2$ support with tars from cedar biomass [56]. At 923 K rhodium and nickel were again seen to be the most active of the catalysts used, however at a lower temperature platinum and palladium became more active suggesting that temperature has an influence on catalytic activity [56].

Overall, a good catalyst for production of hydrogen should have good activity for breaking C-H and C-C bonds by steam reforming, and as such nickel and noble metal catalysts prove to be most suitable. However, whilst rhodium and platinum are two of the most catalytically active metals, they have a very high associated cost, and so as a result nickel catalysts are the most often used in reforming [57].

2.2.5.2 Nickel catalysts

2.2.5.2.1 Activity of nickel catalysts

The activity of nickel catalysts is thought to be related to step sites which are defect sites on the catalyst [21]. Bengard et al proposed that step sites are the main active sites on a catalyst [58], and found lower activation barriers at these locations on the catalyst surface, leading to higher catalytic activity.

Abild-Pederson likewise found that step sites produced a higher catalytic activity when obtaining theoretical and experimental results based on the dissociation of methane [59]. Experiments used an ultra-high vacuum chamber and temperatures of 500 K to decompose methane on a nickel sample. The activity of step sites compared to terraces were analysed on a $\text{Ni}(14\ 13\ 13)$ single crystal sample, with step sites proving to have the higher activity.

Support for the importance of step sites in catalytic activity was also found by Rostrup-Nielsen [60] who saw a correlation between the reaction rate and the density of step sites, as measured by nitrogen adsorption.

In order for the catalytic activity to be high and obtain a large yield of hydrogen it is therefore important to try and increase the number of step sites. Whilst some evidence has suggests that smaller catalyst particles have more step sites, this is not universally upheld [21].

2.2.5.2.2 Sulphur poisoning of nickel catalysts

A key problem with using nickel catalysts is poisoning by sulphur species. Sulphur is a well-known poison to nickel catalysts as it blocks active nickel sites [21]. The mechanism involved in sulphur poisoning of nickel and ruthenium catalysts used in steam reforming was investigated by Chen et al using XANES (X-ray absorption near edge structure) [61]. A liquid hydrocarbon was steam reformed, and metal sulphides, organic sulphides, sulphonates and sulphates were observed on the surface of the catalyst. It is thought that the formation of nickel sulphides causes the deactivation of catalysts as these were present on the nickel catalyst which was rapidly deactivated but not on the ruthenium catalyst which showed much less deactivation. The deactivation of the nickel catalyst by sulphur led to a significantly smaller hydrogen yield even after a small number of hours. Only the initial deactivation of the catalyst is thought to be directly attributable to the presence of nickel sulphides with further deactivation thought to be caused by the build-up of carbons. It is suggested that the presence of sulphur influences the carbon chemistry and restricts the formation of whisker type carbons in favour of amorphous carbons which cause catalyst deactivation.

Whilst sulphur poisoning is a big problem for nickel catalysts, the plastics feedstocks that will be investigated in this study are very unlikely to contain sulphur, and so it is not of great concern.

2.2.5.2.3 Coking of nickel catalysts

A major problem associated with using nickel based catalysts in thermal treatment of hydrocarbons is deactivation by coking [21], where carbon deposition builds on the catalyst surface. This is a result of the decomposition of methane and other hydrocarbons, where breakdown of the C-H bond occurs, leaving carbon to build up on the surface. In an investigation into carbon deposition onto nickel catalysts Rostrup-Nielsen found three distinct types [60]. These were whisker type carbons, which include the valuable nanofilaments and nanotubes, pyrolytic carbons and encapsulating carbons which deactivate the catalyst. Whilst whisker carbons do not necessarily deactivate catalysts they cause parts of the catalyst to fragment [57]. In terms of carbon deposition it is seen that aromatics produce the most carbon, followed by olefins and finally paraffins [57],

showing that deactivation by carbons on nickel catalysts also depends on the feedstock used.

As a result of deactivation by carbon, a number of studies have aimed to reduce the build-up of carbon deposition on catalysts, in order to keep catalyst activities high [62-65]. In terms of coke reduction a number of different methods are thought to prevent coke formation. The nickel particle size is thought to play an important role in the build-up of coke deposits, with Bengaard et al suggesting that nickel particles with facets smaller than 25 Å should not be able to form graphite islands that cause coking [58]. It is also suggested that the blocking of step sites may reduce the amount of coking as these have been shown to be highly active in terms of carbon deposition [57].

2.2.5.2.4 Sintering in nickel catalysts

Another challenge involved in the use of nickel catalysts is sintering, where catalyst particles grow in size [21]. Sintering is of particular importance as it is thought to influence the other three catalytic challenges, since coking limits are determined by catalyst size, sulphur capacity is determined by surface area and the activity of catalysts is related to particle size [21]. Two proposed mechanisms exist for sintering of catalyst particles, particle migration, and Ostwald ripening. Particle migration occurs by entire catalyst particles moving across the support as metal atoms diffuse from one side of the particle to the other, causing translational movement [21]. These particles then coalesce to form larger particles. In contrast the catalyst particles in Ostwald ripening grow by metal transport species being emitted from one particle and migrating via the support or gas phase until it is captured by another catalyst particle, causing growth [21].

The effect of sintering on the activity of a nickel catalyst was investigated by Bai et al [66]. Fresh and sintered nickel methanation catalysts were investigated, with the sintered catalyst showing a smaller nickel and BET surface areas as a result of sintering. As a result there was a reduction in CO conversion in the sintered catalyst.

De La Riva et al likewise reported that sintering of nickel catalysts causes a loss of activity [67]. Reviewing work from the theses of De La Riva and Hansen, it was concluded that Ostwald ripening was the cause of the loss of activity in a Ni/MgAl₂O₄ catalyst. These studies show that sintering of nickel

particles causes a loss of activity, largely through the reduction in nickel surface area.

2.2.5.2.5 Use of different catalyst supports

The use of different catalyst supports also has an effect on the performance of a catalyst, as they offer different surface areas and interactions with the active metal. Miyazawa et al investigated the performance of nickel catalysts on various supports for the steam reforming of tars from biomass pyrolysis [68]. Catalysts were prepared by the incipient wetness technique and used supports of Al_2O_3 , ZrO_2 , TiO_2 , CeO_2 and Ni/MgO . The activity of the catalysts in steam reforming based on tar conversion was as follows $\text{Ni/Al}_2\text{O}_3 > \text{Ni/ZrO}_2 > \text{Ni/TiO}_2 > \text{Ni/CeO}_2 > \text{Ni/MgO}$. Hydrogen production followed a similar pattern with $\text{Ni/Al}_2\text{O}_3$, Ni/ZrO_2 and Ni/TiO_2 producing the largest hydrogen yields, with the $\text{Ni/Al}_2\text{O}_3$ catalyst producing the largest hydrogen yield at 923 K. Hydrogen adsorption of the fresh catalysts was carried out in order to estimate the number of surface nickel atoms, and results for the various catalysts showed that the amount of tars produced from steam reforming reduced with an increase in surface nickel atoms. This suggests a contributing factor in the strong performance of the $\text{Ni/Al}_2\text{O}_3$, Ni/ZrO_2 and Ni/TiO_2 catalysts was a good metal dispersion as these showed the largest amount of surface nickel atoms. The nickel particle sizes measured by hydrogen adsorption and XRD also showed a correlation with catalytic performance, with $\text{Ni/Al}_2\text{O}_3$, Ni/ZrO_2 and Ni/TiO_2 catalysts all showing particle sizes of around 30 nm. In contrast, the catalysts which showed poor activity had nickel particle sizes larger than this, with Ni/CeO_2 having particle sizes of around 50 nm and Ni/MgO having particles sizes of 381 nm. This suggests that the support used has an effect on governing metal particle sizes, which proved to be a key to catalyst activity. Investigations into thermogravimetric analysis (TGA) using steam showed that the Ni/CeO_2 catalyst gasified activated carbons much more readily than the other catalysts, indicating this was good for coke reduction. Overall, the nickel alumina catalyst showed the highest catalytic activity, and that this support provided good nickel dispersion and a catalyst-support interaction which allowed nickel particles of an active size to be formed.

A series of studies on pyrolysis-gasification of polypropylene and other plastic feedstocks, using a variety of nickel based catalysts has been carried out [19]. The catalysts used were $\text{Ni/Al}_2\text{O}_3$, Ni/MgO , Ni/CeO_2 and Ni/ZSM-5

which were prepared by impregnation, a Ni/CeO₂/Al₂O₃ which was prepared by co-impregnation and Ni-Al and Ni-Mg-Al which were produced by co-precipitation. Like the study by Miyazawa et al [68], the Ni/MgO catalyst produced the lowest yield of hydrogen. In this instance the poor performance was attributed to the build-up of monatomic carbon, observed by temperature programmed oxidation (TPO) and scanning electron microscopy (SEM), which blocks access to active sites. Ni/Al₂O₃ and Ni/CeO₂ catalysts also showed large amounts of carbon deposition, however filamentous type carbons were observed which were thought to not deactivate the catalyst to as large an extent. This shows that the support has an effect on the catalysts performance, as it determines the type and amount of carbon deposition which forms. The BET surface area of the Ni/MgO catalyst was also the lowest measured, whilst Ni/Al₂O₃ and Ni/CeO₂, which produced lower hydrogen yields compared to other catalysts, also showed low surface areas. This shows how a low surface area provided by the support also has an impact on catalytic performance. With the exception of the Ni/ZSM-5 catalyst the catalysts prepared by impregnation produced lower hydrogen yields than those produced by other methods. Carbon deposition on the Ni-Al and Ni-Mg-Al catalysts prepared by co-precipitation was also lower. This suggests that the preparation method used also has an effect on catalytic activity. Overall, the results showed that the surface area and carbon deposition are governed by the support used, which have an effect on catalytic performance. Whilst Ni/Al₂O₃ and Ni/CeO₂ catalysts produced large amounts of carbon deposition, activities remained high, whilst Ni/MgO proved an unsuitable catalyst.

Inaba et al investigated Ni/SiO₂, Ni/ZrO₂, Ni/CeO₂ and a series of zeolites for use as catalysts in hydrogen production from the gasification of cellulose [69]. Hydrogen performance for the oxide supports was as follows with Ni/SiO₂ > Ni/ZrO₂ > Ni/CeO₂, whilst the various zeolites obtained higher or lower hydrogen yields depending on the zeolite used. This shows how the support used can have an effect on the activity of the catalyst. The carbon deposition on the catalysts also varied with the catalyst support, as was found by Wu et al [19], with Ni/SiO₂ producing the largest carbon deposition and hydrogen yield. As carbon is produced during hydrocarbon deposition onto the catalyst, larger amounts of carbon deposition would indicate a higher catalyst activity in cracking hydrocarbons. All the catalysts, including zeolites, were investigated by XRD, and it was found that catalysts which had a higher amount of Ni metal relative to NiO after the reaction had a higher catalytic activity, with the exception of Ni/CeO₂. Like Miyazawa et al

[68] this indicates that the interaction between the nickel and the support is an important factor, as catalysts where nickel was more easily reduced produced a higher yield of hydrogen from gasification experiments. XRD was also used to determine the nickel particle size on the catalysts after gasification reactions. Catalysts with nickel particle sizes around 25 nm had the highest activity, with nickel particle sizes larger or smaller than this producing less hydrogen. This too indicates interaction with the support has an effect on the hydrogen yield, as different supports produced nickel particles of different sizes. This is in agreement with the study by Miyazawa et al [68]. Overall, nickel on different supports yielded different hydrogen yields from the gasification of cellulose as a result of interactions between the nickel and support, which is a key component in catalyst activity.

Srinakruang et al investigated the gasification of tar using nickel catalysts supported on $\text{SiO}_2\text{-Al}_2\text{O}_3$, Al_2O_3 and dolomite [63]. As was the case with Wu et al [19] and Inaba et al [69], different supports produced different amounts of carbon deposition. The nickel catalysts on $\text{SiO}_2\text{-Al}_2\text{O}_3$ and Al_2O_3 produced larger amounts of carbon deposition than the Ni-Dolomite catalyst, which led to deactivation. This shows how use of different catalyst supports can effect hydrogen production, as carbon deposition happens more readily on certain supports.

Overall, the use of different catalyst supports effects the activity of the catalyst by determining the surface area, and interactions with the active metal. Interactions with the metal can govern the ease of metal reduction, particle size and carbon deposition, which proved important factors in the production of hydrogen.

2.2.5.2.6 Effect of varying the nickel loading

The metal loading on a catalyst will have an effect as increasing the amount of active nickel species should result in an increase in catalytic activity. Dong et al investigated the effect of varying the nickel content of a Ni/Ce-ZrO₂ catalyst used for the reforming of methane [70]. Nickel contents were varied between 0 and 30 wt%, and it was found that 15 wt% produced the highest catalytic activity. At nickel percentages below this level, catalyst activity decreases with decreasing metal content as a result of a lower surface area of nickel on the catalyst. At nickel percentages above 20 wt% a reduction in the surface area of nickel occurs, as a result of much larger nickel particles being formed via sintering. This led to a reduction in catalytic activity. The 20

wt% catalyst actually had a larger nickel surface area than the 15 wt% catalyst; however its lower catalytic activity occurred as a result of increased carbon deposition. This would suggest above certain particle sizes, carbon deposition occurs more readily. Overall, it was found that catalyst activity towards hydrogen production increases with nickel content as a result of an increase in nickel surface area. However, past a certain point a reduction in the surface area occurs as a result of larger nickel particles being formed, which also cause more carbon deposition.

A Ni-Al₂O₃ catalyst was used by Srinakruang et al for the decomposition of toluene as a model biomass tar compound using nickel contents between 5 and 20 wt% [63]. The conversion of toluene was seen to significantly increase as the nickel content was raised up to 15 wt%, however raising it further to 20 wt% did not give a higher conversion. This is in accordance with Dong et al where increasing nickel content led to an increase in catalytic activity up to a point [70].

Similar results were also obtained by Bimbela et al [71] who varied the weight content of nickel when decomposing biomass pyrolysis oils. In this instance they used a Ni-Al catalyst and nickel loadings of 23, 28 and 33 wt%. Increasing the nickel content up to 28 wt% gave an increase in carbon conversion and hydrogen yield, however further increasing the nickel content had little effect. Likewise, the varying production of carbon deposition at different nickel contents was suggested as a reason for the difference in catalytic activity.

These studies suggest that the nickel content of the catalyst used has an effect on the carbon conversion and hydrogen yield; however beyond a point, increasing the nickel content further has no appreciable effect. The activity of the catalyst is largely related to the nickel surface area of the active species and hence more active sites. Past a certain point however, increasing the metal content leads to increased sintering and a reduction in metal surface area. Increasing the nickel percent also affects the amount of carbon deposition, which can deactivate the catalyst.

2.2.5.2.7 Effect of the calcination temperature

Calcination is often used to prepare catalysts by heating them in air. As such it can be used to prepare different metal particle sizes and metal support interactions. Chen et al investigated the effect of different calcination temperatures on the characteristics of a nickel alumina catalyst [72]. Nickel

alumina catalysts were prepared at calcination temperatures between 673 and 973 K, and it was observed that the nickel particle size increased with calcination temperature before starting to level out around 873 K. This was as a result of an increase in sintering of nickel particles at higher calcination temperatures. It was suggested that less of an increase in particle size was observed above 873 K as nickel aluminate begins to form at this temperature, which is more stable and results in the nickel being strongly bonded to the support. Overall, it was seen how the calcination temperature can not only gauge the particle size of the metal particles, but also how strongly they are attracted to the support.

Clause et al found similar results with nickel/aluminium and nickel /chromium catalysts [73]. Calcination temperatures between 773 and 1273 K were used, with particle size increasing as the calcination temperature was raised for both sets of catalysts. A change in the interaction between nickel and the alumina and chromium supports was also observed at higher temperatures, above 823 K for the nickel/chromium catalyst, and above 1273 K for the nickel/aluminium catalyst. The production of nickel aluminates and different chromates formed at these higher calcination temperatures, with the particle size increasing greatly when chromates were formed. This agrees well with the study by Chen et al [72] in showing how the calcination temperature can control particle size and nickel interactions with its support.

As a result the change in particle size and support interaction, the calcination temperature has an effect on hydrogen production from thermal treatments. Garcia et al investigated two different calcination temperatures with a co-precipitated nickel alumina catalyst for the thermal treatment of biomass [74]. The calcination temperatures used were 750 °C and 850 °C, and it was found that the higher calcination temperature resulted in a higher stability through the formation of spinels, leading to better performance, despite the fact that the initial performance of the catalyst calcined at 750 °C was superior. This suggests that the calcination temperature used influenced the stability and interaction of nickel compounds with the alumina support, and that this in turn had a positive effect on the long term hydrogen production.

Furusawa et al also investigated the effect of the calcination temperature of catalysts on the supercritical water gasification of lignin [75]. Ni/MgO catalysts were used and prepared at calcination temperatures between 773 and 1173 K. As the calcination temperature was increased, the size of the nickel particles increased, because of sintering, which led to a reduction in the metal surface area. As a result of this, changes in the performance of the

catalysts were observed with the catalyst prepared at a calcination temperature of 873 K producing the highest activity. It was concluded that this led to an optimum nickel particle size, which held the highest catalytic activity. This again supports the idea that the calcination temperature can be used to affect the activity of a catalyst by varying its metal particle size.

Overall, the studies have shown that the calcination temperature of catalysts is an important factor in hydrogen production via thermal treatments. Increasing the calcination temperature leads to larger metal particles. This affects the catalysts activity, and can lead to the production of stronger and more stable metal support interactions.

2.2.6 Other effects on hydrogen production

2.2.6.1 Effect of increasing amount of steam

A key factor on the hydrogen yield obtained from gasification is the amount of steam used. Erkiaga et al investigated the gasification of polyethylene in a conical spouted bed reactor at a temperature of 900 °C [40]. The effect of varying the mass ratio of steam to plastic used was investigated using ratios between 0 and 2. With an increase in steam, by raising the steam to plastic ratio, the gas yields were increased, and the hydrogen composition of the gas also increased. This was because with more steam injected, steam reforming and water gas shift reactions are enhanced, leading to more gases, and in particular hydrogen.

Similar results were obtained by Wu and Williams who investigated the effect of varied steam injection into a two stage pyrolysis-gasification process used to produce hydrogen from polypropylene [49]. A gasification temperature of 800 °C was used with a Ni-Mg-Al catalyst, and the steam injection rate of water into the reactor varied between 1.90 and 14.2 g h⁻¹. As was the case with Erkiaga, increasing the steam injection led to an increase in both the gas yield and hydrogen production, with a maximum production of 0.334 g/ g plastic produced at 14.2 g h⁻¹ steam injection. As such increasing the steam rate is a good way of increasing the yield of hydrogen.

2.2.6.2 Effect of feedstock:catalyst ratio

The amount of feedstock relative to the catalyst is also an important factor in thermal treatments. If there is too much feedstock relative to the amount of catalyst, it will not gain sufficient contact with the catalyst for the reaction to

complete successfully. Park et al investigated varying the amount of feedstock relative to the catalyst by changing the WHSV (Weight hourly space velocity) in the gasification of PP [43]. The flow rate of the carrier gas and plastic were kept constant, and so the WHSV was changed by varying the amount of catalyst used. When the WHSV velocity was increased, by using less catalyst relative to the feedstock, there was a reduction in the amount of gases produced. This was because the contact time of the feedstock on the catalyst was reduced and so the reaction was not completed as effectively.

Bimbela et al varied the amount of catalyst relative to an acetol feedstock in gasification experiments [71]. The amount of catalyst used was increased whilst keeping the acetol flow rate constant, and like Park et al at lower amounts of catalyst relative to the feedstock less of the desired gases, including hydrogen were produced.

Overall, the feedstock:catalyst ratio is an important factor in thermal treatments. A lower feedstock:catalyst ratio gives the feedstock a higher contact time on the catalyst, and has more catalyst available for reactions to complete. As a result, more of the desired product is produced.

2.2.6.3 Effect of reaction temperature

The reaction temperature used for the production of hydrogen has an effect on the yield obtained, as higher temperatures increase the rate of reactions for cracking, steam reforming and water gas shift. Some feedstocks also require a larger amount of energy to breakdown the chemical bonds within them and so increasing the temperature can lead to increased production of hydrogen and smaller gases. He et al investigated the effect of varying the temperature between 700 °C and 900 °C on the production of syngas from the gasification of polyethylene [3]. Increasing the reaction temperature led to an increase in the production of hydrogen with the largest yield achieved at 900 °C. This was because steam reforming, carbon gasification and cracking reactions are endothermic, and so increasing the temperature favours the production of the products rather than the reactants.

Bimbela et al also investigated the effect of reaction temperature on the hydrogen yield from acetol [71]. Temperatures of 550, 650 and 750 °C were used with the Ni-Al catalysts. Increasing the temperature led to increased hydrogen yield, and like He et al's study it was attributed to the fact that the steam reforming reactions are endothermic, and so increasing the

temperature shifts the equilibrium towards hydrogen production. It is also likely that there is an increased rate of reaction.

In their study on the degradation of pyrolysis oils from biomass, Miyazawa et al also studied the effect of temperature on Ni-Al₂O₃ catalysts using temperatures of 823, 873 and 923 K [68]. Like Bimbela et al's study it was found that increasing the temperature led to an increase in carbon and conversion, whilst the tar conversion and hydrogen formation rate are also seen to increase.

Ahmed and Gupta also investigated different temperatures for the production of hydrogen from the pyrolysis and gasification of polystyrene [39].

Temperatures were varied between 700 and 900 °C for both pyrolysis and gasification. As with the other the other studies, increasing the temperature led to an increase in hydrogen production from both pyrolysis and gasification.

The results suggest that the temperature used for the steam reforming is a key factor in hydrogen production from plastics via thermal routes. Higher temperatures produce larger yields of hydrogen as a result of an increase in production via endothermic steam reforming and gasification reactions.

2.3 Carbon nanotube production

2.3.1 Carbon nanotube properties

Carbon nanotubes have been identified as a valuable product of thermal treatments. They have gained a great deal of interest in recent years, as a result of the desirable properties and applications they could be used for [76]. CNTs are an allotrope of carbon and form cylindrical hollow tubes which have diameters of the range 0.1-100 nm. Whilst knowledge of the similar fibrous and filamentous carbon types have been known for several years, the discovery of carbon nanotubes is a recent phenomenon, having been first identified by Iijima in 1991 [77].

The characteristics that distinguish carbon nanotubes from other types of carbon stem from their structural make up. Carbon nanotubes are comprised of sheets of graphitic carbon that are rolled up to form hollow cylinders and can either contain single or multiple walls coaxially aligned. When there is a singular tube in isolation they are referred to as single walled carbon nanotubes (SWCNTs), whereas when there are multiple tubes within in each

other they are called multi-walled carbon nanotubes (MWCNTs). The bonding between the carbon atoms is similar to the sp^2 seen in graphite, but because of the cylindrical nature of carbon nanotubes the bonding is slightly deformed, leading to the electrons being more delocalised outside the tube [78]. This in turn leads to high values for strength, thermal and electrical conductivity and chemical and biological reactivity. Table 2.1 shows some of the mechanical properties of CNTs in comparison to that of steel [79].

Table 2.1 Mechanical properties of CNTs compared to steel [79]

	Young's modulus (GPa)	Tensile Strength (GPa)
MWNT	1200	~150
SWNT	1054	75
SWNT bundle	563	~150
Graphite (in plane)	350	2.5
Steel	208	0.4

In terms of their electrical conductivity, CNTs can either be metallic or semi-conducting depending on the orientation of the hexagonal structure with respect to the alignment of the tube itself [80]. For example 'arm chair' alignment, where hexagons are exactly perpendicular to the orientation of the tube, gives metallic CNTs whilst other orientations give semiconducting tubes where the band gap is proportional to the diameter of the tube [80]. Figure 2.2 shows arm chair (a) and two other possible alignments of the hexagonal lattice within carbon nanotubes; (b) and (c) are 'zig-zag' and (d) is 'chiral' [81].

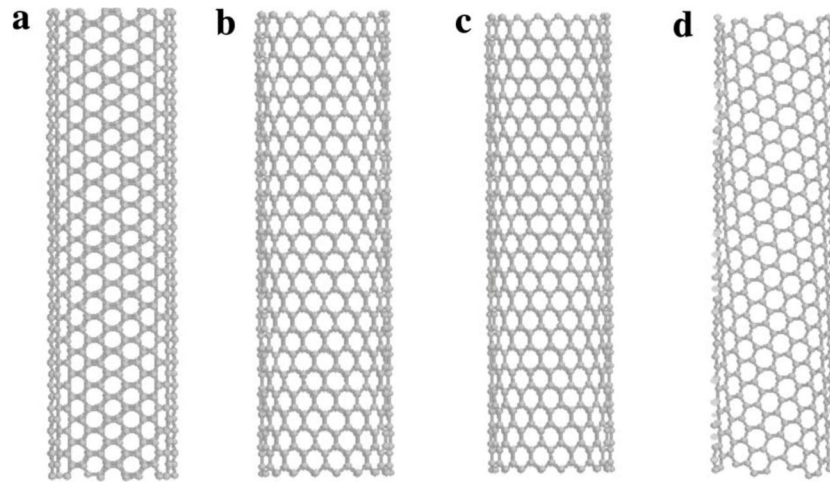


Figure 2.2 Alignment of hexagonal lattice within CNTs [81]

Because of their delocalised electrons, carbon nanotubes also exhibit good thermal conductivity, whilst their high surface areas could lead to applications involving purification, catalysis and separation [78].

2.3.2 Methods of carbon nanotube production

There are three main methods by which CNTs are currently produced; arc discharge, laser ablation and chemical vapour deposition [82]. Arc discharge production makes use of a direct current arc that is placed between two graphite electrodes which are water cooled and placed in a chamber filled with an inert atmosphere of helium. Once the arc is switched on, the positive graphite anode is consumed and a deposit starts to form on the negative graphite cathode. For the production of single walled nanotubes a catalyst is required. Co-vaporisation of the graphite and catalyst is undertaken by densely packing a small hole drilled in the graphite anode with metal and graphite powders.

Laser ablation makes use of a laser oven, and carbon nanotubes were first discovered in this way during fullerene production in the gas phase of a graphite sample [82]. Carbon nanotubes can be formed via this process using temperatures of around 1200°C where graphite is ablated and the carbon is vaporised [82]. Carbon nanotubes form and are then carried away in a gas stream.

Major production of CNTs on a large scale is done through chemical vapour deposition, as it offers better scalability and controllability than other techniques [83]. In chemical vapour deposition (CVD), carbon containing

gases or volatiles are decomposed onto metallic particles which act both as a catalyst and nucleation site for the production of carbon nanotubes [83]. A simplified mechanism for the formation of CNTs is thought to be similar to carbon fibre formation, and can be thought of as follows [84]:

- Carbon containing gas is absorbed onto the catalyst and decomposes releasing gases and solid carbon
- The carbon dissolves and diffuses into the metal particle
- Once the metal is supersaturated carbon begins to precipitate in solid form as carbon nanotubes

Typically the feedstock in CVD uses pure carbon containing gases, with examples being methane [85], acetylene [86], carbon monoxide [87] and aromatic hydrocarbons [88]. Chemical vapour deposition requires use of a catalyst to act as the nucleation site for carbon nanotube formation.

Transition metals are used as catalysts, with the most common being nickel [89], iron [85], and cobalt [90].

2.3.3 Purification of carbon nanotubes

Carbon nanotubes produced from chemical vapour deposition contain a great deal of impurities including amorphous carbons, particles of the metal catalyst or catalyst support and carbon nanoparticles [83]. In order for the carbon nanotubes to be used in valuable applications they are often required to be of a high purity, and so purification methods exist to remove non-CNT materials. There are two main techniques used for the purification of CNTs; dry methods such as oxidation with air, and wet methods such as acid treatment [83]. These techniques can be used in isolation but are often used in conjunction with one another. Dry methods use the higher reactivity of other compounds compared to that of CNTs to remove the impurities. This is done by oxidation in air at a selected temperature as CNTs are less easily oxidised than amorphous carbons or other carbon contaminants [91]. Wet methods use acid treatment to dissolve metal catalysts and metal oxides, and are usually undertaken after the dry methods have taken place [83]. Nitric acid is the most commonly used acid, and filtration and centrifugation steps often follow to increase the yield of CNTs obtained.

Ebbesen et al used oxidation in air to purify CNTs originally from arc-discharge production [92]. The sample was heated to 750 °C and held for 30 minutes. As a result, a large weight loss occurred as other types of carbon

and impurities were burnt off. This included the caps of the CNTs which proved more reactive than the tubes. This left CNTs in isolation, however 99 wt% of the original weight was oxidised.

Xu et al likewise investigated the purification of CNT using oxidation in air [93]. CNTs were produced from CVD of carbon monoxide, and the deposits obtained were treated with air to oxidise any amorphous carbons produced, as these are more reactive. Acid treatment with HCl was then used to remove any iron particles. Oxidation temperatures up to 350 °C were used and CNT purities of over 98% were obtained, with a reduction in iron from 30 wt% to 1 wt%. The CNT yield was maintained at 70 wt% of its original mass, substantially better than was obtained by Ebbesen et al [92]. This was because $C_2H_2F_4$ and SF_6 were also added to the gas stream, so that the iron particles exposed by the gasification of amorphous carbons became deactivated, and CNTs were not destroyed.

Thermal treatment using air was also used as an initial purification method by Moon et al [94]. CNTs produced by arc discharge were purified by first heating the obtained powders in a rotating quartz reactor at a temperature of 470 °C, for 50 minutes in air to remove amorphous carbons. A second acid treatment stage was then undertaken to remove the catalysts, where the nanotubes were dropped into HCl until the acid stopped changing in colour. A final step to unbundle the CNTs was also undertaken, where the nanotubes were boiled in 30% nitric acid. This method obtained a CNT purity of 96%.

Yang et al used a one-step acid treatment for purifying CNTs and compared it with a two-step purification process using oxidation in air followed by acid treatment [95]. CNTs were obtained by CVD of carbon monoxide and were single walled. Acid treatment was undertaken by immersing the as-obtained CNTs in HCl and then filtering the precipitates, whilst oxidation was undertaken by heating in air at 623 K for 30 minutes. Purification led to a reduction in the amount of iron in the CNTs, with a reduction from 30 wt% for the as-obtained CNTs to 18 wt% for the acid treated sample, and 6 wt% for the oxidation and acid treated sample. This shows that the two stage process was a more effective purification treatment than just acid on its own. It was more effective, as the gasification of carbon deposits in air exposed more iron that could then be removed by acid. The purification techniques also had an effect on the properties of the CNTs obtained. After purification the CNTs had a higher surface area and higher volume of micro-pores. This was attributed to the removal of amorphous carbons and metal particles

from the tips of the carbon nanotubes meaning they then had open ends. The two-step purification technique produced a larger surface area and micro-pore volume than the one-step process, consistent with the fact that more iron and carbon deposits were removed by gasification followed by acid treatment. Overall, a better purification performance was achieved by using a two-step process compared with just acid treatment in isolation.

Overall, purification of CNTs can be undertaken to remove metal catalyst particles and carbon contaminants using acid and oxidation treatments. High purities of CNTs are achieved by using both in combination.

2.3.4 Uses for carbon nanotubes

Once CNTs have been purified, they have the potential to be used in a wide range of applications as a result of the useful properties they exhibit. In the long term it is possible that CNTs may find uses in electronics, as transistors and interconnects on the nanoscale, energy applications, with use in batteries, fuel cells, solar cells and hydrogen storage, biological applications, sensors, display devices by field emission display, and high strength materials, as fibres or polymer composites [76, 96].

Whilst carbon nanotubes have a number of possible applications, some of these are limited by the quality of carbon nanotubes that have been produced. For example, nanotubes that could be used in electronics would require specific CNT types, with SWCNTs needed for use as transistors and bundled closely packed, aligned and defect free CNTs required for use as interconnects. Current production from both CVD of pure sources such as methane, as well as production from plastics does not currently give CNTs that are suitable for these applications. Limitations in the length, strength, and consistency all prevent CNTs that are currently in production from being used in high end future applications. SWCNTs also require much more process controls than the production of MWCNTs, resulting in MWCNTs being cheaper and therefore more commonly used [76]. The MWCNTs produced however could find a number of uses in a series of different industries, as they are often used in current technologies.

2.3.4.1 Use in high strength applications

Allaouia et al produced a composite material using MWCNTs and an epoxy resin [97]. MWCNTs produced from CVD of benzene were dispersed in

methanol to reduce the size of aggregates before the methanol was evaporated. The obtained powder was then injected into an epoxy resin mixture which was then left to set in moulds. Using 1 wt% CNTs led to a 100% and 200% increase in the Young's modulus and yield strength respectively, whilst electrical conductivity was also markedly increased.

Montazeri et al likewise used MWCNTs to produce epoxy-CNT composites [98]. The CNTs were mixed with the resin, and then sonicated before hardening. The amount of CNTs added was varied between 0 and 3 wt%, and it was observed that tensile strength and Young's modulus increased with the CNT wt% in the plastic, before starting to level out at around 2 wt% addition.

Coleman et al used MWCNTs to produce polymer composites from different plastics [99]. Poly vinyl alcohol-CNT composites were formed by mixing the MWCNTs into a solution of poly vinyl alcohol, whilst PP-CNT composites were produced by covalently attaching chlorinated PP to the MWCNTs. As was the case with Allaouia et al [97], the composites had significantly increased physical properties. The Young's modulus, tensile strength and toughness increased 3.7, 4.3 and 1.7 times respectively for the PVA-CNT composite, and 3.1, 3.9 and 4.4 times respectively for the PP-CNT composite.

A number of companies in the USA and Japan such as Zyvex, Mitsui and Toray, make current use of MWCNTs from CVD for their high strength properties [96]. They are used in composite plastics as a matrix enhancer rather than being load bearing structures, however they also find uses in constructing superior sporting goods [96].

Overall, MWCNTs can be used to successfully enhance the properties of plastics by creation of composites. The composites have significantly increased Young's modulus and strength compared to the plastics on their own. This shows promise for the use of MWCNTs for use in high strength applications.

2.3.4.2 Use in energy applications

Carbon nanotubes also find many uses in energy applications including batteries, fuel cells and solar cells [76]. For example, Li et al investigated the use of MWCNTs as catalyst supports in a methanol fuel cell [100]. It was found that using CNTs as a support led to increased performance when compared with other support types.

The use of CNTs to improve batteries was investigated by Sotowa et al [101]. MWCNTs were used to improve the positive electrode in Li-ion batteries by adding acetylene blacks and the MWCNTs to the Li-CoO₂ materials used. As a result, the electrode had enhanced density and thermal and electrical properties.

2.3.4.3 Use in filtration and separation

Another possible use for CNTs that could be suited to the CNTs produced from plastics is filtration and separation technologies. For example, Sae-Khow and Mitra [102] investigated the performance of composite filter membrane that was modified to include MWCNTs as part of its structure. The membranes were sonicated with MWCNT dispersions so they were introduced into the membrane pores. Removal efficiencies of the unmodified and CNT modified membranes were undertaken for solutions containing either dichloromethane, chloroform, benzene, trichlorethylene or toluene. The experiments were undertaken for different temperatures, concentrations and flow rates, with the CNT modified membrane outperforming the unmodified membrane in all circumstances. The enhancement in performance between the two membranes was most prevalent at low concentrations, high flow rates and low temperatures, however the CNT membrane enhanced removal of the solvent in all conditions and for all the solvents tested. Overall, results show that MWCNTs can be used to enhance the performance of membrane filters, particularly at low concentrations and temperatures.

Another method by which CNTs can be employed for filtration and separation is by creating 'Bucky paper' as was investigated by Sears et al [103]. Bucky paper is a membrane randomly arranged but non-woven CNTs that are produced by a filtration procedure, which creates a flexible but robust paper like substance. In their research, the group prepared Bucky papers from MWCNTs and used them in isolation and in composite membranes for desalination via membrane distillation [104-107]. Excellent desalination performances were obtained, with salt rejections of 95% and lifetimes of 39 hours of continuous use.

In combination with other researchers Vecitis studied the use of MWCNTs for use in filtration [108, 109]. MWCNTs were used to produce an electrochemical filter, which was successfully used to remove and oxidise aqueous chemicals such as methyl-orange, methylene-blue, phenol,

methanol and formaldehyde and viral or natural organic matter. Various treatments were undertaken on the CNTs to vary their performance including calcination, acid treatment and the addition of various functional groups. The electrochemical filter was able to oxidise 95% of methyl orange within a water sample [108]. The use of MWCNTs in an electrochemical filter also demonstrated the complete removal of viral particles and organic matter from water from the Suwannee river [109].

Overall, MWCNTs have shown potential applications in water treatment. They have proved successful in removal of pollutants or salt from water using membranes and filtration.

2.3.5 Carbon nanotube identification and metrology

A number of analyses can be used to confirm the presence of CNTs, measure their dimensions and assess their quality. Electron microscopy is an important tool used to identify CNTs as their presence can be visibly observed. Scanning electron microscopy, (SEM), allows the nature of carbon deposits to be observed, to determine whether filamentous carbons have been produced. However, as SEM only images the surface no distinction can be made between carbon filaments and CNTs. Transmission microscopy, (TEM), however is a far more useful tool to both confirm the presence of CNTs and determine their nature. This is because TEM images are taken through a thin section, and so the individual walls of the CNTs can be observed. The discovery of CNTs by Iijima used TEM to confirm the presence of CNTs and identify the walls and hollow core [77]. Since then, almost all studies on CNTs have used TEM to observe the presence and nature of the carbon deposits.

Raman spectroscopy is often used to characterise CNTs. CNTs exhibit characteristic peaks in their Raman spectrum, and so the presence of these allows the presence of CNTs to be confirmed. Peaks are seen at 1589, 1348 and 2709 cm^{-1} for CNTs. The peak at 1589 cm^{-1} corresponds to the G peak associated with graphitic carbon within the sample, the peak at 1348 cm^{-1} corresponds with the D peak and is associated with defects within the graphitic lattice; while the G' peak at the Raman shift around 2709 cm^{-1} indicates the two photon elastic scattering process, indicating the purity of CNTs. A number of studies have used Raman spectroscopy to characterise CNTs and confirm their presence [110-114]. For example, Arena et al performed Raman spectroscopy on carbon deposits obtained from the

fluidised bed pyrolysis of polypropylene [110]. It was used to help confirm the presence of CNTs as the spectrum was compared to that of a commercial MWCNT sample. The Raman spectrum of both samples were very similar, and contained the characteristic G and D peaks associated with CNTs. Combined with TEM this helped to confirm the presence of CNTs in the carbon deposits. The ratio between the size of the G peak and D peak is a useful way of comparing the quality of the carbon nanotubes obtained in terms of how ordered and graphitic they are [115-118]. This enables the purity of the deposits in terms of CNTs produced to be evaluated, with a larger G/D ratio indicating a higher purity. For example, instead of using the G/D ratio Yen et al used the D/G ratio to compare the quality of CNTs produced from the pyrolysis of PE, with a low value demonstrating higher quality CNTs [118]. Using different amounts of hydrogen in the gas stream, it was observed that a reduction in the D/G ratio was obtained with an increase in hydrogen, indicating that there was a higher degree of graphitisation in the CNTs.

Temperature programmed oxidation (TPO) can also help to establish whether carbon nanotubes are present in carbon deposits. Carbon nanotubes and filamentous carbons oxidise at a different temperature to amorphous carbons as a result of containing stronger bonds which are hard to breakdown. Wang et al studied the oxidation of amorphous carbon, graphitic carbon, such as that found in CNTs, and Bucky tubes, another name for CNTs, using a thermo-gravimetric analyser [119]. It was found that amorphous carbons were oxidised at a lower temperature, around 550 – 600 °C, than graphitic carbon, around 700 °C. Likewise Bucky tubes (CNTs) were oxidised at a comparable temperature to the graphite, around 700 °C. As such TPO can be used to distinguish between amorphous carbons and the graphitic carbons in filamentous and CNTs, with amorphous carbons being oxidised at a lower temperature.

2.3.6 Carbon nanotube production mechanisms

The deposition of carbon onto transition metal catalysts was identified earlier when discussing the production of hydrogen via thermal treatments.

Rostrup-Nielsen found three distinct types of carbon deposition, encapsulating, pyrolytic and filamentous carbons, such as CNTs [60]. It was also suggested that filamentous carbons, unlike encapsulating and pyrolytic carbons, do not deactivate catalysts, but can cause fragmentation of the catalyst [57]. As such the production of filamentous carbons, such as CNTs,

over amorphous or encapsulating carbons is preferable. The production of filamentous carbons depends on the nature of the hydrocarbon feedstock. Rostrup-Nielsen found that larger molecules form more filamentous carbons and that aromatic precursors form more filamentous carbons than olefins [120]. This is also in accordance with the mechanism for production of CNTs from plastics as proposed by Gong et al, who suggested that CNTs are produced from polymerisation of aromatics compounds on the catalyst surface [121]. Filamentous carbon growth is thought to stop once the catalyst particle is covered in encapsulating carbons [122].

Before the ultimate discovery of CNTs by Iijima in 1991 [77], work was undertaken on the similar material of carbon nanofibres. Baker et al proposed a three stage mechanism [122-124], which was suggested to be the same mechanism as the vapour-liquid-solid (VLS) mechanism of growth developed by Wagener and Ellis to describe the growth of Si whiskers [125]. The first stage for the VLS growth of carbon nanofibres is the adsorption and dissociation of carbon containing gases onto the surface of a catalyst particle to form elementary carbon atoms. This is followed by the carbon atoms dissolving into the catalyst nanoparticles to form a liquid carbide, where the carbon then diffuses throughout the particle. The final step is the precipitation of the carbon on the catalyst particles to form the carbon nanofibres [126]. The VLS mechanism has also since been used to describe the formation of CNTs with Kukovitsky et al using it to describe the growth of CNTs from polyethylene pyrolysis [127]. Snoeck et al described how the diffusion of carbon was as a result of a concentration gradient within the metal particle [128]

A modified version of VLS has also been proposed; the vapour-solid-solid mechanism [126, 129]. In the VSS mechanism, the carbon precursor dissociates on the catalyst, where surface diffusion of carbon atoms then occurs and CNTs then grow from precipitation of the carbon [126]. This was supported by a study by Helveg et al who produced in situ HRTEM images of CNT growth from nickel particles, which showed that CNTs can grow by a mechanism involving surface diffusion of carbons on solid catalyst particles [130].

A mechanism for the initial formation of CNTs, 'yarmulke' mechanism was proposed by Dai et al [87]. Metal particles with diameter nanometres in length have very high surface energy due to the high percentage of surface atoms. The formation of a graphene cap, from excess carbon from deposition, reduces this energy. The growth of multi walled carbon

nanotubes occurs by the formation of subsequent caps which cause the first cap to lift up and form a cylindrical tube, whilst single walled nanotubes grow by new carbon simply being deposited as a cylinder beneath the cap. The mechanism suggests that the diameter of single and multi-walled CNTs are governed by the size of the catalyst particle. Other studies which suggest the ‘yarmulke’ mechanism include work by Pol and Thiyagarajan [131].

CNTs can either grow from catalyst particles at the tip, tip growth, or at the base near the catalyst, base growth [129]. Tip growth is where catalyst particles are found at the end of CNT, as nanotube growth lifts the catalyst from the substrate and then grows from beneath the catalyst [129]. Figure 2.3 by Hofmann et al details how CNT synthesis by tip growth occurs in the following steps [132]:

- (1) Adsorption of the gas precursor molecule on the catalyst surface,
- (2) Dissociation of the precursor molecule,
- (3) Diffusion of the growth species in or on the catalyst particle, and
- (4) Nucleation and incorporation of carbon into the growing structure

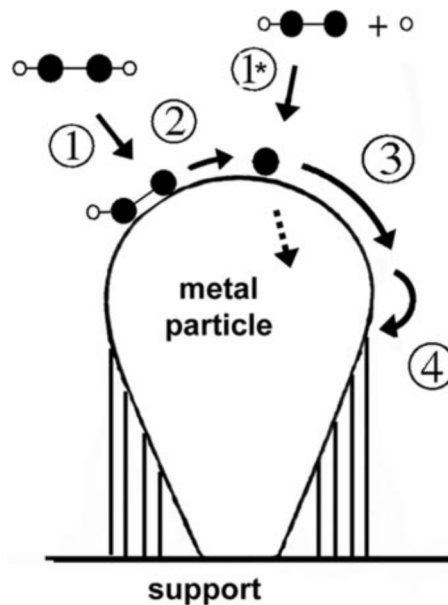


Figure 2.3 Tip growth mechanism for carbon nanotube formation [132]

Other examples of studies which have identified catalyst particles at the end of the CNTs suggesting tip growth include Ducati et al [133] and Kukovitsky et al [127].

The base growth model in contrast sees the CNT grow from above the catalyst particle, which remains attached to the substrate [129]. Figure 2.4 by Puretsky et al details how CNTs are synthesised by the base growth mechanism by the following steps [134]:

- (1) Impingement of carbon precursor molecules into the catalyst particle surface
- (2) Chemisorptions and catalytic decomposition of carbon precursor molecules on the surface of the catalyst particle
- (3) Surface-bulk penetration of carbon atoms
- (4) Formation of disordered surface layer
- (5) Diffusion of carbon atoms channelled by the disordered layer
- (6) Precipitation of carbon species into a nanotube

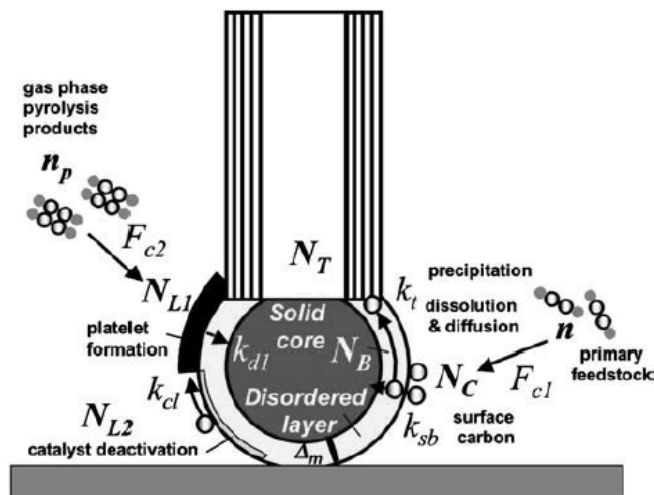


Figure 2.4 Base growth mechanism for carbon nanotube formation [134]

Like tip growth, there have been other studies which have found CNTs produced with no catalyst particles at the tip suggesting the base growth model including work by Hata et al [135] and Ermakova et al [136]. The growth mechanism that occurs depends on the interaction of the catalyst particle and the substrate [129], with metal particles that adhere strongly to the substrate likely to yield base growth.

There no general consensus about the exact mechanism by which CNTs are produced, however a number of steps are thought to be universally upheld [137]:

- (1) Carbon precursor molecules, such as methane or acetylene, catalytically decompose onto the surface of a metal catalyst.
- (2) Diffusion of the carbon atoms which are released into the metal particles.
- (3) The metal becomes supersaturated with carbon and results in solid carbon precipitating on the metal particle
- (4) Depending on the catalyst particle size and precipitation rate, CNTs start to grow from the metal particle.

2.3.7 Catalysis in carbon nanotube production

The use of catalysts in CVD of CNTs is widespread and is thought to play a crucial role in their formation. This section will investigate the role catalysts play in CNT production and a series of factors which affect the catalyst.

2.3.7.1 *Use of different metals*

Transition metals are frequently used as catalysts for CNT production by CVD. This is based on past research which proved them to be successful in terms of filamentous carbon production. Baker et al [122] studied the growth of carbon filaments from acetylene and used catalysts composed of nickel, iron and cobalt. Whilst different rates of filament growth were observed, the graphs followed a similar shape of initial acceleration, constant growth and deactivation, suggesting a similar mechanism, regardless of catalyst metal. Since then a large number of studies have successfully generated CNTs from iron [85, 86, 135, 138-147], nickel [85, 86, 138, 143, 144, 148-155] and cobalt catalysts [85, 90, 138, 143, 144, 147, 151, 152, 156-158]. Recently a study has also made use of a copper catalyst for CNT production [159], suggesting this may also be a suitable catalyst.

In terms of direct comparison between the different metals a number of studies have tried to investigate which metal is most suitable for CNT growth. Kong et al [85] also investigated the use of nickel, iron and cobalt catalysts and compared their relative ability to produce SWCNTs. The catalysts were oxides of the various metals and were impregnated onto either silica or alumina supports and used for the decomposition of methane at 1000 °C. SWCNTs were only produced on the iron and cobalt catalysts,

with nickel only producing them when mixed with cobalt. The nickel catalyst produced MWCNTs, but only on an alumina support. The yield of nanotubes produced from the iron catalyst was significantly larger than was obtained from the cobalt catalyst, with some double walled carbon nanotubes also being produced on the iron catalyst. At the time of publishing no explanation for iron's superior performance was given.

A suggestion for the good performance of iron as a catalyst for CNTs was proposed in a study by Liu et al [144]. The effect of using iron, cobalt and nickel catalysts on CNT production from CVD of methane was investigated. The CNTs were investigated by Raman spectroscopy and TEM, with iron producing the highest quality carbon nanotubes, followed by cobalt and finally nickel. The superior performance of the iron catalyst was attributed to the higher carbon solubility of iron, which helps to promote the production of carbon nanotubes. Carbon solubility was suggested to be a key aspect of CNT growth, since it increases the amount of carbon available for CNT growth, and is thought to produce a higher concentration driving force which accelerates the CNT formation rate. Support for the importance of carbon solubility was provided by Moisala et al when reviewing the production of single walled CNTs [137]. It was noted that amongst transition metals copper had much lower carbon solubility, and likewise was unsuitable for CNT production. Nasbulin et al also concluded that the carbon solubility was an important factor in the production of CNTs [160]. When comparing the production of carbon nanomaterials from nickel and copper catalysts, nickel's higher carbon solubility was suggested to be the reason nickel produced CNTs whilst copper did not.

Other studies have also shown that iron is a good catalyst for CNT production compared to other transition metals. Govindaraj et al likewise compared Co, Fe and Ni catalysts for the production of CNTs from methane [143]. It was found that whilst Fe gave the largest yield of CNTs, it favoured the production of MWCNTs, whilst Co and Ni produced more SWCNTs. One suggestion as to why MWCNTs were produced on the Fe catalyst was due to larger metal particles being formed.

When investigating the production of hydrogen and filamentous carbon from methane decomposition Ermakova and Ermakov discovered CNTs on the surface of an iron catalyst, but not on a nickel catalyst [142]. The catalysts were prepared by a sol-gel method and were supported on SiO₂, however different experimental temperatures were used for each catalyst, with 550 °C used for Ni and 700 °C used for Fe. The iron catalyst was found to produce

CNTs whilst in contrast the nickel catalyst only produced filaments. However the different temperatures used could have influenced the CNT growth.

Work by Tan et al also investigated the effect of different transition metals as catalysts [147]. Once again iron, cobalt and nickel were used as catalysts, this time with alumina used as the support. Methane was the feedstock and the temperature of reaction was 950 °C. In accordance with Kong et al [85], it was found that Fe was the most effective catalyst, with a mixture of single and multi-walled CNTs produced depending on the calcination temperature used. Likewise Co was also seen to produce CNTs, with again the calcination temperature affecting the structure of the carbons obtained. As was seen in Kong et al's study [85] the Ni catalyst proved to be the least effective at producing CNTs, with none produced at any calcination temperature.

Similarly, Ago et al also investigated catalysts based on iron, cobalt and nickel using a MgO support [138]. The catalysts were prepared by impregnation and were utilised with a methane feedstock and temperatures of 800 °C. Based on methane conversion, into either CNTs or amorphous carbons, it was seen that Fe is the most effective by a large stretch, with Co the next most effective and Ni the least suitable. This is again similar to results from Kong et al [85] and Tan et al [147]. The TEM results correlate to the results of methane conversion, with a larger number of CNTs seen on the Fe catalyst, and the smallest amount seen on the Ni catalyst. This again suggests a dependence on the metal catalyst used for CNT production, with Fe being the most effective and Ni the least.

The influence of the catalyst metal on the carbon nanotubes obtained was investigated by Choi et al, who used both nickel and cobalt catalysts [151]. Acetylene was used as the feedstock in this instance, with the metals being supported upon a silicon substrate. Whilst different temperatures and feedstocks were used, CNTs were produced on both metals. A difference in the CNTs obtained was observed, with the nanotubes from the Ni catalyst having a smaller diameter than those from the Co catalyst. This suggests that the different metals formed catalyst particles of different sizes, which could be a result of different interactions with their support material.

Hsieh et al also discussed the differences between CNTs produced from nickel and cobalt catalysts, this time using a CaCO₃ support was used with an acetylene feedstock and temperatures of between 700 °C and 850 °C [152]. The catalysts were prepared by impregnation. A larger inner diameter, of the hollow centre, was also observed on the CNTs from Co compared to

Ni, however the outer diameters for both were similar. It was suggested that the Co particles where CNT growth occurred were larger and resulted in a larger inner diameter. A kinetic study of the catalysts suggested that whilst nickel required a higher activation energy for CNT production, the growth rate from nickel was higher.

Overall, iron, nickel and cobalt catalysts have all proved effective catalysts for the production of CNTs via CVD. However, iron catalysts were found to be the most effective, with nickel and cobalt frequently producing smaller yields. It is suggested that the high carbon solubility that iron in comparison to nickel and cobalt's is the reason for the superior performance of iron. Different diameters of CNTs were also produced from CNTs, which could be a result of the metals having different interactions with the support, and so undergoing varying degrees of sintering.

2.3.7.2 Use of different supports

The catalyst support also has an effect on the production of CNTs. As is the case for hydrogen production, this is because the support is an important part of the catalyst and can control the surface area, dispersion and interaction with the active metal. A number of studies have successfully yielded CNTs from a variety of supports, with Al₂O₃ [85, 89, 136, 138, 146, 147, 161, 162], MgO [162-165] and SiO₂ [85, 89, 136, 138, 142, 146, 162] being the most commonly used.

Studies have also compared the use of different supports, to see the effect on CNT production. Kong et al investigated both alumina and silica supports [85]. Whilst alumina and silica supports both yielded CNTs results varied with catalyst metal. Iron supported on silica produced large bundles of CNTs, however, the alumina support produced individual single and double walled CNTs rather than in bundles. For nickel and cobalt catalysts however, the silica support proved completely ineffective as no tubular materials were synthesised at all, whilst the alumina support saw the growth of CNTs. This suggests that more needs to be considered than just choosing a support, as whilst it may be effective for one metal, it may give a poor performance with others. This could be a result of the different way some metals interact with supports. In this study it is suggested that the anisotropic properties of the alumina leads to a range of catalyst particle sizes and shapes and so therefore a mixture of CNTs are formed, resulting in the individual tubes

observed. In contrast silica is thought to have an isotropic surface leading to uniformly and closely distributed catalyst particles.

Ermakova et al used a number of different catalyst supports for the decomposition of methane and quantified the amount of carbon deposited [136, 166, 167]. The decomposition of methane was undertaken for the production of filamentous carbons rather than CNTs, however both materials are similar in nature. When nickel catalysts were investigated using supports including SiO₂, Al₂O₃, ZrO₂, TiO₂ and MgO, SiO₂ is found to give more carbon deposits [166, 167]. The SiO₂ support was reported to be effective as a catalyst as it allowed metal particles of the correct size for filaments to grow. The metal-support interactions in the study were deliberately weak, as it is suggested that when interactions are too strong they interfere with carbon diffusion, and hence the production of filamentous carbons such as CNTs. Likewise the strong performance of a SiO₂ support was obtained with iron catalysts [136]. In terms of the nature of the carbon deposits obtained using Fe, silica supports produced bamboo like CNTs, filamentous carbons and a small amount of CNTs, whilst alumina supports produced far straighter CNTs. This suggests that alumina is a more favourable support for CNT production, backed up by results for the amount of graphitisation in the carbon deposits where silica produces 0% compared with alumina's 35%.

Takenaka et al also investigated the use of different catalyst supports for nickel catalysts used in the decomposition of methane [162]. The catalysts were produced by impregnation, and used reaction temperatures of 550 °C. The Ni/SiO₂ catalyst gave the highest carbon yield, with Ni/TiO₂ producing a reasonable yield and Ni/Al₂O₃ producing significantly less. The catalysts which provided larger yields of carbon showed nickel present in the form of crystallised Ni, whereas, the catalysts which performed poorly showed nickel present in the form of NiO. It was suggested that a compound oxide was formed between the metal and support for the Al₂O₃ and MgO and their poor performance was attributed to this. A compound oxide would indicate a strong interaction between the support and metal, and so it is likely that the interaction proved too strong and inhibited CNT growth. SEM analysis showed the presence of filamentous carbons on the SiO₂, TiO₂, ZrO₂ and graphite supports, whilst none were seen on MgO, however no results are shown for the Ni/Al₂O₃ catalyst.

Chai et al also investigated the formation of carbon nanotubes and filaments from the decomposition of methane using nickel catalysts on a range of supports [89]. In terms of the amount of carbon deposited it was observed

that $\text{NiO/SiO}_2 > \text{NiO/HZSM-5} > \text{NiO/CeO}_2 > \text{NiO/Al}_2\text{O}_3$. However, TEM results showed the presence of CNTs on the $\text{Ni/Al}_2\text{O}_3$ catalyst at a reaction temperature of 550 °C, whilst all other supports, including SiO_2 , only produced carbon fibres. The alumina support produced NiO crystals which were significantly smaller than those produced from the supports used, which could be an attributing factor in the production of CNTs. When a higher temperature of 700 °C was investigated the SiO_2 and CeO_2 as well as the Al_2O_3 catalyst were seen to produce CNTs suggesting that whilst the catalyst support is important, other factors such as temperature also have an influence. Zeolites however proved unsuccessful at both temperatures suggesting that these supports may be unsuitable for CNT production. The $\text{Ni/Al}_2\text{O}_3$ catalyst showed a strong adhesion between the support and active metal which prevents sintering and leads to smaller particles which favour CNT growth.

The use of MgO , SiO_2 and Al_2O_3 as catalyst supports using Fe for the production of CNTs from methane was investigated by Liu et al [144]. Results were interpreted by Raman spectroscopy and electron microscopy. It was found that MgO produced the highest quality CNTs in terms of the D/G ratio and also showed the highest intensity of radial breathing modes which are representative of single walled CNTs. The results in terms of the D/G ratio was $\text{MgO} < \text{Al}_2\text{O}_3 < \text{SiO}_2$, with a smaller D/G ratio showing less defects in the CNTs and hence a higher quality. The high performance of the MgO catalyst was attributed to its strong catalyst-support interaction, which prevents sintering of the metal particles, and gives a good dispersion of the active metal. This contrasts with the results obtained by Takenaka et al [162], where MgO and Al_2O_3 catalysts had interactions which were too strong and inhibited carbon deposition. However, different methods of catalyst preparation were used, suggesting this might be another important factor in CNT production.

Overall, it has been seen that Al_2O_3 , SiO_2 and MgO are suitable catalyst supports for the production of CNTs, with SiO_2 suggested to be the best in a number of studies. An important factor in choosing a suitable support for CNT production is its interaction with the active metal. Strong metal-support interactions can prevent sintering and allow good dispersion and particle sizes of the active metal. However, it is also suggested that if metal support interactions become too strong, CNT production is inhibited.

2.3.7.3 Use of different loadings of metal

Studies have also investigated the metal loading when studying CNT production [143, 146, 155, 161, 168-170]. For example, Govindaraj et al investigated the nickel, cobalt and iron catalysts for the production of CNTs, with varying amounts of the active metal used, between around 3 and 13 wt% [143]. A temperature of 1070 °C was used to decompose methane over the catalysts. Results are given for the amount of carbon deposited as well as for the increase in surface area of the catalyst after carbon deposition per gram of carbon, representing the quality of the CNTs produced. For all the metals tested the carbon yield increases with metal loading, however the quality is seen to decrease. It is suggested that increasing the metal loading of the catalyst yields a larger amount of CNTs as a result of more catalytically active metal particles being present. Above 10 wt% metal the yield is not thought to increase further as a result of larger metal particles being produced which do not yield CNTs. The quality is thought to reduce as a result of more multi-walled as opposed to single walled CNTs.

A study by Avdeeva et al found a similar increase in activity with metal loading when investigating the use of nickel-copper alumina catalysts for the deposition of methane [161]. The temperature used was 827 K and the amount of nickel and copper within the catalyst was varied. Increasing the amount of nickel between 57 wt% and 90 wt% saw increases in the amount of carbon deposited, however further increasing to 100 wt% nickel saw a drastic reduction. No carbon nanotubes were observed, with the carbons obtained being filamentous in nature.

Takenaka et al undertook a series of studies for the formation of filamentous carbons from methane decomposition over nickel and iron catalysts [146, 168, 169]. The first study [168] used two different nickel contents, 5 wt% and 10 wt%, in nickel silica catalysts at 803 K and found the amount of carbon deposited on the 10 wt% nickel catalyst to be higher. The subsequent study [169] concentrated further on the effect of the metal content and once again used nickel silica catalysts, with nickel contents of between 1 wt% and 90 wt%. The yield of carbon depositions increased up to around 40 wt% nickel, upon which point further increases in nickel content led to a reduction in carbon yield. The diameters of the fibres grown showed a positive correlation with the metal percentage in the catalyst, particularly at the early stage of growth, and it is suggested that certain diameter metal particles are more effective at producing fibres as these diameters saw a longer growth time. It was reported that the reduction in carbon yield observed for higher

metal percentages was due to a reduction in the amount of the optimum fibre growth diameter metal particles, and that likewise the highest yield was due to an abundance of these particle diameters. This correlates with the findings of Govindaraj et al [143] who also suggested higher metal contents give smaller yields as a result of larger metal particles. Another study by Takenaka et al switched to iron catalysts for the decomposition of methane, with metal loadings of 7 wt%, 14 wt%, 38 wt% and 77 wt% [146]. Similarly to nickel, the optimum metal percentage was 38 wt%, with reductions in carbon deposition yield either side of this metal content. It was also found that the size of the metal particles formed increased with the metal content of the catalysts and that as with nickel, the catalyst particle size governs the carbon deposition performance.

Tian et al used nickel catalysts of different metal contents, 5 wt%, 10 wt% and 15 wt%, to produce CNTs from the chemical vapour deposition of methane [155]. The increase in metal content leads to an increase in the yield of CNTs, which is a similar result as was found by Takenaka et al [169], who saw increases in the yield of carbon nanofibres with these nickel contents. However it is reported that the thermal stability of the CNTs and quality, as observed by TEM, reduces as nickel content is increased. This is in agreement with the work by Govindaraj et al [143] who likewise saw a reduction in CNT quality as the metal content of the catalyst was increased.

Overall, it can be seen that increasing the active metal content in the catalysts leads to a larger yield of CNTs as a result of more active sites. The catalyst particle size is also affected by metal loading, and whilst certain particle sizes are more effective for CNT growth past a certain point the catalyst particles then become too large to large for CNT formation. MWCNTs rather than SWCNTs are also formed at higher metal loadings, possibly as a result of larger catalyst particles.

2.3.7.4 Influence of catalyst preparation

In addition to the influence of metal and supports used on CNT production, the calcination temperature used during catalyst preparation is also an important factor. This can govern the size of catalyst particles on the support, which is an important factor in CNT production. For example, Baker et al found that the diameter of filamentous carbons, such as CNTs, has an inverse square root dependence on their growth rate [122], and larger

diameter CNTs are thought to be produced from larger metal particles [171-173].

Lee et al investigated the effect of varying the catalyst particle size by using different treatment methods [174]. Iron catalysts were used, and were deposited onto silicon oxide. As with Baker et al's study, an inverse relationship was found between the particle size and the growth rate of CNTs. It was suggested that the growth rate increases with a smaller particle as the time taken for the carbon to diffuse through the particle is reduced as the distance to cover is shorter.

Ermakova et al also investigated the effect of the calcination temperature on the growth of filamentous carbons [142, 166, 167]. The results found that the size of the catalyst particles increase as the calcination temperatures is raised. In terms of filamentous carbon production it was found that there was an optimum particle size range, between around 10-40 nm. When higher calcination temperatures formed metal particles larger than this, the amount of filamentous carbons deposited was significantly reduced.

Tan et al also studied the effect of calcination temperature on the growth of CNTs, including nickel, iron and cobalt catalysts [147]. With cobalt catalysts it was seen that higher calcination temperatures formed SWCNTs whilst lower temperatures formed a mixture of MWCNTs and SWCNTs. This was attributed to higher calcination temperatures allowing the metal to melt and form the smaller catalyst particles which form SWCNTs. Iron on the other hand produced more SWCNTs at lower calcination temperatures, with higher temperatures yielding MWCNTs. In this case the iron catalyst is thought to agglomerate at the higher calcination temperatures, yielding the larger particles responsible for MWCNTs. This is more similar to Ermakova et al's results for nickel catalysts [167], since an increase in calcination temperature yielded larger catalyst particles. No CNTs were produced on the nickel catalyst regardless of calcination temperature, and this was thought to be a result of the high reaction temperature used.

Chai et al investigated the effect of the calcination temperature of a cobalt catalyst on CNT production in a CVD process [148]. Methane was used as the feedstock and the calcination temperatures investigated were between 300 and 750 °C. At low calcination temperatures, the interaction between the catalyst metal and support was weak, and during CNT production the catalyst underwent sintering, leading to metal particles too large for CNT production. As the calcination temperature was increased, however, the metal support interaction became stronger and as a result, the carbon

nanotube yield increased. This was only true up to a certain point however, as the catalyst can become hindered by too strong a metal support interaction. The same was identified when discussing the use of different catalyst supports. Transition metals can bond strongly to supports, for example Garcia et al investigated the production of metal aluminates [74]. It was found that iron, cobalt, nickel and copper all form aluminates when calcinated at different temperatures.

Overall, the calcination temperature used in catalyst preparation has an effect on the CNT production. Calcination can affect the metal particle size produced, which controls the diameter and also affects the growth of CNTs. The calcination temperature can also effect the interaction between metal and support. At high calcination temperatures metals can become strongly bonded to the support, which restricts mobility of metal particles and prevents CNT production.

2.3.7.5 Catalyst lifetime

Another important factor in the growth of CNTs is the catalyst lifetime, and has an effect on both the decomposition of the feedstock and the length of CNTs obtained [117, 138, 140, 163, 175, 176]. Ago et al investigated the amount of methane that was decomposed onto various metal catalysts supported on MgO in order to calculate the amount of carbon deposition [138]. The initial conversion rate of methane was high at the start before beginning to decrease as the reaction time was increased, and tended towards zero conversion after about 5 minutes for all catalysts. The short conversion time in this instance was attributed to deactivation of the catalyst occurring as a result of the build-up of amorphous carbons.

Likewise Bronikowski et al [140] found that the growth of CNTs on iron deposited onto silicon substrates only grew in length for a short period of time before their growth halted. The growth period was reported to be up to around 5 minutes, similar to the point where decomposition of methane stopped as seen in Ago et al [138]. It is also suggested that the reason for the termination of the growth of the CNTs is due to overcoating of the catalyst with carbon, again consistent with Ago et al [138]. The growth reported by Bronikowski et al is linear, and so it is suggested that the time the feedstock is exposed to the catalyst can be varied to control the length of the CNTs produced.

With the use of different catalysts however some studies have seen longer growth periods, whilst maintaining the linear growth rate observed. Yang et al utilised a different method of catalysis, whereby a floating catalyst was used by subliming ferrocene in the flow of the inlet gas [117]. The ferrocene would sublime to form particles of iron, which would catalyse the growth of CNTs onto a substrate. Linear growth of CNTs was observed up to 40 minutes. Li et al instead of silica used and alumina buffer layer above the silica substrate and saw longer growth times of up to two hours [175]. Studies by Li et al [163] and Zhao et al [176] investigated the amount of CNTs obtained against time rather than the length, but still found that the increase was linear. Li et al used a Ni/Mo/MgO catalyst and saw increased growth times of up to two hours, whilst Zhao et al used a Ni/Cu/Al catalyst and saw growth times of more than three hours. Zhao et al whilst seeing longer CNTs also saw that a longer reaction time may have led to an increase in the diameter of some of the CNTs obtained.

Overall, it can be seen that increasing the length of CNTs increases linearly with time, but that the time until deactivation occurs is controlled by other factors such as the catalyst used. Catalyst deactivation occurs by the production of amorphous carbons which encapsulate the catalyst. It is also likely that other factors such as the temperature used for CNT growth will influence the time until deactivation.

2.3.8 Effect of reaction temperature

In addition to catalysts, other factors also have an effect on carbon nanotube production such as reaction conditions and the addition of other substances to the process. A number of studies have investigated the effect of temperature on the production of CNTs. Lee et al investigated the effect of different temperatures on the chemical vapour deposition of acetylene over iron deposited silicon substrates, using temperatures between 750-950 °C [177]. It was found that as growth temperature was increased the rate of growth of the CNTs increased substantially, with the diameter also increasing with temperature. It was suggested that the growth rate increased as a result of higher diffusion and reaction rates of carbon. The diameter of the CNTs is thought to increase with reaction temperature as a result of agglomeration of iron particles on the catalyst surface, leading to the formation of larger iron particles and hence larger diameter CNTs. As a result of the agglomeration of the iron particles, the CNTs were also observed to be more sparsely spread across the catalyst leading to a lower

density of CNTs. The crystallinity of the walls of the CNTs as observed in TEM also increased as the growth temperature was raised. TPO and Raman spectra of the CNTs also confirmed the increased crystallinity, with oxidation of the carbon deposits occurring at a higher temperature, and a reduction in the D/G ratio observed.

Other studies including those by Gallego et al [116], Li et al [175], Liu et al [178] and Wu and Tzeng [170] also investigated the effect of temperature on the growth of CNTs. In accordance to Lee et al [177], an increase in the amount of carbon deposits and CNTs was observed as the temperature was raised. In each case a maximum temperature was reached after which CNT growth was inhibited.

Sengupta et al likewise investigated the effect of reaction temperature on the production of CNT via CVD of iron(III) acetylacetonate [179]. Temperatures between 550 °C and 950 °C were used. As was observed by Lee et al [177], the crystallinity of the CNTs obtained increased with reaction temperature. This was confirmed by Raman spectroscopy, where a change in the D/G ratio was observed. The D peak is associated with defects within the CNTs whilst the G peak is associated with ordered graphitic carbon, and so a low D/G ratio relates to high quality CNTs. The D/G ratios obtained reduced from 1.23 at 550 °C, to 0.24 at 950 °C, indicating that the CNTs obtained at 950 °C were the most crystalline and of the highest quality.

Ducati et al investigated the effect of temperature on the growth of CNTs using nickel catalysts [133]. Acetylene was used as the feedstock and deposited over nickel silica catalysts at temperatures in the range of 550 °C to 850 °C. It was found that the diameter and number of walls in the CNTs increased with reaction temperature, whilst the density of the CNTs decreased. Larger CNT diameters were a result of growth of metal particles via sintering. The shape of the catalyst particles was also seen to vary with growth temperature, with ellipsoid particles at the lower temperature and more spherical particles at the higher temperatures.

Juang investigated the growth of bamboo type CNTs from ethylene at a range of growth temperatures between 800 °C and 900 °C [153]. In correlation with the results from Ducati and Lee [133, 177], an increase in temperature led to a larger diameter of CNT. It was also observed that the rate that formation of 'diaphragms' in bamboo type CNTs, caps inside the hollow centre of the CNT, increased with reaction temperature. This was attributed to high surface and bulk diffusion at higher temperatures, which

meant caps formed more through the bulk diffusion of carbon from the bottom of the metal particle to the top.

With regards to the growth rate of CNTs Bronikowski et al investigated temperatures between 550 °C and 800 °C on iron deposited on silicon substrates to see the effect on the length obtained [140]. The length of CNTs increased up to temperatures of 700 °C, with no CNTs observed at all at 500 °C, however at temperatures above 700 °C the CNT length obtained was shorter. It is suggested that at lower temperatures decomposition of carbon may be too slow to form the growth of CNTs, and that metal particles of a suitable size for CNT growth cannot form through agglomeration. The reason for the lack of growth at higher temperatures is attributed to the catalyst particles growing to a size too large to yield CNTs.

An investigation into the effect of temperature on CNT growth was also undertaken by Ohashi et al [180]. Methane was used as the feedstock with a Mo/Fe/Al catalyst on a Si support in a CVD process. As the temperature was raised, between 900 °C and 975 °C, larger catalyst particles were formed, and as a result less CNTs were formed, as it was suggested they were too big for CNT production. Carbon filaments were produced instead. With an increase in reaction temperature there was also a change from base to tip growth of the CNTs. The increase in temperature also yielded an increase in the rate of formation of filamentous carbons. The temperatures used in this study were high, and suggest that above a certain temperature the production of CNTs is inhibited as catalyst particles become too large.

Kukovisty et al investigated the effect of different reaction temperatures, 700 °C and 800 °C, on the production of CNTs from PE pyrolysis products [127]. In contrast to the other works, it was found that at the higher temperature CNT diameters were smaller and within a smaller range. In addition, whilst lower temperature CNTs matched the size of the catalyst particles no such correlation was observed at higher temperatures, with a Gaussian distribution of diameters obtained instead. It was suggested that a transformation in growth mechanism takes place between the two temperatures, where liquid metal particles are formed at the higher temperature, leading to a different shape of metal particle and hence the smaller diameter. The mechanism of CNT production also changed from base growth to tip growth as the temperature was raised, as was observed by Ohashi et al [180]. In accordance with Lee et al [177] and Sengupta et al [179], an increase in the crystallinity of the CNTs and continuity of the hollow core was observed at higher temperatures.

Takenaka et al investigated a number of growth temperatures for the decomposition of methane over nickel silica catalysts [169]. Growth temperatures were between 500 °C and 700 °C. The results showed that like Kukovitsky et al [127], the diameter of the nanofibres obtained reduced at the higher temperature, however, a change in the catalyst particle shape was observed as temperature increased. At the higher temperature metal particles in the carbon fibres became almost spherical, and the nature of the carbon changed from solid fibres to CNTs with a hollow core. As with all the previous studies, Raman spectra showed that the graphitic order, and hence quality of the fibres increased with an increase in temperature. In fact, whilst only carbon nanofibres are seen at the lower temperatures, CNTs are only produced at the higher temperatures.

Overall, the reaction temperature has shown to be an important factor in CNT growth. The rate of carbon deposition increases with reaction temperature leading to an increase in CNT production. The diameter of metal particles also increase with reaction temperature through sintering, and led to larger diameter CNTs, however past a certain point the diameter of metal particles become too large and CNT production is hindered. Some studies also show that a change in CNT production occurs at higher temperatures, with a switch from base to tip growth, and a change in the shape of catalyst particles. This will depend on the catalyst metal and how it interacts with its support. Another effect of increasing temperature is an increase in the quality and crystallinity of CNTs.

2.3.9 Super growth and the effect of steam

A number of studies have investigated the effect of adding steam to the reaction atmosphere to try and improve the yield of CNTs obtained. Hata et al reported the benefits of the addition of water vapour into the CVD reactor when using ethylene and iron deposited onto various substrates [135]. The addition of steam led to the production of very long, pure and compact CNTs, as the steam reacted with any amorphous carbons impurities that act to deactivate the catalyst. The relative amounts of ethylene and water vapour was found to be of great importance to increase the catalyst lifetime. The best results yielded CNTs on the mm scale within 10 minutes of growth, and were thought to have grown by the base growth mechanism.

Ago et al also investigated the effect of adding water in varying concentrations into the CVD reactor [138]. An Fe/Mo/MgO catalyst was used

with a methane feedstock with water concentrations varying from 0 to 16000 ppm. As the water concentration increased, the conversion of methane and carbon yield increased up to concentrations of 13700 ppm of water at which point decreases were seen. SEM and TEM also confirmed the presence of more CNTs. Like Hata et al [135], the increase in CNT yield was attributed to the reaction of the steam with amorphous carbons. When the water concentration was raised to 15900 ppm the amount of carbon deposited decreased significantly, and it is thought that an excess of water deactivated the catalyst, hence demonstrating the importance of the amount of water injected to CNT growth.

Li et al found that the lifetime of the catalyst used was increased when water was added to the reaction of ethylene over the iron, alumina, silicon catalysts [175]. However, it was seen that the growth rate of the CNTs was unaffected for temperatures of 750 °C and that the longer CNTs achieved were solely as a result of prolonged activation of the catalyst. When the temperature of reaction was increased to 780 °C however the rate of CNT growth was increased compared to when no steam was used. In support of Hata et al's study [135] it was also found that there were less amorphous carbons observed when steam was utilised and that the CNTs grew by the base growth mechanism.

In addition to increasing the catalyst lifetime by reacting with amorphous carbons, Amama et al suggest that the addition of water also increases the catalyst lifetime by suppressing Ostwald ripening [139]. Ostwald ripening is a process where larger catalyst particles grow in size whilst smaller particles disappear by atomic diffusion leading to a smaller amount of catalyst particles, and particles with a larger diameter. The study annealed iron catalysts with and without water to see the effect on the amount and diameters of the resulting nanoparticles. The results showed that the addition of water yielded a larger amount of catalyst particles and that the average diameter of the particles was smaller. It is suggested that the water prevents ripening since the oxygen and hydroxyl groups suppress the diffusion of metal particles and help to stabilise the smaller catalyst particles. The results of the study concluded that the addition of water did lead to a longer catalyst lifetime, with growth continuing even after 6 hours.

Yun et al likewise investigated the production of CNTs via CVD using steam to increase the yield [181]. Ethylene was used as the feedstock with use of an iron catalyst supported on an alumina, silica, silicon substrate. The

addition of steam into the system led to longer CNTs being produced and increased the lifetime of the catalyst.

The effect of water on the growth of CNTs has been seen to lead to longer CNTs as a result of longer catalyst activation times and growth rates. It is suggested that this is due to water's reaction with amorphous carbons which deactivate the catalyst, however the amount of water used is crucial as too much water can suppress CNT growth by deactivating the catalyst. It is also thought that the addition of water increases catalyst reaction times by preventing Ostwald ripening.

2.3.10 **Simultaneous production of hydrogen and carbon nanotubes**

Research has also concentrated on the simultaneous production of carbon nanotubes and hydrogen from methane sources. This takes advantage of the fact that when methane deposits onto the catalyst to form CNTs, hydrogen is given off at the same time. Logically as the amount of methane deposited increases and hence the amount of CNTs, the amount of hydrogen should also increase meaning that large CNT yields will be synonymous with large hydrogen yields. A study undertaken by Gallego et al found this to be true with results showing that higher yields of hydrogen also lead to a higher yield of carbon nanotubes [116]. A Ni/La₂O₃ catalyst was used in a horizontal reactor, with the highest CNT and hydrogen yields both obtained at a reaction temperature of 700 °C. MWCNTs were obtained with diameters up to 40 nm. A reaction time of 4 hours achieved the highest rate of production of both CNTs and hydrogen, with a reaction time of 22 hours producing a larger overall yield, but a slower rate of production as the catalysts became deactivated by carbon deposition.

The relationship between production of hydrogen and CNTs was also observed by Takenaka et al [169]. Methane was decomposed into CNTs and hydrogen with the use of a nickel catalyst. The largest catalytic life and hence hydrogen production was obtained at 40 wt% nickel, which likewise saw the largest yield of CNTs. A similar pattern was observed when varying the temperature, with the highest yield of both hydrogen and CNTs achieved at 773 K, with an increase in temperature leading to a reduction in both products.

Zein and Mohamed also found similar results when investigating the decomposition of methane [182]. NiO/MnO/TiO₂ catalysts were prepared by

impregnation, sol-gel and polyvinyl methods. It was observed that a larger amount of CNTs compared to other carbon types was obtained on the impregnated catalyst, whereas the other catalysts produced more encapsulating carbons. As a result the impregnated catalyst gave the highest conversions of methane into hydrogen, as the sol-gel and vinyl catalysts became deactivated by encapsulating carbons. This shows that catalysts that favour the production of CNTs over other carbon types are also more suitable for hydrogen production, as CNTs do not deactivate the catalyst to as large an extent.

Ermakova et al likewise investigated the simultaneous production of hydrogen and carbon nanotubes from the decomposition of methane [142, 167]. Various nickel and iron catalysts were used, and large conversions of methane into hydrogen and CNTs were obtained, with the catalyst metal, support, and calcination temperature and reaction temperature all affecting the yields obtained.

Overall, the simultaneous production of CNTs and hydrogen has been demonstrated in a number of studies. Their production is related; with the highest yields of hydrogen also corresponding to the highest yield of CNTs. Production of CNTs is favourable for hydrogen production as they deactivate the catalyst less than other carbon types such as encapsulating or amorphous carbons.

2.3.11 Carbon Nanotube Production from Plastics

2.3.11.1 Production techniques

Whilst CVD is widely used to produce CNTs from pure gas streams, CNTs have also been produced from plastic sources. The potential to produce CNTs from the pyrolysis of plastics was demonstrated by Kukovitsky et al [15]. Generating CNTs from waste plastics holds the benefit of simultaneously dealing with waste management problems, and also providing a cheap and abundant feedstock for CNT production. Kukovitsky et al used granular polyethylene (PE) which was pyrolysed with a nickel catalyst at temperatures of 420-450°C. Whilst CNTs were produced, the yield was small with the majority of the deposits being carbon fibres. Later work by the same research group obtained a larger CNT yield at the higher temperature of 800°C [183]. Further studies have produced CNTs from the pyrolysis of plastics, either by a one pot autoclave process [131], or in a fluidised bed [110] or fixed bed [184] reactor.

A variation on CVD is the floating catalyst technique, which introduces the catalyst metal unsupported, most often by sublimation of a solid metal source such as ferrocene [185]. This technique can also be used to produce CNTs from plastics using ferrocene as a catalyst. For example, Kong and Zhang used a ferrocene catalyst to produce CNTs from the pyrolysis of PE and maleated PP [112]. The plastics and ferrocene catalyst were placed in an autoclave and heated up to 700 °C over 100 minutes and left for a hold time of 12 hours. Straight and helical MWCNTs were produced with diameters between 20 nm and 60 nm. It was suggested that the ferrocene decomposed when the temperature was increased and led to the production iron nanoparticles which acted as a catalyst for CNT growth.

CNTs can also be produced when hydrocarbons are combusted, with CNTs arising in the carbon deposits in their soot [186]. Likewise plastics also yield CNTs when they are combusted. For example, Tang et al used catalytic combustion using organically modified clay and a nickel supported catalyst to produce MWCNTs from polypropylene [113]. The catalysts and plastics were mixed together with maleated PP and then heated with flame of gas lamp at 600 °C. The combustion led to the production of small carbon containing molecules such as CO and CH₄ which were then shielded from combustion by the clay layers, and led to the production of CNTs on the Ni catalyst particles. Jiang et al similarly used catalytic combustion to produce MWCNTs from polypropylene [111]. The polypropylene was similarly mixed with nickel catalysts and clay, in this case organically modified montmorillonite, and were combusted together to form carbon deposits.

2.3.11.2 **Production from pyrolysis of plastics**

2.3.11.2.1 Use of different plastics

Following the production of CNTs from plastics by Kukovitsky et al, numerous studies have since been undertaken using different plastics for CNT production. Early work by Kukovitsky et al on the use of polyethylene as a precursor for CNTs used a pyrolysis process and nickel catalysts [15, 127, 187]. A quartz reactor was used with temperatures of 420-450 °C [15], and 700-800 °C [15, 127, 187] used. The lower temperature study however yielded mainly nanofibres with some CNTs of diameters mainly between 10-40 nm. At the higher temperature more CNTs were yielded with various diameters and yields depending on the temperature and catalyst used. Other studies within the same research group likewise used PE as a feedstock and

nickel plate as a catalyst and used temperatures between 500 °C and 800 °C [183, 188]. As was the case with Kukovitsky et al's studies MWCNTs were successfully obtained.

Maksimova et al [189, 190] also utilised polyethylene as a precursor for CNT growth but instead of pyrolysing solid PE over a catalyst, the catalyst was instead distributed throughout the plastic. This was done by forming a solution of the plastic by mixing with xylene, before adding iron hydroxide, as the catalyst precursor. The mixture was then evaporated leaving a plastic film with iron catalyst particles distributed throughout it. The films were then heated in nitrogen within a quartz reactor up to 750 °C to produce CNTs with an average diameter of 20 nm.

Yen et al investigated the use of a fluidised bed reactor to produce CNTs from PE via pyrolysis [118]. PE was placed in with an Fe/MgO catalyst and a Ni shot bed which was fluidised with the flow of a mixture of Ar and H₂. The gas entered through the bottom of the reactor. The reactor was heated with two furnaces, one where the catalyst bed and sample were placed at a temperature of 750 °C, and another above it at a temperature of 850 °C. MWCNTs were successfully obtained with diameters between 25 and 50 nm.

In the study detailed earlier as an example of a floating catalyst, Kong et al also made use of PE as a source for the production of CNTs via pyrolysis [112]. An autoclave was used with ferrocene as a catalyst and maleated PP as a compatibilizer to help disperse the iron throughout the sample. The autoclave was heated up to a temperature of 700 °C over 100 minutes with a hold time of 12 hours. MWCNTs were obtained with diameters between 20 nm and 60nm. These studies demonstrate how a number of studies have used PE as a feedstock for the production of CNTs.

PP is another plastic which has been used as a feedstock for the production of CNTs. Gong et al produced CNTs from a polypropylene source via pyrolysis [121]. Using nickel catalysts along with activated carbon, pyrolysis of PP was undertaken at temperatures between 720 °C and 920 °C, and it was found that the addition of activated carbon led to increased production of CNTs. It was suggested that the activated carbon helped cracking of the PP, and also helped the formation of aromatic compounds which were more easily converted into CNTs.

Zhang et al used an autoclave heated to 700 °C for 12 hours, with PP and nickel powder used in place of PE and ferrocene, [165]. In this instance the

main yield was straight MWCNTs with diameters of up to 160 nm. Maleated PP was again suggested to play a role in helping the dispersion of the catalyst, whilst in the absence of the nickel catalyst carbon spheres were formed in the place of CNTs, suggesting that the use of the catalyst is key to the production of CNTs.

Yang et al likewise used a floating catalyst technique with a plastic feedstock to produce CNTs [117]. As described earlier, the floating catalyst technique used makes use of a ferrocene catalyst which is sublimed creating catalyst particles within the stream of pyrolysis gases. The plastic used as the feedstock in this instance was PP, which was pyrolysed at 450 °C, and passed into a CVD zone at a temperature of 800 °C with a total reaction time of 30 minutes used. The CNTs formed on a quartz substrate, and were the MWCNT type. They were well aligned and depending on various factors had mean diameters of between 22 and 36 nm. By modulating various factors including the feed rate of the catalyst precursor, the temperature and growth time, different lengths and diameters of CNTs were obtained. Increasing the CVD temperature led to changes in the CNT diameter, with larger diameter CNTs observed. This is also thought to be as a result of catalyst formation, with higher temperatures increasing collision frequency and sintering, leading to larger catalyst particles, and hence CNTs.

Arena et al used both virgin and recycled PP in a steel fluidised bed reactor with a bed of either alumina or quartz sand and pyrolysis temperatures between 450 °C and 850 °C [110]. The CNTs obtained were multi-walled and were comparable to those available commercially. The steel walls of the reactor must have acted as the catalyst as traces of iron were found within the CNTs obtained. These studies show how a number of techniques can be used to successfully prepare CNTs from PP, and that this is a suitable feedstock for CNT production.

As well as using virgin plastics, waste plastics have also been recently used as the feedstock for the production of CNTs. Pol and Thiyagarajan [131] used an autoclave with a nitrogen atmosphere to convert used HDPE bags into CNTs. Cobalt acetate was used as the catalyst and temperatures of 700 °C employed. Bundles of MWCNTs were obtained with diameters of around 80 nm, proving that plastic waste samples can be used to generate CNTs.

Mishra et al also produced CNTs from a waste PP in a single stage pyrolysis reactor [184]. Shredded waste PP and a nickel catalyst were placed in a reactor and heated in an inert atmosphere up to 600-800 °C with a 1 hour dwell time. MWCNTs were obtained with diameters between 10 and 25 nm,

with the temperature used influencing the quality of the CNTs obtained. In accordance with Lee et al [177], an increase in reaction temperature led to an increase in the G/D ratio obtained by Raman spectroscopy of the CNTs, indicating higher quality CNTs.

Zhang et al used an autoclave to produce CNTs from PP, using ferrocene and NaN_3 as catalysts [191]. Temperatures between 500 and 700 °C were used. MWCNTs were observed on the iron metal particles and referred to as Fe/carbon nanocomposites. These studies show how waste plastics can be used to produce CNTs. This is important as waste plastics make up a significant proportion of municipal solid waste and are often difficult to recycle. Demonstrating CNT production from waste plastics opens up the possibility of diverting plastics from landfill in favour of pyrolysis to produce CNTs.

Whilst PP and PE have proved suitable feedstocks for CNT production, studies have also investigated comparing different plastic feedstocks. Chung et al investigated the use of both polypropylene (PP) and polystyrene (PS) as CNT precursors [192]. CNTs were produced from each of the plastics, however the morphology of the CNTs varied depending on the feedstock due to the aromatic and olefinic nature of the precursors. The plastics were dissolved in xylene or toluene and mixed with iron nanoparticles before being coated onto a silicon wafer substrate. Pyrolysis temperatures varied between 500 and 900 °C. 500 °C proved too low a temperature for CNT formation, whilst at 900 °C CNT production was limited as metal particles became too large. 700 °C proved a suitable temperature for production of CNTs, demonstrating that as is the case with CVD, CNT production from plastics is affected by temperature. PP yielded MWCNTs with diameters in the range 16.5-40 nm, whereas PS gave smaller diameter CNTs but with thicker walls. It was suggested that this was because the aromatic precursors that form from PS pyrolysis are more susceptible to the production of thicker walls by secondary pyrolytic deposition. It is also suggested that higher temperatures may be required to produce CNTs from aromatic plastics such as PS than is required for PP and PE. This suggests that the plastic feedstock used will have an effect on the CNTs produced.

Arena and Mastellone also compared the production of MWCNTs from PP and PET feedstocks using fluidised bed pyrolysis [193]. Using a temperature of 600 °C and quartz sand as a bed MWCNTs were obtained from both plastics. No catalyst was used, and so it is likely the iron in the steel walls of the reactor acted as a catalyst, as was the case with Arena et al's other work

[110]. The work demonstrated that PET can be used to produce CNTs via pyrolysis.

Yang et al investigated the use of PP for the production of CNTs via a floating catalyst pyrolysis process as detailed earlier [117]. Other plastics such as PE and PVC were also used as feedstocks. CNTs from PE were similar to those from PP, however whilst PVC still produced CNTs, the graphite walls were more disordered and contained more defects. The defects obtained were attributed to the presence of Cl within the PVC sample, as the Cl can bond with the carbon and affect the dissolution of carbon into the metal. This suggests the presence of other elements in plastic samples could interfere with CNT production. Nevertheless, CNTs were produced from the PVC sample, showing that it is a suitable feedstock.

Overall, it has been seen that a number of different plastics can be used to produce CNTs, with all the major plastics found in municipal solid waste, namely PS, PE, PP, PET and PVC, all producing MWCNTs via pyrolysis. Waste plastics were also successfully utilised as a feedstock, opening the possibility of pyrolysis for CNT production being a genuine alternative to current landfilling practices.

2.3.11.2.2 Two stage process

As well as using one step processes, two step processes have recently been used to produce CNTs from plastic feedstocks. A two stage reactor was used by Liu et al, with the first stage being used to create pyrolysis gases and the second stage used to deposit these gases onto a catalyst to form CNTs [178]. The first stage used a screw kiln reactor and a zeolite catalyst to produce pyrolysis gases from PP, whilst the second stage used a moving bed reactor and a NiO catalyst prepared by a sol-gel method. Liquid fractions from pyrolysis were separated out by a condenser leaving just the gases to pass through to the second deposition stage. The temperatures of pyrolysis, in the screw kiln, and deposition, in the moving bed reactor, were varied to investigate the effect on CNT growth. When the decomposition temperature was varied between 500 and 800 °C, the quality of the CNTs increased as shown by TGA and TEM analyses. The inner diameter of the CNTs is also shown to increase, suggesting larger catalyst particles; however the outer diameter actually showed a smaller range. As the pyrolysis temperature was varied, different proportions of gases were obtained as the precursor for CNT growth. It was found that the amount of

CNTs varied, with a larger amount produced at 650 and 700 °C when amounts of larger hydrocarbons had decreased. The largest yield of CNTs was obtained at a pyrolysis temperature of 650 °C and a decomposition temperature of 700 °C with a value of 37.6 g/ 100 g PP obtained. The process also produced large yields of hydrogen gas simultaneously with CNTs. The largest amount of hydrogen in the gas stream was obtained at the same process conditions where the largest CNT yield was achieved, with hydrogen making up 77.0 vol% of the gas stream.

Arnaiz et al simulated a two stage process by running pyrolysis experiments for CNT production using a gas stream which was representative of the pyrolysis of PE [115]. Pyrolysis of the gas stream with an iron catalyst was undertaken at temperatures between 600 °C and 800 °C, and MWCNTs with a diameter of around 20nm were successfully produced. As is the case with CVD, the temperature had an effect on the production of CNTs, with the highest yield obtained at 650 °C, but the highest quality CNTs, as determined by TEM and Raman spectroscopy, produced at 750 °C. The lower yield at 750 °C was attributed to sintering of the iron particles in the catalyst.

Other studies have also used a two stage reactor to produce CNTs. and investigated the effect of introducing steam into the reactor [194, 195]. Using nickel catalysts, a pyrolysis temperature of 500 °C and a catalyst temperature of 800 °C, feedstocks including PP, HDPE, PVC mixed with HDPE and a waste plastic were successfully used to generate CNTs. MWCNTs were obtained for all the samples, however electron microscopy and TPO analyses showed that there were less produced from the PVC, and it was again suggested that the presence of Cl in the feedstock inhibited CNT production by poisoning the catalyst. As was the case with Liu et al's study, large yields of hydrogen were also produced, with hydrogen production increasing with steam injection into the reactor. As a result of the steam injection, gasification of the carbon deposits occurred, however amorphous carbons were more readily destroyed resulting in the proportion of filamentous carbons relative to amorphous carbons increasing. Introducing steam did lead to a reduction in the yield of CNTs however, with Raman spectroscopy showing steam caused extra defects in the CNT structure.

Overall, it has been found that the production of CNTs from plastics is possible, with a large amount of studies using PP and PE with either pyrolysis or autoclaving processes. The CNTs obtained are MWCNTs rather

than SWCNTs. Other plastics have also yielded CNTs such as PVC and PS. Recycled and used plastics also produced CNTs. Two stage processes have also been undertaken and can be used to simultaneously produce large yields of CNTs and hydrogen gas.

References

1. Kruse, T.M., H.-W. Wong, and L.J. Broadbelt, *Mechanistic Modeling of Polymer Pyrolysis: Polypropylene*. *Macromolecules*, 2003. **36**: p. 9594-9607.
2. Faravelli, T., et al., *Thermal degradation of polystyrene*. *Journal of Analytical and Applied Pyrolysis*, 2001. **60**: p. 103-121.
3. He, M., et al., *Syngas production from catalytic gasification of waste polyethylene: Influence of temperature on gas yield and composition*. *International Journal of Hydrogen Energy*, 2009. **34**(3): p. 1342-1348.
4. Bridgwater, A.V., *Review of fast pyrolysis of biomass and product upgrading*. *Biomass and Bioenergy*, 2012. **38**: p. 68-94.
5. *EU renewable ethanol production and consumption for fuel*. 2014 01/04/2015]; Available from: <http://www.epure.org/resources/statistics>.
6. Hall, W.J. and P.T. Williams, *Analysis of products from the pyrolysis of plastics recovered from the commercial scale recycling of waste electrical and electronic equipment*. *Journal of Analytical and Applied Pyrolysis*, 2007. **79**(1-2): p. 375-386.
7. Lopez, A., et al., *Pyrolysis of municipal plastic wastes II: Influence of raw material composition under catalytic conditions*. *Waste Manag*, 2011. **31**(9-10): p. 1973-83.
8. Siddiqui, M.N. and H.H. Redhwi, *Pyrolysis of mixed plastics for the recovery of useful products*. *Fuel Processing Technology*, 2009. **90**(4): p. 545-552.
9. Demirbas, A., *Pyrolysis of municipal plastic wastes for recovery of gasoline-range hydrocarbons*. *Journal of Analytical and Applied Pyrolysis*, 2004. **72**(1): p. 97-102.
10. Sharma, B.K., et al., *Production, characterization and fuel properties of alternative diesel fuel from pyrolysis of waste plastic grocery bags*. *Fuel Processing Technology*, 2014. **122**: p. 79-90.
11. Devaraj, J., Y. Robinson, and P. Ganapathi, *Experimental investigation of performance, emission and combustion characteristics of waste plastic pyrolysis oil blended with diethyl ether used as fuel for diesel engine*. *Energy*, 2015.
12. Mani, M., C. Subash, and G. Nagarajan, *Performance, emission and combustion characteristics of a DI diesel engine using waste plastic oil*. *Applied Thermal Engineering*, 2009. **29**(13): p. 2738-2744.
13. Achilias, D.S., et al., *Chemical Recycling of Polystyrene by Pyrolysis: Potential Use of the Liquid Product for the Reproduction of Polymer*. *Macromolecular Materials and Engineering*, 2007. **292**(8): p. 923-934.

14. Esfandiari, A., T. Kaghazchi, and M. Soleimani, *Preparation and evaluation of activated carbons obtained by physical activation of polyethyleneterephthalate (PET) wastes*. Journal of the Taiwan Institute of Chemical Engineers, 2012.
15. Kukovitskii, E.F., et al., *Carbon nanotubes of polyethylene*. Chemical Physics Letters, 1997. **266**: p. 323-328.
16. Kodera, Y. and Y. Ishihara, *Novel Process for Recycling Waste Plastics To Fuel Gas Using a Moving-Bed Reactor*. Energy & Fuels, 2006. **20**: p. 155-158.
17. Tsuji, T., et al., *Two-stage thermal gasification of polyethylene*. Nippon Kagaku Kaishi, 1999. **11**: p. 759-763
18. Tsuji, T., Y. Tanaka, and H. Itoh, *Two-stage thermal gasification of polyolefins*. Journal of Material Cycles and Waste Management, 2000(3): p. 2 - 7.
19. Wu, C. and P.T. Williams, *Hydrogen production by steam gasification of polypropylene with various nickel catalysts*. Applied Catalysis B: Environmental, 2009. **87**(3-4): p. 152-161.
20. Busby, R.L., *Hydrogen and Fuel Cells: A Comprehensive Guide*. 1st American Edition ed2005: PennWell.
21. Sehested, J., *Four challenges for nickel steam-reforming catalysts*. Catalysis Today, 2006. **111**(1-2): p. 103-110.
22. El-Rub, Z.A., E.A. Bramer, and G. Brem, *Review of Catalysts for Tar Elimination in Biomass Gasification Processes*. Industrial and Engineering Chemistry Research, 2004. **43**: p. 6911-6919.
23. Dayton, D., *A Review of the Literature on Catalytic Biomass Tar Destruction*, in *Milestone report2002*, National Renewable Energy Laboratory
24. Li, T.S., et al., *Chlorine contaminants poisoning of solid oxide fuel cells*. Journal of Solid State Electrochemistry, 2010. **15**(6): p. 1077-1085.
25. Trembly, J.P., R.S. Gemmen, and D.J. Bayless, *The effect of coal syngas containing HCl on the performance of solid oxide fuel cells: Investigations into the effect of operational temperature and HCl concentration*. Journal of Power Sources, 2007. **169**(2): p. 347-354.
26. Chang, A.C.C., et al., *Biomass gasification for hydrogen production*. International Journal of Hydrogen Energy, 2011. **36**(21): p. 14252-14260.
27. Demirbas, M.F., *Hydrogen from Various Biomass Species via Pyrolysis and Steam Gasification Processes*. Energy Sources, Part A: Recovery, Utilization, and Environmental Effects, 2006. **28**(3): p. 245-252.
28. Fremaux, S., et al., *An experimental study on hydrogen-rich gas production via steam gasification of biomass in a research-scale fluidized bed*. Energy Conversion and Management, 2015. **91**: p. 427-432.
29. Huang, B.-S., et al., *Hydrogen production by biomass gasification in a fluidized-bed reactor promoted by an Fe/CaO catalyst*. International Journal of Hydrogen Energy, 2012. **37**(8): p. 6511-6518.
30. Luo, S., et al., *Hydrogen-rich gas from catalytic steam gasification of biomass in a fixed bed reactor: Influence of particle size on*

- gasification performance. *International Journal of Hydrogen Energy*, 2009. **34**(3): p. 1260-1264.
31. Lv, X., et al., *Experimental study on biomass steam gasification for hydrogen-rich gas in double-bed reactor*. *International Journal of Hydrogen Energy*, 2014. **39**(36): p. 20968-20978.
 32. Song, T., et al., *Experimental investigation on hydrogen production from biomass gasification in interconnected fluidized beds*. *Biomass and Bioenergy*, 2012. **36**: p. 258-267.
 33. Ahmed, I. and A.K. Gupta, *Syngas yield during pyrolysis and steam gasification of paper*. *Applied Energy*, 2009. **86**(9): p. 1813-1821.
 34. Ahmed, I.I. and A.K. Gupta, *Pyrolysis and gasification of food waste: Syngas characteristics and char gasification kinetics*. *Applied Energy*, 2010. **87**(1): p. 101-108.
 35. Dalai, A.K., et al., *Gasification of refuse derived fuel in a fixed bed reactor for syngas production*. *Waste Manag*, 2009. **29**(1): p. 252-8.
 36. He, M., et al., *Hydrogen-rich gas from catalytic steam gasification of municipal solid waste (MSW): Influence of catalyst and temperature on yield and product composition*. *International Journal of Hydrogen Energy*, 2009. **34**(1): p. 195-203.
 37. He, M., et al., *Syngas production from pyrolysis of municipal solid waste (MSW) with dolomite as downstream catalysts*. *Journal of Analytical and Applied Pyrolysis*, 2010. **87**(2): p. 181-187.
 38. Wang, J., et al., *Hydrogen-rich gas production by steam gasification of municipal solid waste (MSW) using NiO supported on modified dolomite*. *International Journal of Hydrogen Energy*, 2012. **37**(8): p. 6503-6510.
 39. Ahmed, I.I. and A.K. Gupta, *Hydrogen production from polystyrene pyrolysis and gasification: Characteristics and kinetics*. *International Journal of Hydrogen Energy*, 2009. **34**(15): p. 6253-6264.
 40. Erkiaga, A., et al., *Syngas from steam gasification of polyethylene in a conical spouted bed reactor*. *Fuel*, 2013. **109**: p. 461-469.
 41. Wu, C. and P.T. Williams, *Investigation of Ni-Al, Ni-Mg-Al and Ni-Cu-Al catalyst for hydrogen production from pyrolysis-gasification of polypropylene*. *Applied Catalysis B: Environmental*, 2009. **90**(1-2): p. 147-156.
 42. Czernik, S. and R.J. French, *Production of Hydrogen from Plastics by Pyrolysis and Catalytic Steam Reform*. *Energy & Fuels*, 2006. **20**: p. 754-758.
 43. Park, Y., et al., *Optimum operating conditions for a two-stage gasification process fueled by polypropylene by means of continuous reactor over ruthenium catalyst*. *Fuel Processing Technology*, 2010. **91**: p. 951-957.
 44. Wu, C. and P.T. Williams, *Pyrolysis-gasification of plastics, mixed plastics and real-world plastic waste with and without Ni-Mg-Al catalyst*. *Fuel*, 2010. **89**(10): p. 3022-3032.
 45. Tsuji, T., et al., *Steam Reforming of Oils Produced from Waste Plastics*. *Journal of Chemical Engineering of Japan*, 2005. **38**(10): p. 859-864.
 46. Namioka, T., et al., *Hydrogen-rich gas production from waste plastics by pyrolysis and low-temperature steam reforming over a ruthenium catalyst*. *Applied Energy*, 2011. **88**(6): p. 2019-2026.

47. Friengfung, P., et al., *NiO/Dolomite Catalyzed Steam/O₂ Gasification of Different Plastics and Their Mixtures*. Industrial & Engineering Chemistry Research, 2014. **53**(5): p. 1909-1915.
48. Wilk, V. and H. Hofbauer, *Conversion of mixed plastic wastes in a dual fluidized bed steam gasifier*. Fuel, 2013. **107**: p. 787-799.
49. Wu, C. and P.T. Williams, *Pyrolysis–gasification of post-consumer municipal solid plastic waste for hydrogen production*. International Journal of Hydrogen Energy, 2010. **35**(3): p. 949-957.
50. Kaewpengkrow, P., D. Atong, and V. Sricharoenchaikul, *Pyrolysis and gasification of landfilled plastic wastes with Ni-Mg-La/Al₂O₃ catalyst*. Environ Technol, 2012. **33**(22-24): p. 2489-95.
51. Arena, U. and F. Di Gregorio, *Energy generation by air gasification of two industrial plastic wastes in a pilot scale fluidized bed reactor*. Energy, 2014. **68**: p. 735-743.
52. Cho, M.-H., et al., *Two-stage air gasification of mixed plastic waste: Olivine as the bed material and effects of various additives and a nickel-plated distributor on the tar removal*. Energy, 2014. **70**: p. 128-134.
53. Cho, M.-H., T.-Y. Mun, and J.-S. Kim, *Air gasification of mixed plastic wastes using calcined dolomite and activated carbon in a two-stage gasifier to reduce tar*. Energy, 2013. **53**: p. 299-305.
54. Aupretre, F., C. Descorme, and D. Duprez, *Bio-ethanol catalytic steam reforming over supported metal catalysts*. Catalysis Communications, 2002. **3**: p. 263-267.
55. Hu, X. and G. Lu, *Comparative study of alumina-supported transition metal catalysts for hydrogen generation by steam reforming of acetic acid*. Applied Catalysis B: Environmental, 2010. **99**(1-2): p. 289-297.
56. Tomishige, K., et al., *Catalyst performance in reforming of tar derived from biomass over noble metal catalysts*. Green Chemistry, 2003. **5**(4): p. 399.
57. Yung, M.M., W.S. Jablonski, and K.A. Magrini-Bair, *Review of Catalytic Conditioning of Biomass-Derived Syngas*. Energy & Fuels, 2009. **23**: p. 1874–1887.
58. Bengaard, H., *Steam Reforming and Graphite Formation on Ni Catalysts*. Journal of Catalysis, 2002. **209**(2): p. 365-384.
59. Abild-Pedersen, F., et al., *Methane activation on Ni(111): Effects of poisons and step defects*. Surface Science, 2005. **590**(2-3): p. 127-137.
60. Rostrup-Nielsen, J.R., *Steam Reforming Catalysts 1975*, Copenhagen: Danish Technical Press.
61. Chen, Y., et al., *Sulfur poisoning mechanism of steam reforming catalysts: an X-ray absorption near edge structure (XANES) spectroscopic study*. Phys Chem Chem Phys, 2010. **12**(21): p. 5707-11.
62. Sato, K. and K. Fujimoto, *Development of new nickel based catalyst for tar reforming with superior resistance to sulfur poisoning and coking in biomass gasification*. Catalysis Communications, 2007. **8**(11): p. 1697-1701.
63. Srinakruang, J., et al., *A highly efficient catalyst for tar gasification with steam*. Catalysis Communications, 2005. **6**(6): p. 437-440.

64. Trimm, D.L., *Catalysts for the control of coking during steam reforming*. Catalysis Today, 1999. **49**: p. 3-10.
65. Wu, C. and P.T. Williams, *Investigation of coke formation on Ni-Mg-Al catalyst for hydrogen production from the catalytic steam pyrolysis-gasification of polypropylene*. Applied Catalysis B: Environmental, 2010. **96**(1-2): p. 198-207.
66. Bai, X., et al., *The sintering of Ni/Al₂O₃ methanation catalyst for substitute natural gas production*. Reaction Kinetics, Mechanisms and Catalysis, 2014. **112**(2): p. 437-451.
67. DeLaRiva, A.T., et al., *In situ Transmission Electron Microscopy of catalyst sintering*. Journal of Catalysis, 2013. **308**: p. 291-305.
68. Miyazawa, T., et al., *Catalytic performance of supported Ni catalysts in partial oxidation and steam reforming of tar derived from the pyrolysis of wood biomass*. Catalysis Today, 2006. **115**(1-4): p. 254-262.
69. Inaba, M., et al., *Hydrogen Production by Gasification of Cellulose over Ni Catalysts Supported on Zeolites*. Energy and Fuels, 2006. **20**: p. 432 - 438.
70. Dong, W.-S., et al., *Methane reforming over Ni/Ce-ZrO₂ catalysts: effect of nickel content*. Applied Catalysis A: General, 2002. **226**: p. 63 - 72.
71. Bimbela, F., et al., *Catalytic steam reforming of model compounds of biomass pyrolysis liquids in fixed bed: Acetol and n-butanol*. Journal of Analytical and Applied Pyrolysis, 2009. **85**(1-2): p. 204-213.
72. Chen, I., S.-Y. Lin, and D.-W. Shiue, *Calcination of Nickel/Alumina Catalysts*. Industrial and Engineering Chemistry Research, 1988. **27**: p. 926-929.
73. Clause, O., et al., *Preparation and thermal reactivity of nickel/chromium and nickel/aluminium hydrotalcite-type precursors*. Applied Catalysis 1991. **73**: p. 217-236.
74. Garcia, L., et al., *Influence of Calcination and Reduction Conditions on the Catalyst Performance in the Pyrolysis Process of Biomass*. Energy & Fuels, 1998. **12**: p. 139-143.
75. Furusawa, T., et al., *Hydrogen production from the gasification of lignin with nickel catalysts in supercritical water*. International Journal of Hydrogen Energy, 2007. **32**: p. 699-704.
76. Volder, M.F.L.D., et al., *Carbon Nanotubes: Present and Future Commercial Applications*. Science, 2013. **339**: p. 535 - 539.
77. Iijima, S., *Helical Microtubules of Graphitic Carbon*. Letters to Nature, 1991. **354**: p. 56-58.
78. Han, J., *Structures and Properties of Carbon Nanotubes*, in *Carbon Nanotubes: Science and Applications*, M. Meyyappan, Editor 2005, CRC Press.
79. Lu, J. and J. Han, *Carbon Nanotubes and Nanotube-based Nano Devices*. International journal of High Speed Electronics and Systems, 1998. **9**(1): p. 101-123.
80. Baughman, R.H., A.A. Zakhidov, and W.A. de Heer, *Carbon nanotubes--the route toward applications*. Science, 2002. **297**(5582): p. 787-92.
81. Dai, H., *Carbon nanotubes: opportunities and challenges*. Surface Science, 2002. **500**: p. 218-241.

82. Moravsky, A.P., E.M. Wexler, and R.O. Loutfy, *Growth of Carbon Nanotubes by Arc Discharge and Laser Ablation*, in *Carbon Nanotubes: Science and Applications*, M. Meyyappan, Editor 2005, CRC Press.
83. Joselevich, E., et al., *Carbon Nanotube Synthesis and Organization*, in *Carbon Nanotubes: Advanced Topics in the Synthesis, Structure, Properties and Applications*, A. Jorio, M. Dresselhaus, and G. Dresselhaus, Editors. 2008, Springer.
84. Meyyappan, M., *Growth: CVD and PECVD*, in *Carbon Nanotubes: Science and Applications*, M. Meyyappan, Editor 2005, CRC Press.
85. Kong, J., A.M. Cassell, and H. Dai, *Chemical vapor deposition of methane for single-walled carbon nanotubes*. *Chemical Physics Letters*, 1998. **292**: p. 567-574.
86. Wei, Y.Y., et al., *Effect of catalyst film thickness on carbon nanotube growth by selective area chemical vapor deposition*. *Applied Physics Letters*, 2001. **78**(10): p. 1394.
87. Dai, H., et al., *Single-wall nanotubes produced by metal-catalyzed disproportionation of carbon monoxide*. *Chemical Physics Letters*, 1996. **260**: p. 471-475.
88. Das, N., et al., *The effect of feedstock and process conditions on the synthesis of high purity CNTs from aromatic hydrocarbons*. *Carbon*, 2006. **44**(11): p. 2236-2245.
89. Chai, S.-P., S.H.S. Zein, and A.R. Mohamed, *Synthesizing carbon nanotubes and carbon nanofibers over supported-nickel oxide catalysts via catalytic decomposition of methane*. *Diamond and Related Materials*, 2007. **16**(8): p. 1656-1664.
90. Jung, M.J., et al., *Effect of NH₃ environmental gas on the growth of aligned carbon nanotube in catalytically pyrolyzing C₂H₂*. *Thin Solid Films*, 2001. **398**: p. 150-155.
91. Park, T.-J., et al., *Purification strategies and purity visualization techniques for single-walled carbon nanotubes*. *Journal of Materials Chemistry*, 2006. **16**(2): p. 141.
92. Ebbesen, T.W., et al., *Purification of nanotubes*. *Nature*, 1994. **367**: p. 519-519.
93. Xu, Y.-Q., et al., *Controlled Multistep Purification of Single-Walled Carbon Nanotubes*. *Nano Letters*, 2004. **5**(1): p. 163-168.
94. Moon, J.-M., K.H. An, and Y.H. Lee, *High-Yield Purification Process of Singlewalled Carbon Nanotubes*. *Journal of Physical Chemistry B*, 2001. **105**: p. 5677-5681.
95. Yang, C.-M., et al., *Effect of Purification on Pore Structure of HiPco Single-Walled Carbon Nanotube Aggregates*. *Nano Letters*, 2002. **2**(4): p. 385-388.
96. Endo, M., M.S. Strano, and P.M. Ajayan, *Potential Applications of Carbon Nanotubes*, in *Carbon nanotubes: Advanced Topics in the Synthesis, Structure, Properties and Applications*, A. Jorio, M. Dresselhaus, and G. Dresselhaus, Editors. 2008, Springer
97. Allaouia, A., et al., *Mechanical and electrical properties of a MWNT/epoxy composite*. *Composites Science and Technology*, 2002. **62**: p. 1993-1998.

98. Montazeri, A., et al., *Mechanical properties of multi-walled carbon nanotube/epoxy composites*. *Materials & Design*, 2010. **31**(9): p. 4202-4208.
99. Coleman, J.N., et al., *High-Performance Nanotube-Reinforced Plastics: Understanding the Mechanism of Strength Increase*. *Advanced Functional Materials*, 2004. **14**(8): p. 791-798.
100. Li, W., et al., *Carbon nanotubes as support for cathode catalyst of a direct methanol fuel cell*. *Carbon*, 2002. **40**: p. 787-803.
101. Sotowa, C., et al., *The reinforcing effect of combined carbon nanotubes and acetylene blacks on the positive electrode of lithium-ion batteries*. *ChemSusChem*, 2008. **1**(11): p. 911-5.
102. Sae-Khow, O. and S. Mitra, *Carbon Nanotube Immobilized Composite Hollow Fiber Membranes for Pervaporative Removal of Volatile Organics from Water*. *Journal of Physical Chemistry C*, 2010. **114**: p. 16351-16356.
103. Sears, K., et al., *Recent Developments in Carbon Nanotube Membranes for Water Purification and Gas Separation*. *Materials*, 2010. **3**(1): p. 127-149.
104. Dumée, L., et al., *Enhanced durability and hydrophobicity of carbon nanotube bucky paper membranes in membrane distillation*. *Journal of Membrane Science*, 2011. **376**(1-2): p. 241-246.
105. Dumée, L., et al., *Fabrication of thin film composite poly(amide)-carbon-nanotube supported membranes for enhanced performance in osmotically driven desalination systems*. *Journal of Membrane Science*, 2013. **427**: p. 422-430.
106. Dumée, L., et al., *Carbon nanotube based composite membranes for water desalination by membrane distillation*. *Desalination and Water Treatment*, 2012. **17**(1-3): p. 72-79.
107. Dumée, L.F., et al., *Characterization and evaluation of carbon nanotube Bucky-Paper membranes for direct contact membrane distillation*. *Journal of Membrane Science*, 2010. **351**(1-2): p. 36-43.
108. Gao, G. and C.D. Vecitis, *Electrochemical carbon nanotube filter oxidative performance as a function of surface chemistry*. *Environ Sci Technol*, 2011. **45**(22): p. 9726-34.
109. Rahaman, M.S., C.D. Vecitis, and M. Elimelech, *Electrochemical carbon-nanotube filter performance toward virus removal and inactivation in the presence of natural organic matter*. *Environ Sci Technol*, 2012. **46**(3): p. 1556-64.
110. Arena, U., et al., *An innovative process for mass production of multi-wall carbon nanotubes by means of low-cost pyrolysis of polyolefins*. *Polymer Degradation and Stability*, 2006. **91**(4): p. 763-768.
111. Jiang, Z.W., et al., *Polypropylene as a carbon source for the synthesis of multi-walled carbon nanotubes via catalytic combustion*. *Carbon*, 2007. **45**(2): p. 449-458.
112. Kong, Q.H. and J.H. Zhang, *Synthesis of straight and helical carbon nanotubes from catalytic pyrolysis of polyethylene*. *Polymer Degradation and Stability*, 2007. **92**(11): p. 2005-2010.
113. Tang, T., et al., *Synthesis of multiwalled carbon nanotubes by catalytic combustion of polypropylene*. *Angew Chem Int Ed Engl*, 2005. **44**(10): p. 1517-20.

114. Zhuo, C., et al., *Synthesis of carbon nanotubes by sequential pyrolysis and combustion of polyethylene*. Carbon, 2010. **48**(14): p. 4024-4034.
115. Arnaiz, N., et al., *Production of Carbon Nanotubes from Polyethylene Pyrolysis Gas and Effect of Temperature*. Industrial & Engineering Chemistry Research, 2013. **52**(42): p. 14847-14854.
116. Gallego, G.S., et al., *Production of hydrogen and MWCNTs by methane decomposition over catalysts originated from LaNiO(3) perovskite*. Catalysis Today, 2010. **149**(3-4): p. 365-371.
117. Yang, Z., et al., *Coupled process of plastics pyrolysis and chemical vapor deposition for controllable synthesis of vertically aligned carbon nanotube arrays*. Applied Physics A, 2010. **100**(2): p. 533-540.
118. Yen, Y.W., M.D. Huang, and F.J. Lin, *Synthesize carbon nanotubes by a novel method using chemical vapor deposition-fluidized bed reactor from solid-stated polymers*. Diamond and Related Materials, 2008. **17**(4-5): p. 567-570.
119. Wang, P., et al., *Filamentous carbon prepared by the catalytic pyrolysis of CH₄ on Ni/SiO₂*. Applied Catalysis A: General, 2002. **231**: p. 34-44.
120. Rostrup-Nielsen, J.R., *Coking on nickel catalysts for steam reforming of hydrocarbons*. Journal of Catalysis, 1974. **33**(2): p. 184-201.
121. Gong, J., et al., *Catalytic carbonization of polypropylene by the combined catalysis of activated carbon with Ni₂O₃ into carbon nanotubes and its mechanism*. Applied Catalysis A: General, 2012. **449**: p. 112-120.
122. Baker, R.T.K., *Catalytic Growth of Carbon Filaments*. Carbon, 1989. **27**(3): p. 315-323.
123. Baker, R.T.K., et al., *Nucleation and growth of carbon deposits from the nickel catalyzed decomposition of acetylene*. Journal of Catalysis, 1972. **26**(1): p. 52-62.
124. Baker, R.T.K., et al., *Formation of filamentous carbon from iron, cobalt and chromium catalyzed decomposition of acetylene*. Journal of Catalysis, 1973. **30**(1): p. 86-95.
125. Wagner, R.S. and W.C. Ellis, *Vapor-Liquid-Solid Mechanism of Single Crystal Growth*. Applied Physics Letters, 1964. **4**(5): p. 89.
126. Tessonier, J.P. and D.S. Su, *Recent progress on the growth mechanism of carbon nanotubes: a review*. ChemSusChem, 2011. **4**(7): p. 824-47.
127. Kukovitsky, E.F., et al., *Correlation between metal catalyst particle size and carbon nanotube growth*. Chemical Physics Letters, 2002. **355**(5-6): p. 497-503.
128. Snoeck, J.W., G.F. Froment, and M. Fowles, *Filamentous Carbon Formation and Gasification: Thermodynamics, Driving Force, Nucleation, and Steady-State Growth*. Journal of Catalysis, 1997. **169**: p. 240-249.
129. Nessim, G.D., *Properties, synthesis, and growth mechanisms of carbon nanotubes with special focus on thermal chemical vapor deposition*. Nanoscale, 2010. **2**(8): p. 1306-23.
130. Helveg, S., et al., *Atomic-scale imaging of carbon nanofibre growth*. Nature, 2004. **427**: p. 426-429.

131. Pol, V.G. and P. Thiyagarajan, *Remediating plastic waste into carbon nanotubes*. Journal of Environmental Monitoring, 2010. **12**(2): p. 455-459.
132. Hofmann, S., et al., *Surface Diffusion: The Low Activation Energy Path for Nanotube Growth*. Physical Review Letters, 2005. **95**(3).
133. Ducati, C., et al., *Temperature selective growth of carbon nanotubes by chemical vapor deposition*. Journal of Applied Physics, 2002. **92**(6): p. 3299.
134. Poretzky, A.A., et al., *In situ measurements and modeling of carbon nanotube array growth kinetics during chemical vapour deposition*. Applied Physics A: Materials Science & Processing, 2005. **81**: p. 223-240.
135. Hata, K., et al., *Water-assisted highly efficient synthesis of impurity-free single-walled carbon nanotubes*. Science, 2004. **306**(5700): p. 1362-4.
136. Ermakova, M., et al., *Decomposition of Methane over Iron Catalysts at the Range of Moderate Temperatures: The Influence of Structure of the Catalytic Systems and the Reaction Conditions on the Yield of Carbon and Morphology of Carbon Filaments*. Journal of Catalysis, 2001. **201**(2): p. 183-197.
137. Moisala, A., A.G. Nasibulin, and E.I. Kauppinen, *The role of metal nanoparticles in the catalytic production of single-walled carbon nanotubes—a review*. Journal of Physics: Condensed matter, 2003. **15**: p. S3011-S3035.
138. Ago, H., et al., *Gas analysis of the CVD process for high yield growth of carbon nanotubes over metal-supported catalysts*. Carbon, 2006. **44**(14): p. 2912-2918.
139. Amama, P.B., et al., *Role of Water in Super Growth of Single-Walled Carbon Nanotube Carpets*. Nano Letters, 2009. **9**(1): p. 44-49.
140. Bronikowski, M., *CVD growth of carbon nanotube bundle arrays*. Carbon, 2006. **44**(13): p. 2822-2832.
141. El-Hendawy, A.-N.A., R.J. Andrews, and A.J. Alexander, *Impact of Mo and Ce on growth of single-walled carbon nanotubes by chemical vapour deposition using MgO-supported Fe catalysts*. Applied Surface Science, 2009. **255**(16): p. 7446-7450.
142. Ermakova, M.A. and D.Y. Ermakov, *Ni/SiO₂ and Fe/SiO₂ catalysts for production of hydrogen and filamentous carbon via methane decomposition*. Catalysis Today, 2002. **77**: p. 225-235.
143. Govindaraj, A., et al., *An investigation of carbon nanotubes obtained from the decomposition of methane over reduced Mg_{1-x}M_xAl₂O₄ spinel catalysts*. Journal of Materials Research, 1999. **14**(6): p. 2567-2576.
144. Liu, W.-W., et al., *Synthesis of Single-Walled Carbon Nanotubes: Effects of Active Metals, Catalyst Supports, and Metal Loading Percentage*. Journal of Nanomaterials, 2013. **2013**: p. 1-8.
145. Sohn, J.I., et al., *Growth behavior of carbon nanotubes on Fe-deposited (001) Si substrates*. Applied Physics Letters, 2001. **78**(20): p. 3130.
146. Takenaka, S., *Formation of filamentous carbons over supported Fe catalysts through methane decomposition*. Journal of Catalysis, 2004. **222**(2): p. 520-531.

147. Tan, S.-M., et al., *Effects of FeOx, CoOx, and NiO catalysts and calcination temperatures on the synthesis of single-walled carbon nanotubes through chemical vapor deposition of methane*. Journal of Alloys and Compounds, 2009. **477**(1-2): p. 785-788.
148. Chai, S.-P., S.H. Sharif Zein, and A.R. Mohamed, *The effect of catalyst calcination temperature on the diameter of carbon nanotubes synthesized by the decomposition of methane*. Carbon, 2007. **45**(7): p. 1535-1541.
149. Chen, P., et al., *Growth of carbon nanotubes by catalytic decomposition of CH₄, or CO on a Ni-MgO catalyst*. Carbon, 1997. **35**: p. 1495-1501.
150. Choi, G.S., et al., *Carbon nanotubes synthesized by Ni-assisted atmospheric pressure thermal chemical vapor deposition*. Journal of Applied Physics, 2002. **91**(6): p. 3847.
151. Choi, Y.C., et al., *Growth mechanism of vertically aligned carbon nanotubes on silicon substrates*. Synthetic Metals, 2001. **117**: p. 81-86.
152. Hsieh, C.-T., et al., *Synthesis of carbon nanotubes over Ni- and Co-supported CaCO₃ catalysts using catalytic chemical vapor deposition*. Materials Chemistry and Physics, 2009. **114**(2-3): p. 702-708.
153. Juang, Z., *On the kinetics of carbon nanotube growth by thermal CVD method*. Diamond and Related Materials, 2004. **13**(11-12): p. 2140-2146.
154. Kovalenko, G.A., et al., *Synthesis of catalytic filamentous carbon by the pyrolysis of alkanes on alumina-silica foam supporting nickel nanoparticles*. Carbon, 2009. **47**(2): p. 428-435.
155. Tian, F., et al., *Catalyst effects of fabrication of carbon nanotubes synthesized by chemical vapor deposition*. Materials Chemistry and Physics, 2009. **115**(2-3): p. 493-495.
156. Chai, S.-P., et al., *The Examination of NiO and CoOx Catalysts Supported on Al₂O₃ and SiO₂ for Carbon Nanotubes Production by Catalytic Chemical Vapor Deposition of Methane*. Carbon Science and Technology, 2008. **1**: p. 24-29.
157. Lee, C.J., J.H. Park, and J. Park, *Synthesis of bamboo-shaped multiwalled carbon nanotubes using thermal chemical vapor deposition*. Chemical Physics Letters, 2000. **323**(5-6): p. 560-565.
158. Yeoh, W.-M., et al., *Synthesis of high purity multi-walled carbon nanotubes over Co-Mo/MgO catalyst by the catalytic chemical vapor deposition of methane*. New Carbon Materials, 2009. **24**(2): p. 119-123.
159. Lin, Y.-C. and J.-H. Lin, *Purity-controllable growth of bamboo-like multi-walled carbon nanotubes over copper-based catalysts*. Catalysis Communications, 2013. **34**: p. 41-44.
160. Nasibulin, A.G., et al., *Carbon nanotubes and onions from carbon monoxide using Ni(acac)₂ and Cu(acac)₂ as catalyst precursors*. Carbon, 2003. **41**(14): p. 2711-2724.
161. Avdeeva, L.B., et al., *Coprecipitated Ni-alumina and Ni-Cu-alumina catalysts of methane decomposition and carbon deposition. II. Evolution of the catalysts in reaction*. Applied Catalysis A: General, 1996. **141**: p. 117-129.

162. Takenaka, S., et al., *Decomposition of methane over supported-Ni catalysts: effects of the supports on the catalytic lifetime*. Applied Catalysis A: General, 2001. **217**: p. 101-110.
163. Li, Y., et al., *Mass production of high-quality multi-walled carbon nanotube bundles on a Ni/Mo/MgO catalyst*. Carbon, 2005. **43**(2): p. 295-301.
164. Yang, W., et al., *Cerium Oxide Promoted Ni/MgO Catalyst for the Synthesis of Multi-walled Carbon Nanotubes*. Chinese Journal of Catalysis, 2011. **32**(6-8): p. 1323-1328.
165. Zhang, Q., et al., *Radial growth of vertically aligned carbon nanotube arrays from ethylene on ceramic spheres*. Carbon, 2008. **46**(8): p. 1152-1158.
166. Ermakova, M.A., et al., *New Nickel Catalysts for the Formation of Filamentous Carbon in the Reaction of Methane Decomposition*. Journal of Catalysis, 1999. **187**: p. 77-84.
167. Ermakova, M.A., D.Y. Ermakov, and G.G. Kuvshinov, *Effective catalysts for direct cracking of methane to produce hydrogen and filamentous carbon: Part I. Nickel catalysts*. Applied Catalysis A: General 2000. **201**: p. 61-70.
168. Takenaka, S., *Structural Change of Ni Species in Ni/SiO₂ Catalyst during Decomposition of Methane*. Journal of Catalysis, 2002. **208**(1): p. 54-63.
169. Takenaka, S., *Ni/SiO₂ catalyst effective for methane decomposition into hydrogen and carbon nanofiber*. Journal of Catalysis, 2003.
170. Wu, T.-Y. and S.-S. Tzeng, *Effect of nitrogen in the reaction atmosphere on the microstructure of carbon nanofibers grown by thermal chemical vapor deposition*. Journal of Materials Research, 2011. **24**(09): p. 2997-3002.
171. Cheung, C.L., et al., *Diameter-Controlled Synthesis of Carbon Nanotubes*. Journal of Physical Chemistry B, 2002. **106**: p. 2429-2433.
172. Jourdain, V. and C. Bichara, *Current understanding of the growth of carbon nanotubes in catalytic chemical vapour deposition*. Carbon, 2013. **58**: p. 2-39.
173. Nasibulin, A., et al., *Correlation between catalyst particle and single-walled carbon nanotube diameters*. Carbon, 2005. **43**(11): p. 2251-2257.
174. Lee, C.J., et al., *Diameter-controlled growth of carbon nanotubes using thermal chemical vapor deposition*. Chemical Physics Letters, 2001. **341**: p. 245-249.
175. Li, Q.W., et al., *Sustained Growth of Ultralong Carbon Nanotube Arrays for Fiber Spinning*. Advanced Materials, 2006. **18**(23): p. 3160-3163.
176. Zhao, N., et al., *Fabrication and growth mechanism of carbon nanotubes by catalytic chemical vapor deposition*. Materials Letters, 2006. **60**(2): p. 159-163.
177. Lee, C.J., et al., *Temperature effect on the growth of carbon nanotubes using thermal chemical vapor deposition*. Chemical Physics Letters, 2001. **343**: p. 33-38.

178. Liu, J., et al., *Catalytic pyrolysis of polypropylene to synthesize carbon nanotubes and hydrogen through a two-stage process*. Polymer Degradation and Stability, 2011. **96**(10): p. 1711-1719.
179. Sengupta, J., et al., *Effect of growth temperature on the CVD grown Fe filled multi-walled carbon nanotubes using a modified photoresist*. Materials Research Bulletin, 2010. **45**(9): p. 1189-1193.
180. Ohashi, F., et al., *The role of the gas species on the formation of carbon nanotubes during thermal chemical vapour deposition*. Nanotechnology, 2008. **19**(44): p. 445605.
181. Yun, Y.H., et al., *Growth Mechanism of Long Aligned Multiwall Carbon Nanotube Arrays by Water-Assisted Chemical Vapor Deposition*. Journal of Physical Chemistry B, 2006. **110**: p. 23920-23925.
182. Hussein, S.Z.S. and A.R. Mohamed, *Mn/Ni/TiO₂ Catalyst for the Production of Hydrogen and Carbon Nanotubes from Methane Decomposition*. Energy and Fuels, 2004. **18**: p. 1336-1345.
183. Chernozatonskii, L.A., et al., *Carbon crooked nanotube layers of polyethylene: Synthesis, structure and electron emission*. Carbon, 1998. **36**(5-6): p. 713-715.
184. Mishra, N., et al., *Pyrolysis of waste polypropylene for the synthesis of carbon nanotubes*. Journal of Analytical and Applied Pyrolysis, 2012. **94**: p. 91-98.
185. Mohlala, M.S. and N.J. Coville, *Floating catalyst CVD synthesis of carbon nanotubes from CpFe(CO)₂X (X=Me, I): Poisoning effects of I*. Journal of Organometallic Chemistry, 2007. **692**(14): p. 2965-2970.
186. Yuan, L., et al., *Nanotubes from methane flames*. Chemical Physics Letters, 2001. **340**: p. 237-241.
187. Kukovitsky, E.F., et al., *CVD growth of carbon nanotube films on nickel substrates*. Applied Surface Science, 2003. **215**(1-4): p. 201-208.
188. Kiselev, N.A., et al., *Carbon nanotubes from polyethylene precursors: Structure and structural changes caused by thermal and chemical treatment revealed by HREM*. Carbon, 1998. **36**(7-8): p. 1149-1157.
189. Maksimova, N.I., et al., *Preparation of nanoscale thin-walled carbon tubules from a polyethylene precursor*. Carbon, 1999. **37**: p. 1657-1661.
190. Maksimova, N.I., et al., *Catalytic synthesis of carbon nanostructures from polymer precursors*. Journal of Molecular Catalysis A: Chemical, 2000. **158**: p. 301-307.
191. Zhang, J., et al., *Sustainable processing of waste polypropylene to produce high yield valuable Fe/carbon nanotube nanocomposites*. CrystEngComm, 2014. **16**(37): p. 8832.
192. Chung, Y.-H. and S. Jou, *Carbon nanotubes from catalytic pyrolysis of polypropylene*. Materials Chemistry and Physics, 2005. **92**(1): p. 256-259.
193. Arena, U. and M.L. Mastellone, *Production of Multi-wall Carbon Nanotubes by Means of Fluidized Bed Pyrolysis of Virgin or Recycled Polymers*. Proceedings of ENS-European Nano System, Paris 2005, TIMA Editions, 2005: p. 7-12.

194. Wu, C., et al., *Processing real-world waste plastics by pyrolysis-reforming for hydrogen and high-value carbon nanotubes*. Environ Sci Technol, 2014. **48**(1): p. 819-26.
195. Wu, C., et al., *Sustainable processing of waste plastics to produce high yield hydrogen rich synthesis gas and high quality carbon nanotubes*. RSC Advances, 2012. **2**: p. 4045 - 4047.

3 Materials and methods

3.1 Materials

3.1.1 Plastics samples used

A Waste Electrical and Electronic equipment (WEEE) plastic waste sample was collected from a commercial WEEE recycling plant, with waste from computer monitors and television sets. The computer monitors and television sets are recycled by removing the plastic outer casing before separation of the glass screen from the electronic components. The glass and circuit boards are separated for recycling while the plastic fraction is ground into small flakes of approximately 10-20 mm in size and then sold for low level recycling applications, such as plastic fencing, pallets, garden furniture, and traffic cones. A representative 1 kg sample of the plastic was taken from a large 1 tonne mixed batch of the WEEE plastic. This was carefully sampled using a multiple grab procedure to ensure that it was a representative sample of the WEEE plastic waste. The WEEE plastic sample was investigated in chapter 4.

High impact polystyrene (HIPS) pellets of around 2mm were supplied by Atofina (UK) Ltd. Acrylonitrile butadiene styrene (ABS) pellets of around 2mm were supplied by Vamptech (Italy). Both the HIPS and ABS samples were investigated in chapter 4.

Polypropylene (PP) was obtained as 2 mm virgin polymer pellets provided by BP Chemicals UK. Low density polyethylene (about 2 mm) (LDPE) was obtained from ACROS Organics UK. Polystyrene (about 2 mm) (PS) was obtained from ACROS Organics UK. PP and PS were investigated in chapter 5, whilst the LDPE was investigated in chapters 5, 6 and 7.

Elemental analyses of the plastics samples was carried out using an elemental analyser (Carlo Erba Flash EA 1112) to achieve the precise determination of nitrogen, carbon, hydrogen, and sulphur. Table 3.1 below shows the results obtained from elemental analysis, and the maximum hydrogen yield that can be obtained from each plastic if all the hydrogen in the plastic is converted to hydrogen gas. Oxygen was calculated by difference for the LDPE, PP and PS samples, however as the WEEE plastic samples contained other elements such as bromine and chlorine, this was not undertaken for these samples. Instead, a proximate analysis was undertaken to determine the moisture, volatiles, fixed carbons and ash contents.

Table 3.1 Elemental composition and maximum H₂ yield from plastic samples used

Plastic	C (%)	H (%)	N (%)	S (%)	O (%)*	Maximum H ₂ yield (g/100g plastic)
LDPE	81.9	13.9	1.1	0.0	3.1	13.9
PP	82.7	13.9	1.2	0.0	2.2	13.9
PS	91.0	8.8	0.0	0.0	0.2	8.8

* Oxygen calculated by difference

Table 3.2 Elemental composition, maximum H₂ yield, and proximate analysis of WEEE plastic samples used

Plastic	Elemental analysis				Proximate analysis				Maximum H ₂ yield (g/100g plastic)
	C	H	N	S	Moisture	Volatiles	Fixed carbons	Ash	
	(wt %)	(wt %)	(wt %)	(wt%)	(wt %)	(wt %)	(wt %)	(wt %)	
WEEE	83.3	8.5	4.1	0.0	0.06	96.74	1.18	2.02	8.5
ABS	73.3	6.0	4.5	0.0	0.02	95.67	2.59	1.72	6.0
HIPS	78.8	6.6	1.2	0.0	0.04	95.16	2.22	2.58	6.6

3.1.2 Catalysts prepared

Nickel catalysts were prepared by an impregnation method using nickel nitrate ($\text{Ni}(\text{NO}_3)_2 \cdot 6\text{H}_2\text{O}$), deionised water and gamma Al_2O_3 as the raw materials. The desired amount of $\text{Ni}(\text{NO}_3)_2 \cdot 6\text{H}_2\text{O}$ was mixed in deionised water and heated at 80 °C until dissolved, at which point the Al_2O_3 was added. This mixture was then left to mix until a slurry was formed. This was then dried overnight in the oven at 105 °C to remove the remaining water before the precursor was calcined at 500 °C in an air atmosphere for 3 hours. Catalysts with a wt% of 5 and 10% were used in chapter 4, whilst catalysts with a wt% of 5% were used in chapter 5.

Catalysts using different metals were also prepared by impregnation. Nickel, iron, cobalt and copper nitrates and gamma Al_2O_3 were used as the raw materials. Metal nitrates were dissolved in ethanol, following which the alumina was added and the mixture left until it formed a slurry. This was then dried overnight in an oven at 50 °C to remove the remaining ethanol before calcination was undertaken. The catalysts were heated to either 500 or 750 °C at a heating rate of 2 °Cmin⁻¹ in an air atmosphere with a hold time of 3 hours. Iron, nickel, cobalt and copper catalysts with 5 and 10 wt% were used in chapter 6, whilst iron catalysts with 10 wt% were used in chapter 7.

3.2 Experimental reactors

Experiments were carried out using a two stage pyrolysis-gasification reactor as shown in figure 3.1. The two reactors were placed directly after one another and heated by electric furnaces. The temperature was measured with the use of thermocouples inside each of the two reactors. Samples were placed in the pyrolysis reactor where they were pyrolysed under the flow of nitrogen. Pyrolysis products were then passed to the second reactor where steam was injected via a syringe pump and passed over the catalyst bed causing gasification to occur. The procedure was to heat the catalytic reactor up to the desired temperature and then heat the pyrolysis reactor at a set heating rate. Liquid products were collected in a two stage condenser system, with the first being held at room temperature and the second cooled by dry ice. The non-condensed gases were then collected in a Tedlar gas sample bag. Gases were collected for 20 minutes after the experiment had finished allowing all gases to pass through the reactor and collect in the sample bag. The reactor was weighed before and after the experiment to determine the amount of solids produced in each experiment. These included waxes in the reactor and carbon deposition on the surface of the catalyst. The sample boat which held the plastic sample was also weighed before and after the experiment to determine the weight of any ash or char. Where steam was injected, the amount used was determined by weighing the syringe before and after each experiment. Mass balances were determined by summing the mass of gases collected, liquids obtained in the condensers and solids in the reactor and comparing this to the amount of sample and water used.

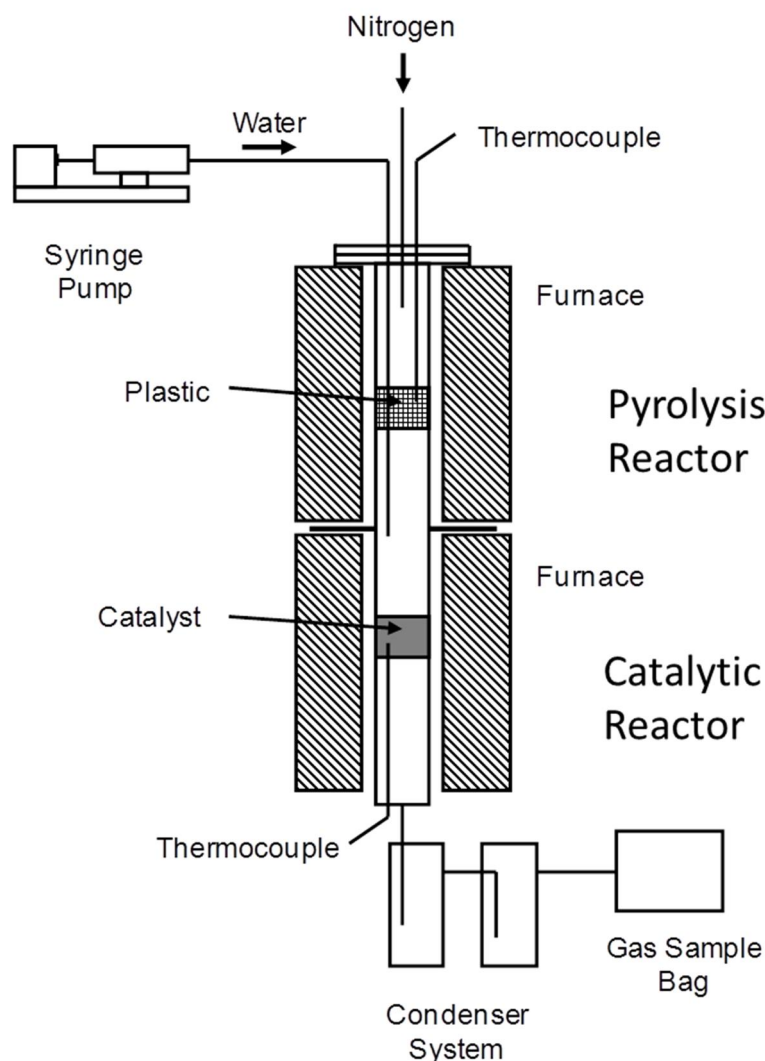


Figure 3.1 Schematic diagram of pyrolysis-gasification reactor

The process conditions used were temperatures of 700-900 °C for the catalyst reactor and a temperature of 600 °C for the pyrolysis reactor which was heated at a rate of 40 or 50 °Cmin⁻¹. For chapters 4 to 6 a catalyst reactor temperature of 800 °C was used, whilst for chapter 7, the effect of varying the temperature between 700 and 900 °C was investigated.

The injection rate of water used was between 0 and 4.74 g h⁻¹. For chapter 4 an injection rate of 4.74 g h⁻¹ was used, for chapter 5 the injection rate was varied between 0 and 4.74 g h⁻¹, using 0, 0.25, 1.90 and 4.74 g h⁻¹. These equate to weight hourly space velocities of 9.48, 3.8, 0.5 and 0 h⁻¹. For chapters 6 and 7 no steam was injected to the reactor.

1 g of the plastic sample was used in chapters 4, 5 and 6, whilst for chapter 7 the amount of plastic was varied between 0.5 and 1.25 g.

In each case 0.5 g of catalyst or sand was used.

For chapters 6 and 7 a new reactor was created in order to address mass balance issues and aid with cleaning and maintenance of the reactor, such as changing thermocouples. The reactor was changed to one continuous tube, with the connection and flange moved to the top where both thermocouples were placed. The width and dimensions of the reactor were kept the same, and the experimental procedure was unchanged, including using the same furnaces, condensers and gas bags.

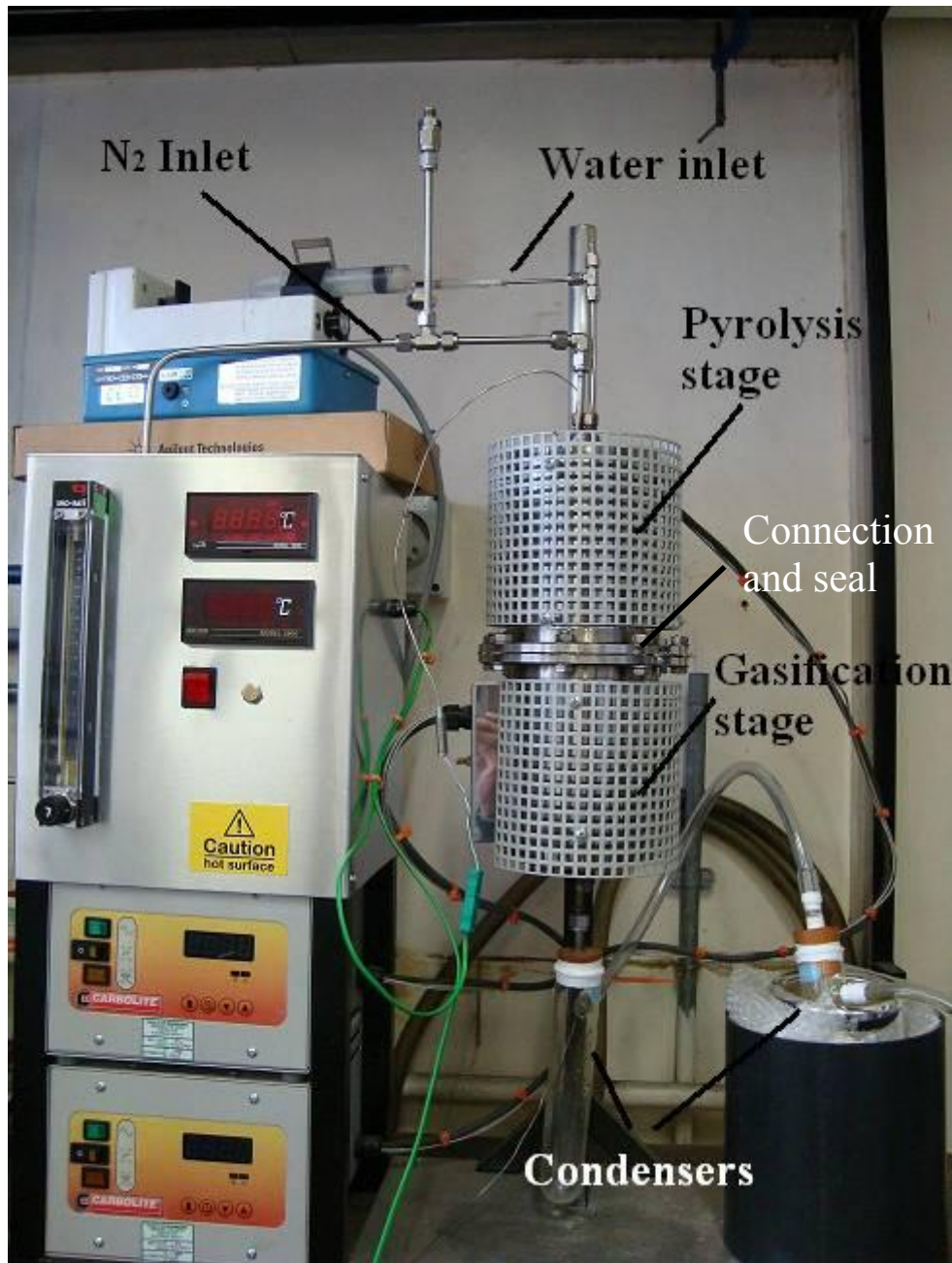


Figure 3.2 Original reactor setup used for chapters 4 and 5

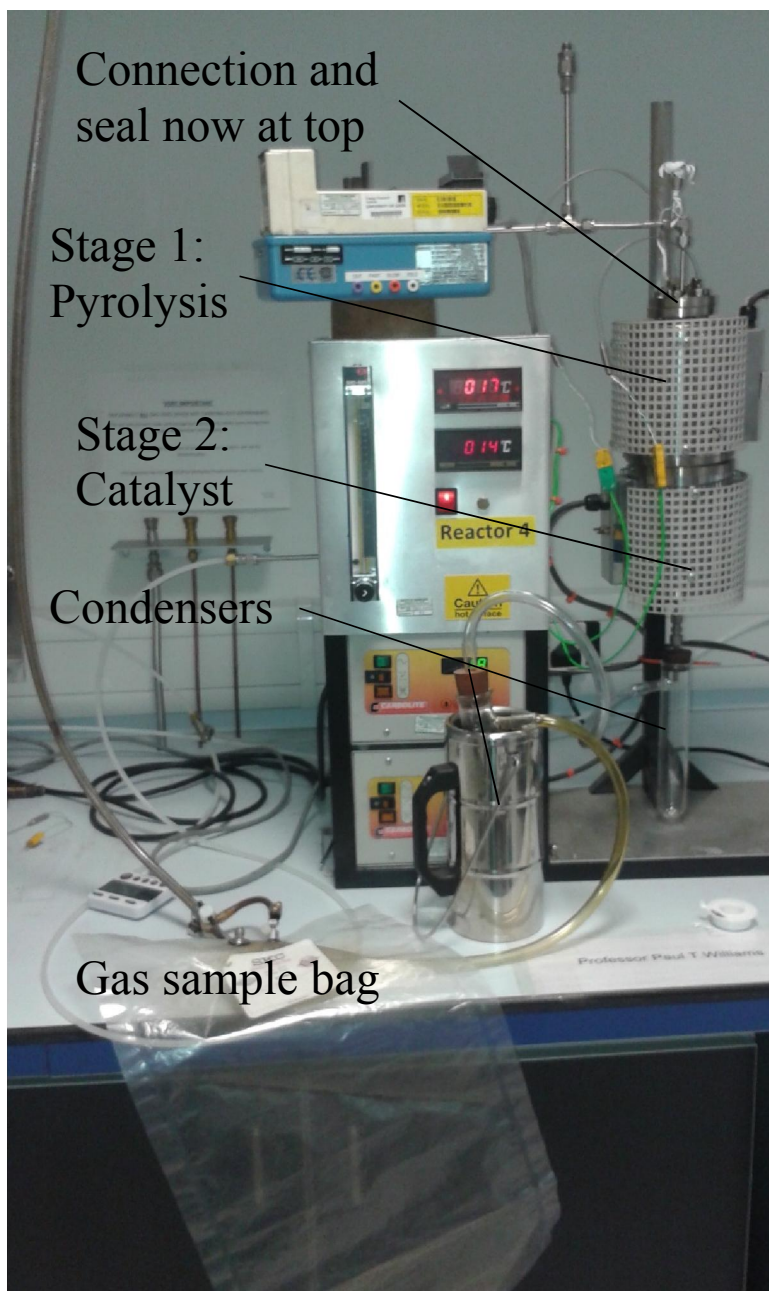


Figure 3.3 Modified reactor setup used for chapters 6 and 7

Research results were undertaken and repeated. Where the mass balance was lower than 85 wt %, experiments were repeated until a mass balance higher than this was achieved. This was to ensure that results were as accurate as possible, and errors and losses kept to a minimum. A notable exception to this was with the use of acrylonitrile butadiene styrene, where mass balances were lower due to losses from volatiles. Typical repetitions for each of the reactors are seen in tables 3.1 and 3.2, along with the mass balances obtained.

Table 3.3 Repetition of research results reactor 1

	WEEE	WEEE	Mean
	Run 1	Run 2	
Gas (wt%)	10.8	14.1	12.5
Oils (wt%)	76.0	77.0	76.5
Solids (wt%)	3.7	3.5	3.6
Mass balance (%)	90.5	94.6	
H ₂ (vol%)	36.0	39.5	37.8
CH ₄ (vol%)	29.1	25.0	27.1
CO (vol%)	6.2	7.3	6.75
CO ₂ (vol%)	4.5	5.8	5.2
C ₂ -C ₄ (vol%)	24.3	22.4	23.4

Table 3.4 Repetition of research results reactor 2

	LDPE	LDPE	Mean
	Run 1	Run 2	
Gas (wt%)	59.2	63.2	61.2
Oils (wt%)	24.0	25.0	24.5
Solids (wt%)	3.0	3.0	3.0
Mass balance (%)	86.2	91.2	
H ₂ (vol%)	16.5	16.4	16.5
CH ₄ (vol%)	26.6	27.0	26.8
CO (vol%)	0.0	0.0	0
CO ₂ (vol%)	0.0	0.0	0
C ₂ -C ₄ (vol%)	56.9	56.6	56.75

3.3 Analytical techniques

All analytical techniques were undertaken by the author, except where University policy and laboratory procedures required help or assistance from technicians because of health and safety.

3.3.1 Gas Analysis

3.3.1.1 C₁-C₄ hydrocarbons

The gases collected in the sample bag were analysed by gas chromatography (GC). The system used to analyse C₁-C₄ hydrocarbons was a Varian 3380 gas chromatograph with an 80-100 mesh HayeSep column, a flame ionisation detector and nitrogen used as the carrier gas.

3.3.1.2 Permanent gases

The permanent gases hydrogen, nitrogen, oxygen and carbon monoxide were analysed using a separate Varian 3380 GC/TCD, with a thermal conductivity detector with two packed columns. The first column was 2m long and 2mm diameter and was packed with a 60-80 mesh molecular sieve and was used to analyse the hydrogen, nitrogen, oxygen and carbon monoxide. Carbon dioxide however was analysed using another Varian 3380 with a 2m long and 2mm diameter column with HayeSep 60-80 (80-100) mesh molecular sieve. The carrier gas in both instances was argon.

3.3.1.3 Calculation of sample gas concentration

Gas standards for permanent gases, (nitrogen, carbon monoxide, carbon dioxide, hydrogen and oxygen) alkanes (methane, ethane, propane and butane) and alkenes (ethene, propene, butene and butadiene) were obtained from Scientific and Technical gases, and used for the calculation of the concentration of the gases collected in the gas sample bag. The standard gas for permanent gases contained 1Vol. % CO, 1Vol. % CO₂, 1Vol. % H₂, 1Vol. % O₂, and was balanced with 96 Vol. % N₂. The standard gas for alkanes contained 1Vol. % CH₄, 1Vol. % C₂H₆, 1Vol. % C₃H₈, and 1Vol. % C₄H₁₀. The standard gas for alkenes contained 1Vol. % C₂H₄, 1Vol. % C₃H₆, and 1Vol. % 1-3-C₄H₈. Both the alkane and alkene standard gases were balanced with nitrogen. 1ml of each of the standards was injected into

the relevant GC in order to obtain response peaks for each of the gases. Figures 3.4 – 3.7 show the chromatograms obtained.

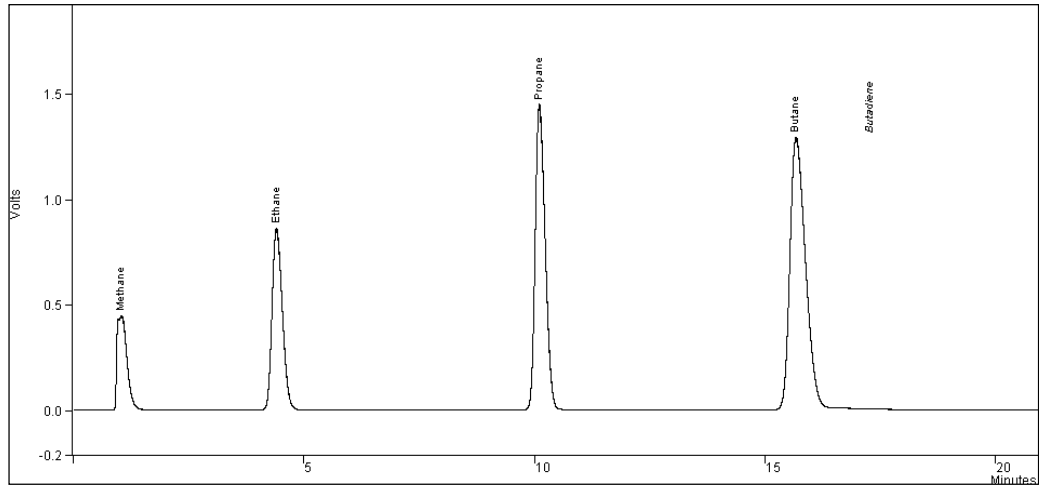


Figure 3.4 GC standard gas chromatogram alkanes

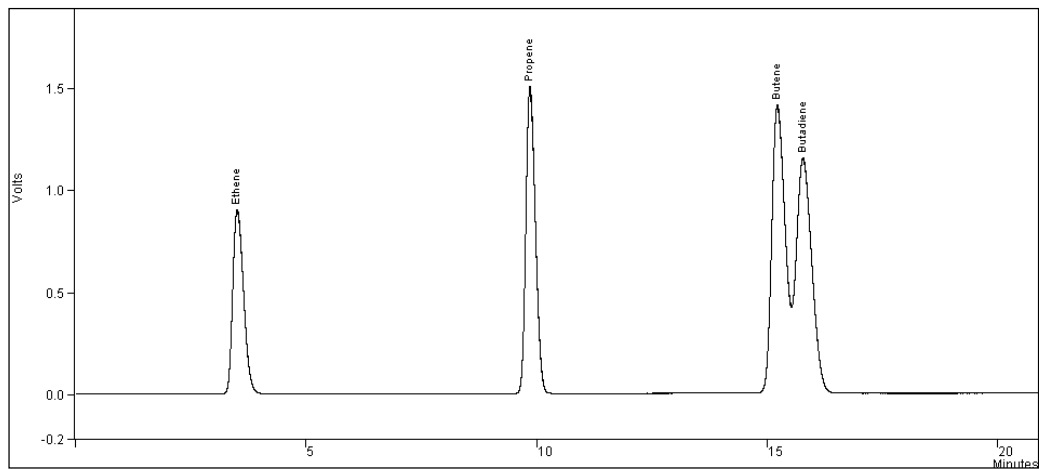


Figure 3.5 GC standard gas chromatogram alkenes

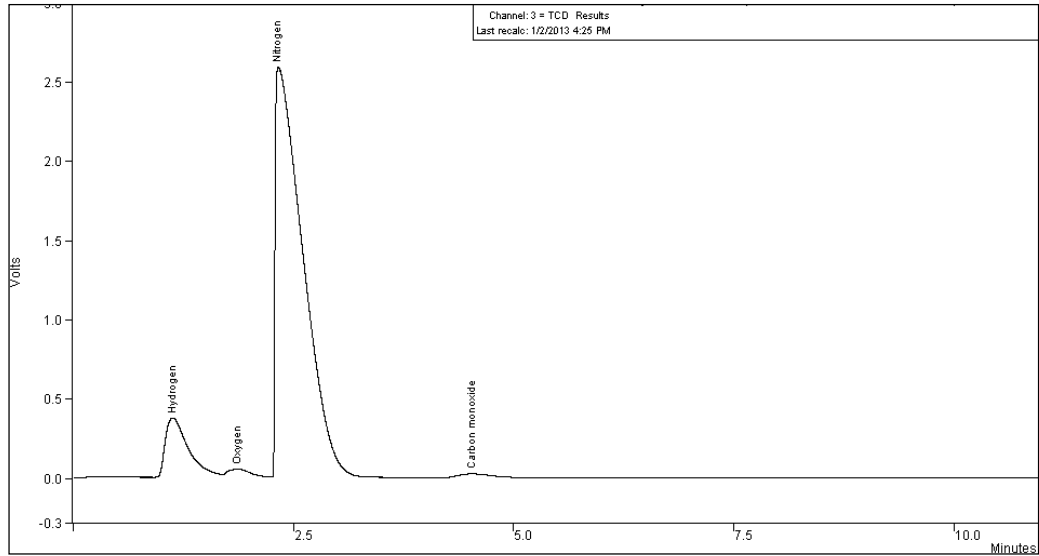


Figure 3.6 GC standard gas chromatogram permanent gases

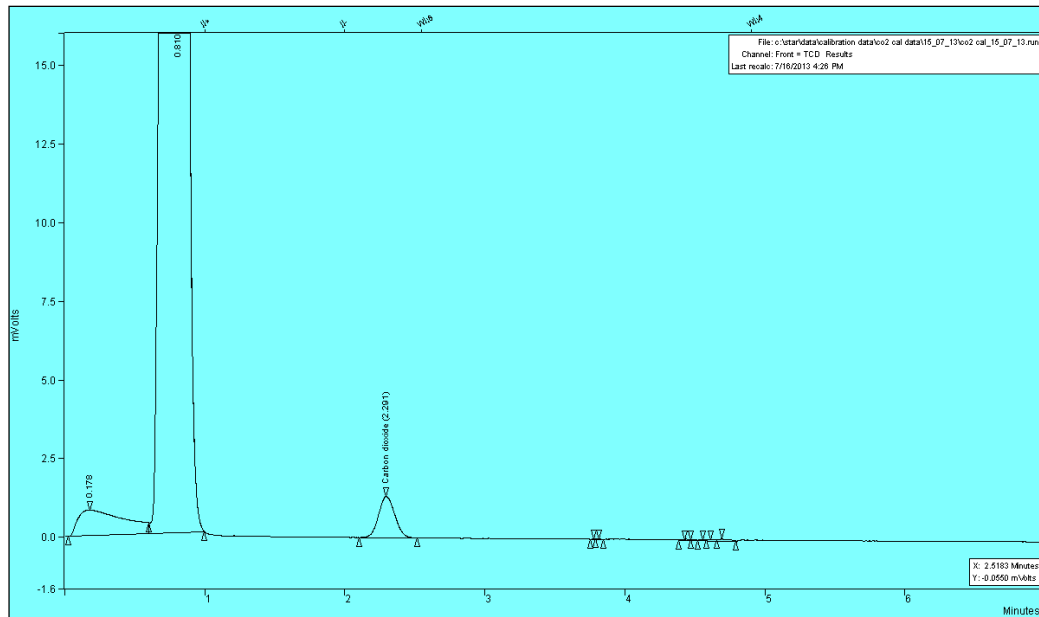


Figure 3.7 GC standard gas chromatogram carbon dioxide

The analytical software used for the GCs could then be used to obtain the peak areas for each of the gases from the standard. 1ml of the sample obtained from the gas sample bag was then injected into the GC and the corresponding peak area obtained. The concentration of each gas in the gas sample bag could then be calculated as follows:

$$C_{sample} = C_i \cdot A_{sample} / A_i \quad (3.1)$$

Where C_{sample} is the concentration of the sample gas, C_i is the concentration of the standard gas, A_{sample} is the peak area obtained from the GC for the sample gas, and A_i is the peak area obtained from the GC for the standard gas.

Corrections to the concentrations were made for the presence of oxygen, and to normalise the total concentrations up to 100 %. For each gas sample, the GC analysis was repeated to ensure reliability of the research results.

Using an Excel spreadsheet, the mass of the sample gas was then calculated based on the concentration of nitrogen present, by first calculating the total volume of the gas sample as follows:

$$V_{\text{total}} = Q_n \cdot t_c \cdot \frac{100}{C_n} \quad (3.2)$$

Where V_{total} is the total volume of the gas sample collected, Q_n is the flow rate of nitrogen used in the experiment, t_c is the collection time for the gas sample and C_n is the concentration of nitrogen in the gas in percent.

If we assume STP, 1 mol has a volume of 22.4 litres. The mass of each constituent gas 'x' can then be calculated as follows:

$$\text{Mass}_x = R_m \cdot \left(\frac{C_x}{100} \cdot V_{\text{total}} \right) / 22.4 \quad (3.3)$$

Where Mass_x is the mass of the compound 'x' produced, R_m is the molecular mass of the compound 'x', C_x is the concentration of gas 'x' in percent obtained from GC analysis and V_{total} is the total volume of the gas sample collected.

The total mass of the gases produced used for the mass balance can then simply be calculated by summing the masses for each constituent gas.

3.3.2 Gas Chromatography/Mass Spectrometry

Oils obtained during the pyrolysis-gasification of the plastic samples were analysed by gas chromatography/mass spectrometry (GC/MS). The GC/MS system used consisted of a Hewlett Packard 5280 gas chromatograph coupled to a HP 5271 ion trap detector. The gas chromatographic column was a Restek RTX-5MS column 30 m in length and had an internal diameter of 0.25 mm. It was fitted with fused silica 5% diphenyl and 95% dimethyl polysiloxane of 25 μm film thickness. The carrier gas used was helium.

3.3.3 Thermo gravimetric analysis

A thermo gravimetric analyser contains a microbalance coupled with a furnace which precisely controls the temperature.

3.3.3.1 Temperature Programmed Oxidation

Temperature programmed oxidation (TPO) is an analysis which is carried out on a thermo gravimetric analyser, using an air atmosphere. The instrument used for the analysis was a Shimadzu TGA 50. The reacted catalysts were analysed by temperature programmed oxidation to investigate the carbon deposits on their surfaces. Around 30 mg of the reacted catalyst was heated in a thermo gravimetric analyser in an atmosphere of air at a heating rate of 15 $^{\circ}\text{Cmin}^{-1}$ up to a temperature of 800 $^{\circ}\text{C}$, with a dwell time of 10 min. Due to the different reactivity of the types of carbon deposits, they are oxidised at different temperatures. By using a derivative plot, peaks are shown at the temperatures where the different types of carbon are oxidised. A typical TPO and derivative plot is shown in figure 3.8. Amorphous carbons are reported to show a peak at lower temperatures than filamentous carbons, due to being more reactive [1]. As such the low temperature peak is associated with the oxidation of amorphous carbons whilst the high temperature peak is associated with the oxidation of filamentous carbons such as carbon nanotubes. Weight loss that occurs below 100 $^{\circ}\text{C}$ is associated with the loss of moisture from the sample.

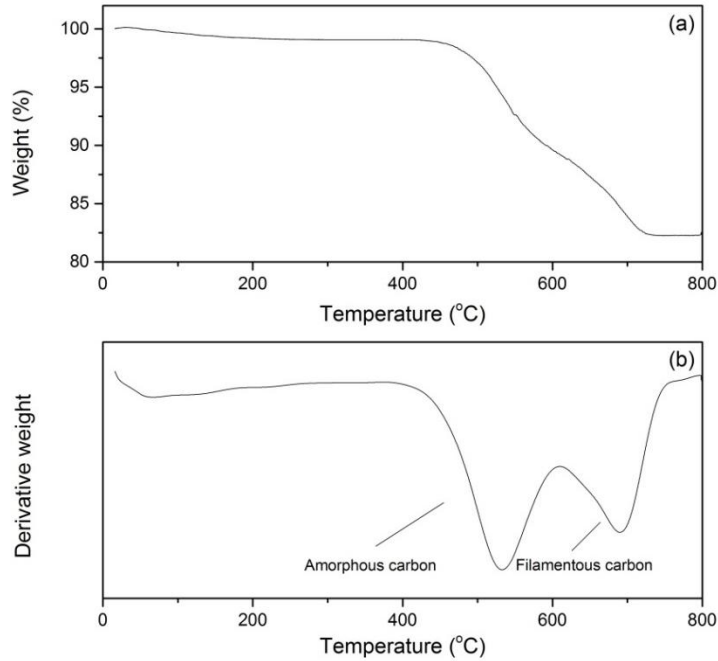


Figure 3.8 (a) Temperature programmed oxidation plot, (b) Derivative of temperature programmed oxidation

The amounts of each carbon type and the total carbon deposited were calculated from TPO analysis. This was done by first calculating the amount of each carbons oxidised during the TPO. For amorphous carbons the calculation would be as follows:

$$m_{amorphous} = m_{amorphous\ end} - m_{amorphous\ start} \quad (3.4)$$

Where $m_{amorphous}$ is the mass of amorphous carbons oxidised in TPO, $m_{amorphous\ end}$ is the mass from the TPO plot corresponding to the end of the amorphous peak and $m_{amorphous\ start}$ is the mass from the TPO plot corresponding to the start of the amorphous peak.

This was then scaled up from the small amount of catalyst used in TPO to the total amount of catalyst used in each experiment. To obtain the result in mg this means:

$$M_{amorphous} = m_{amorphous} \cdot (500/m_{cat\ end}) \quad (3.5)$$

Where $M_{\text{amorphous}}$ is the mass of amorphous carbons produced in the experiment, $m_{\text{amorphous}}$ is the mass of amorphous carbons oxidised in TPO and $m_{\text{cat end}}$ is the mass of catalyst left at the end of the TPO analysis.

The same procedure is conducted for filamentous carbons, and the total carbon deposition can be determined by the summation of the two. TPO analyses were repeated to ensure reliability of the results.

For TPO catalyst sampling was carefully carried out to ensure a representative sample was used.

3.3.3.2 Temperature Programmed Reduction

Temperature programmed reduction of the fresh catalysts was undertaken to help determine what metals and oxides were present in the catalyst. The analysis involves using a thermo gravimetric analyser with a reducing hydrogen atmosphere, where a derivative plot reveals peaks where the catalyst is reduced by hydrogen. The analyses were undertaken using a Stanton-Redcroft thermo gravimetric analyser. The samples were heated at $20\text{ }^{\circ}\text{C min}^{-1}$ up to $150\text{ }^{\circ}\text{C}$ to remove moisture, and then held for 30 min in a hydrogen atmosphere (5 % H_2 balanced with N_2). The samples were then heated in the hydrogen atmosphere at $10\text{ }^{\circ}\text{Cmin}^{-1}$ to $900\text{ }^{\circ}\text{C}$.

3.3.3.3 Proximate analysis

Proximate analyses are used to determine the moisture content, volatiles, fixed carbons and ash contents of samples, using thermo gravimetric analysis. The proximate analysis was completed using a Shimadzu TGA-50H thermo gravimetric analyser, using roughly 15 mg of each sample. Moisture content was determined by the weight loss associated with heating the sample in nitrogen up to $100\text{ }^{\circ}\text{C}$. The composition of volatiles then corresponded to the weight loss associated with an increase in temperature up to $925\text{ }^{\circ}\text{C}$, with fixed carbon then determined from the weight loss when the atmosphere was switched to air. Any remaining mass then determined the ash content of the plastic samples.

3.3.4 Scanning Electron Microscopy

High resolution scanning electron microscopy was undertaken to characterise the nature of the carbon that was deposited on the surface of the catalysts during the experimental procedure, and the raw unused catalysts. A scanning electron microscope allows high magnification images to be obtained by scanning the surface of a sample with a high energy beam of electrons. The microscopes used were a SEM, LEO 1530 (chapters 4-6) and a Hitachi SU8230 (chapters 6-7). Samples were imaged under vacuum at working distances between 2-6 mm, with an accelerating voltage between 2 and 5 KV. For the LEO the catalysts were attached to a specimen holder with carbon conductive adhesive tape, dusted with compressed air to remove loose particles and then coated with 5 nm of platinum. For the Hitachi microscope, coating was not required and so the samples were simply attached to the sample holder and dusted.

3.3.5 Transmission Electron Microscopy and TEM-EDX

Transmission electron microscopy (TEM) was used to further characterise the carbon deposits on the surface of the reacted catalysts. TEM is a microscopy analysis similar to SEM which can likewise be used to obtain high magnification images of a sample. In TEM the beam of electrons is transmitted through an ultra-thin specimen, where the transmitted electrons interact with the sample and form an image. TEM was undertaken to further characterise the nature of the carbon deposits to see if CNTs were produced, as unlike SEM, TEM allows individual walls of CNTs to be observed. The microscope used was a Phillips CM200, and the samples were prepared by dispersing them in acetone and then being deposited onto a Cu grid covered with a perforated carbon membrane. Energy Dispersive X-Ray analysis (EDX) was undertaken in conjunction with TEM. EDX detects X-rays that are produced when the electron beam interacts with the sample. Each element produces a characteristic X-ray spectrum, and so the elements present in a sample can be determined. Combined with TEM, the EDX can be targeted at specific points to determine what elements are present in particular parts of the sample. TEM-EDX was carried out using procedure described above, and inserting an Oxford Instruments INCA 350 EDX system to record EDX spectra at certain points. A typical EDX spectrum obtained during the experimental work is shown in figure 3.9. Peaks show the presence of nickel, oxygen and aluminium. Copper peaks are also present due to the copper grid used during TEM.

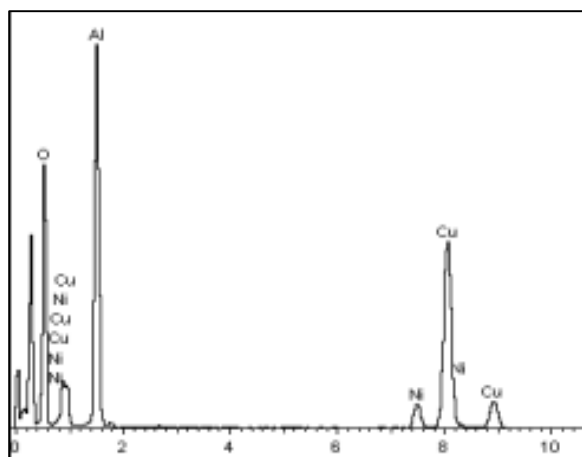


Figure 3.9 Typical EDX spectrum obtained from a catalyst

3.3.6 Raman Spectroscopy

Raman spectroscopy was undertaken on the carbon deposits on the catalyst surface to determine their graphitic quality. Raman spectroscopy is often used to characterise CNTs [2-6]. Peaks are observed at 1589 and 1348 cm^{-1} corresponding to the G peak associated with graphitic carbon within the sample, and the D peak associated with defects within the graphitic lattice respectively. A G' peak is also obtained at Raman shifts around 2709 cm^{-1} and is a further indication of CNT purity. The ratio between the size of the G peak and D peak is a useful way of comparing the quality of the carbon nanotubes obtained in terms of how ordered and graphitic they are [7-10]. A higher G:D ratio indicates better quality carbon deposits with regards to CNTs. Results were obtained using a Renishaw Invia Raman spectrometer at a wavelength of 514 nm at Raman shifts between 100 and 3200 cm^{-1} . The used catalysts were placed onto a glass slide, and a flat surface created before the sample was analysed. Raman spectra were obtained from at least three points for each sample to ensure the spectrum obtained was indicative of the sample. Figure 3.10 shows a typical Raman spectrum obtained during analyses. G, D and G' peaks can be seen on the spectrum, with the G:D ratio also calculated.

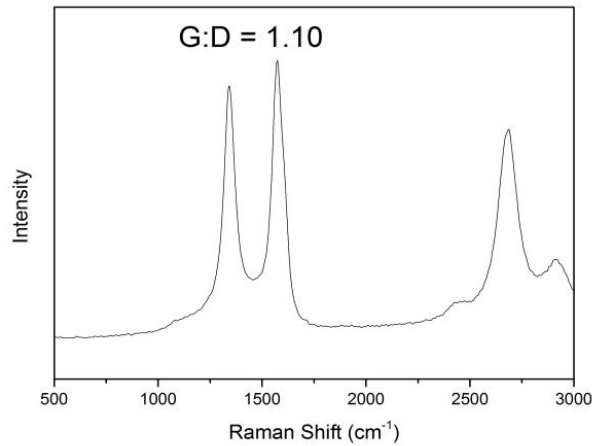


Figure 3.10 A typical Raman spectrum of catalyst carbon deposits

3.3.7 X-Ray Diffraction

X ray diffraction (XRD) of the fresh catalysts was undertaken with a Bruker D-8 diffractometer using a Cu-K α X-ray source with a Vantec position sensitive detector. In XRD, X-rays are fired at a sample and the incident X-rays are diffracted by crystalline atoms within the sample structure. According to the different angles of diffraction, and the relative intensities of the diffracted X-rays, specific compounds can be identified. A typical XRD spectrum is shown in figure 3.11, showing the peaks that appear on the spectrum at a range of diffraction angles. The spectra were analysed with a database of known spectra from Pan Analytical Xpert High score plus, to identify the peaks.

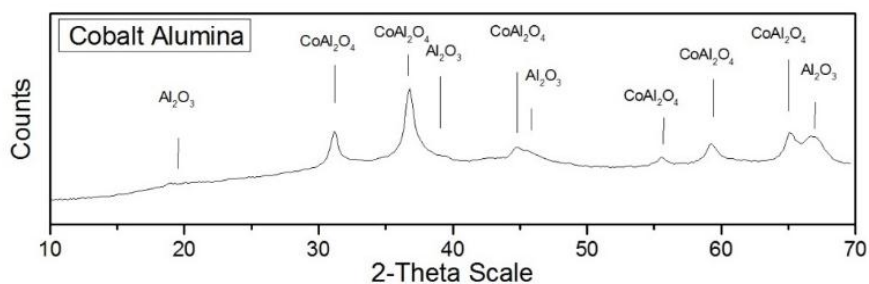


Figure 3.11 A typical XRD plot of a fresh catalyst

References

1. Wang, P., et al., *Filamentous carbon prepared by the catalytic pyrolysis of CH₄ on Ni/SiO₂*. *Applied Catalysis A: General*, 2002. **231**: p. 34-44.
2. Arena, U., et al., *An innovative process for mass production of multi-wall carbon nanotubes by means of low-cost pyrolysis of polyolefins*. *Polymer Degradation and Stability*, 2006. **91**(4): p. 763-768.
3. Jiang, Z.W., et al., *Polypropylene as a carbon source for the synthesis of multi-walled carbon nanotubes via catalytic combustion*. *Carbon*, 2007. **45**(2): p. 449-458.
4. Kong, Q.H. and J.H. Zhang, *Synthesis of straight and helical carbon nanotubes from catalytic pyrolysis of polyethylene*. *Polymer Degradation and Stability*, 2007. **92**(11): p. 2005-2010.
5. Tang, T., et al., *Synthesis of multiwalled carbon nanotubes by catalytic combustion of polypropylene*. *Angew Chem Int Ed Engl*, 2005. **44**(10): p. 1517-20.
6. Zhuo, C., et al., *Synthesis of carbon nanotubes by sequential pyrolysis and combustion of polyethylene*. *Carbon*, 2010. **48**(14): p. 4024-4034.
7. Arnaiz, N., et al., *Production of Carbon Nanotubes from Polyethylene Pyrolysis Gas and Effect of Temperature*. *Industrial & Engineering Chemistry Research*, 2013. **52**(42): p. 14847-14854.
8. Gallego, G.S., et al., *Production of hydrogen and MWCNTs by methane decomposition over catalysts originated from LaNiO₃ perovskite*. *Catalysis Today*, 2010. **149**(3-4): p. 365-371.
9. Yang, Z., et al., *Coupled process of plastics pyrolysis and chemical vapor deposition for controllable synthesis of vertically aligned carbon nanotube arrays*. *Applied Physics A*, 2010. **100**(2): p. 533-540.
10. Yen, Y.W., M.D. Huang, and F.J. Lin, *Synthesize carbon nanotubes by a novel method using chemical vapor deposition-fluidized bed reactor from solid-stated polymers*. *Diamond and Related Materials*, 2008. **17**(4-5): p. 567-570.

4 Pyrolysis-gasification of WEEE plastics for the production of hydrogen

In this chapter, the potential to produce hydrogen gas from waste electrical and electronic equipment (WEEE) plastics by a two stage pyrolysis gasification process was investigated. A temperature of 600 °C was used for the pyrolysis reactor, whilst a temperature of 800 °C was used for the catalytic reactor. A WEEE plastic from waste cathode ray tube material was used along with two plastics which are commonly used in WEEE; Acrylonitrile Butadiene Styrene (ABS) and High Impact Polystyrene (HIPS). Hydrogen production has been demonstrated from the thermal treatment of other waste plastics, but the potential to produce from WEEE plastics is not as well researched. The use of catalysts is considered as a key factor to maximise the production of hydrogen [1, 2]. Nickel-based catalysts have been reported as the most appropriate catalysts for hydrogen production due to their availability, catalytic activity and comparatively low cost [3-5]. The percentage of nickel in the catalyst used plays an important role in determining the performance of the catalyst [6, 7], with the amount of hydrogen produced and carbon deposited on the catalyst being affected. Whilst there are various preparation methods for the production of Ni-Al₂O₃ the impregnation method is one that much shows promise for the production of catalysts [8]. As nickel catalysts have proven successful for hydrogen production from other plastics, in this work a nickel catalyst produced by impregnation onto a gamma Al₂O₃ support was used, with nickel loadings of 5 and 10 wt% used. Where hydrogen production from the thermal treatment of plastics has been investigated before, carbon deposits on the catalyst often show the presence of valuable filamentous carbons and carbon nanotubes. As a result the carbon deposition on the surface of the catalyst in this work was also investigated, to see if carbon nanotubes had been produced.

4.1 Gas yield

Table 4.1 shows the gas and solid yields (wt %) from the two-stage pyrolysis gasification of WEEE, HIPS and ABS. Oils were calculated by difference as the exact yield produced was unable to be determined as they were not able to be separated from the water injected. The results are presented in the case of no steam or catalyst, where sand was used in place of the catalysts,

for the addition of steam to the second reactor, also with sand instead of catalysts, and for the catalytic steam gasification of the plastics and also in relation to the Ni content of the catalyst.

Table 4.1 Product yield from pyrolysis-gasification of plastics

Plastic	WEEE	WEEE	WEEE	WEEE	HIPS	HIPS	HIPS	HIPS	ABS	ABS	ABS	ABS
Water flow rate (g/h)	0	4.74	4.74	4.74	0	4.74	4.74	4.74	0	4.74	4.74	4.74
Catalyst	Sand	Sand	5% Ni	10% Ni	Sand	Sand	5% Ni	10% Ni	Sand	Sand	5% Ni	10% Ni
Gas (wt %)	10.8	12.7	21.5	28.3	5.9	6.0	32.0	40.5	11.6	11.3	15.4	16.2
Solid (wt %)	3.7	3.0	4.3	3.0	8.0	5.0	4.6	5.8	12.2	10.7	14.5	11.7
Oils (wt %)*	85.5	84.3	74.2	68.7	86.1	89.0	63.4	53.7	76.2	78.0	70.1	72.1

* Oils calculated by difference

As shown in table 4.1, when no catalyst or steam was used the WEEE plastic produced 10.8 wt% gas, similar to that produced from ABS 11.6 wt%, whereas HIPS only produced 5.9 wt% gas. Encinar and Gonzalez [9] undertook a thermo gravimetric investigation of the pyrolysis of thermosetting plastics and thermoplastics. They found that the yield of gases from ABS (thermoset) was significantly lower, between 2.89 and 8.86 wt% (depending on heating rate), compared to polyethylene and polypropylene (thermoplastics) which gave between 18.17 - 38.76 wt% gas and 16.55 – 31.84 wt% gas respectively. In addition, styrene based polymers such as ABS and polystyrene have been shown to produce less gas than polyalkene plastics such as polyethylene and polypropylene [10]. The solid yield for the plastics for each of the plastics mostly consisted of solid residue in the sample holder in the pyrolysis stage, since carbon deposition on the catalyst surface was visibly low. As a result for each of the plastics, the solid yield varied little from experiment to experiment, with the WEEE producing on average 3.5 wt%, HIPS producing on average 5.9 wt% and ABS producing on average 12.3 wt%.

The addition of steam to the non-catalytic pyrolysis-gasification of WEEE, HIPS and ABS showed only a small influence on gas yield (table 4.1). However, with the introduction of the nickel catalysts there was a marked increase in yield of gas, particularly for the HIPS plastic sample which

produced 32.0 wt% and 40.5 wt% gas yield for the 5 wt% and 10 wt% nickel catalysts. Whilst ABS also saw an increase in the gas yield when the catalyst was added, the increase observed was far more modest with values of 15.4 wt% and 16.2 wt% obtained for the 5 wt% and 10 wt% nickel catalysts. The results for the WEEE plastic gave gas yields of 21.5 wt% and 28.3 wt% for the 5 wt% and 10 wt% nickel catalysts respectively which are between the values obtained for both HIPS and ABS, suggesting that the WEEE may be comprised of a mixture of the two plastics.

4.2 Hydrogen production

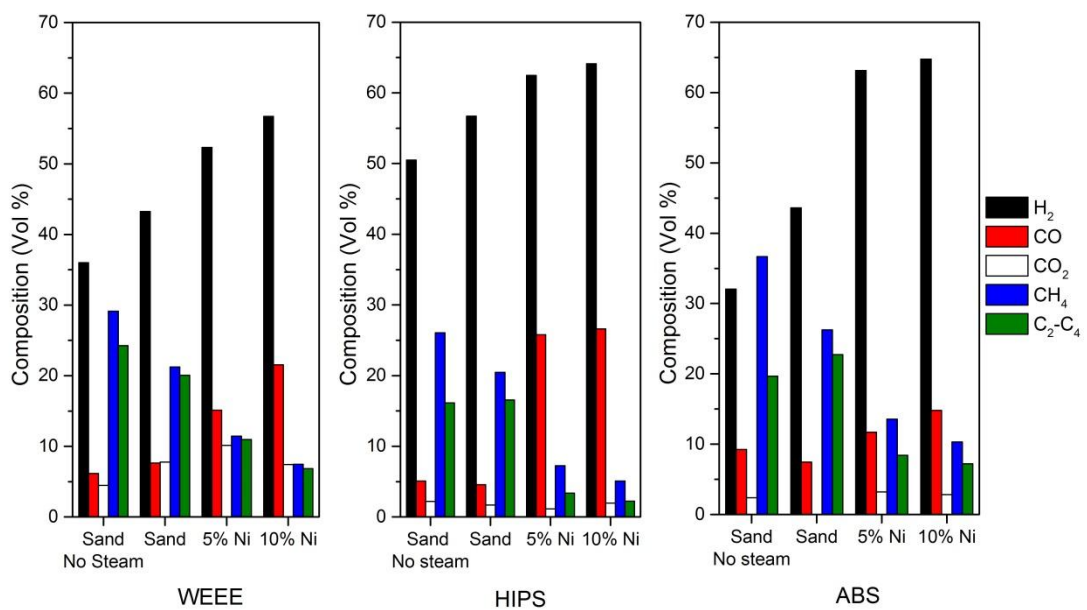
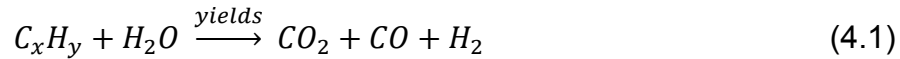


Figure 4.1 Gas compositions from the pyrolysis-gasification of WEEE, HIPS and ABS

Figure 4.1 shows the volume percent of hydrogen displayed along with that of carbon monoxide (CO), carbon dioxide (CO₂), methane (CH₄) and C₂-C₄ hydrocarbons for the pyrolysis-gasification of the WEEE plastic, HIPS and ABS and the influence of steam and the Ni/Al₂O₃ catalysts.

Hydrogen is produced from the thermal treatment of plastics through a series of different chemical reactions. These include the steam reforming of the hydrocarbons produced from the pyrolysis stage (reaction 4.1), gasification of solid carbon deposits with steam (reaction 4.2) and via the forward reaction of the water gas shift reaction 4.3).



As shown in figure 4.1, all the samples give a roughly similar gas composition when no catalyst or steam is used, with varying amounts of hydrogen, CH₄ and C₂-C₄ hydrocarbons and then smaller amounts of CO and CO₂. The thermal treatment of the HIPS sample produced the largest hydrogen composition at around 50 vol% compared with 36 vol% for WEEE and 32 vol% for ABS. In relation to ABS, the HIPS plastic itself has a larger hydrogen content, as shown in table 3.2 in its elemental analysis, suggesting why more gaseous hydrogen is produced. ABS is constructed from an acrylonitrile-styrene polymer being grafted onto a polybutadiene backbone, whilst HIPS is similar but contains no acrylonitrile monomers [10]. As a result it has a comparatively larger amount of styrene monomers and hence a larger amount of hydrogen. HIPS also shows the smallest methane yield, 26 vol%, whilst ABS displays the highest, 36 vol%. WEEE shows a methane yield in between the two pure plastics further suggesting that it is comprised of a mixture of the HIPS and ABS polymers. The similarity in the yield and composition of gas obtained from WEEE and ABS suggests that ABS makes up a larger proportion of the WEEE sample.

As shown in figure 4.1, when steam is introduced into the second stage the hydrogen composition of the gas increases, with a corresponding decrease in the amount of methane and C₂-C₄ hydrocarbons which suggests that they are consumed in a steam reforming reaction. The hydrogen composition of the gas in the presence of steam, but no catalyst, was higher for HIPS compared to WEEE and ABS.

The addition of the 5 wt% Ni/Al₂O₃ catalyst to the catalytic gasification of the plastics showed an increase in hydrogen composition of the gas (figure 4.1). This was the case for all three plastic samples tested, however as before, HIPS and ABS produced the largest amount of hydrogen at around 63 vol%, with WEEE producing 52 vol% hydrogen gas by composition. Methane and C₂-C₄ hydrocarbons decreased with corresponding increase in the formation of CO with the introduction of the catalyst, suggesting that the catalyst may

promote hydrogen production by decomposition of hydrocarbons and the reaction of steam with carbon on the coked catalyst to produce CO.

Compared to the 5 wt% Ni catalyst, the 10 wt% catalyst was an improvement on catalytic activity. Figure 4.1 shows a clear increase in the hydrogen yield from the pyrolysis-gasification of the WEEE plastic, as the hydrogen composition of the gas rises to 57 vol%. The increase in nickel content raises the catalytic activity in terms of decomposition of the hydrocarbon gases into hydrogen as decreases in the yield of methane and C₂-C₄ are seen. The amount of CO is also seen to increase significantly as the nickel content of the catalyst is raised.

Table 4.2 Hydrogen production and conversion from the pyrolysis-gasification of WEEE, HIPS and ABS

Plastic	WEEE	WEEE	WEEE	WEEE	HIPS	HIPS	HIPS	HIPS	ABS	ABS	ABS	ABS
Water flow rate (g/h)	0	4.74	4.74	4.74	0	4.74	4.74	4.74	0	4.74	4.74	4.74
Catalyst	-	-	5% Ni	10% Ni	-	-	5% Ni	10% Ni	-	-	5% Ni	10% Ni
Hydrogen yield (g/100g sample)	0.47	0.69	1.50	2.35	0.48	0.58	3.59	4.72	0.46	0.68	1.82	1.99
Hydrogen conversion (%)	5.5	8.1	17.7	27.6	7.3	8.9	54.5	71.5	7.7	11.3	30.4	33.1

Table 4.2 shows the hydrogen yield and conversion of hydrogen in the plastic into hydrogen gas for each of the three plastic samples tested. Based on their elemental composition the theoretical yields of hydrogen that could be obtained if all the hydrogen in the sample was converted into gas was calculated (table 3.1). Based on this the hydrogen conversion of the sample into hydrogen was calculated as a percentage of this theoretical maximum. As steam was injected, hydrogen could also be produced from water gas shift and gasification of carbon deposits, meaning conversions of more than 100% are possible. When no catalyst or steam was used the hydrogen conversion was consistently low for each of the plastics, with conversions of below 10%. Whilst the addition of steam led to an increase in the hydrogen yield, it was not until the nickel catalyst was used that the hydrogen

conversions began to rise significantly. The increase was seen for all the samples but was largest for the HIPS plastic which had a conversion of 54.5% compared with 30.4% and 17.7% for ABS and WEEE respectively. The high value for HIPS is attributed to a high hydrogen content in the gas coupled with a high yield of gas due to catalytic cracking. Raising the nickel content of the catalyst continued the increasing trend in the hydrogen conversion again with HIPS giving the largest conversion with values of 71.5%, compared with 33.1% and 27.6% for ABS and WEEE respectively. Despite having the lowest conversion WEEE actually generated a higher yield of hydrogen than ABS, 2.35 g/ 100g sample compared with 1.99 g/ 100g sample. Its low conversion value is due to the WEEE plastics higher hydrogen content. Again ABS and WEEE gave similar results, suggesting the ABS proportion in the WEEE is large.

4.3 Characterisation of oils

Table 4.3 shows the GC/MS results for the oils obtained from the two stage pyrolysis of the three plastics when no catalyst or steam was used. Fifteen of the most abundant compounds in the oils are shown for the WEEE, HIPS and ABS. Styrene was present in all of the oil samples, which is to be expected since all of the plastics are formed from styrene based polymers.

Nitrogen containing compounds including benzyl nitrile, benzonitrile-3-methyl, and naphthalene, 1-isocyano are seen in ABS and WEEE but not in HIPS. In contrast to HIPS, ABS contains acrylonitrile monomers which could breakdown to form the nitrogen containing compounds found in both ABS and WEEE oils. This suggests that these compounds in the WEEE oil are likely to have originated from ABS within the WEEE plastic. Similarly there are some compounds including indene and Phenanthrene, 3-methyl which are present in HIPS and WEEE but not in ABS. This suggests that the WEEE plastic also contains HIPS, further cementing the idea that it is comprised of a mixture of the HIPS and ABS plastics.

Table 4.3 GC-MS identified species in WEEE, HIPS and ABS pyrolysis

Retention Time (min)	Identified species		
	WEEE	HIPS	ABS
9.74-9.99	Ethylbenzene	Ethylbenzene	Ethylbenzene
11.94-12.15	Styrene	Styrene	Styrene
17.01-17.05	Phenol	-	Phenol
19.51	Indene	Indene	-
20.35-20.49	Benzonitrile, 3- methyl-	-	Benzonitrile, 3- methyl-
22.90-23.03	Benzyl nitrile	-	Benzyl nitrile
24.34-24.47	Naphthalene	Naphthalene	Naphthalene
30-30.08	Biphenyl	Biphenyl	Biphenyl
32.88-32.94	Naphthalene, 1- isocyano-	-	Naphthalene, 1- isocyano-
37.94-37.96	1,2-Diphenylethylene	1,2-Diphenylethylene	1,2-Diphenylethylene
39.45-39.47	Phenanthrene	Phenanthrene	Phenanthrene
41.01	1H-Indene, 1- (phenylmethylene)-	1H-Indene, 1- (phenylmethylene)-	1H-Indene, 1- (phenylmethylene)-
42.25	Phenanthrene, 3- methyl-	Phenanthrene, 3- methyl-	-
43.30	2- Phenylnaphthalene	2- Phenylnaphthalene	2- Phenylnaphthalene
51.74	Benz[a]anthracene	Benz[a]anthracene	Benz[a]anthracene

The effect of steam and the catalyst on the oils is shown table 4.4 and figure 4.2. Table 4.4 shows the same fifteen compounds that were displayed in table 4.3, with the relative abundance of each compound denoted by the number of stars. Smaller aromatics such as ethylbenzene, styrene, phenol and indene increase when the catalyst is added however, there is a subsequent reduction seen when the nickel content of the catalyst is increased. It is suggested that larger aromatics are cracked into these smaller compounds with the introduction of the catalyst, leading to the initial increase shown. Once the nickel percentage is increased the smaller compounds are themselves broken down into gases due to the higher catalytic activity that result. Bimbela et al and Srinakruang et al found similar results with catalytic activity increasing with increasing nickel content leading to the production of smaller hydrocarbons [11, 12]. Larger compounds such as phenanthrene and benz[a]anthracene on the other hand show a reduction in abundance when the 5 wt% nickel catalyst is introduced and also a subsequent reduction when the nickel content is increased. This suggests that these larger compounds are cracked when the catalyst is used, and are broken down into smaller molecules.

The GC/MS profiles in figure 4.2 mirror the results that are shown in table 4.4, with reductions seen in the concentration of larger compounds at higher retention times. Figure 4.2 a shows the profile for WEEE pyrolysis without steam and without a catalyst. The major peaks seen are at 12.15 and 24.47 minutes which are styrene and naphthalene respectively, however there are also a substantial amount of peaks seen at the higher retention times. The peaks at the higher retention times are seen to reduce with the addition of steam (figure 4.2 b) and reduce further when the catalyst is used (figures 4.2 c and d), with some disappearing completely. This reinforces the theory that the nickel catalyst promotes the breakdown of oils via cracking, with the products being smaller aromatics or even gaseous hydrocarbons.

Table 4.4 GC-MS results showing the effect of catalyst on WEEE oils

Identified Species	Concentration ^a			
	WEEE + Sand	WEEE + Sand + Steam	WEEE + 5 wt% Ni/Al ₂ O ₃ + Steam	WEEE + 10 wt% Ni/Al ₂ O ₃ + Steam
Ethylbenzene	*	**	****	**
Styrene	*****	***	****	***
Phenol	***	**	****	**
Indene	*****	**	***	*
Benzonitrile, 3-methyl-	****	***	**	**
Benzyl nitrile	****	**	***	**
Naphthalene	*****	**	***	*
Biphenyl	****	**	**	*
Naphthalene, 1-isocyano-	****	**	**	*
1,2-Diphenylethylene	****	**	**	*
Phenanthrene	*****	**	**	*
1H-Indene, 1-(phenylmethylene)-	****	**	**	*
Phenanthrene, 3-methyl-	**	*	*	-
2-Phenyl-naphthalene	****	**	**	*
Benz[a]anthracene	***	**	*	-

^a Relative abundance of species in oil fraction based on peak area. More asterisks means higher concentration.

Using methodology of Blanco et al, Energy Fuels, 2012, 26, 2107–2115

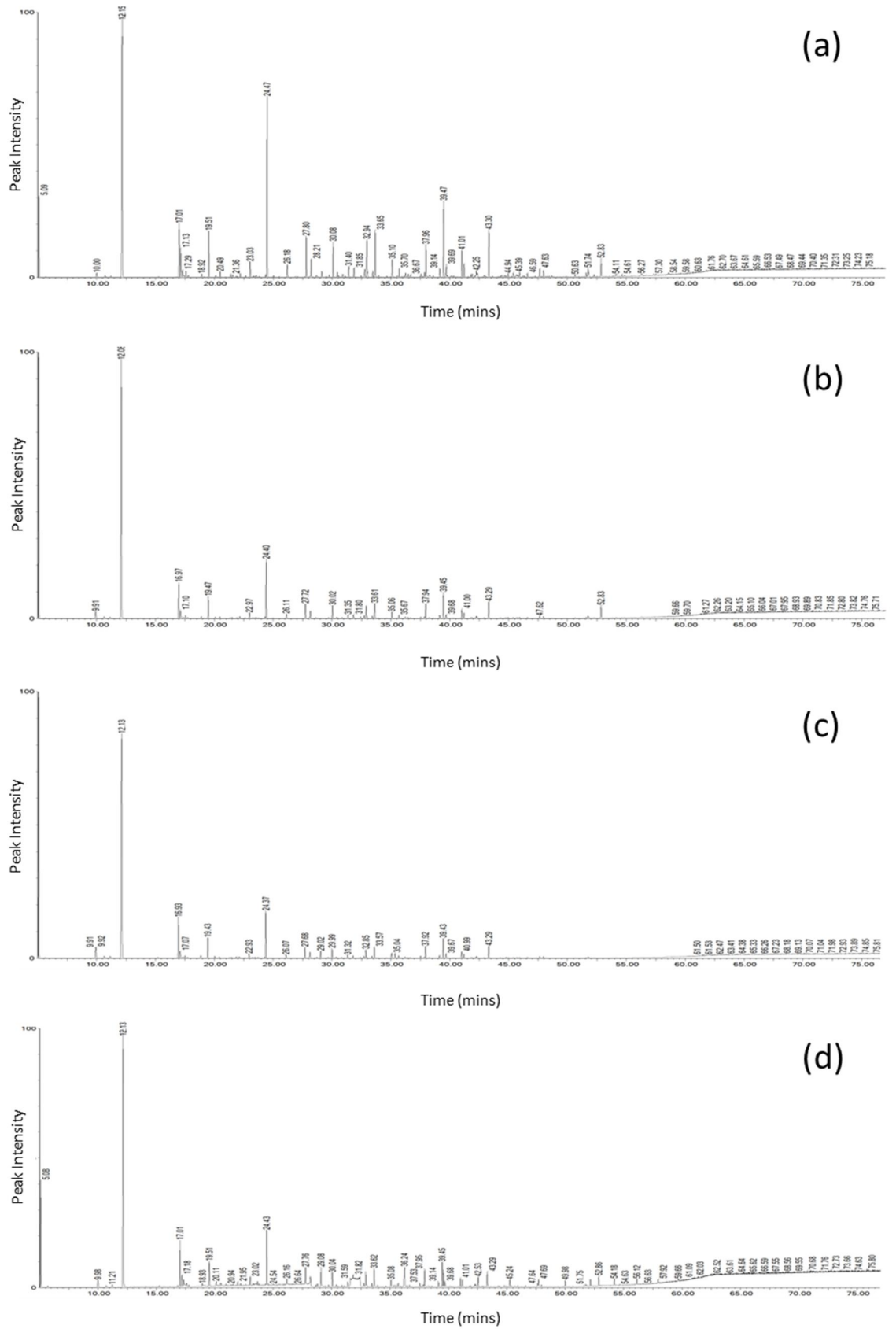


Figure 4.2 GC-MS total ion chromatograms of oils obtained from WEEE pyrolysis-gasification using (a) no steam, no catalyst, (b) steam, no catalyst, (c) steam and 5 wt% Ni (d) steam and 10 wt% Ni

4.4 Characterisation of coke on Ni/Al₂O₃ catalyst

Carbon deposition on the surface of nickel catalysts poses a major challenge to hydrogen production, since it can deactivate the catalyst. Rostrup-Nielsen [11] identified three types of carbon deposition, whisker type carbons, such as filamentous carbons, in addition to pyrolytic and encapsulating carbons which deactivate the catalyst. As a result a number of recent publications have aimed to reduce the build-up of carbon on the surface of nickel catalysts, by use of different supports or promoters [12-15]. However, it was demonstrated by Kukovitsky et al [16] that valuable carbon nanotubes are also produced in the filamentous carbon deposits on nickel catalysts during pyrolysis of polyethylene. Carbon nanotubes (CNTs) are high value materials which have generated a great deal of research interest in recent years as they have potential uses in a wide range of applications [17-24]. This stems from their remarkable properties including high strength, a large surface area and good electrical conductivity [25]. As a result a series of analyses were undertaken on the carbon deposits produced to investigate whether carbon deposition has contributed to the deactivation of the catalyst, and to establish whether carbon nanotubes have been produced.

4.4.1 SEM analysis

SEM images of the reacted catalysts obtained from the pyrolysis-gasification of the plastics samples can be seen in figure 4.3. The images of the catalysts in figure 4.3 (a-f) show the nature of the carbon deposits on their surfaces. Figure 4.3(a) shows an image of the used 5 wt% nickel catalyst from the pyrolysis-gasification of WEEE, where sparsely scattered filamentous carbons are seen on the catalyst surface. The SEM image of the reacted 10% nickel catalyst used in the experiments with the WEEE sample is shown in figure 4.3(b). It shows a similarly sparse scattering of filamentous carbons.

The reacted catalyst surface shown in figures 4.3(c) and (d) show the catalyst particles from the pyrolysis-gasification of HIPS and are for 5 wt% and 10 wt% nickel loadings respectively. A large amount of carbon deposition can be seen in the form of filamentous carbons. The filamentous carbons on both catalysts from pyrolysis-gasification of HIPS appear to be longer and more thickly spread than those when WEEE was the feedstock, however there is very little difference between the two different metal

loadings. This shows the feedstock used has a larger effect on the carbon deposits than the nickel loading.

Figures 4.3(e) and (f) show the SEM images of the used 5 wt% and 10 wt% nickel catalysts obtained from pyrolysis-gasification of ABS. Filamentous carbons are again observed however the nature of the carbons are distinctly different from those from the other feedstocks, as the filaments appear thicker and bound together; themselves forming larger cylindrical structures. The 5% and 10% nickel catalysts again produce similar results with the nature of the carbon deposits remaining largely unchanged.

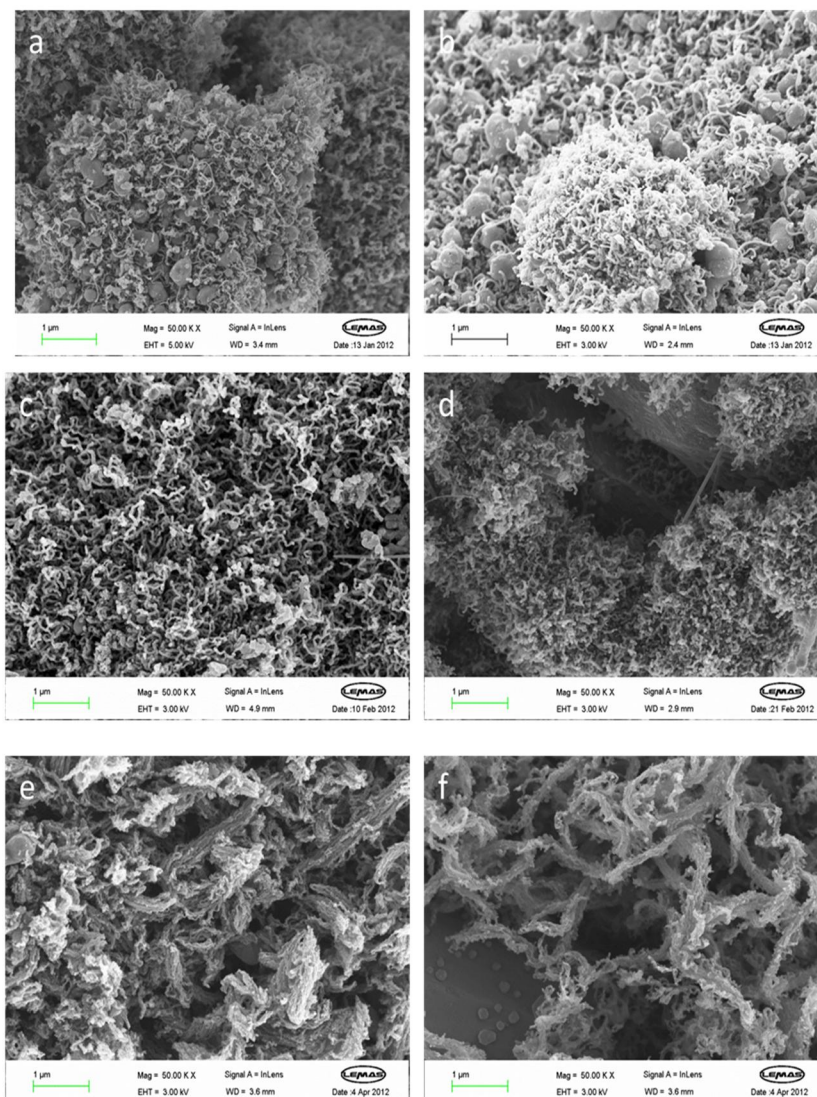


Figure 4.3 SEM images of carbon deposition on used catalyst from pyrolysis gasification of (a) WEEE using 5 wt% Ni, (b) WEEE using 10 wt% Ni, (c) HIPS using 5 wt% Ni, (d) HIPS 10 wt% Ni, (e) ABS using 5 wt% Ni and (f) ABS using 10 wt% Ni

4.4.2 TEM analysis

TEM analysis was carried out on the used catalysts in order to determine the nature of the carbon deposition, and determine whether CNTs had been produced. Figure 4.4 shows the TEM images obtained. Carbon deposits on the surface of the catalyst used for experiments using the WEEE sample, shown in figure 4.4 (a) and (b), revealed that the majority of filamentous carbons did not have a hollow centre, and were around 50 – 100 nm diameter. For both 5 and 10 wt% nickel loading, the filaments appear to be made up of series of roughly circular segments of carbon, some of which contain a hollow centre. This suggests a similar mechanism of formation to those of CNTs. CNTs were observed from the carbon deposits on the catalyst used for experiments with the WEEE sample, however they were uncommon, with more observed at 10 wt% nickel loading than 5 wt%. CNTs obtained from the carbon deposits on the catalyst used in WEEE experiments are shown in figure 4.5 (a). The CNTs are multi walled, fairly short in length and between 20 and 50 nm in diameter.

TEM images of the carbon deposits on the catalyst used in the pyrolysis gasification of the HIPS plastic bare a strong resemblance to those obtained from the WEEE sample, with filaments being composed of roughly circular segments of carbon, with some being hollow. Likewise, CNTs were also observed in the carbon deposits from the HIPS experiments with a typical CNT shown in figure 4.5 (b). As was the case with the deposits from the WEEE experiments, more CNTs were seen at the nickel loading of 10 wt%. The CNT is multi walled and again fairly short, but has a smaller diameter than those obtained from the carbon deposits on the catalyst using the WEEE sample, with the CNT observed having a diameter of roughly 10 nm.

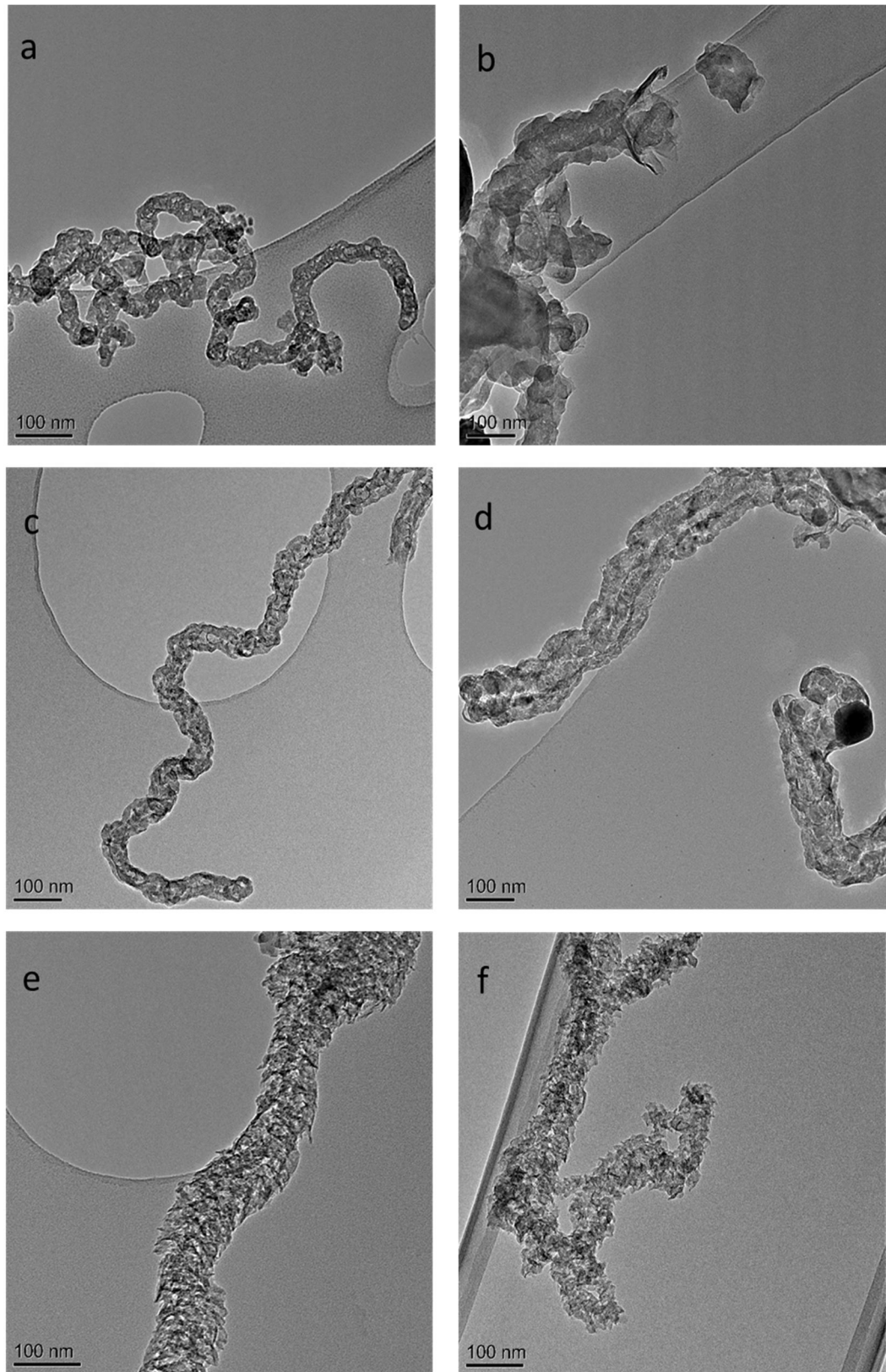


Figure 4.4 TEM images of carbon deposition on used catalyst from pyrolysis gasification of (a) WEEE using 5 wt% Ni, (b) WEEE using 10 wt% Ni, (c) HIPS using 5 wt% Ni, (d) HIPS 10 wt% Ni, (e) ABS using 5 wt% Ni and (f) ABS using 10 wt% Ni

In contrast to the filaments produced on the catalyst used in the pyrolysis gasification of WEEE, those from ABS experiments, figures 4.4 (c) and (d), are distinctly different. The diameter of the filaments is larger, above 100 nm, and there is more branching and variation in width along the course of the filament. The nature of the filaments themselves are also different, and appear to be composed of smaller more irregularly shaped particles of carbon. Whilst a small number of CNTs were found from carbon deposits on the catalysts from the WEEE and HIPS experiments, none were found in the deposits from ABS experiments. Together with the different nature of the filaments, this suggests the mechanism of formation for the ABS sample varies from that of CNTs.

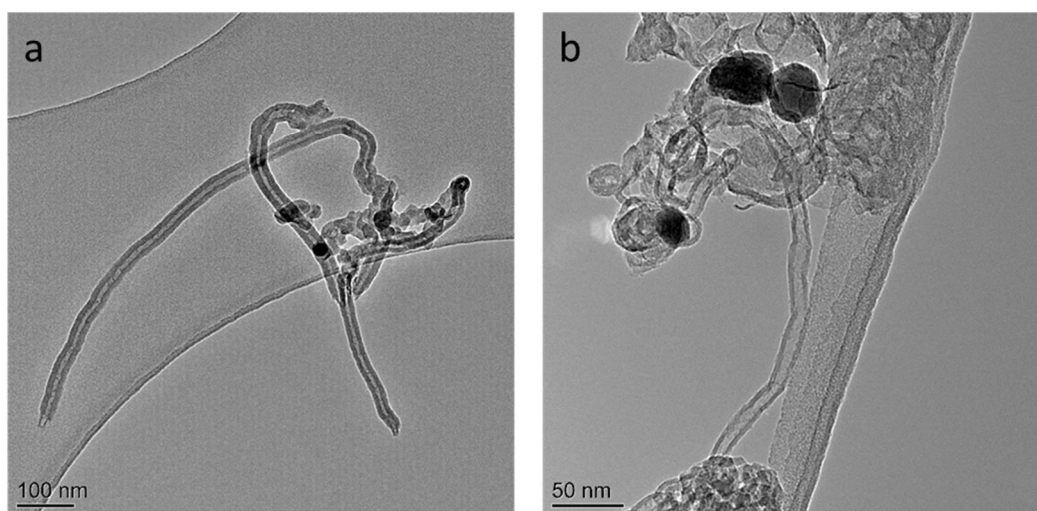


Figure 4.5 TEM images of CNTs produced from the pyrolysis-gasification of (a) WEEE, (b) HIPS

4.4.3 Temperature programmed oxidation

Temperature programmed oxidation of the catalysts used in the pyrolysis-gasification of WEEE, HIPS and ABS was undertaken to investigate the carbon deposits on the catalyst surface. Figure 4.6 shows the TPO plots and derivative plots obtained.

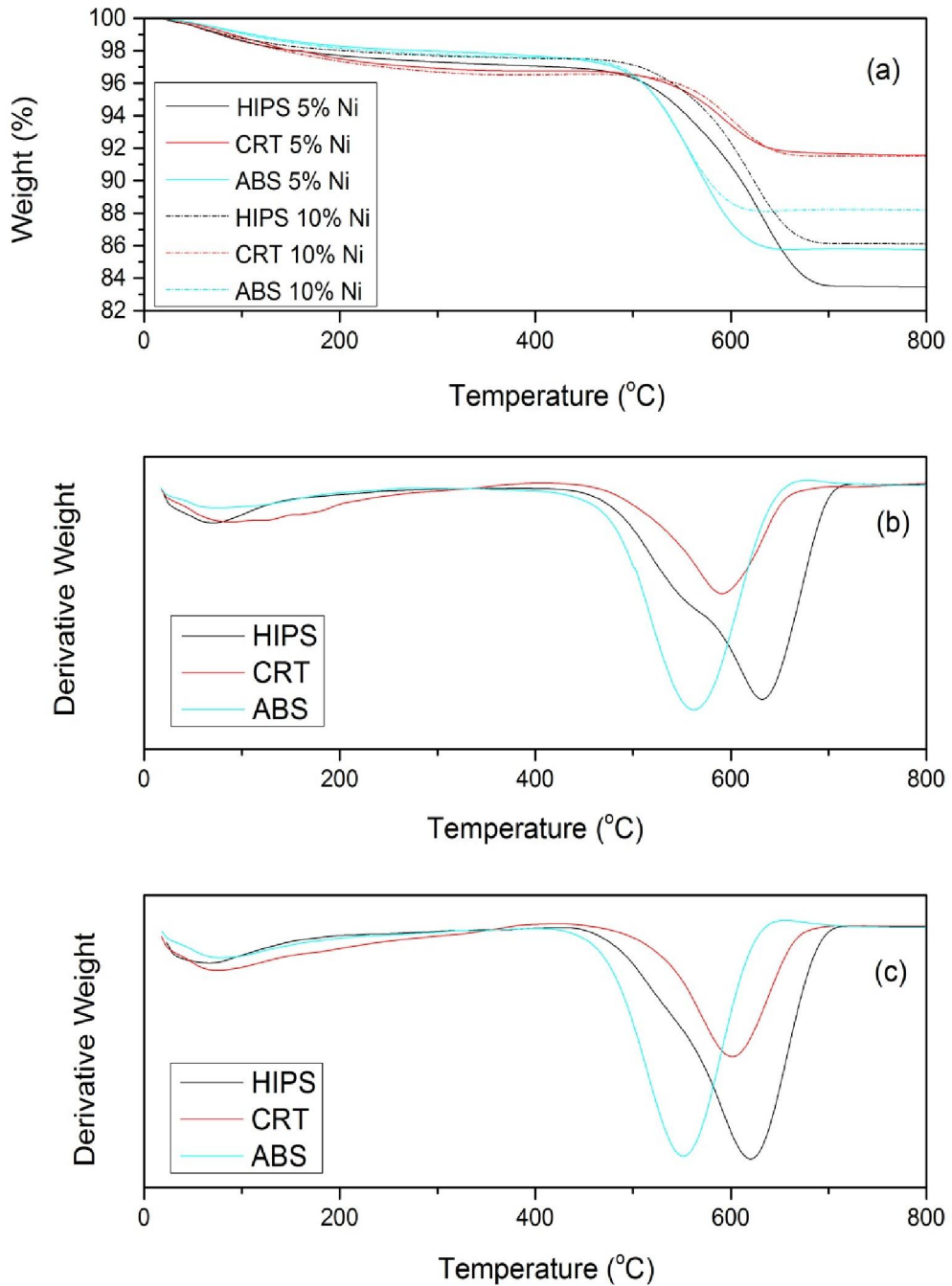


Figure 4.6 (a) Temperature programmed oxidation results from carbon deposits on catalysts used in pyrolysis-gasification of plastics, (b) Derivative plot of 5wt % Ni catalysts used and (c) Derivative plot of 10 wt% Ni catalysts used

The TPO results shown in figure 4.6 (a) show that as the amount of nickel in the catalyst is increased, the amount of carbon deposition actually decreases for the HIPS and ABS feedstocks. As steam is injected into the reactor, the reduction in carbon could suggest that the increase in loading

led to increased gasification of carbon deposits on the surface as shown in reaction 4.2.

From the derivative plots, seen in figures 4.6 (a) and (b), the carbon deposits on the catalyst from experiments with each of samples produce peaks between 500 and 700 °C. The ABS experiments produced carbon deposits which were oxidised at the lowest temperature. This is consistent with the different type of carbon observed from TEM and suggests that the irregular and unstructured filaments seen with this feedstock are more reactive with oxygen. Experiments using the HIPS sample produced carbon deposits which were oxidised at the highest temperature, but also showed a shoulder peak at a lower temperature on the 5 wt% nickel catalyst. This suggests that these more reactive carbons could impede hydrogen production, as when larger amounts are seen in the deposits from ABS, and HIPS at 5 wt% nickel loading, the hydrogen yield is lower.

The WEEE plastic, despite producing a small amount of hydrogen, produced a smaller amount of carbon deposition on the catalyst surface than the other plastics. The oxidation of the carbons in TPO occurs at a similar temperature to those from the HIPS sample, agreeing with the similar nature of carbon deposits observed in TEM. The smaller amount of these carbons in deposits from pyrolysis gasification of WEEE suggests that the carbon deposited does not cause the catalyst to deactivate, since HIPS produced more carbon deposition, but a higher hydrogen yield. There is also no significant change in the nature of the carbon deposits when the metal loading is increased, suggesting instead that the higher hydrogen yield observed is due to an increase in catalytic cracking and carbon gasification. This is likely since cracking was seen from the analysis of the oils, gases and mass balances. Overall, whilst the type of carbon deposited from the plastics has an influence on the hydrogen yield, other factors appear to be more significant.

4.5 Conclusions

Nickel catalysts have proven successful in increasing the yield of hydrogen obtained from WEEE plastics. The addition of the catalyst yielded higher hydrogen and carbon monoxide levels, and it is thought that these are produced by cracking of hydrocarbons and reaction of steam with the coke deposited on the catalyst surface. Increasing the nickel content of the catalyst also saw a corresponding increase in the yield of hydrogen,

suggesting that this plays an important role in catalytic activity. When comparing the three different plastics investigated, HIPS was seen to produce the largest amount of hydrogen, with ABS and the WEEE plastic giving smaller yields. Larger polyaromatic hydrocarbons are broken down via cracking when the nickel catalysts are used, forming smaller aromatics and hydrocarbon gases. Based upon the GC/MS of the pyrolysis oils and GC results from the gases, it has been deduced that the WEEE plastic is formed of both HIPS and ABS. Due to its similar performance however, it is thought that the WEEE plastic contains a higher proportion of ABS. The carbon deposits seen on the nickel catalysts were all of the filamentous type, however the nature and abundance of the filaments varied with the feedstock. TEM images showed that only a very small amount of CNTs were produced from the HIPS and WEEE samples, with none produced from the ABS feedstock.

References

1. Chen, L., et al., *Development of a Co–Ni bimetallic aerogel catalyst for hydrogen production via methane oxidative CO₂ reforming in a magnetic assisted fluidized bed*. International Journal of Hydrogen Energy, 2010. **35**(16): p. 8494-8502.
2. Tanksale, A., J.N. Beltramini, and G.M. Lu, *A review of catalytic hydrogen production processes from biomass*. Renewable and Sustainable Energy Reviews, 2010. **14**(1): p. 166-182.
3. Yoon, S.J., Y.-C. Choi, and J.-G. Lee, *Hydrogen production from biomass tar by catalytic steam reforming*. Energy Conversion and Management, 2010. **51**(1): p. 42-47.
4. de Lima, S.M., et al., *Hydrogen production through oxidative steam reforming of ethanol over Ni-based catalysts derived from La_{1-x}Ce_xNiO₃ perovskite-type oxides*. Applied Catalysis B: Environmental, 2012. **121–122**(0): p. 1-9.
5. Xie, Q., et al., *Syngas production by two-stage method of biomass catalytic pyrolysis and gasification*. Bioresource Technology, 2012. **110**(0): p. 603-609.
6. Avdeeva, L.B., et al., *Coprecipitated Ni-alumina and Ni-Cu-alumina catalysts of methane decomposition and carbon deposition. II. Evolution of the catalysts in reaction*. Applied Catalysis A: General, 1996. **141**: p. 117-129.
7. Takenaka, S., *Ni/SiO₂ catalyst effective for methane decomposition into hydrogen and carbon nanofiber*. Journal of Catalysis, 2003.
8. Lu, Y., et al., *Hydrogen production by biomass gasification in supercritical water over Ni/γAl₂O₃ and Ni/CeO₂-γAl₂O₃ catalysts*.

- International Journal of Hydrogen Energy, 2010. **35**(13): p. 7161-7168.
9. Encinar, J.M. and J.F. González, *Pyrolysis of synthetic polymers and plastic wastes. Kinetic study*. Fuel Processing Technology, 2008. **89**: p. 678 - 686.
 10. MAUL, J., et al., *Polystyrene and Styrene Copolymers*, in *Ulmann's Encyclopedia of Industrial Chemistry* 2007, Wiley-VCH.
 11. Rostrup-Nielsen, J.R., *Steam Reforming Catalysts* 1975, Copenhagen: Danish Technical Press.
 12. Alipour, Z., M. Rezaei, and F. Meshkani, *Effect of alkaline earth promoters (MgO, CaO, and BaO) on the activity and coke formation of Ni catalysts supported on nanocrystalline Al₂O₃ in dry reforming of methane*. Journal of Industrial and Engineering Chemistry, 2014. **20**(5): p. 2858-2863.
 13. Bhavani, A.G., et al., *Improved activity and coke resistance by promoters of nanosized trimetallic catalysts for autothermal carbon dioxide reforming of methane*. Applied Catalysis A: General, 2013. **450**: p. 63-72.
 14. Chiou, J.Y.Z., et al., *Effect of Co, Fe and Rh addition on coke deposition over Ni/Ce_{0.5}Zr_{0.5}O₂ catalysts for steam reforming of ethanol*. International Journal of Hydrogen Energy, 2014. **39**(35): p. 20689-20699.
 15. Zhang, Y., et al., *Steam reforming of methane over Ni/SiO₂ catalyst with enhanced coke resistance at low steam to methane ratio*. Catalysis Today, 2015.
 16. Kukovitskii, E.F., et al., *Carbon nanotubes of polyethylene*. Chemical Physics Letters, 1997. **266**: p. 323-328.
 17. Ajayan, P.M., et al., *Single-walled carbon nanotube-polymer composites: Strength and weakness*. Advanced Materials, 2000. **12**: p. 750-753.
 18. Hinds, B.J., et al., *Aligned multiwalled carbon nanotube membranes*. Science, 2004. **303**(5654): p. 62-5.
 19. Javey, A., *Ballistic carbon nanotube field-effect transistors*. Nature, 2003. **424**: p. 654-657.
 20. Kymakis, E., I. Alexandrou, and G.A.J. Amaratunga, *High open-circuit voltage photovoltaic devices from carbon-nanotube-polymer composites*. Journal of Applied Physics, 2003. **93**(3): p. 1764.
 21. Li, W., et al., *Carbon nanotubes as support for cathode catalyst of a direct methanol fuel cell*. Carbon, 2002. **40**: p. 787-803.
 22. Sae-Khow, O. and S. Mitra, *Carbon Nanotube Immobilized Composite Hollow Fiber Membranes for Pervaporative Removal of Volatile Organics from Water*. Journal of Physical Chemistry C, 2010. **114**: p. 16351-16356.
 23. Shimoda, H., et al., *Lithium Intercalation into Opened Single-Wall Carbon Nanotubes: Storage Capacity and Electronic Properties*. Physical Review Letters, 2001. **88**(1): p. 015502-1 - 015502-4.
 24. Snow, E.S., et al., *Chemical detection with a single-walled carbon nanotube capacitor*. Science, 2005. **307**(5717): p. 1942-5.
 25. Nessim, G.D., *Properties, synthesis, and growth mechanisms of carbon nanotubes with special focus on thermal chemical vapor deposition*. Nanoscale, 2010. **2**(8): p. 1306-23.

5 Effect of steam injection rate and plastic type on production of hydrogen and carbon nanotubes

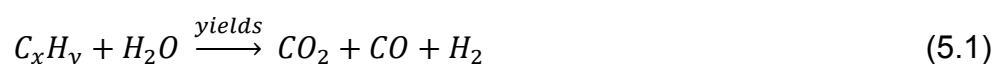
In the previous chapter, whilst hydrogen production was successful from the thermal treatment of WEEE plastics, only small yields of filamentous carbons were observed. Likewise gas yields from the WEEE plastics were low compared to previous studies using polyalkane plastics. In an effort to produce a large yield of carbon nanotubes along with hydrogen, in this chapter the effect of varying the steam injection rate was investigated. The steam injection rates used were 0, 0.25, 1.90 and 4.74 g h⁻¹. These equate to weight hourly space velocities of 9.48, 3.8, 0.5 and 0 h⁻¹. The effect of using different plastics was also investigated using polyalkane plastics, i.e. low density polyethylene and polypropylene, and aromatic plastics similar to those in WEEE i.e. polystyrene. The same 5% nickel catalyst prepared by impregnation was also used, along with the same pyrolysis and catalyst reactor temperatures of 600 and 800 °C. The amounts of catalyst, 0.5 g, and plastic sample, 1 g, were also kept the same.

5.1 Hydrogen production

5.1.1 Effect of steam injection

Tables 5.1-5.3 show the mass balances in terms of the amount of gases, oils and solids produced for each of the plastics used. The mass balances obtained were all above 93%.

For all three samples as the flow rate of steam injected into the reactor was increased, the amount of oils and solids decreased, whilst the amount of gases increased. This is to be expected as steam reforming reactions produce larger amounts of gas, at the expense of oils and solids via reactions 5.1 and 5.2.



This is also in agreement with results from Erkiaga et al [1] who found that increasing steam/plastic ratio gave a reduction in tars and chars and an increase in gas production, particularly hydrogen. The composition of the gases produced from the plastics samples are shown in tables 5.1-5.3 and are typically composed of H₂, CO, CO₂, CH₄ and C₂-C₄ hydrocarbons. Hydrogen makes up the largest constituent of the gas and is above 50 vol.% for all the results. When no steam was injected, methane and C₂-C₄ hydrocarbons also made up a significant proportion of the gas, however once the steam rate into the reactor was increased, hydrocarbons decreased and CO and CO₂ increased via the steam reforming reaction in reactions 5.1. The higher concentration of CO relative to CO₂ seen is due to the high temperatures used being unfavourable for the water gas shift reaction. To increase the hydrogen yield further a third stage could be employed to convert CO into CO₂ and H₂ via reaction with water. Hydrogen production for each of the plastics is also shown in tables 5.1-5.3 and shows how, as expected by reactions 5.1 and 5.2, the yield obtained increases with increasing steam injection rate.

5.1.2 Effect of plastic type

5.1.2.1 Low density polyethylene

The largest gas yields were obtained for the pyrolysis-catalytic gasification of LDPE and reached over 80 wt% for a steam injection rate of 4.74 g h⁻¹ as can be seen in table 5.1. Wax was produced at the low steam injection rates, particularly at 0 steam injection, accounting for the large solid yields observed. The amount of wax produced visibly reduced once higher steam injection rates were applied. Overall the yield of solids reduced as the steam injection rate was increased, as a result of steam reforming of waxes and oils and gasification of carbon deposition. Yields of oils were low, 14 wt% or less, and reduced until none were obtained when 1.90 g h⁻¹ or higher steam rates were used. Methane and other hydrocarbons were produced in similar amounts and reduced from around 20 vol. % each to roughly half that at the highest steam injection rate. Reduction of hydrocarbons and oils are a result of increased steam reforming as more steam is injected. The hydrogen content of the gas ranged between 50 vol.% and 58 vol.% depending on the steam injection rate as shown in table 5.1. A reduction in the content of

hydrogen is seen when steam was injected (reactions 5.1 and 5.2), as a result of CO and CO₂ now becoming part of the gas stream, however in actual terms the amount of hydrogen produced from the plastic was increased, as seen in table 5.1. CO and CO₂ also increase with the steam injection rate as a result of steam reforming and gasification.

Table 5.1 Mass balance, gas composition and hydrogen yield from the pyrolysis-gasification of LDPE

Sample	LDPE	LDPE	LDPE	LDPE
Water injection (g h ⁻¹)	0	0.25	1.90	4.74
Catalyst	Ni 5%	Ni 5%	Ni 5%	Ni 5%
Gas (wt %)	30.9	58.8	78.9	85.7
Oils (wt %)	14.0	8.2	0.0	0.0
Solid * (wt %)	52.0	25.0	15.5	12.5
H ₂ (Vol.%)	58.3	50.3	53.8	53.1
CO (Vol.%)	0.0	13.1	26.4	21.1
CO ₂ (Vol.%)	0.0	0.7	3.1	6.2
CH ₄ (Vol.%)	20.3	16.1	7.1	7.1
C ₂ -C ₄ (Vol.%)	21.4	19.7	9.7	12.5
H ₂ yield (g/100g sample)	3.3	4.7	9.0	9.2
Hydrogen conversion (%)	22.7	33.0	62.9	64.6

*Solid fraction includes carbon deposition, solid residue and waxes obtained after reaction

The yield of hydrogen obtained when no steam was injected was 3.3 g/100g sample. This increased with the steam injection rate. Based on its elemental composition the theoretical yield of 13.9 g/100g sample could be obtained if all the hydrogen in the sample was converted into gas (table 3.1). Based on this the hydrogen conversion of the sample into hydrogen was calculated as a percentage of this theoretical maximum. As steam was injected, hydrogen could also be produced from water gas shift and gasification of carbon deposits, meaning conversions of more than 100% are possible. The maximum hydrogen yield obtained from LDPE at 4.74 g h⁻¹ steam injection was of 9.2 g/100g of sample, a hydrogen conversion of 64.6%. A

comparison can also be made with the WEEE plastics with the 5% catalyst. The LDPE sample at 4.74 g h^{-1} gave a larger hydrogen conversion than all three of the WEEE plastics, which gave values of 18, 30 and 55% for WEEE, ABS and HIPS respectively. LDPE also gave a higher yield of hydrogen in actual terms, with $9.2 \text{ g}/100\text{g}$ sample compared with 1.5, 1.8, $3.6 \text{ g}/100\text{g}$ sample for WEEE, ABS and HIPS respectively. This shows that the LDPE plastic sample was more suitable for hydrogen production.

5.1.2.2 Polypropylene

Table 5.2 Mass balance, gas composition and hydrogen yield from the pyrolysis-gasification of PP

Sample	PP	PP	PP	PP
Water injection (g h^{-1})	0	0.25	1.90	4.74
Catalyst	Ni 5%	Ni 5%	Ni 5%	Ni 5%
Gas (wt %)	44.8	57.1	69.8	80.3
Oils (wt %)	16.0	6.5	8.3	0.0
Solid * (wt %)	35.0	30.9	20.0	14.0
H ₂ (Vol.%)	51.1	50.0	51.60	49.5
CO (Vol.%)	0.0	14.9	18.3	21.6
CO ₂ (Vol.%)	0.0	1.0	4.7	6.4
CH ₄ (Vol.%)	19.3	13.7	9.0	5.5
C ₂ -C ₄ (Vol.%)	29.7	20.4	16.3	17.0
H ₂ yield ($\text{g}/100\text{g}$ sample)	3.3	4.4	6.2	6.9
Hydrogen conversion (%)	23.3	31.0	43.2	48.5

*Solid fraction includes carbon deposition, solid residue and waxes obtained after reaction

Results from the pyrolysis-catalytic gasification of PP are detailed in table 5.2. PP also gave a high gas yield, with smaller amounts of wax also being produced at lower steam injection rates. This gave rise to the lower proportion of solids, without steam injection, of 35 wt% compared with 52 wt% for LDPE. Oils produced were initially of a comparable amount to those

from LDPE, around 15 wt%, however oils were still present at 1.90 g h⁻¹ steam injection before being reduced to zero at 4.74 g h⁻¹ of steam. The presence of oils at a higher steam injection rate could be attributed to larger hydrocarbon molecules produced from the pyrolysis of PP compared with LDPE, since PP is made of a larger monomer molecule. Encinar and Gonzalez found similar results, with higher yields of oil obtained from the pyrolysis of PP when compared with PE [2]. The content of hydrogen in the gas is slightly lower than was observed for LDPE and remains around 50 vol.% irrespective of the steam injection rate. The amount of methane and C₂-C₄ hydrocarbons was also higher than was obtained for LDPE, between 17.0 and 29.7 vol.% compared with 12.5 and 21.4% for LDPE, again as a result of the larger molecules in the pyrolysis gas. As was the case for LDPE carbon monoxide and carbon dioxide in the gas stream increase with the steam injection rate, from 0 to 21.6 vol.% for CO and 6.4 vol.% for CO₂, with CO again in higher proportions than CO₂, as was observed for the LDPE sample. The hydrogen yield for PP when no steam was injected is comparable to that of LDPE at 3.3 g/100g sample, however, whilst increasing the steam injection rate does produce a larger yield, the increase is not as substantial as was observed for LDPE. The maximum hydrogen yield obtained was again achieved with the highest steam injection rate and had a value of 6.9 g/100g sample, compared with 9.2 g/100g sample for LDPE. This is a hydrogen conversion of 48.5%, also lower than was obtained for LDPE. This shows that less of the PP sample was converted into hydrogen than was the case with LDPE. The hydrogen conversion for PP was higher than that obtained for the WEEE plastic sample and ABS from chapter 4, which gave values of 18 and 30%, but actually lower than the 55% that was obtained for the HIPS sample. However PP gave a higher yield in actual terms with 6.9 g/100g sample compared with 1.5, 1.8, 3.6 g/100g sample for WEEE, ABS and HIPS respectively. This shows that whilst less of the hydrogen in the PP sample is converted than in HIPS, it remains a more suitable plastic for hydrogen production as a result of its large yield.

5.1.2.3 Polystyrene

From the pyrolysis-catalytic gasification of PS a smaller yield of solids than LDPE when no steam was injected, 35 wt% compared with 52 wt%, largely because almost no waxes were produced in the reactor. Unlike LDPE and PP, PS produced a larger oil yield and smaller proportion of gases as can be

seen in table 5.3. The proportion of oils was as high as 53.0 wt% without steam injection for PS, whilst LDPE and PP only gave values of 14 and 16 wt% respectively. Enicar and Gonzalez [3] also undertook pyrolysis of various plastics and found that polystyrene gave higher oil yields and lower gas yields than PP and LDPE. This is likely due to the aromatic nature of the PS plastic, making it more difficult to breakdown into smaller hydrocarbon gases. Oil yields make up more than half of the mass balance when no steam was injected, but reduces with increasing water injection rate to 25.1 wt% at 4.74 g h⁻¹. This is still a higher proportion than was obtained for either LDPE or PP when no steam was injected, demonstrating how difficult it is to break down the aromatic structure of the plastic.

Table 5.3 Mass balance, gas composition and hydrogen yield from the pyrolysis-gasification of PS

Sample	PS	PS	PS	PS
Water injection (g h ⁻¹)	0	0.25	1.90	4.74
Catalyst	Ni 5%	Ni 5%	Ni 5%	Ni 5%
Gas (wt %)	11.7	23.9	46.4	56.1
Oils (wt %)	53.0	37.7	31.0	25.1
Solid * (wt %)	35.0	38.4	18.2	12.3
H ₂ (Vol.%)	77.2	68.5	64.4	60.0
CO (Vol.%)	0.0	16.7	22.2	26.3
CO ₂ (Vol.%)	0.0	0.9	6.3	8.2
CH ₄ (Vol.%)	12.0	8.5	4.0	2.2
C ₂ -C ₄ (Vol.%)	10.7	5.4	3.2	3.2
H ₂ yield (g/100g sample)	2.7	3.8	6.9	7.4
Hydrogen conversion (%)	30.9	43.4	78.4	83.6

*Solid fraction includes carbon deposition, solid residue and waxes obtained after reaction

PS also shows a comparatively higher hydrogen content in the gas phase compared with PP and LDPE, with values of up to 77 vol.% obtained, as seen in table 5.3. This is due to the proportion of hydrocarbons in the gas stream being significantly lower than was observed for the other samples,

with C₂-C₄ hydrocarbons particularly less abundant. This was again attributed to the aromatic nature of the PS sample, since these gases are harder to produce from aromatic carbons. As was the case with the other plastics hydrocarbon gases were reduced and carbon monoxide and carbon dioxide were increased as the steam injection rate was increased, as seen in table 5.3, due to increased steam reforming. C₂-C₄ hydrocarbons reduce from 10.7 to 3.2 vol%, whilst CO and CO₂ increase from 0 to 26.3 and 8.2 vol.% respectively. When no steam was injected to the reactor the hydrogen yield from PS was lower than was obtained for each of the other plastics, at a value of 2.7 g/100g sample compared with 3.3 g/100g sample for both LDPE and PP. With increased steam injection the hydrogen yields increased. The maximum hydrogen yield obtained with PS was at 4.74 g h⁻¹ steam injection rate and had a value of 7.4 g/100g sample, a conversion of 83.6%. The yield of 7.4 g/100g sample was higher than was obtained for PP, 6.9 g/100g sample, but lower than was obtained for the LDPE plastic, 9.2 g/100g sample. The hydrogen conversions at large steam injection rates were high with a maximum value of 83.6%, and were higher than was obtained for either LDPE or PP at all steam injection rates. Hydrogen yields and conversions were also both higher than was obtained for the WEEE plastics in chapter 4.

5.1.3 Study of catalyst

XRD plots of the fresh catalyst and used catalysts from PP pyrolysis-gasification experiments with and without steam injection are found in figure 5.1. The fresh catalyst shows the presence of alumina, and nickel oxide with a particle size of around 5 to 10 nm. The used catalyst without steam instead shows peaks for Ni as opposed to NiO, and has larger particle sizes of around 50 to 100 nm. This suggests that hydrogen produced during the process reduces the NiO to Ni, and that sintering of the Ni particles occur as a result of the high temperature. The presence of a peak at 26 ° indicates graphitised carbon build up on the catalyst surface. The XRD plot for the used catalyst when steam was injected at a rate of 4.74 g h⁻¹ shows a similar profile to that of the used catalyst without steam, with nickel and alumina peaks observed. A marked difference between the two samples is the lack of a peak representing carbon on the surface, suggesting carbon has reacted with the steam injected.

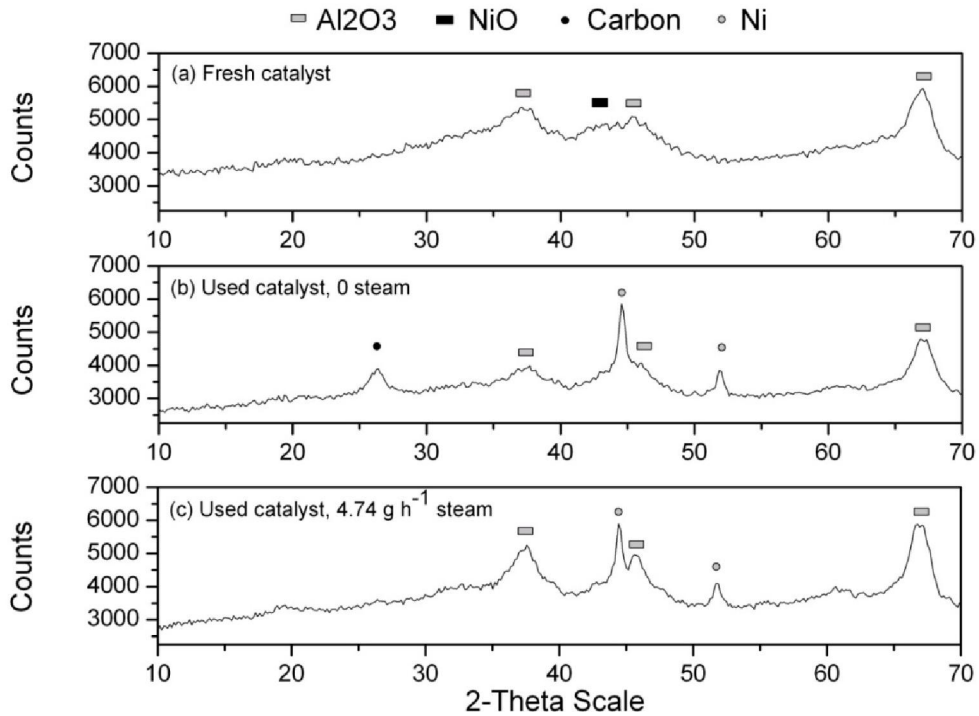


Figure 5.1 XRD analysis of (a) fresh Ni Al₂O₃ catalyst, (b) used Ni Al₂O₃ catalyst with 0 steam injection and (c) used Al₂O₃ catalyst with 4.74 g h⁻¹ steam injection

5.2 Carbon deposits

The solid carbons deposited on the surface of the catalyst were analysed by a range of techniques including scanning and transmission electron microscopy (SEM and TEM), temperature programmed oxidation (TPO) and Raman spectroscopy.

5.2.1 Low Density Polyethylene

For LDPE scanning electron microscopy images of the carbon deposits obtained at different steam injection rates are shown in figure 5.2. Figure 5.2 (a) shows that the deposits on the catalyst surface with no steam injection are predominantly filamentous type carbons. There was a dense covering of these carbons which were fairly long and thin. When steam was added to the reactor, the SEM images shown in figure 5.2 (b) for 0.25 g h⁻¹ steam injection continue to show long thin filamentous type carbons. However they were not as densely covered across the catalyst surface due to steam reacting with the carbons on the catalyst surface.

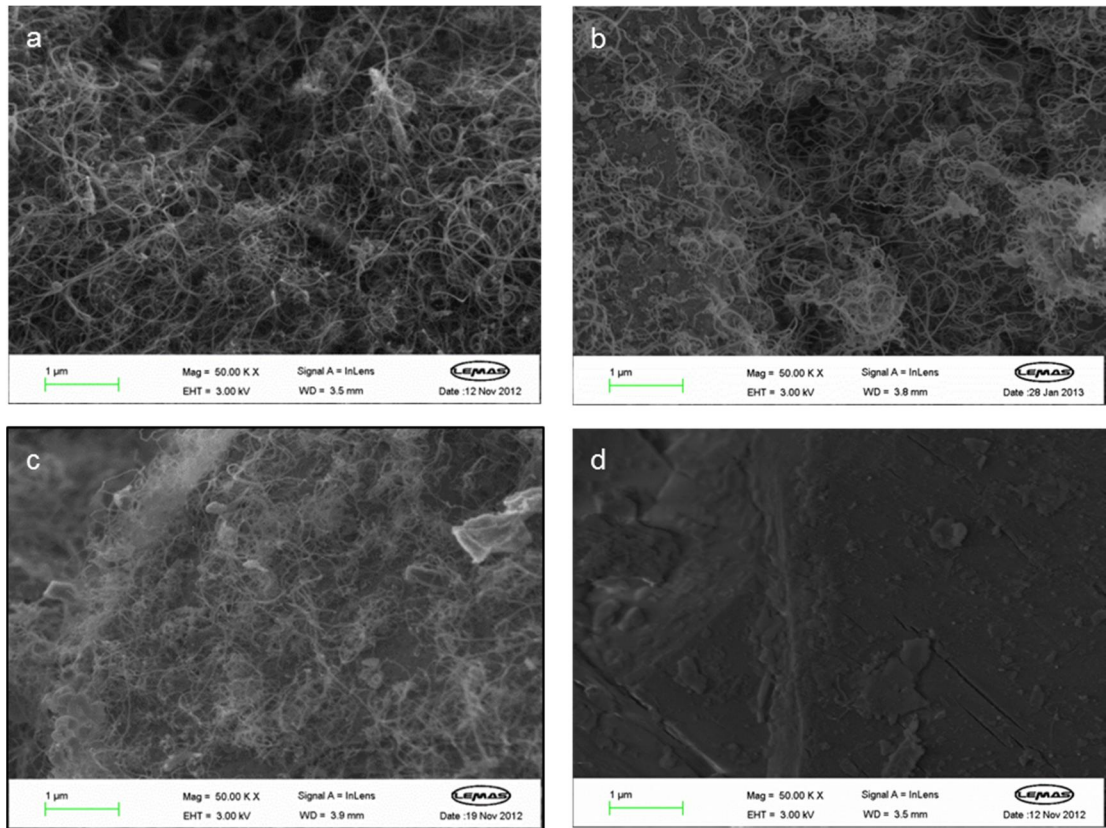


Figure 5.2 SEM images of carbon deposits obtained from LDPE at steam flow rates of (a) 0 g h^{-1} , (b) 0.25 g h^{-1} , (c) 1.90 g h^{-1} and (d) 4.74 g h^{-1}

As the steam flow rate was increased further to 1.90 g h^{-1} and 4.74 g h^{-1} the SEM images in figure 5.2 (c) and (d) show fewer carbon deposits. At 1.90 g h^{-1} steam injection, the filamentous carbons are shorter and much more sparsely spread across the catalyst surface and when the steam injection rate was increased further to 4.74 g h^{-1} , there were no filamentous carbon deposits on the catalyst surface. The increased amount of steam appears to have completely reacted with all carbon deposits. The increase in H_2 production observed at the higher steam injection rates is likely to be a result of steam reacting with carbon deposits, as seen in reaction 5.2 in addition to steam reforming.

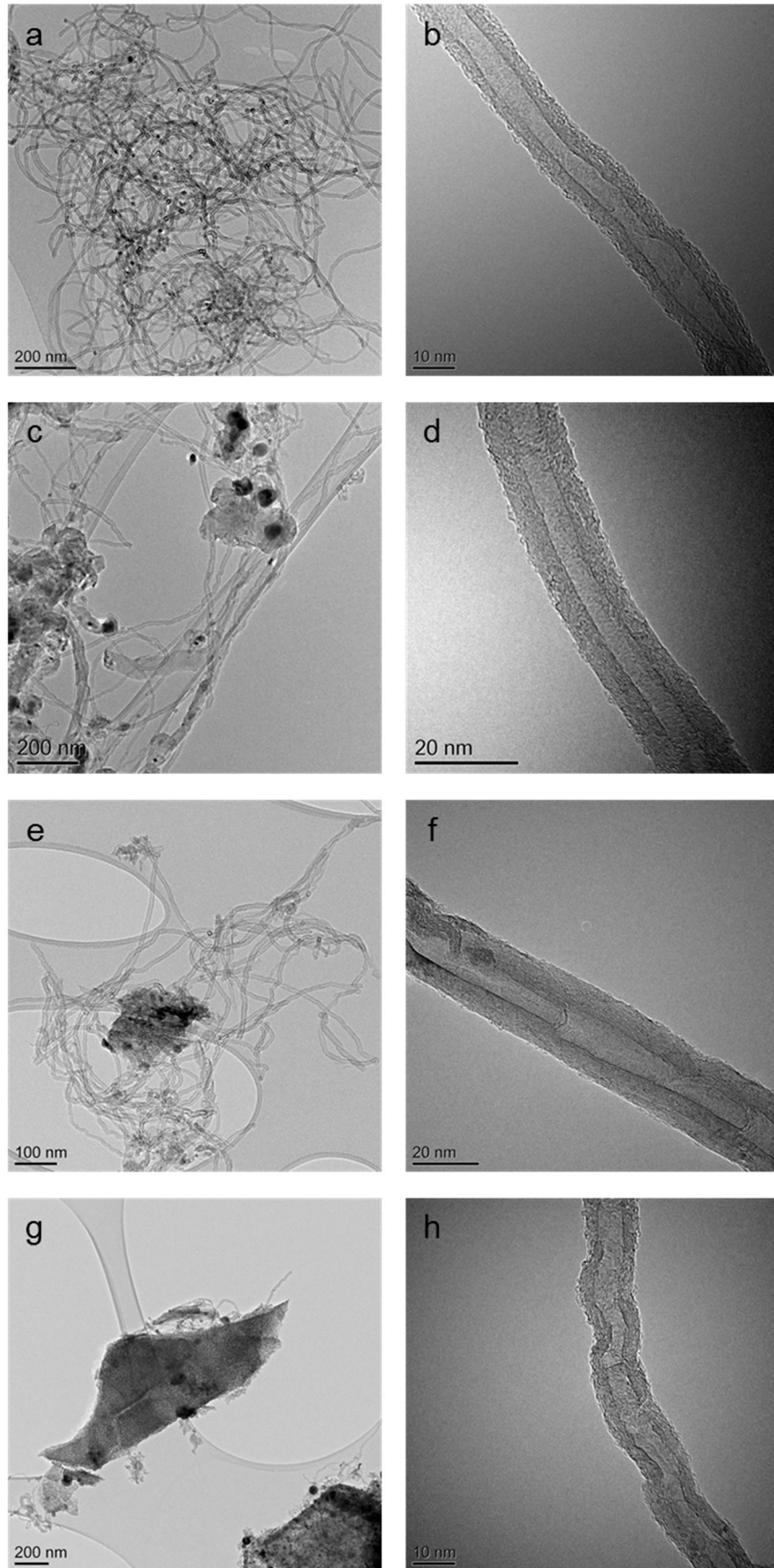


Figure 5.3 TEM images of carbon deposits obtained from LDPE at steam flow rates of (a-b) 0 g h^{-1} (c-d) 0.25 g h^{-1} , (e-f) 1.90 g h^{-1} and (g-h) 4.74 g h^{-1}

Transmission electron microscopy was also undertaken on the used catalysts to further examine the nature of the carbon deposition on the catalyst surface. Figures 5.3 (a-h) show the carbon deposits formed from LDPE with varying steam injection rates. Multi walled carbon nanotubes were confirmed which were between 10 and 20 nm in diameter. With no steam injection TEM images in Figure 5.3 (a) and (b) show that large bundles of these carbon nanotubes were produced. As the steam injection rate was increased to 0.25 g h^{-1} , 1.90 g h^{-1} and 4.74 g h^{-1} figure 5.3 (c) and (d), (e) and (f) and (g) and (h) respectively show how the amount of carbon nanotubes produced was reduced, as seen in the SEM images (figure 5.2). In figure 5.3 (g) and 3(h) for the steam injection rate of 4.74 g h^{-1} only a small number of CNTs were observed whereas none were seen from SEM. The nature of the CNTs appears to stay fairly similar irrespective of steam injection, with irregularities and deformities in the CNT structure apparent at all steam rates, and the CNT diameters remained fairly stable. The length of the carbon nanotubes obtained varied with the rate of steam injection. SEM images in figure 5.2 (a), (b), (c) and (d) show that with no steam injection the CNTs were on the μm scale, around 2-4 μm in length, but when the steam injection was increased the number of longer CNTs decreases to the point where none were observed at 4.74 g h^{-1} steam flow rate.

In order to better determine the relative amounts of the different types of carbon on the catalyst surface, temperature programmed oxidation was carried out on the used catalyst samples. TPO plots for the carbon deposits obtained from LDPE can be seen in figure 5.4 (a), with the corresponding derivative plots seen in figure 5.4 (b). Figure 5.4 (a) shows that increasing the amount of steam added into the reactor leads to a reduction in the amount of carbon on the catalyst surface. This correlates with what was seen from SEM and TEM images seen in figures 5.2 and 5.3 respectively, as higher steam injection rates gasified the carbon deposits.

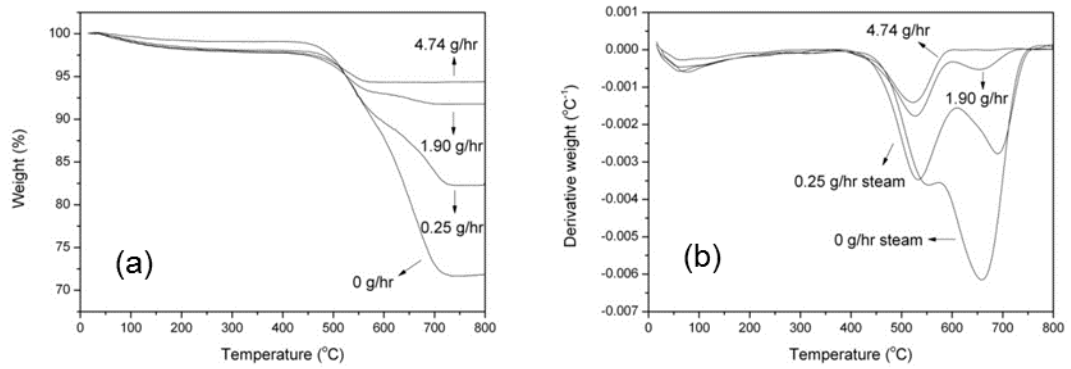


Figure 5.4 Effect of steam on carbon deposition from LDPE: (a) Temperature programmed oxidation, (b) Derivative plot of TPO

The derivative TPO plots in figure 5.4 (b) show two distinct peaks, one at around 540 °C, and another at about 650 °C. Amorphous carbons are reported to show a peak in oxidation and therefore weight loss at lower temperatures than filamentous carbons, due to being more reactive [4]. As such the lower temperature peak was associated with amorphous carbons, whilst the higher temperature peak was associated with filamentous carbons. When no steam was injected the peak associated with the filamentous carbons was large, however the addition of water into the reactor showed that this peak became smaller. This is in accordance with the SEM results in figure 5.2 where a reduction in the amount of filamentous carbons was observed, as steam reacted with carbon deposits via reaction 5.2. Further increasing the steam injection rate produced a reduction in the size of the peak associated with filamentous carbons, until a steam rate of 4.74 g h⁻¹ where virtually none were produced. Table 5.4 shows the mass of filamentous carbons produced from the pyrolysis-catalytic gasification of LDPE. These were calculated from the TPO results and are indicative of CNT production, as CNTs are a type of filamentous carbon observed with TEM. Results show that the yield of filamentous carbons was reduced from 188 mg/ g sample to 0 mg/ g sample as the steam injection rate was increased. Overall there was a downward trend in the production of amorphous carbons as the steam injection rate was increased, with the ratio of filamentous:amorphous carbons, also shown in table 5.4, reducing from 2.30 to 0.

Table 5.4 Production of filamentous and amorphous carbons obtained from LDPE

Plastic	LDPE	LDPE	LDPE	LDPE
Steam injection (g h ⁻¹)	0	0.25	1.90	4.74
Filamentous carbon production (mg/ g sample)	188	76	16	0
Amorphous carbon production (mg/ g sample)	82	113	71	57
Ratio of filamentous carbons: Amorphous carbons	2.30	0.67	0.23	0

Raman spectroscopy was also undertaken to characterise the carbon deposits produced, with the spectrum for LDPE shown in figure 5.5. Peaks are seen at wavenumbers of 1589 cm⁻¹ and 1348 cm⁻¹. The peak at 1589 cm⁻¹ corresponds to the G peak associated with graphitic carbon structures within the sample, including carbon nanotubes, whilst the peak at 1348 cm⁻¹ corresponds with the D peak and is associated with defects within the graphitic lattice or amorphous carbons [5]. For LDPE at 0 g h⁻¹ steam injection rate, figure 5.5 (a) shows that large G and D peaks are observed and that the G peak is significantly larger than the D peak. This suggests a high purity of CNTs since more graphitic carbons are produced than amorphous carbons or defects in the graphitic structure. Figure 5.5 (b) shows that once steam is injected the size of the peaks reduce, particularly the G peak. Higher steam injections of 1.90 g h⁻¹ and 4.74 g h⁻¹ as shown in figure 5.5 (c) and (d) show that the size of the peaks were significantly reduced as carbon deposits are reduced further by increased gasification.

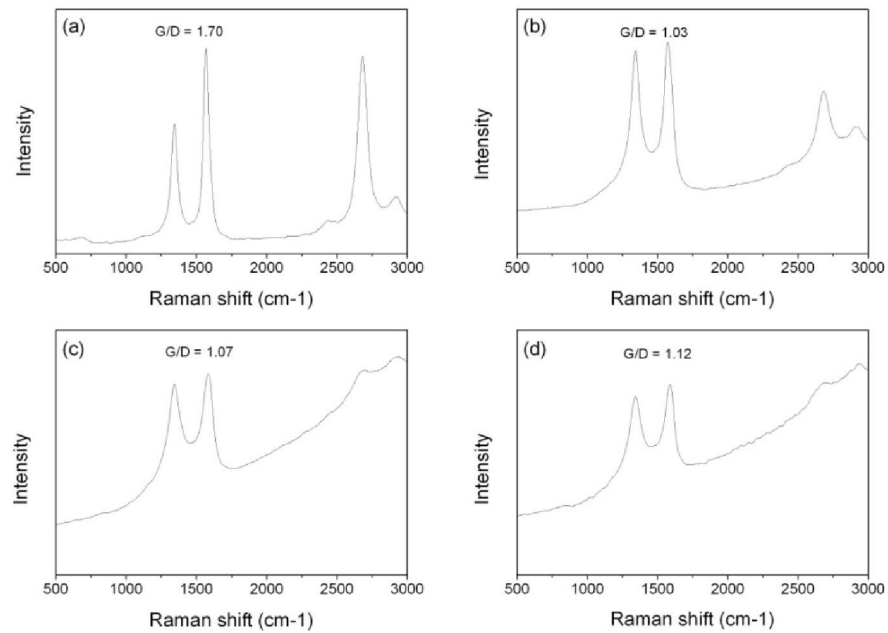


Figure 5.5 Raman spectrums for carbon deposits from LDPE with (a) 0 steam injection, (b) 0.25 g h^{-1} steam injection, (c) 1.90 g h^{-1} steam injection and (d) 4.74 g h^{-1} steam injection

The ratio between the size of the G peak and D peak can be used to compare the quality of the carbon deposits obtained in terms of how ordered and graphitic they are [6-8]. This will enable the purity of the CNTs produced to be evaluated, with a larger G/D ratio indicating a higher purity. For LDPE, the addition of water was detrimental to the purity of CNTs, with a significant decrease observed. A large G/D ratio of over 1.7 was obtained with no steam injection, falling to 1.0 once steam was added.

5.2.2 Polypropylene

The same analyses were also used to investigate the carbon deposits on the catalyst surface produced during the pyrolysis-catalytic gasification of PP. SEM images of the carbon deposits on the catalysts surface obtained using PP as a feedstock can be seen in figure 5.6. Similarly to the images for the carbon deposits on the catalyst when using LDPE, long thin filamentous carbons are observed along with amorphous carbon deposits. With no steam injection filamentous deposits produced from PP appear not as abundant as was seen with LDPE. When a steam injection rate of 0.25 g h^{-1}

was applied, the amount of filamentous carbons appears to remain fairly similar. Raising the steam injection rate further to 1.90 g h^{-1} , figure 5.6 (c), and 4.74 g h^{-1} , figure 5.6 (d), shows a clear reduction in the amount and length of the filamentous carbons deposited on the catalyst. As with LDPE the filaments at no steam injection and a steam injection rate of 0.25 g h^{-1} are on the μm scale, but at higher steam injection rate the length of the filamentous carbons reduce, as can be seen in figures 5.6 (a), (b), (c) and (d). This again suggests that at these higher steam injection rates, gasification of filamentous carbons occurs. This also accounts for the increased hydrogen and carbon monoxide production observed as the steam injection rate was increased.

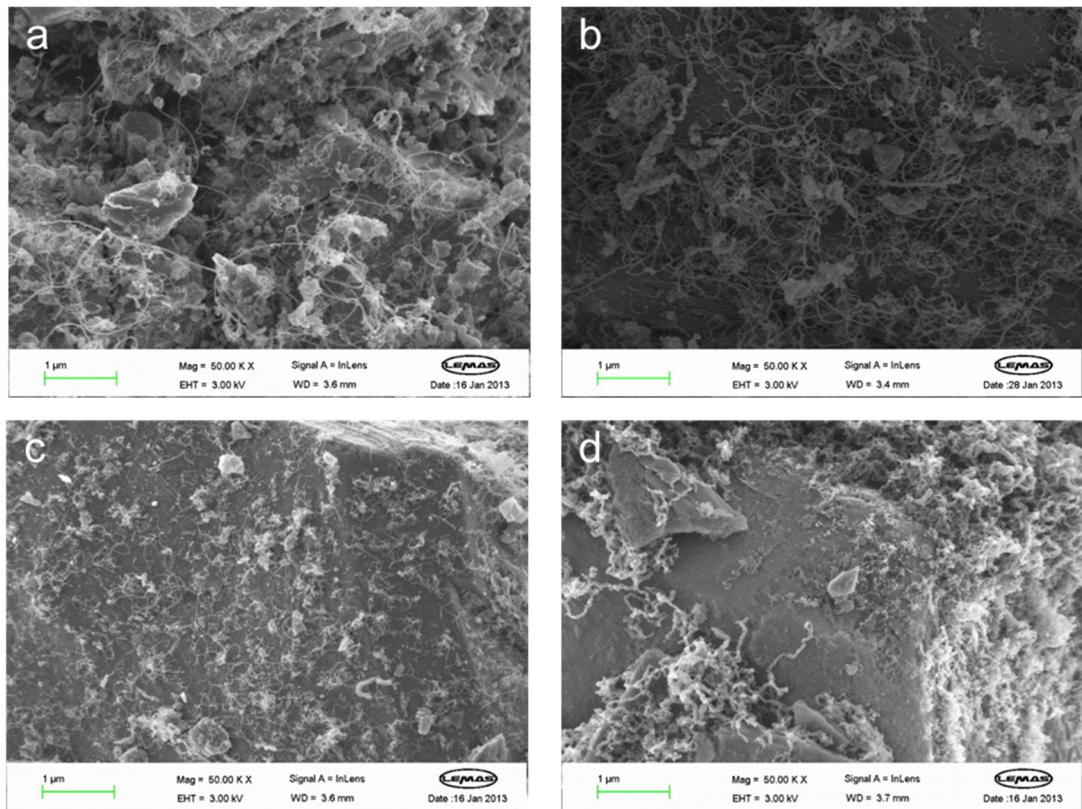


Figure 5.6 SEM images of carbon deposits obtained from PP at steam flow rates of (a) 0 g h^{-1} , (b) 0.25 g h^{-1} , (c) 1.90 g h^{-1} and (d) 4.74 g h^{-1}

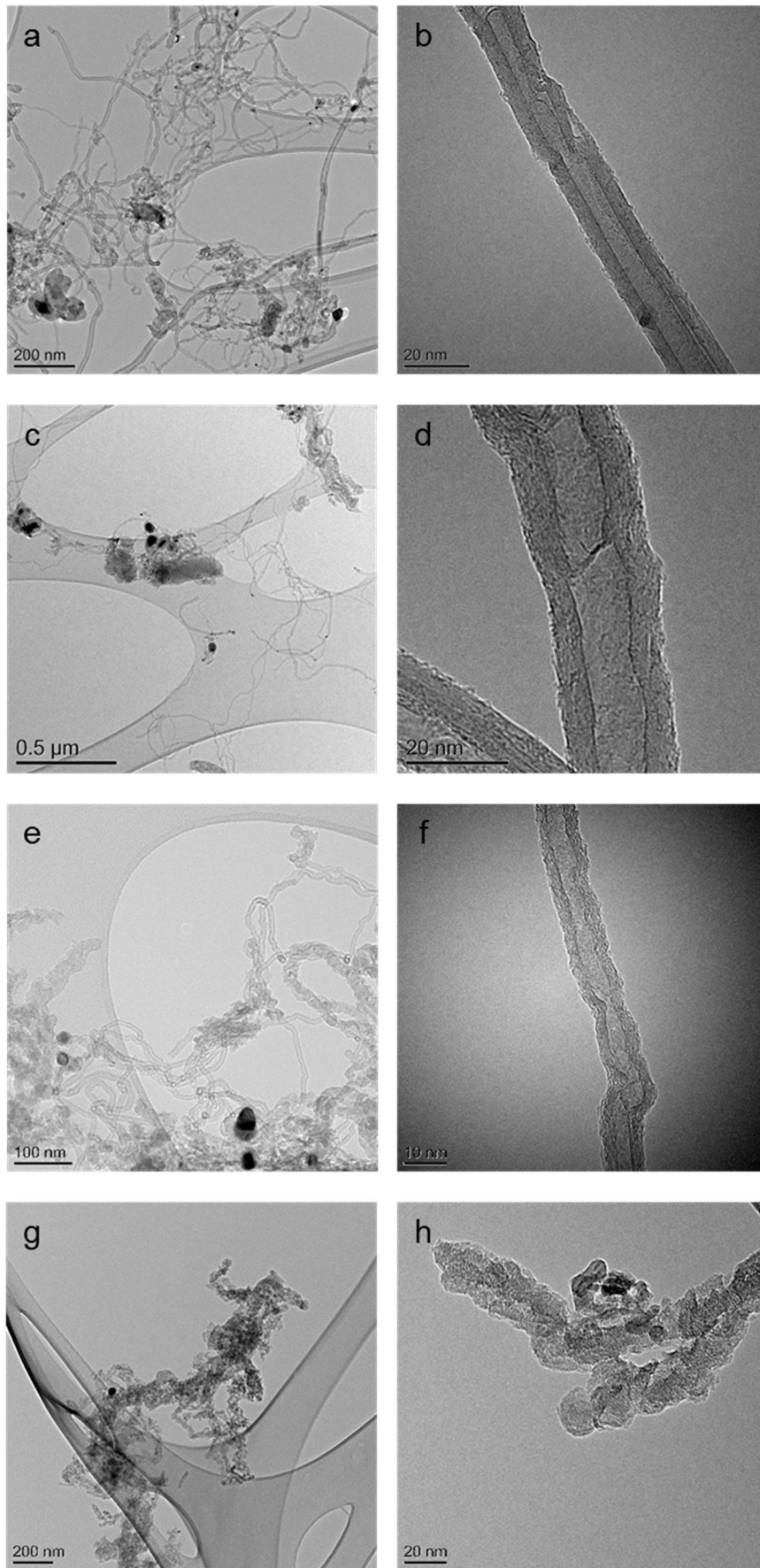


Figure 5.7 TEM images of carbon deposits from PP (a-b) 0 steam, (c-d) 0.25 g h⁻¹ steam, (e-f) 1.90 g h⁻¹ steam and (g-h) 4.74 g h⁻¹ steam

Figures 5.7 (a) to (h) show the TEM images of the carbon deposits on the catalyst obtained from the pyrolysis-catalytic gasification of the PP feedstock. Similarly to the deposits from LDPE the images show that CNTs are produced for steam injection rates of 0, 0.25 and 1.90 g h⁻¹. Similar diameters between around 10 and 20 nm were also obtained for the CNTs produced from PP feedstock as was found with LDPE. Whilst only CNTs are seen at 0 and 0.25 g h⁻¹ steam injection rate, as the steam injection rate was increased the relative amount of CNTs decreases, to the point where at a steam injection rate of 4.74 g h⁻¹ (figures 5.7 (e) and (f)), only carbon filaments rather than nanotubes were observed. This suggests a change in growth mechanism at higher steam injection rates.

TPO results for the carbon deposition on the catalyst used for the pyrolysis-catalytic gasification of the PP feedstock are shown in figure 5.8 (a), with the corresponding derivative plots shown in figure 5.8 (b). Similarly to LDPE, as the steam injection rate was increased the amount of carbon oxidised from the catalyst surface was reduced as suggested by the SEM and TEM results (figures 5.6 and 5.7 respectively).

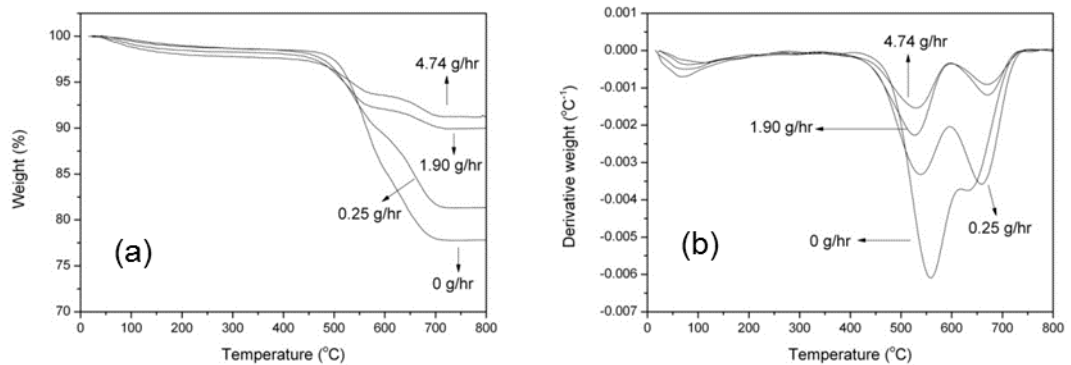


Figure 5.8 Effect of steam on carbon deposition from PP: (a) Temperature programmed oxidation, (b) Derivative plot of TPO

The derivative TPO plots show similarities to those obtained from LDPE, with two distinct peaks observed, again representing amorphous and filamentous carbons. The amount of filamentous carbons produced is shown in table 5.5. Contrary to what was seen with LDPE, a small increase in filamentous carbons was seen from 88 to 104 mg/ g sample at 0.25 g h⁻¹ steam flow rate. The amount of amorphous carbons reduces and as a result the ratio of filamentous to amorphous carbons increases from 0.44 to 0.89.

At higher steam injection flow rates filamentous carbon production falls to around 30 mg/ g sample, with amorphous carbons reducing as well, leading to the filamentous:amorphous ratio falling to 0.33.

Table 5.5 Production of filamentous and amorphous carbons obtained from PP

Plastic	PP	PP	PP	PP
Steam injection (g h ⁻¹)	0	0.25	1.90	4.74
Filamentous carbon production (mg/ g sample)	88	104	33	34
Amorphous carbon production (mg/ g sample)	201	117	97	60
Ratio of filamentous carbons: Amorphous carbons	0.44	0.89	0.33	0.57

Raman spectra for the carbon deposits on the catalyst obtained from the pyrolysis-catalytic gasification of PP are shown in figures 5.9 (a) to (d) and show a similar pattern those obtained from the pyrolysis-catalytic gasification of LDPE. For all the spectra D and G peaks are observed, with larger peaks observed at low steam injection rates and significantly smaller peaks seen at steam injections of 1.90 g h⁻¹ and 4.74 g h⁻¹. The relative height of the G peak compared to the D peak reduces when steam was introduced suggesting that, as was seen with LDPE, the amount of ordered graphitic carbon decreases, and with it the purity of the CNTs. This suggests that whilst an increase in the amount of filamentous carbons was observed for PP at 0.25 g h⁻¹ steam injection, the purity or quality of the CNTs is low. At 4.74 g h⁻¹ the D band is actually larger than the G band, which suggests the deposits are more disordered; in agreement with the TEM images in figure 5.7, since a larger proportion of filaments were seen in comparison to CNTs. The injection of steam into the system resulted in a decrease in the G/D ratio, falling from 1.2 to 1.0, indicating the purity of CNTs in the carbon deposits was decreased.

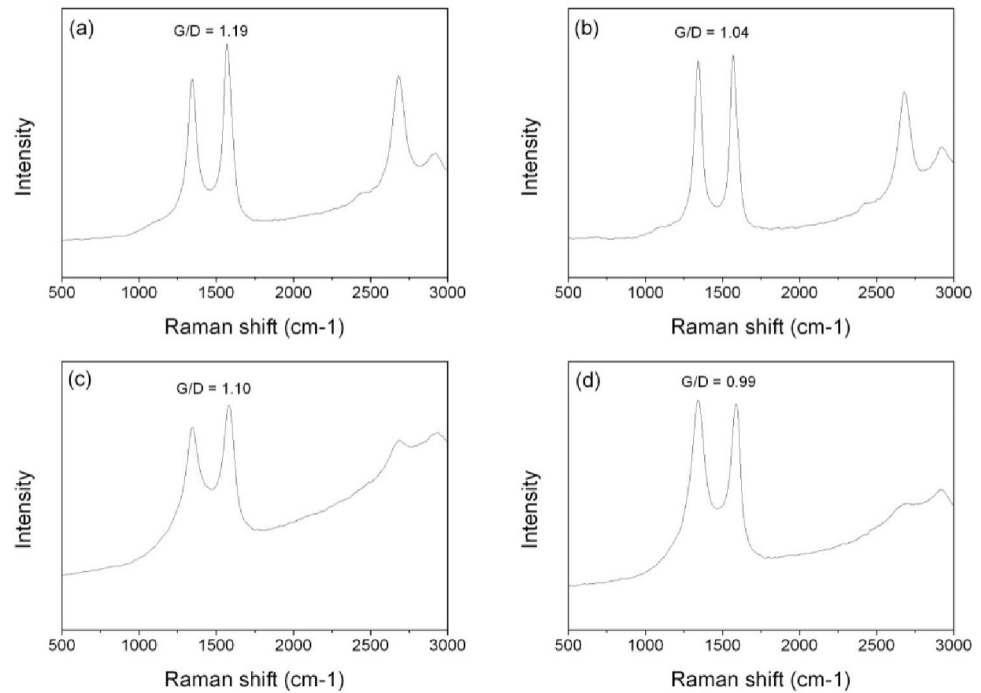


Figure 5.9 Raman spectra for carbon deposits from PP with (a) 0 steam injection, (b) 0.25 g h⁻¹ steam injection, (c) 1.90 g h⁻¹ steam injection and (d) 4.74 g h⁻¹ steam injection

5.2.3 Polystyrene

The SEM images (figure 5.10) of carbon deposits produced on the catalyst used in the pyrolysis-catalytic gasification of PS show long thin filamentous carbons similar to those seen from other plastic samples. The 0 and 0.25 g h⁻¹ steam injection rates show a much larger amount of the long thin filamentous deposits associated with carbon nanotubes than can be seen in figures 5.10 (c) and (d) for steam injections of 1.90 and 4.74 g h⁻¹. The deposits at the higher steam injection rates do however show more carbon deposits than those obtained from the other plastics, but the nature of the filamentous carbons are much thicker and shorter, and more likely to be carbon filaments rather than CNTs. The length of the CNTs obtained without steam injection and at 0.25 g h⁻¹ are comparable to those seen with the other plastic samples, on the μm scale. At higher steam injection rates, some CNTs are still of a μm length, but tend to be shorter at around 1 to 2 μm as opposed to the 3 to 4 μm seen at low steam injection rates as can be seen in the SEM images in figures 5.10 (a), (b), (c), and (d).

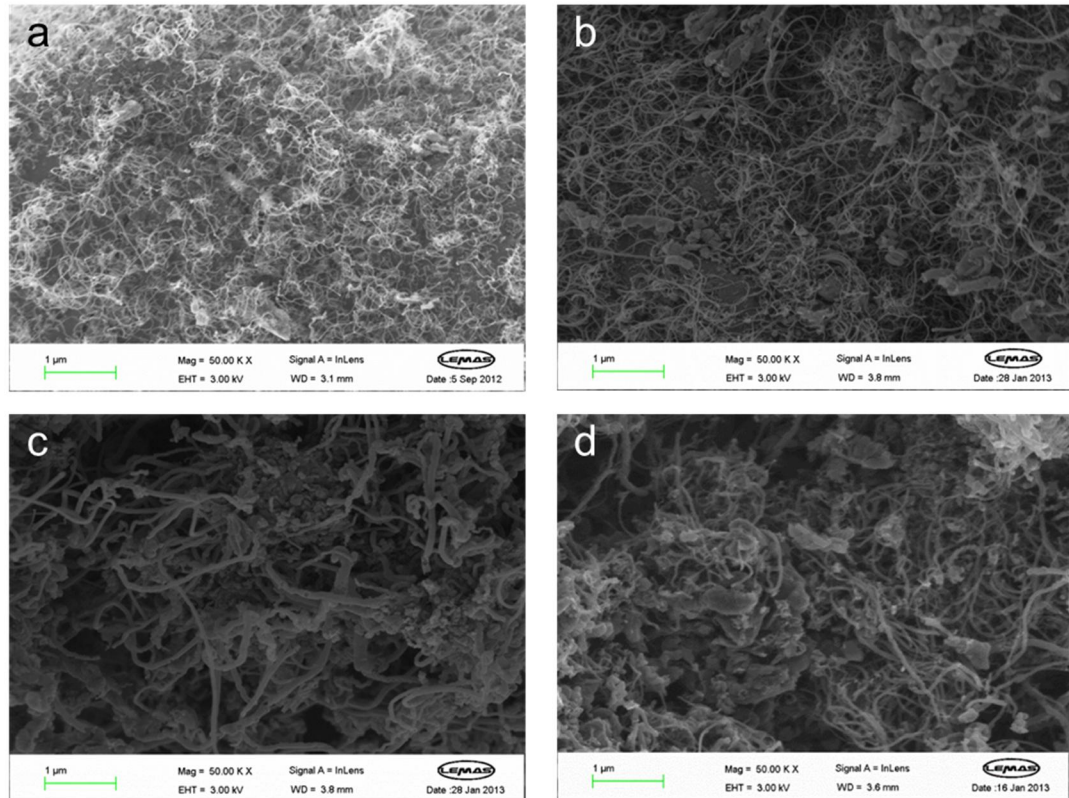


Figure 5.10 SEM images of carbon deposits obtained from PS at steam flow rates of (a) 0 g h^{-1} , (b) 0.25 g h^{-1} , (c) 1.90 g h^{-1} and (d) 4.74 g h^{-1}

The TEM images of the carbon deposits produced on the surface of the catalyst from pyrolysis-catalytic gasification of PS are shown in figures 5.11 (a) to (h). They show that multi walled CNTs are also produced from this feedstock. At 0, 0.25 and 1.90 g h^{-1} steam injection rates the CNTs have diameters of around 10-20 nm as was seen with the other plastics, with some larger diameters also produced, as is seen in figures 5.11 (a) to (f). When the steam injection rate was increased to 4.74 g h^{-1} however, there were very few CNTs observed, with amorphous and filamentous carbons being the predominant deposits. The nanotubes that were observed at this steam injection rate also had a very large diameter, as seen in figures 5.11 (g) and (h).

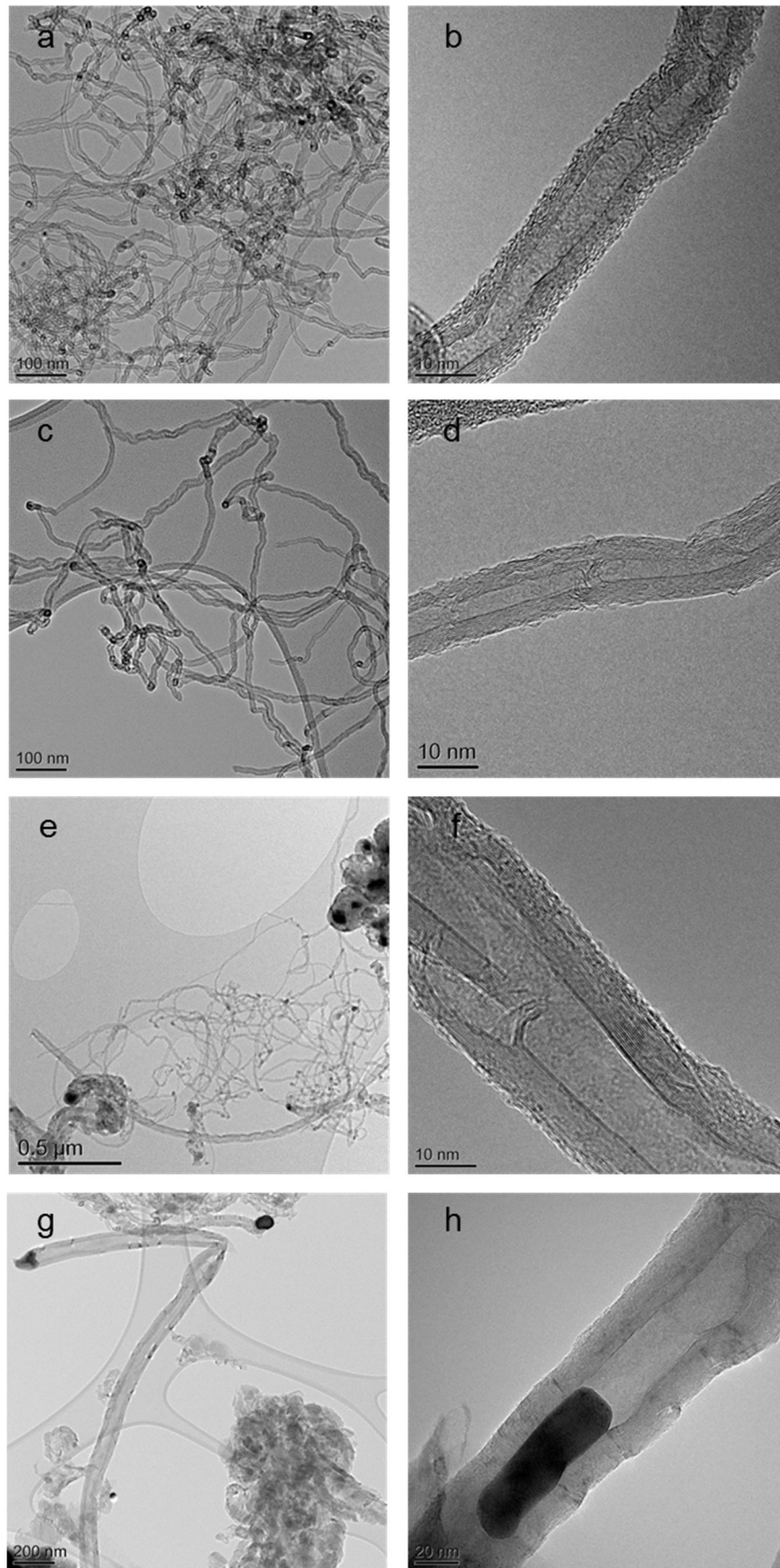


Figure 5.11 TEM images of carbon deposits from PS (a-b) 0 steam, (c-d) 0.25 g h⁻¹ steam, (e-f) 1.90 g h⁻¹ steam and (g-h) 4.74 g h⁻¹ steam

For PS the TPO results of the carbon deposited on the catalyst are particularly interesting, with figure 5.12 showing that unlike the results seen for LDPE and PP, there is actually an increase in the amount of carbon deposition on the surface on the catalyst at a steam injection rate of 0.25 g h^{-1} . At steam rates beyond this the amount of carbon deposition once again drops as witnessed with the other plastic samples. The derivative TPO plot, figure 5.12 (b), reveals that the type of carbon produced at 0.25 g h^{-1} steam injection rate is predominantly filamentous carbon such as carbon nanotubes, along with a small amount of amorphous carbons. The amount of amorphous carbons produced is less than was observed for 0 g h^{-1} steam injection and remains low for the other steam injection rates.

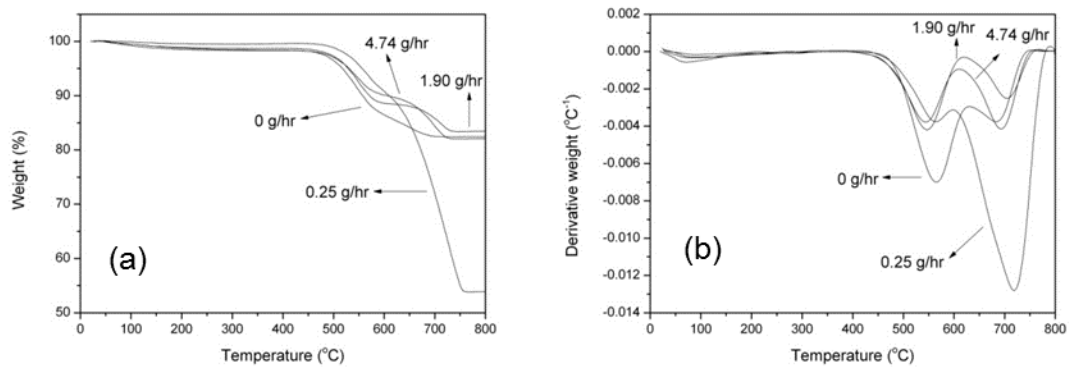


Figure 5.12 Effect of steam on carbon deposition from PS: (a) Temperature programmed oxidation, (b) Derivative plot of TPO

Table 5.6 shows that the amount of filamentous carbons produced from pyrolysis-catalytic gasification of PS first increases when 0.25 g h^{-1} of steam is added up to 324 mg/g sample, before reducing at the higher steam injection rates to 70 mg/g sample. The ratio of filamentous:amorphous carbons at 0.25 g h^{-1} steam flow rate is high, at a value of 4.47. It then shows a similar pattern to the carbons produced with PP, with a reduction at higher steam injection rates as the amount of filamentous carbons reduce.

Table 5.6 Production of filamentous and amorphous carbons obtained from PS

Plastic	PS	PS	PS	PS
Steam injection (g h ⁻¹)	0	0.25	1.90	4.74
Filamentous carbon production (mg/ g sample)	96	324	63	70
Amorphous carbon production (mg/ g sample)	209	73	130	75
Ratio of filamentous carbons: Amorphous carbons	0.46	4.47	0.49	0.92

Raman spectra obtained for the carbon deposits from the pyrolysis-catalytic gasification of PS can be seen in figures 5.13 (a) to (d). As with the spectra obtained from the carbon deposits from experiments with LDPE and PP, G and D peaks are observed, with the relative heights of these varying with the steam injection rate. At 0 and 0.25 g h⁻¹ steam injection rate, (figures 5.13 (a) and (b) respectively) the peaks observed are large, but for PS it can be seen that the height of the G peak compared to the D peak actually increases when 0.25 g h⁻¹ of steam is injected. This contrasts with the results obtained from the other plastic feedstocks where the injection of steam results in a significant reduction in the relative height of the G peak. The rise in this instance is likely to be due to the large increase in the amount of CNTs produced at this steam injection rate, giving more graphitic carbon.

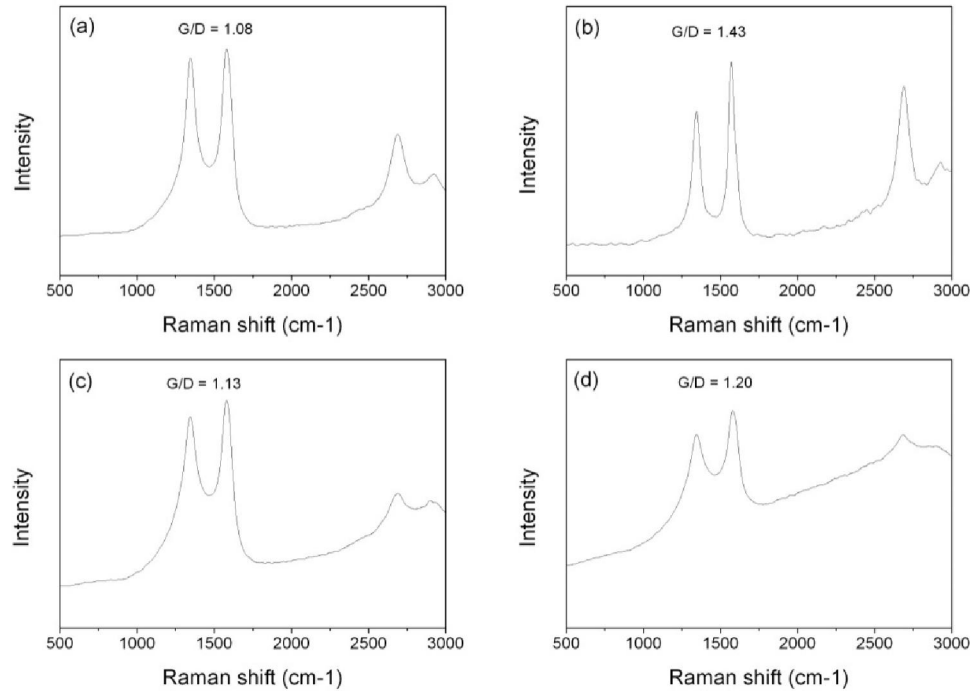


Figure 5.13 Raman spectrums for carbon deposits from PS with (a) 0 steam injection, (b) 0.25 g h^{-1} steam injection, (c) 1.90 g h^{-1} steam injection and (d) 4.74 g h^{-1} steam injection

5.3 Discussion

5.3.1 Production of hydrogen

For each of the plastics, increasing the steam injection rate for the pyrolysis-catalytic gasification process produced an increase in the yield of hydrogen. This was because of an increase in steam reforming and gasification reactions. LDPE produced the highest yields, both with and without steam injection. This can be attributed to two factors; the comparatively small hydrocarbons produced from the pyrolysis stage, and the comparatively small amount of amorphous carbons produced. Smaller hydrocarbons are produced from LDPE pyrolysis due to its comparatively simple structure, and smaller monomers used. As the smaller gases produced from the LDPE sample, such as methane, are easier to break down by steam reforming, more hydrogen is produced. Likewise the catalyst will be deactivated less as a result of the smaller amounts of amorphous carbons produced when no steam is injected. When studying the pyrolysis of different plastics Encinar

and Gonzalez found that PP produced a larger proportion of oils, and smaller amounts of gases compared to PE [2]. These oils are more difficult to breakdown by steam reforming and gasification, and as a result PP gives a lower hydrogen yield. When no steam is injected, the pyrolysis-catalytic gasification of PS produces a low hydrogen yield. This is a result of the aromatic nature of the plastic, but the large amount of amorphous carbons produced could also be a contributing factor, as such carbons deactivate the catalyst. The increase in hydrogen yield observed when steam is injected into the pyrolysis-gasification system then gives PS a higher yield than for PP. Pyrolysis-catalytic gasification of PS produced a larger amount of CNTs compared to PP, as seen in tables 5.5 and 5.6, and this could help explain the larger hydrogen yield obtained. Hydrogen is produced when hydrocarbons decompose on the surface of the catalyst to form solid carbons. As filamentous carbons such as CNTs do not encapsulate and deactivate the catalyst like amorphous carbons do, they allow for a continuous process of hydrocarbon decomposition into solid carbon and hydrogen gas.

Compared to the WEEE plastics from chapter 4, LDPE, PP and PS produced larger yields and conversions of the plastic into of hydrogen. This is partly attributable to the aromatic nature of the WEEE plastics used, which are more difficult to break down via steam reforming. However the aromatic plastic PS also gave significantly higher yields of hydrogen for the pyrolysis-gasification experiment. Therefore another explanation could be the presence of other contaminants or elements in the WEEE plastics disrupting the catalyst or hydrogen production. The ABS, HIPS and WEEE samples used in this study, contained bromine and chlorine [9, 10]. These could potentially have an effect on production of both hydrogen and CNTs, and further work on this topic should be considered for the future.

5.3.2 Effect of steam on carbon deposition

Overall, increasing the amount of steam in the pyrolysis-gasification of the plastics had the effect of reducing the amount of carbon deposits on the catalyst. This is in agreement with the reduction in solid yields observed in tables 5.1-5.3, as steam reacts with the carbon deposits to produce CO and H₂ (reaction 5.2). TPO analyses for each of the carbons, seen in figures 5.4, 5.8 and 5.12, show how the amount of total carbon deposition on the catalyst surface decreases as more steam is injected. This is true for each of

the plastics with the exception of PS at 0.25 g h⁻¹ steam flow rate, which will be discussed later.

Furthermore, increasing the steam injection rate appears to also reduce the amount of filamentous carbons produced, with SEM images in figures 5.2, 5.6 and 5.10 showing the smallest amount observed at steam injection rates of 4.74 g h⁻¹. It is reported by Figueiredo and Trimm [11] that the gasification of filamentous carbons, such as CNTs, occurs as the reverse of their formation mechanism, and that the rate of gasification is independent of the amount of carbon deposited on the supported catalysts. This would suggest that CNTs are formed when the rate of gasification of the deposited carbons is less than the rate of formation. As steam is injected into the reactor, the rate of gasification will increase, and result in the reduction in the yield of filamentous carbons observed. The gasification of these carbon deposits would also account for the increase in hydrogen and carbon monoxide levels at higher steam injection rates as seen in tables 5.1-5.3. When undertaking steam reforming of a model bio-oil compound Wu and Liu [12] found similar results, with increased steam injection leading to a decrease in filamentous carbons produced.

Another effect that steam has on carbon deposits is an increase in the formation of CNTs by increased activity of the catalyst, as a result of destruction of amorphous carbons [13]. For the pyrolysis-gasification of PP and PS at 0.25 g h⁻¹ steam injection rate TPO results of the used catalysts seen in tables 5.5 and 5.6 show an increase in the amount of filamentous deposits produced. Derivative plots shown in figures 5.8 and 5.12 also show that the addition of steam into the reactor leads to a reduction in amorphous carbons. This suggests that the effect of increased CNT production by increased catalytic activity outweighs the effect of steam disrupting the production of CNTs. So whilst some filamentous carbons are destroyed by gasification, the higher activity of the catalyst leads to an overall increase in CNT production.

At steam injection rates beyond 0.25 g h⁻¹ however tables 5.4 – 5.6 show a reduction in the yield of filamentous carbons obtained for each of the plastics. This suggests that more CNTs are prevented by steam inhibition than enabled by increased catalyst activity, leading to a reduction in the overall production of CNTs. This shows that the variation of steam is a key attribute to CNT growth, and that whilst the optimum amount can lead to an increase in the yield, too much steam prevents CNT production. From the

results obtained steam injection rates of 1.90 and 4.74 g h⁻¹ have proven to be unsuitable for CNT production.

From the TEM analyses of the carbon deposited on the catalysts from pyrolysis-gasification experiments using PP and PS, shown in figures 5.7 and 5.11, it can be seen that there is a change in the type of carbon deposits which occur with an increase in steam injection. Whilst CNTs are produced at low steam injection rates, at higher steam injection rates, and particularly at 4.74 g h⁻¹ carbon fibres without a hollow central channel are seen. Snoeck et al [14] suggest that the difference in formation of carbon fibres and CNTs is due to the different rate at which carbon deposition nucleates compared to the diffusion through the nickel catalyst. When carbon deposition occurs at a slow rate it is more likely to form fibres, whilst fast carbon deposition forms CNTs since deposition is fast compared to diffusion, meaning it only occurs around the particles edge, forming a tube. A similar mechanism could explain why carbon fibres are formed rather than CNTs at high steam injection rates, since the rate of carbon formation could be slowed due to the presence of steam.

Steam injection has shown to be of crucial importance to both the production of hydrogen and CNTs. However, the maximum yields of each occur at different steam injection rates. Low steam injection rates of 0 g h⁻¹ and 0.25 g h⁻¹ proved most productive for CNT production, whilst the highest hydrogen yields were obtained at 4.74 g h⁻¹ steam flow rate. This gives the potential for an industrial process which has great flexibility over its production, where by simply changing the steam injection rate the major product can be switched between hydrogen and CNTs.

5.3.3 Effect of plastic type on carbon deposition

The pyrolysis products from the pyrolysis-catalytic gasification of the different plastics had different affinities to produce filamentous carbons and amorphous carbons. This had a strong bearing on their CNT production at different steam injection rates. Whilst SEM and TEM images in figures 5.2, 5.3, 5.6, 5.7, 5.10 and 5.11 showed that CNTs were produced from each plastic, there were differences in the relative abundances of both CNTs and amorphous carbons produced from the different feedstocks. Without steam injection tables 5.4, 5.5 and 5.6 show that LDPE produced 188 mg/ g sample of CNTs, much larger than either PP, 88 mg/ g sample, or PS, 96 mg/ g sample.

It is likely that more CNTs are formed from LDPE since a comparatively small amount of amorphous carbons were seen with this feedstock, with a filamentous:amorphous ratio of 2.30 compared with 0.44 for PP and 0.46 for PS, as shown in tables 5.4, 5.5 and 5.6. This would allow more CNT production from LDPE, whilst PP and PS which produce more amorphous carbons would see CNT growth restricted by deactivation of the catalyst. Accordingly results from Raman spectroscopy showed that LDPE had a much higher purity of CNTs with a G/D ratio of 1.7, compared with 1.2 for PP and 1.1 for PS. Amorphous carbons could be higher for the pyrolysis-gasification of PP and PS as a result of larger hydrocarbons being produced from these feedstocks. This correlates with the results shown in tables 5.1-5.3, which show that PP gave a larger amount of C₂-C₄ hydrocarbons, whilst PS gave a much larger yield of larger oil compounds.

Once steam is injected at a flow rate of 0.25 g h⁻¹, significant changes are observed. The results in tables 5.4, 5.5 and 5.6 show that whilst LDPE shows a reduction in the amount of filamentous carbons, to 76 mg/ g sample, PP and PS see increases to 104 and 324 mg/ g sample respectively. The addition of steam has two effects on the production of filamentous carbons, one is to increase the formation of CNTs by increased activity of the catalyst, as a result of destruction of amorphous carbons [13]. The other is the destruction of CNTs by gasification.

For the pyrolysis-gasification of PP and PS at a steam injection rate of 0.25 g h⁻¹ it suggests that the effect of increased CNT production by increased catalytic activity outweighs the effect of steam disrupting the production of CNTs. This was not true for LDPE. For PP this could be due to the fact that it forms larger molecules when pyrolysed than LDPE. The gas composition in table 5.2 confirms more C₂-C₄ hydrocarbons are produced from PP. Rostrup-Nielsen found that larger molecules form more filamentous carbons [15], and since gasification is independent of the amount of carbon, gasification of these filaments will leave a higher proportion for the carbon deposits from the PP experiment than for LDPE. Increased filamentous carbons found for PS is likely to be due to the fact that aromatic precursors form more filamentous carbons than alkenes [15]. This is also in accordance with the mechanism for production of CNTs from plastics as proposed by Gong et al, who suggested that CNTs are produced from polymerisation of aromatic compounds on the catalyst surface [16]. PS is an aromatic based polymer and would form more aromatics on the catalyst surface than the alkene plastics.

Raman spectroscopy results for carbon deposits produced with PS, showed an increase in the G/D ratio as the purity of CNTs increased. For PP a reduction in G/D ratio was observed, however the increase in filamentous carbon production for this feedstock was very small. This suggests that at 0.25 g h⁻¹ steam injection rate for PP the reduction in the G/D band could be a result of filamentous carbons rather than CNTs being produced. For LDPE a significant reduction in the G/D ratio is seen, from 1.7 to 1.0, concurrent with the reduction in CNT purity as less are produced.

For the higher steam injection rates of 1.90 and 4.74 g h⁻¹, PP and LDPE experiments produced similar results with reductions in the amounts of filamentous carbons observed from SEM, in figures 5.2, 5.6 and 5.10, and from TPO in tables 5.4, 5.5 and 5.6. For a steam injection rate of 4.74 g h⁻¹ the filamentous carbon production was severely depleted with values of 0 and 34 mg/ g sample shown for LDPE and PP respectively. This would suggest that these high steam injection rates are unsuitable for CNT production from alkene hydrocarbons, as the ratio of steam to carbon is too high and simply results in a reaction between the two. Whilst TPO results for PS in table 5.6 show that the amount of filamentous carbons reduced at the higher steam injection rates, more are produced than was observed for LDPE and PP with a value for PS of 70 mg/ g sample at 4.74 g h⁻¹. Jackson et al [17] similarly reported that whilst alkane feedstocks such as pentane and hexane resulted in the production of filamentous carbons disappearing at high steam injection rates, aromatic sources such as benzene, toluene and ethyl-benzene continued to show production of filamentous carbons. In this work, as PS is an aromatic based polymer when the pyrolysis products from the first stage pyrolysis step reach the catalyst they will behave in a manner similar to the aromatic sources used by Jackson et al [17].

5.4 Conclusions

The pyrolysis-gasification of plastics has shown that the production of hydrogen was increased when the steam injection rate was increased. This is ascribed to a combination of increased steam reforming reactions, and also gasification of carbon deposits on the catalyst surface. LDPE produced roughly 65% of the maximum theoretical hydrogen yield, with the relative productions of, LDPE > PS > PP for the percentage of maximum theoretical yield achieved.

With no steam injection LDPE produces a small amount of amorphous carbons and so the catalyst is less readily deactivated and a large number of

CNTs are produced. Even though PS and PP have a better affinity to produce filamentous carbons such as CNTs, they also produce more amorphous carbons from large molecular weight hydrocarbons and so the catalyst is quickly deactivated and less CNTs are produced.

For PS and PP the critical point where the increase in activity of the catalyst outweighs the destruction of CNTs by gasification is reached at 0.25 g h⁻¹ steam flow rate since they produce filamentous carbons more readily, leaving a smaller proportion destroyed by gasification. At higher steam injection rates, more CNTs are prevented to form by gasification and at this point it has a larger effect than the increase in catalytic activity. PS produced the largest yield of filamentous carbons, with 324 mg/ g sample.

Results show that the rate of steam injection is crucial for CNT production. The maximum yields for hydrogen and CNTs occurred at different steam injection rates, since gasification at high injection rates of CNTs gives a higher hydrogen production. Therefore, there is potential for a process with good flexibility over production, where by changing the steam injection rate the major product can be shifted from CNTs to hydrogen.

References

1. Erkiaga, A., et al., *Syngas from steam gasification of polyethylene in a conical spouted bed reactor*. Fuel, 2013. **109**: p. 461-469.
2. Encinar, J.M. and J.F. González, *Pyrolysis of synthetic polymers and plastic wastes. Kinetic study*. Fuel Processing Technology, 2008. **89**: p. 678 - 686.
3. JM, E. and G. JF, *Pyrolysis of synthetic polymers and plastic wastes. Kinetic study*. Fuel Processing Technology, 2008. **89**: p. 678 - 686.
4. Wang, P., et al., *Filamentous carbon prepared by the catalytic pyrolysis of CH₄ on Ni/SiO₂*. Applied Catalysis A: General, 2002. **231**: p. 34-44.
5. Jiang, Z.W., et al., *Polypropylene as a carbon source for the synthesis of multi-walled carbon nanotubes via catalytic combustion*. Carbon, 2007. **45**(2): p. 449-458.
6. Das, N., et al., *The effect of feedstock and process conditions on the synthesis of high purity CNTs from aromatic hydrocarbons*. Carbon, 2006. **44**(11): p. 2236-2245.
7. Qian, W., *Quantitative Raman characterization of the mixed samples of the single and multi-wall carbon nanotubes*. Carbon, 2003. **41**(9): p. 1851-1854.

8. Sengupta, J., et al., *Effect of growth temperature on the CVD grown Fe filled multi-walled carbon nanotubes using a modified photoresist*. Materials Research Bulletin, 2010. **45**(9): p. 1189-1193.
9. Hall, W.J. and P.T. Williams, *Analysis of products from the pyrolysis of plastics recovered from the commercial scale recycling of waste electrical and electronic equipment*. Journal of Analytical and Applied Pyrolysis, 2007. **79**(1-2): p. 375-386.
10. Hall, W.J. and P.T. Williams, *Removal of organobromine compounds from the pyrolysis oils of flame retarded plastics using zeolite catalysts*. Journal of Analytical and Applied Pyrolysis, 2008. **81**(2): p. 139-147.
11. Figueiredo, J.L. and D.L. Trimm, *Gasification of carbon deposits on nickel catalysts*. Journal of Catalysis, 1975. **40**(2): p. 154-159.
12. Wu, C. and R. Liu, *Carbon deposition behavior in steam reforming of bio-oil model compound for hydrogen production*. International Journal of Hydrogen Energy, 2010. **35**(14): p. 7386-7398.
13. Hata, K., et al., *Water-assisted highly efficient synthesis of impurity-free single-walled carbon nanotubes*. Science, 2004. **306**(5700): p. 1362-4.
14. Snoeck, J.W., G.F. Froment, and M. Fowles, *Filamentous Carbon Formation and Gasification: Thermodynamics, Driving Force, Nucleation, and Steady-State Growth*. Journal of Catalysis, 1997. **169**: p. 240-249.
15. Rostrup-Nielsen, J.R., *Coking on nickel catalysts for steam reforming of hydrocarbons*. Journal of Catalysis, 1974. **33**(2): p. 184-201.
16. Gong, J., et al., *Catalytic carbonization of polypropylene by the combined catalysis of activated carbon with Ni₂O₃ into carbon nanotubes and its mechanism*. Applied Catalysis A: General, 2012. **449**: p. 112-120.
17. Jackson, S.D., S.J. Thomson, and G. Webb, *Carbonaceous Deposition Associated with the Catalytic Steam-Reforming of Hydrocarbons over Nickel Alumina Catalysts*. Journal of Catalysis, 1981. **70**: p. 249-263.

6 Investigation into the effect of catalyst type on the production of hydrogen and carbon nanotubes

Catalysts play a key role in the production of both carbon nanotubes and hydrogen via the thermal treatment of plastics. This chapter looks at some of the key characteristics of the catalysts used, including the use of different transition metal catalysts, different metal loadings and the calcination temperature used in the preparation of the catalysts. Nickel, iron, cobalt and copper catalysts were all investigated, since these metals are frequently used for either the production of hydrogen or CNTs. Catalysts with loadings of 5 and 10 wt% nickel, iron, cobalt and copper were all used, prepared by impregnation onto an alumina support. The calcination temperature used for the preparation of the catalysts was also investigated, with 750 °C used for each of the catalyst metals, and a calcination temperature of 500 °C also prepared for the nickel catalyst.

6.1 Influence of catalyst metal

To investigate the effect of different transition metal catalysts on the production of hydrogen and CNTs from the two stage catalytic pyrolysis of LDPE, 10 wt% loadings of nickel, iron cobalt and copper catalysts were prepared and used in experiments. A calcination temperature of 750 °C was used.

6.1.1 Characterisation of fresh catalysts

In order to better understand the properties of the catalysts that were used, a number of analyses were carried out on the fresh 10 wt% catalysts. SEM, TEM-EDX, XRD and TPR were all undertaken (Chapter 3).

6.1.1.1 Nickel alumina

SEM images of the fresh 10 wt% nickel catalyst used for the production of hydrogen and CNTs from the two stage catalytic pyrolysis of LDPE are seen in figure 6.1 (a). The surface is largely smooth, with only a small number of particles observed.

The TEM image of the fresh nickel catalyst in figure 6.2(a) shows a particle which is very uniform in its structure. EDX spectrums, figure 6.3, were taken

for the whole catalyst particle, as well as two points in different regions of the catalyst surface. The spectrum obtained for the area A1 showed the presence of Al, Ni and O, which is expected of the Ni/Al₂O₃ catalyst. The spectrums of points 1 and 2 both show peaks for Al, Ni and O suggesting that the particle is consistent throughout, with nickel, aluminium and oxygen all bonded together.

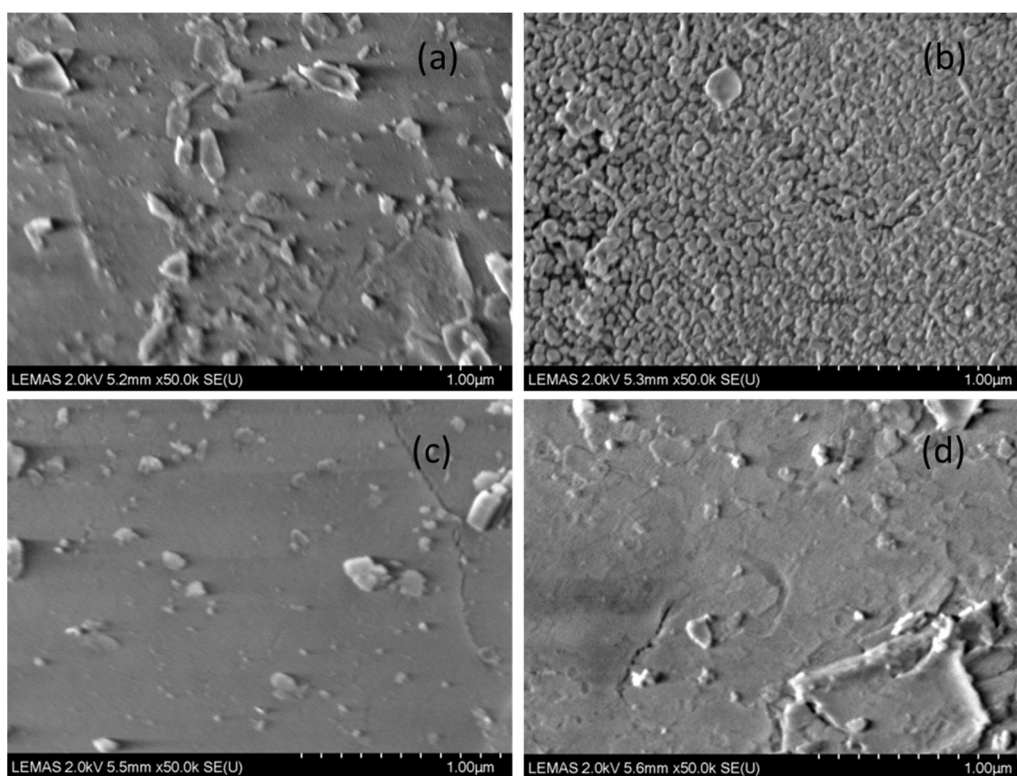


Figure 6.1 SEM images of fresh catalysts used for the two stage pyrolysis of LDPE. (a) Ni/Al₂O₃, (b) Fe/Al₂O₃, (c) Co/Al₂O₃ and (d) Cu/Al₂O₃

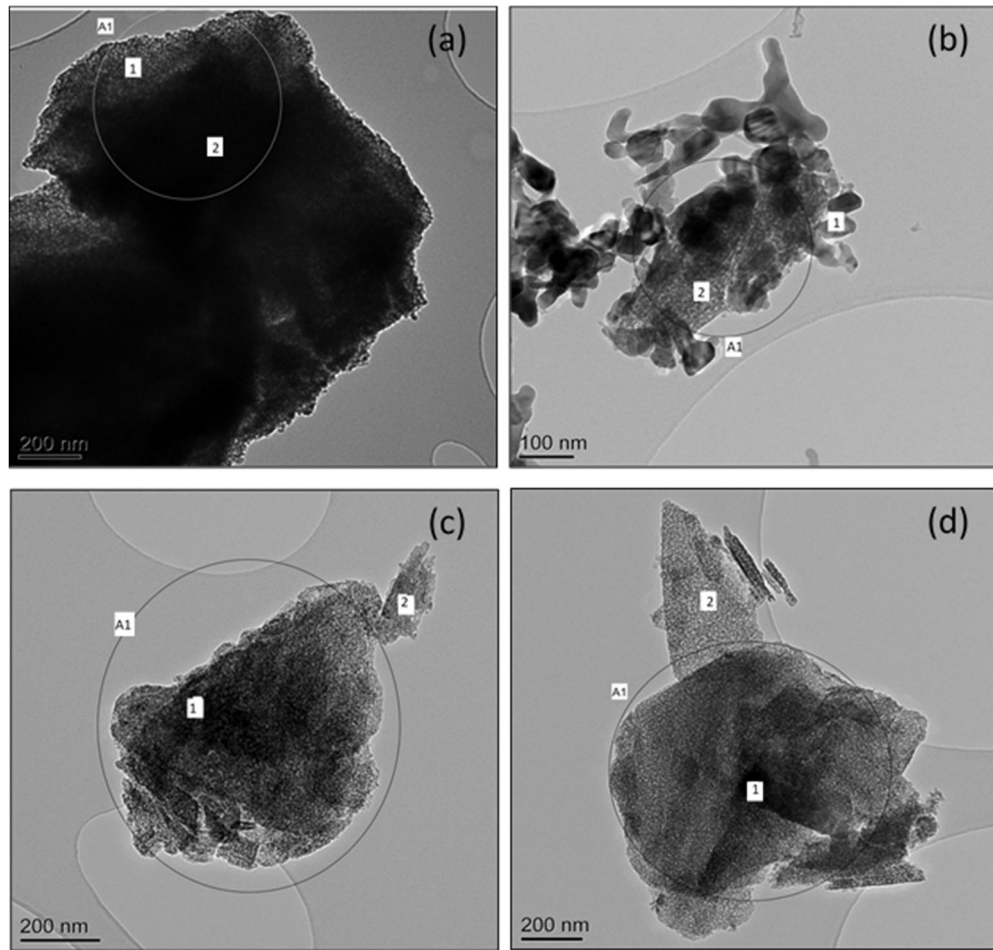


Figure 6.2 TEM images of fresh catalysts used for the two stage pyrolysis of LDPE. Ni/Al₂O₃, (b) Fe/Al₂O₃, (c) Co/Al₂O₃ and (d) Cu/Al₂O₃

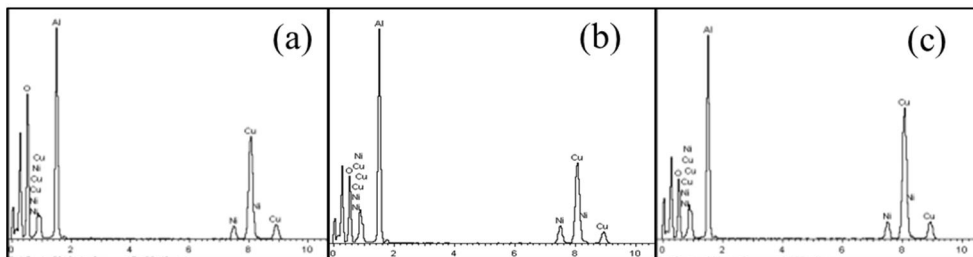


Figure 6.3 EDX spectrums of TEM image of nickel catalyst shown in Figure 6.2(a): (a) Area A1, (b) Point 1, (c) Point 2

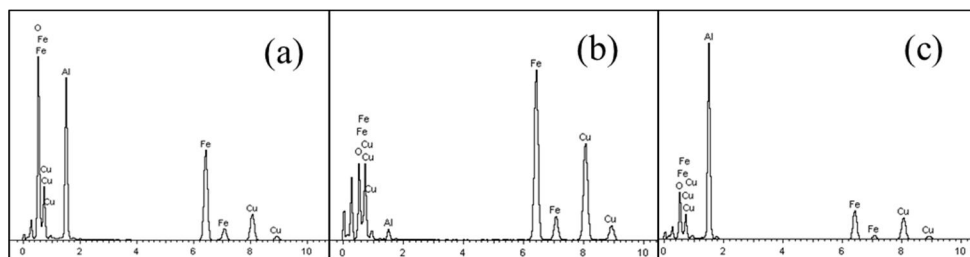


Figure 6.4 EDX spectrums of TEM image of iron catalyst shown in shown in Figure 6.2(b): (a) Area A1, (b) Point 1, (c) Point 2

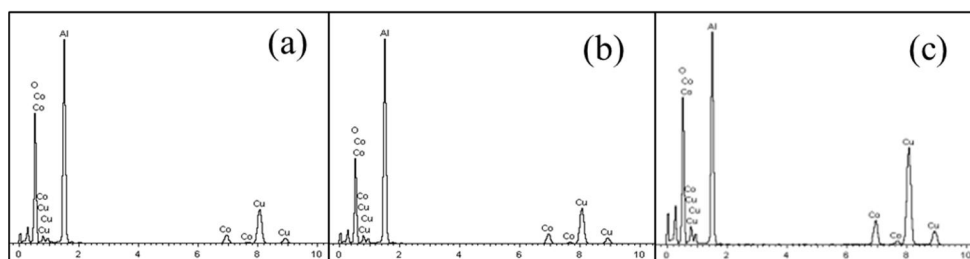


Figure 6.5 EDX spectrums of TEM image of cobalt catalyst shown in shown in Figure 6.2(c): (a) Area A1, (b) Point 1, (c) Point 2

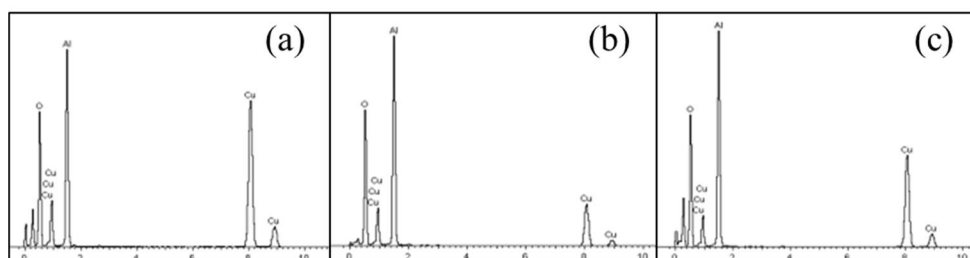


Figure 6.6 EDX spectrums of TEM image of copper catalyst shown in shown in Figure 6.2(d): (a) Area A1, (b) Point 1, (c) Point 2

Results from XRD of the fresh 10 wt% nickel catalyst, seen in figure 6.7, show peaks associated with NiAl_2O_4 (nickel aluminate) and Al_2O_3 and small peaks for NiO . Nickel aluminate is formed at high calcination temperatures such as the one used in this study [1, 2], when NiO bonds to the alumina support. The XRD results agree with the TEM-EDX images and show the presence of a catalyst which is largely comprised of nickel, aluminium and oxygen bonded together as a nickel aluminate.

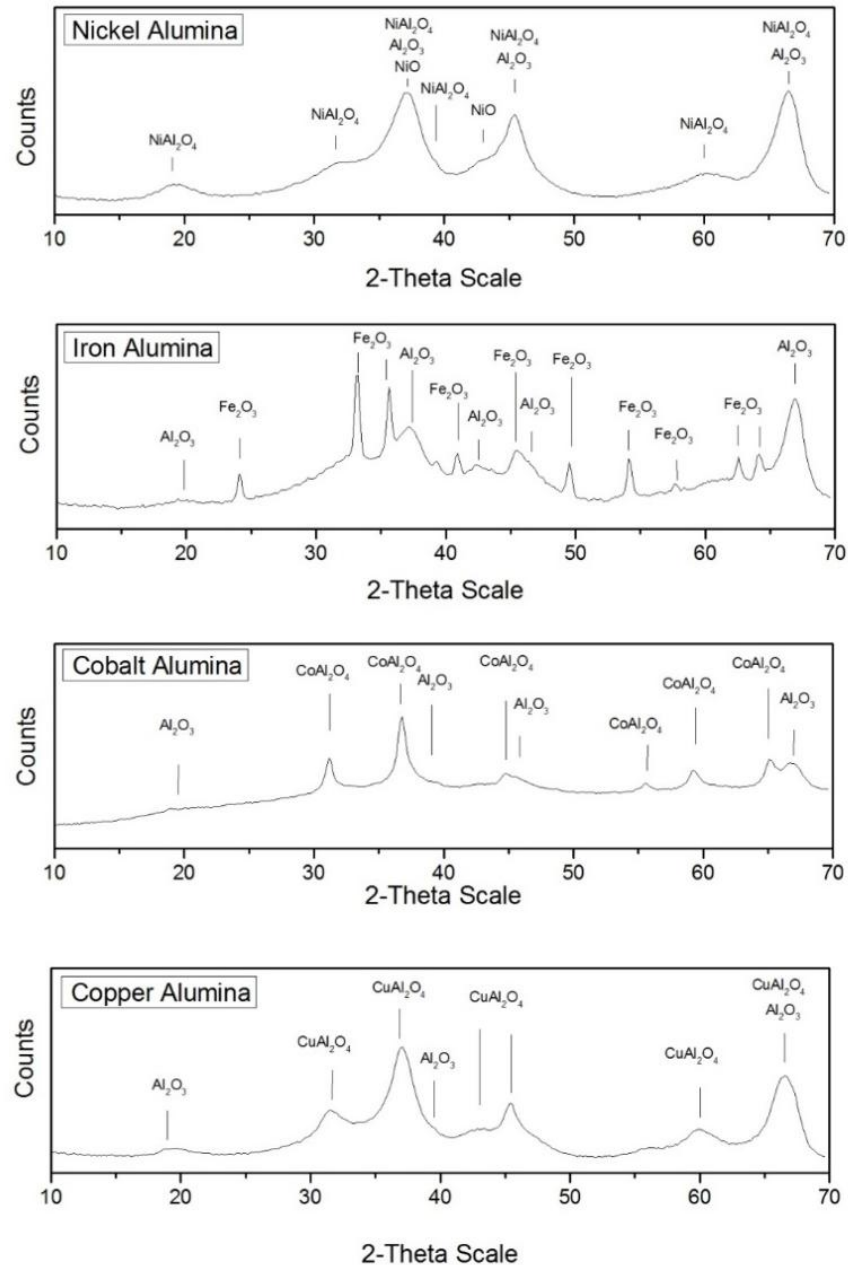


Figure 6.7 XRD investigation of the fresh catalysts used in two stage pyrolysis of LDPE

TPR results for the fresh nickel catalyst are shown in figure 6.8, with a large peak observed at a temperature of 800 °C. A number of studies have found similar results and attribute the peak to the reduction of nickel aluminate [3-5]. Again this agrees well with previous analyses in identifying the catalyst as being predominantly composed of nickel aluminate. NiO particles were not clearly identified from the TEM or TPR analyses, implying that only very small quantities were present.

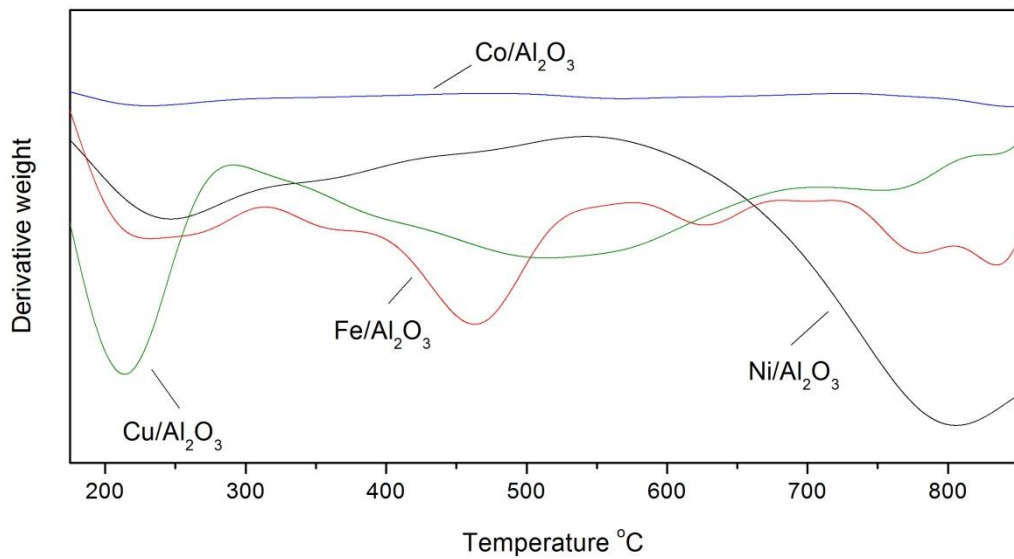


Figure 6.8 Investigation of the fresh catalysts used for the two stage pyrolysis of LDPE by temperature programmed reduction

6.1.1.2 Iron alumina

The SEM image of the fresh 10 wt% iron catalyst used to produce hydrogen and CNTs by two stage catalytic pyrolysis of LDPE is shown in figure 6.1 (b). It shows a marked difference to the nickel catalyst, with a large number of particles spread across the catalyst surface. The TEM image in figure 6.2(b) for the fresh iron catalyst shows differences to the nickel catalyst with two different phases observed. The EDX spectrum, figure 6.4, for the area A1 showed peaks for Fe, Al and O, consistent with an iron alumina catalyst. However, there are notable differences in the spectrums of point 1 and point 2, representing the different parts of the catalyst. Whilst point 2 showed Fe, Al and O, point 1 only produced peaks for Fe and O. This suggests that a form of iron oxide is present on the catalyst. The presence of iron oxide suggests that not all the iron is bonded to the alumina as an aluminate as was the case with the nickel catalyst prepared at the same conditions. This is in accordance with literature which reports that iron forms aluminates less readily than nickel [6].

XRD results of the fresh 10 wt% Fe catalyst, shown in figure 6.7, support the conclusions drawn from the TEM-EDX analysis, with both Fe_2O_3 and Al_2O_3 present in the catalyst. TPR results in figure 6.8 show that the iron catalyst produces a broad peak at 450 °C, with a further series of peaks at temperatures between 700 and 850 °C. The reduction of iron oxide

supported on alumina is complex and occurs in a number of stages [7-9]. Park et al report that a first peak between 400 and 560 °C is related to the conversion of Fe_2O_3 into Fe_3O_4 , which subsequently is reduced into FeO and Fe metal at 600 – 800 °C [9]. As such, the first peak observed in TPR represents the first stage of reduction into Fe_3O_4 , whilst further peaks represent the subsequent reduction to FeO and Fe. Iron aluminate is reported to reduce at temperatures above 850 °C [10], and so the peak observed above 800 °C could be related to this. It is suggested that the iron catalyst contains iron oxide which has not bonded to the alumina to form an aluminate. The main TPR peak for the iron catalyst is at a lower temperature than that of the nickel catalyst, indicating the iron is more easily reduced, and so less strongly bonded to its alumina support.

6.1.1.3 Cobalt alumina

The SEM image of the fresh 10 wt% cobalt catalyst, figure 6.1(c) bares similarities to the nickel catalyst, with a relatively smooth surface, and a small number of particles. Similarly to nickel, the cobalt catalyst also shows a uniform structure in its TEM image in figure 6.2(c). The EDX spectrum, figure 6.5, obtained for the whole particle in area A1, showed the presence of Co, O, and Al, consistent with a $\text{Co}/\text{Al}_2\text{O}_3$ catalyst. To gain more insight into the catalyst structure, as with the other catalysts, two EDX spectrums of specific points on the catalyst surface were obtained, (figure 6.5). Both the points revealed the presence of Co, O and Al, suggesting that as with nickel, the catalyst is all in one phase with Co bonded to the alumina.

XRD results in figure 6.7 show the presence of CoAl_2O_4 (cobalt aluminate) along with alumina, consistent with TEM-EDX results in portraying a catalyst with cobalt bonded to the alumina support. The lack of cobalt oxide agrees well with literature since Co is reported to form aluminates more readily than both nickel and iron [6]. TPR results (figure 6.8) for the fresh 10 wt% cobalt catalyst show no significant peak associated with reduction in the temperature range tested. Previous TPR studies however do not report reduction of cobalt aluminate until temperatures of 1200 K; higher than used here [11]. Along with the lack of a significant peak at lower reduction temperatures, this leads to the suggestion that the cobalt in the catalyst is present in the form of cobalt aluminate. This is in agreement with both TEM-EDX and XRD analyses, and suggests the cobalt is very strongly bonded to the alumina, since it is hardly reduced at temperatures below 900 °C.

6.1.1.4 Copper alumina

The fresh 10 wt% copper catalyst is also noticeably similar in its nature to the cobalt and nickel catalysts in its SEM image, (figure 6.1 (d)). Like the fresh cobalt and nickel catalysts, the TEM image of the fresh copper catalyst in figure 6.2(d) is fairly uniform. The EDX spectrum, figure 6.6, of the whole catalyst particle predictably is comprised of peaks for Cu, Al and O, whilst the spectrums from points 1 and 2 also show the same result. As with the nickel and cobalt catalysts this shows that the fresh copper catalyst is consistent throughout, suggesting a single phase composition such as copper aluminate.

XRD results, shown in figure 6.7, confirm the presence of CuAl_2O_4 (copper aluminate), with alumina also present. TPR results from the fresh copper catalyst, figure 6.8, show a large peak at around 200 °C in addition to a broad peak between 350 and 650 °C. These results are consistent with the reduction of CuO and CuAl_2O_4 for the low and high temperature peaks, respectively [12, 13]. CuO was barely observed in XRD, however Luo et al found similar results [12], and attributed the lack of CuO in XRD to its highly disperse nature. As such it is thought that the peak observed in this case is similarly highly disperse CuO which has not formed into bulk CuO.

6.1.2 Mass balance and hydrogen production

Results for the mass balance in terms the amount of gases, solids and liquids produced from the two stage catalytic pyrolysis experiments using the 10 wt% metal catalysts, and also the uncatalysed pyrolysis, can be seen in table 6.1. Solids constitute carbon deposition on the catalyst, and the small amounts of wax which were also obtained. When no catalyst is used, the proportion of gases, 63.2 wt%, is large compared to the proportions of oils and solids, 25.0 wt% and 3.0 wt% respectively. The addition of a catalyst leads to a reduction in the gas yield for each of the catalysts in favour of solid products. As a reduction in waxes was observed this suggests that hydrocarbons in the gas streams are converted into solid carbons when a catalyst is used. Other than for the iron catalyst, where a reduction to 17.0 wt% is observed, the proportion of liquids remains largely unchanged. The nickel catalyst shows a small reduction in oils to 24.0 wt%, whilst the cobalt and copper catalysts show slight increases to 27.0 wt% and 29.0 wt% respectively. In terms of the performance of different metals, the iron catalyst produced a smaller amount of gases than the nickel; 51.5 wt% compared

with 55.2 wt%. The iron catalyst also produced a much larger yield of solids with 24.0 wt% compared with 11.0 wt%, suggesting a larger amount of carbon deposition. The cobalt and copper catalysts on the other hand produce results far more comparable to the nickel catalyst in terms of gases, solids and liquids with both producing only slightly more oils, and less solids than the nickel catalyst.

Gas compositions and hydrogen conversions for the different catalysts are shown in table 6.1. The hydrogen conversion is based upon the amount of hydrogen in the LDPE sample from results obtained from an elemental analysis (table 3.1). When no catalyst is used, the gas composition is largely comprised of C₂-C₄ hydrocarbons, 56.6 vol%, with 27.0 vol% methane, and smaller amounts of hydrogen, 16.4 vol%. The addition of a catalyst leads to a significant reduction in the yield of C₂-C₄ hydrocarbons, with values of 39.8, 29.6, 43.8 and 47.4 vol% for the nickel, iron, cobalt and copper catalysts respectively. Methane sees smaller reductions from 27.0 vol% uncatalysed to 23.6, 19.8, 24.9 and 26.6 vol% for the nickel, iron, cobalt and copper catalysts respectively. The reduction in the proportion of hydrocarbons is met with an increase in the proportion of hydrogen. Values increase from 16.4 vol% for the uncatalysed reaction up to 36.6 vol% for the nickel catalyst, 50.6 vol% for the iron catalyst, 31.3 vol% for the cobalt catalyst and 26.0 vol% for the copper catalyst. This suggests that hydrocarbons are deposited on the surface of the catalysts to produce an increase in solid carbons and hydrogen. The hydrogen conversion from the uncatalysed reaction is fairly low with a value of 6.5%. All the catalysts used resulted in an increase in the hydrogen yield and hydrogen conversion. Whilst the amount of gases produced from the iron catalyst was less compared to that of the nickel, the relative concentration of hydrogen in the gas is significantly higher and the concentrations of hydrocarbons are lower. This results in a large hydrogen conversion of 26.8%. Cobalt and copper catalysts however produce a lower yield of hydrogen than the other catalysts, with conversion values of 12.8% and 10.1% for cobalt and copper respectively, compared with a value of 16.5% for nickel. Nickel catalysts are widely reported to be effective at hydrogen production when compared to iron, cobalt and copper, however in this instance it has been outperformed by iron. The large yield for iron in this instance could be due to the fact that a larger amount of carbon deposition occurred, as shown by its high solid yield in the mass balance. Since hydrogen is given off during carbon deposition, a larger amount of carbon would result in a corresponding high yield in hydrogen. It is noted

that steam was not introduced in the experiment; therefore catalytic thermo-cracking reactions are dominant during the pyrolysis of plastics.

Table 6.1 Effect of catalyst metal on mass balance, gas composition and hydrogen conversion from the two stage pyrolysis of LDPE

Catalyst	-	Ni Al ₂ O ₃	Fe Al ₂ O ₃	Co Al ₂ O ₃	Cu Al ₂ O ₃
Loading (wt%)	-	10	10	10	10
Gas (wt%)	63.2	55.2	51.5	54.6	55.0
Oils (wt%)	25.0	24.0	17.0	27.0	29.0
Solid (wt%)	3.0	11.0	24.0	9.0	7.0
H ₂ (vol%)	16.4	36.6	50.6	31.3	26.0
CH ₄ (vol%)	27.0	23.6	19.8	24.9	26.6
C ₂ -C ₄ (vol %)	56.6	39.8	29.6	43.8	47.4
Hydrogen production (g/100g sample)	0.9	2.3	3.7	1.8	1.4
Hydrogen conversion (%)	6.5	16.5	26.8	12.8	10.1

6.1.3 Carbon nanotube production

6.1.3.1 Scanning and Transmission Electron Microscopy

Both scanning electron microscopy (SEM) and transmission electron microscopy (TEM) were undertaken on the used catalysts from the two stage catalytic pyrolysis of LDPE. This was done in order to investigate the carbon deposition on the surface, with particular interest in carbon nanotubes. SEM images of the used 10 wt% nickel catalyst are shown in figure 6.9(a), where the catalyst shows a covering of filamentous carbons.

TEM images shown in figure 6.10(a) confirmed that the filaments observed were carbon nanotubes. The images reveal the presence of carbon nanotubes along with a number of loose metal particles, which have separated from the catalyst surface. Metal particles are also seen inside the carbon nanotubes, indicating the tip, rather than base growth mechanism [14].

Like the SEM images for nickel catalyst, the images seen for the carbon deposits on the used iron catalyst in figure 6.9(b) also show a dense covering of filamentous carbons. TEM images in figure 6.10 (b) confirm the presence of carbon nanotubes, which are multi walled. The TEM images also show the presence of a greater number of metal particles than was observed from the used nickel catalyst, and CNTs with a larger diameter. Larger diameter CNTs are thought to be produced from larger metal particles [15-17], which could have formed as a result of the weaker metal support interaction the iron catalyst demonstrates. A weaker support interaction would allow sintering of the iron to form larger metal particles. The weak support interaction would also explain the presence of a larger amount of loose metal particles, since they would separate from the support more readily.

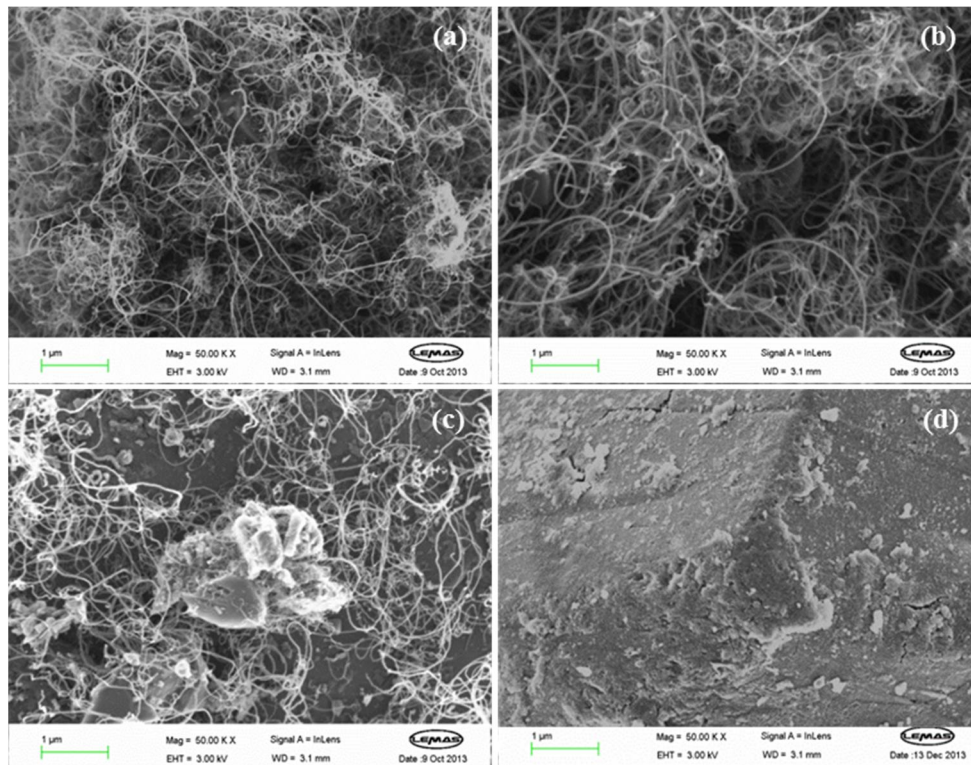


Figure 6.9 Scanning electron microscopy of the carbon deposits on the used catalysts from the two stage pyrolysis of LDPE: (a) Ni/Al₂O₃, (b) Fe/Al₂O₃, (c) Co/Al₂O₃ and (d) Cu/Al₂O₃

The SEM images of carbon deposits from the cobalt catalyst used for the two stage catalytic pyrolysis of LDPE are seen in figure 6.9(c). The images show the presence of long thin filamentous carbons. However they are not as densely packed as on the surface of the iron or nickel catalysts, suggesting that less are produced. TEM images in figure 6.10(c) also confirmed the presence of multi walled carbon nanotubes. The CNTs show a much narrower diameter, and very few loose metal particles. TPR results of the fresh catalyst (figure 6.8) revealed cobalt to have a very strong support interaction, which would restrict sintering of the metal catalyst and result in smaller CNT diameters. It is also possible that the strong interaction could inhibit the production of CNTs, by restricting sintering to such an extent that the metal particles formed are either too small for CNT growth or too strongly attached. The strong metal-support interaction would also prevent metal particles from becoming detached from the catalyst surface, supporting the lack of metal particles observed from this catalyst.

The used copper catalyst in contrast to the other metals shows almost no filamentous carbons on the SEM image in figure 6.9(d). This indicates that almost no carbon nanotubes were produced on this catalyst. TEM images of the carbon deposits on the catalyst in figure 6.10(d) accordingly only showed the presence of amorphous carbons, with no filamentous or carbon nanotubes observed. The TEM image revealed very large metal particles produced on the copper catalyst, suggesting the presence of weakly attached copper oxides particles which have sintered. It is suggested that the dispersed CuO particles can be easily reduced (figure 6.8), leading to a significant amount of sintering and metal particles which are too large to form carbon nanotubes.

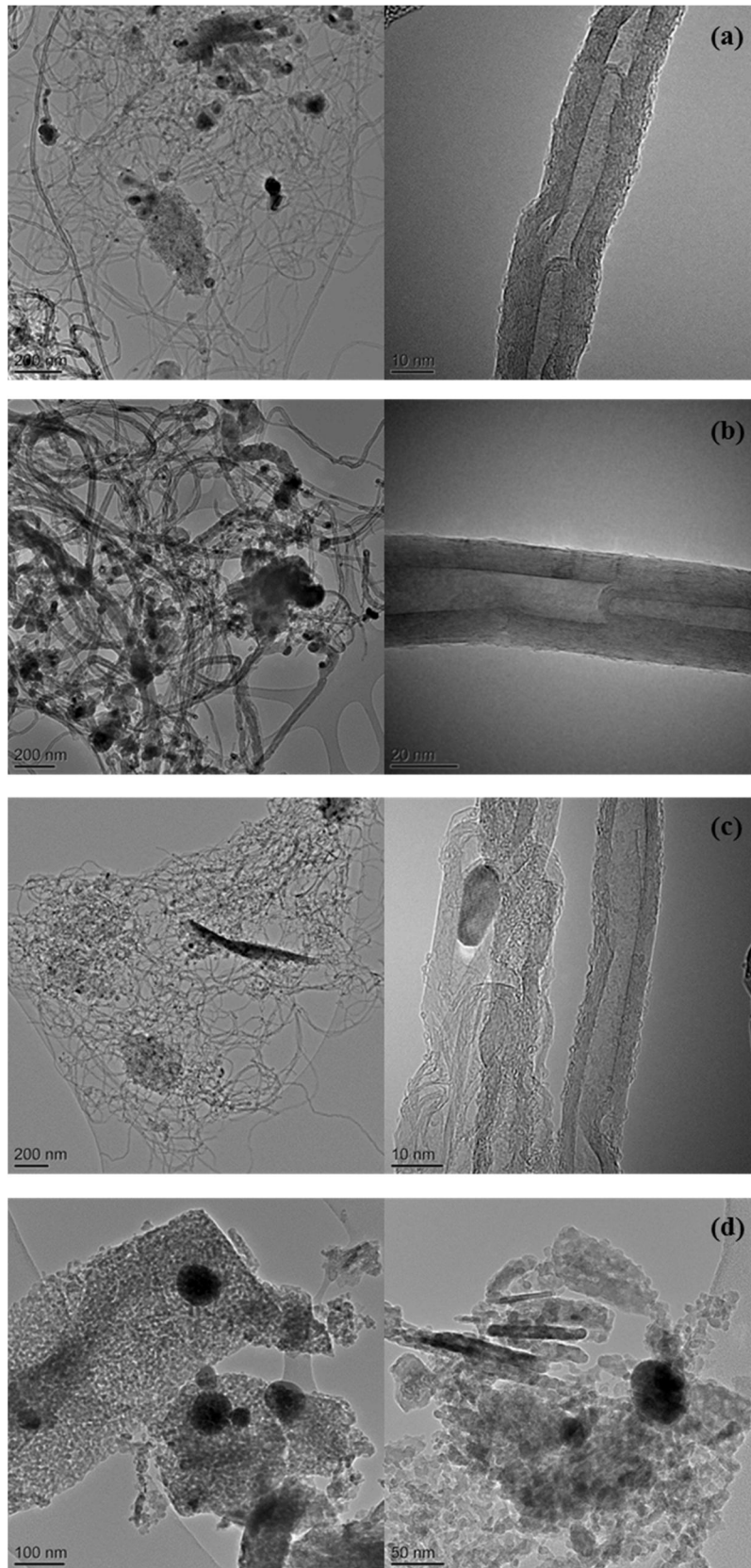


Figure 6.10 Transmission electron microscopy of the carbon deposits on the used catalysts from the two stage pyrolysis of LDPE: (a) Ni/Al₂O₃, (b) Fe/Al₂O₃, (c) Co/Al₂O₃ and (d) Cu/Al₂O₃

6.1.3.2 X-Ray Diffraction of the used catalysts

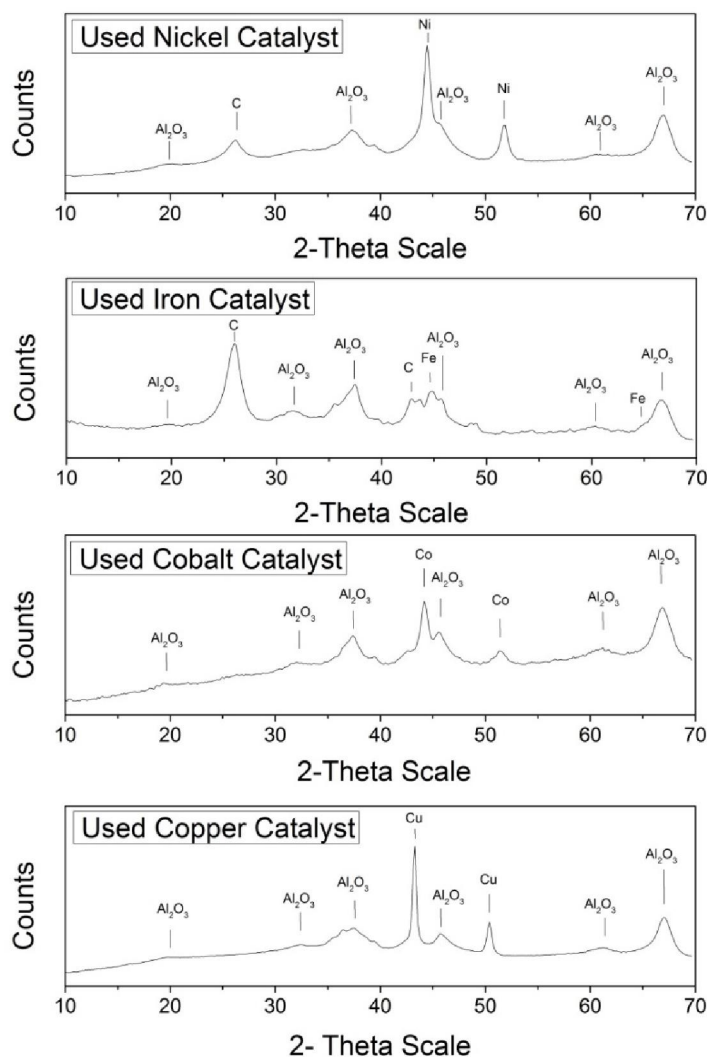


Figure 6.11 XRD of the used catalysts from the two stage pyrolysis of LDPE

XRD of the 10 wt% metal catalysts used in the two stage pyrolysis of LDPE is shown in figure 6.11. The nickel, iron, cobalt and copper in the catalysts were all reduced to their metallic form, with no other oxides or aluminates of the metals observed. This indicates that the metal oxides and aluminates were all reduced by reducing agents e.g. hydrogen in the pyrolysis gases in situ. The nickel and iron catalysts also show a peak for graphitic carbon, indicating significant carbon formation on the surfaces of these catalysts.

6.1.3.3 Temperature programmed oxidation

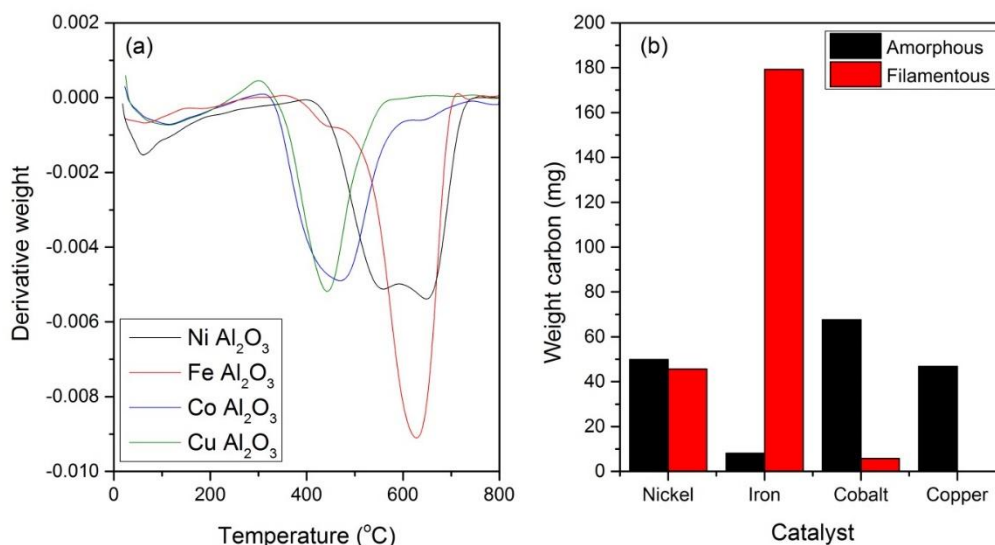


Figure 6.12 Temperature programmed oxidation investigation of the used catalysts from the two stage pyrolysis of LDPE: (a) Derivative TPO plot and (b) Amount of different carbon types deposited on the catalysts

Temperature programmed oxidation of the catalysts used in the two stage pyrolysis of LDPE was undertaken to give a better understanding of the types of carbon deposited on the catalyst surface and their abundance. TPO of the used catalysts gave two peaks around 550 °C and around 650 °C on the derivative plot, seen in figure 6.12(a). Amorphous carbons are reported to show a peak at lower temperatures than filamentous carbons, due to being more reactive [18]. As such the low temperature peak is associated with the oxidation of amorphous carbons whilst the high temperature peak is associated with the oxidation of filamentous carbons. Since all the filamentous carbons observed from TEM were CNTs, it is a fair assumption that the peak associated with filamentous represents CNTs alone. The carbon deposition on the nickel catalyst shows the peaks associated with amorphous and filamentous carbons on the derivative TPO plot, shown in figure 6.12(a). Both peaks are of a similar size, suggesting both carbon types are produced in roughly equal amounts. Based on the TPO results, calculations were undertaken to determine the amount of each carbon type, with results shown in figure 6.12(b). The deposits on the nickel catalyst produced a yield of 49.9 mg g⁻¹ sample of amorphous carbons and 45.7 mg g⁻¹ sample of CNTs. This is lower than was obtained in chapter 5 using a similar conditions, but with a different catalyst preparation technique [19].

The lower yield is likely due to a change in reactor design altering the pyrolysis gases obtained.

TPO plots for the used iron catalyst in figure 6.12(a) likewise show the presence of two peaks, associated with amorphous carbons and CNTs, however, unlike the nickel catalyst the filamentous peak is much larger. The values associated with each type of carbon were found to be 8 and 179 mg g⁻¹ sample for amorphous and CNTs, respectively. This shows that the iron catalyst produced a great deal more carbon nanotubes than its nickel counterpart. This is consistent with a number of studies which have reported iron to give higher yields of CNTs than other transition metals [20-23]. This also agrees well with the larger hydrogen yield from the iron catalyst, since a larger amount would be produced during the deposition of CNTs.

Whilst carbon nanotubes were observed on the cobalt catalyst, TPO plots seen in figure 6.12(a) suggest that the predominant type of carbon deposition was amorphous carbons. This is because the oxidation peak associated with filamentous carbons is much smaller than that of the amorphous carbons. The values for each type of carbon calculated mirror this, with amorphous carbons, 68 mg g⁻¹ sample, vastly outweighing filamentous carbons, 6 mg g⁻¹ sample. This is in accordance with the SEM images since less filamentous carbons were obtained than for both the nickel and iron catalysts. It also indicates why no significant peak for carbon was observed in XRD (figure 6.11). The results show that the cobalt catalyst clearly favours the production of amorphous carbons over filamentous carbons and is not an effective catalyst for carbon nanotube production. This is consistent with other studies comparing cobalt with iron catalysts, where cobalt proved less effective for CNT production [20-23]. Similarly low yields of CNTs were also obtained from a cobalt catalyst containing CoAl₂O₄ by Chai et al [24], where metal-support interactions were too strong and inhibited CNT growth.

TPO results for the used copper catalyst, shown in figure 6.12(a), reinforce the findings from electron microscopy with no peak seen for filamentous carbons. A peak for amorphous carbons is observed, and gave a value for amorphous carbon deposition of 47 mg g⁻¹ sample. The small amount of carbon deposition on the used copper catalyst ties in with XRD, where no significant peak was observed. This demonstrates that copper is not a suitable catalyst metal for the production of carbon nanotubes from a plastic feedstock.

6.1.3.4 Raman Spectroscopy

Raman spectroscopy is an analytical technique that can be used to characterise CNTs. It was undertaken on the catalysts used in the two stage pyrolysis of LDPE to analyse the carbon deposits produced. Spectrums produced (figure 6.13) show peaks at 1589 and 1348 cm^{-1} corresponding to the G peak, associated with graphitic carbon structures within the sample, and the D peak associated with defects within the graphic lattice or amorphous carbons, respectively [25]. The ratio between the height of these peaks, G:D ratio, is often used as a tool to determine the quality of CNTs produced with a higher value representing better quality or purity CNTs [26]. Figure 6.13(a) shows that the spectrum obtained for the nickel catalyst used in the two stage pyrolysis of LDPE. It shows the presence of the G and D peaks that are commonly associated with carbon nanotubes and gave a G:D ratio of 1.35. This shows CNTs are present in the carbon deposits on the catalyst surface. Raman spectroscopy of the used iron catalyst (figure 6.13(b)) likewise showed G and D peaks. In comparison to the nickel catalyst however, the size of the D peak is much smaller. The G:D ratio of the iron catalyst is accordingly higher than that obtained for nickel, with a values of 1.96, indicating the carbon deposition on the catalyst has a higher purity of carbon nanotubes. The used cobalt catalyst gave a Raman spectrum, shown in figure 6.13(c), with G and D peaks of a similar size. The corresponding G:D ratio obtained was 1.22; smaller than obtained for the used iron and nickel catalysts. This correlates with the other analyses in suggesting that the purity and quantity of carbon nanotubes is lower on the surface of the used cobalt catalyst. Raman spectroscopy of the used copper catalyst (figure 6.13(d)) shows two small peaks at the G and D position. The G:D ratio obtained is low at a value of 1.18, also indicating the poor quality of carbon deposits obtained from this catalyst. The copper catalyst showed that carbon deposits have almost no carbon nanotubes from TEM which would account for the low ratio obtained.

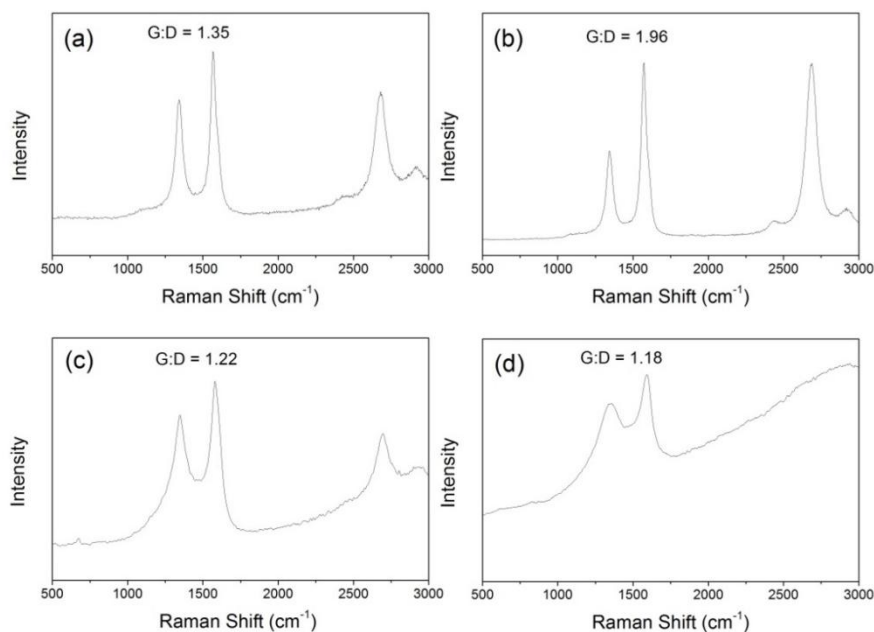


Figure 6.13 Investigation of the used catalysts from the two stage pyrolysis of LDPE by Raman spectroscopy: (a) Ni/Al₂O₃, (b) Fe/Al₂O₃, (c) Co/Al₂O₃ and (d) Cu/Al₂O₃

6.1.4 Discussion

The results show that the catalyst metal used has a strong influence on the CNT yield, with catalyst support interactions playing an important role. TPR and TEM analyses showed that the cobalt catalyst had a strong interaction with alumina, which prevented the formation of metal particles that could readily detach from the catalyst surface or were of a suitable size for CNT growth. Whilst the cobalt catalyst had a metal-support interaction which was too strong, the dispersed copper oxide particles in the copper-based catalyst could be easily reduced (TPR results, figure 6.8); as a result, a great deal of sintering of copper occurred, leading to the large copper particles observed in TEM of the reacted catalyst figure 6.10 (d). These were unsuitable for CNT production. The nickel and iron catalysts in contrast showed metal-support interactions which were suitable for CNT production, since both gave significant yields. The TPR results showed that these catalysts gave reduction peaks at intermediate values between 400 and 900 °C, which were clearly associated with support interactions which were neither too weak nor too strong.

TEM images also showed that these catalysts had a great deal more loose metal particles than the cobalt catalyst, suggesting the ability of metals to detach from the surface could be an important factor in CNT growth. This

supports the conclusion that CNT production is best suited to metal support interactions of intermediate strength. Chai et al. found similar results when investigating cobalt catalysts prepared at different calcination temperatures, with weaker interactions producing catalyst particles too large for CNT growth, but interactions which were too strong resulting in drastic reductions in CNT yield [24].

6.2 Effect of calcination temperature

In order to investigate the effect of metal support interactions further, a nickel catalyst was prepared at a lower calcination temperature of 500 °C (Nickel500 catalyst as opposed to the Nickel750 catalyst). The effect of the resulting lower catalyst support interaction on the production of hydrogen and carbon nanotubes could then be determined.

6.2.1 Characterisation of fresh catalysts

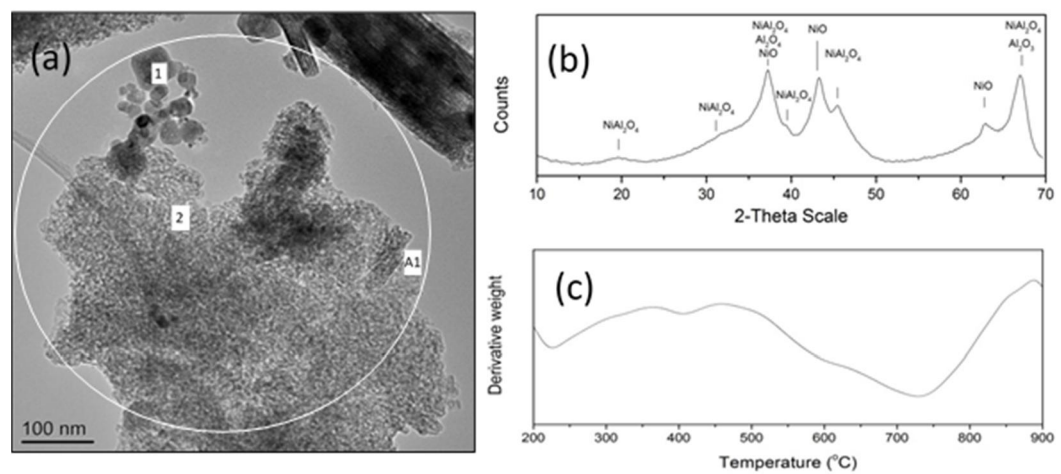


Figure 6.14 Analysis of the fresh Nickel500 catalyst used for the two stage pyrolysis of LDPE: (a) TEM image, (b) XRD and (c) TPR

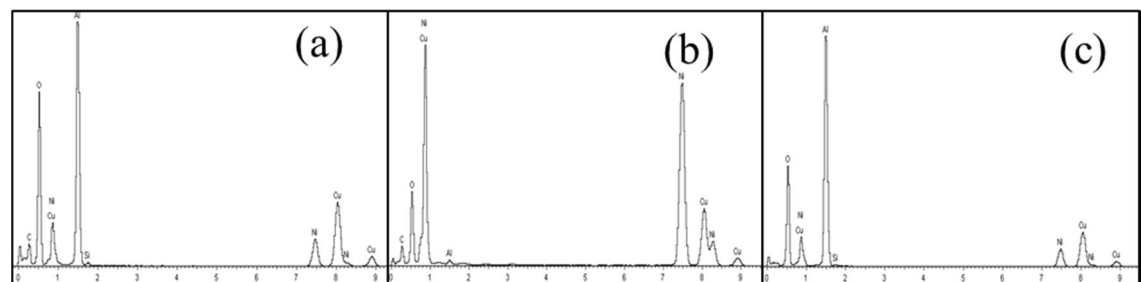


Figure 6.15 EDX spectrums of TEM image of Nickel500 catalyst shown in shown in figure 6.14(a): (a) Area A1, (b) Point 1, (c) Point 2

The TEM image of the fresh Nickel500 catalyst in figure 6.14(a) reveals that it is made of two distinct phases. The EDX spectrum in figure 6.15 of the whole catalyst particle, in area A1, showed the presence of Ni, Al and O, consistent with the Ni/Al₂O₃ catalyst. EDX spectrums were also taken at the two different phases observed. The spectrum, figure 6.15, observed at point 1 showed peaks for Ni and O, indicating that this is a form of nickel oxide. In contrast the spectrum of point 2 showed Ni, Al and O suggesting the presence of nickel aluminate as was observed in the nickel catalyst prepared by calcination at 750 °C. Nickel oxide is reported to interact with alumina at relatively low temperatures such as the 500 °C calcination temperature used to form nickel aluminate, suggesting this could be compound formed [2].

XRD analysis of the fresh Nickel500 catalyst was carried out, with the results shown in figure 6.14(b). It shows the presence of a number nickel and alumina compounds. The nickel in the catalyst is present as both NiO and NiAl₂O₄, with alumina present as Al₂O₃, reaffirming conclusions from SEM and TEM that the catalyst structure contains nickel oxide particles bonded to the alumina support in addition to nickel aluminate.

TPR of the fresh catalyst calcined at 500 °C shown in figure 6.14(c) shows a large peak at around 725 °C and a smaller peak at around 400 °C. Peaks at 400 and 725 °C are consistent with literature with the reduction of NiO and NiAl₂O₄ respectively, on a nickel alumina catalyst prepared by impregnation [5]. The peak associated with the reduction of the nickel aluminate has shifted to a lower temperature compared to reduction obtained from the Nickel750 catalyst (figure 6.8). This agrees well with results obtained by Garcia et al., where a nickel catalyst calcined at a lower temperature gave a reduction peak at a lower temperature because of smaller amounts of nickel aluminate [3]. The presence of the NiO peak is consistent with TEM-EDX and XRD results (figure 6.14), which show that a lower calcination temperature leads to less of the nickel bonding to the catalyst support in the form of nickel aluminates, and instead remains as nickel oxide. This agrees well with work by Chen et al where nickel aluminate formation increases at higher calcination temperatures through a reaction between the alumina support and NiO [1]. When compared to the catalyst prepared at a higher calcination temperature, the reduction peak has shifted to a lower temperature, indicating a weaker metal-support interaction. Overall the Nickel500 catalyst has a weaker metal-support interaction due to the presence of the nickel oxide, which is more easily reduced, and in turn appears to make the nickel aluminate more easily reducible.

6.2.2 Mass balance and hydrogen production

The product distribution in terms of gases, solids and liquids produced from the two stage pyrolysis of LDPE using the Nickel500 catalyst is seen in table 6.2 along with the composition of the gas stream. There is very little difference between the catalyst calcined at 500 °C and 750 °C, with both producing large amounts of gas and smaller amounts of solids and oils. In terms of the gas composition, there is no large difference seen between the two calcination temperatures used, with the Nickel500 catalyst producing slightly less hydrogen and slightly more hydrocarbons. The Nickel750 catalyst however does give a slightly larger hydrogen conversion of 16.5% compared with 15.2% for the 500 °C calcined catalyst. This result would suggest that the calcination temperature has not had a strong influence on hydrogen production in this instance.

Table 6.2 Effect of calcination temperature of nickel catalysts on mass balance, gas composition and hydrogen conversion from the two stage pyrolysis of LDPE

Calcination temperature (°C)	500	750
Gas (wt%)	57.3	55.2
Oils (wt%)	25.0	24.0
Solid (wt%)	12.0	11.0
H ₂ (vol%)	34.1	36.6
CH ₄ (vol%)	23.5	23.6
C ₂ -C ₄ (vol %)	42.4	39.8
Hydrogen production (g/100g sample)	2.1	2.3
Hydrogen conversion (%)	15.2	16.5

6.2.3 Carbon nanotube production

6.2.3.1 Scanning and Transmission Electron Microscopy

Figure 6.16 shows a number of analyses which were undertaken on the used Nickel500 catalyst in order to determine the nature of the carbon deposition on its surface. The deposition on the Nickel500 catalyst in the SEM image in figure 6.16(a) shows the presence of filamentous carbons on the catalyst surface. As was the case with the catalyst prepared at 750 °C the TEM images shown in figure 6.16(c) confirmed that the filaments observed were multi walled carbon nanotubes. TEM images also show that similarly to the nickel and iron catalysts prepared at the higher calcination temperature, there are a number of loose metal particles. However, the size of these particles appears larger than was observed from the Nickel750 catalyst. This indicates that the weaker metal-support interaction, indicated by TPR, has allowed greater sintering of the nickel particles.

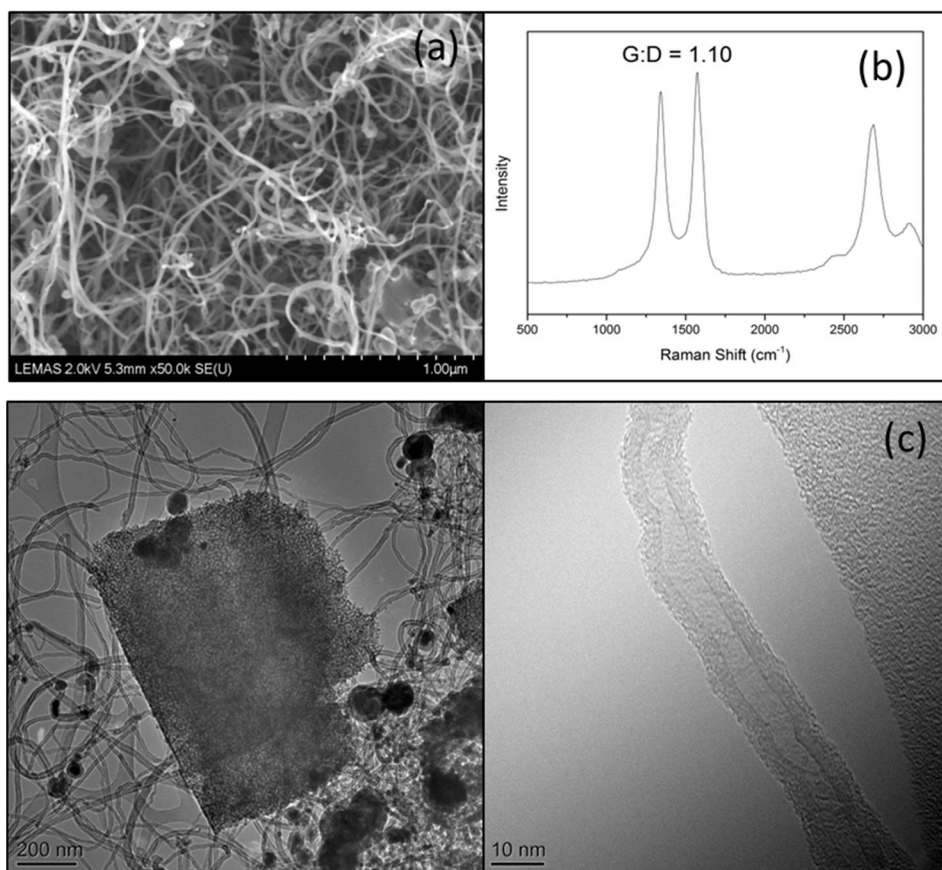


Figure 6.16 Analysis of the used Nickel500 catalyst from the two stage pyrolysis of LDPE (a) SEM, (b) Raman spectroscopy and (c) TEM

6.2.3.2 Temperature Programmed Oxidation

TPO of the Nickel500 catalyst used in the two stage pyrolysis of LDPE was also undertaken in order to determine the nature and quantity of the carbon deposited on its surface. In the TPO results in figure 6.17(a) the peak associated with amorphous carbons is much larger than that of the filamentous carbons, showing that a larger amount of amorphous carbons have been produced from the two stage pyrolysis of LDPE. Calculations based upon these TPO results proved this to be the case with 65.0 and 17.7 mg g⁻¹ sample of amorphous and filamentous carbons produced respectively as shown in figure 6.17(b). This is a smaller yield of CNTs than was obtained with the nickel catalyst prepared at a higher calcination temperature. As such, the calcination temperature of the catalyst is an important factor in determining the yield of CNTs with a higher calcination temperature giving a larger amount of CNTs and smaller amounts of amorphous carbons. This strengthens the conclusion that the catalyst support interaction is an important factor in CNT growth, since a weaker interaction has yielded smaller amounts of CNTs. The larger production of amorphous carbons on the Nickel500 compared to the Nickel750 catalyst could also be responsible for the smaller hydrogen yield, since amorphous carbons are known to deactivate catalysts by encapsulating catalyst particles [27].

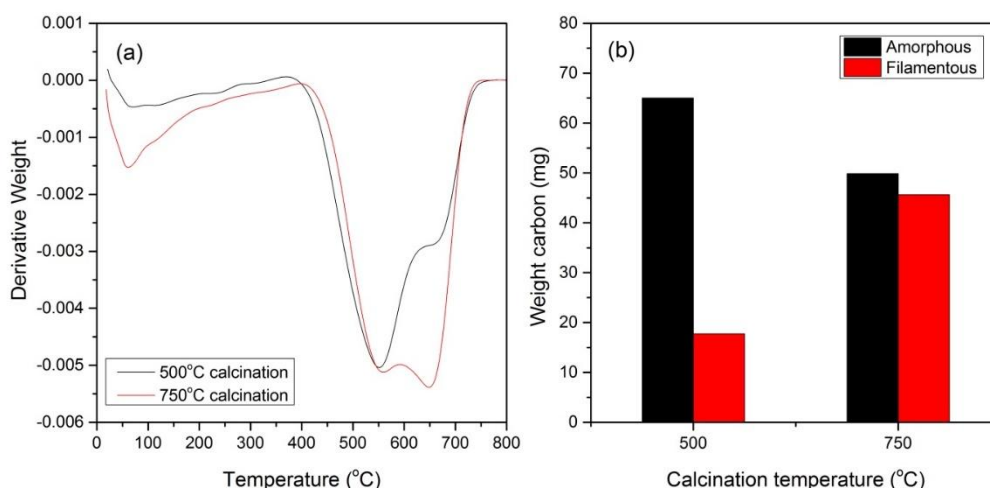


Figure 6.17 The effect of calcination temperature on the yield of CNTs from the two stage pyrolysis of LDPE: (a) Derivative TPO graph from used catalysts and (b) Amount of different carbon types deposited on the catalysts

6.2.3.3 Raman Spectroscopy

Raman analysis of the used Nickel500 catalyst is shown in figure 6.16(b). It shows the presence of both G and D peaks, with the peaks being of a similar height. This gave a G:D ratio of 1.10, lower than was obtained for the Nickel750 catalyst indicating less purity in terms of CNTs. This is consistent with TPO results where the Nickel750 catalyst showed a larger yield of CNTs and smaller amounts of amorphous carbons.

6.2.4 Discussion

From the analyses on the fresh catalysts it was found that the lower calcination temperature produced weaker catalyst-support interactions, forming NiO rather than NiAl_2O_4 . The interaction between the metal and support proved to be an important factor when using different catalysts, with the weak interaction of the copper catalyst allowing sintering of the metal to occur, and yielding catalyst particles which were too large for CNT production. Similarly, a larger yield of amorphous carbons, rather than CNTs, were produced from the catalyst with a lower calcination temperature as a result of its weaker metal support interaction.

The weaker metal-support interaction allowed sintering of the nickel, resulting in larger particles which yielded more amorphous carbons. Chai et al, found similar results where increasing the calcination temperature yielded more CNTs when using a cobalt catalyst and a methane feedstock [24]. It was suggested that at lower calcination temperatures, sintering produced catalyst particles too large to form CNTs. Liu et al also obtained higher yields of CNTs with stronger catalyst support interactions when investigating different supports with an iron catalyst, again using methane as a feedstock [22].

Results show that the Nickel500 catalyst had a weaker metal support interaction than the Nickel750 catalyst, and produced less CNTs as a result. However TPR and TEM analyses showed that the iron catalyst had a similar interaction to the Nickel500, but yielded significantly more CNTs. This suggests that catalyst support interactions are not the only factor governing CNT production. It has been suggested that iron catalysts in particular produce large yields of CNTs because of iron's large carbon solubility compared to other metals [22]. This could help to indicate why copper aluminate particles, which show a reduction peak comparable to iron and nickel, produce almost no CNTs, since copper has a much lower carbon

solubility [28]. Carbon solubility is thought to be a key aspect of CNT growth, since it increases the amount of carbon available for CNT growth, and is thought to accelerate the CNT formation rate [22, 28]. In this instance, the iron catalysts large CNT yield could be a result of a desirable catalyst-support interaction coupled with a large carbon solubility.

6.3 Effect of metal loading

The effect of reducing the metal loading of the catalysts to 5 wt% on the results from the two stage pyrolysis of LDPE using nickel, iron, cobalt and copper catalysts is shown in table 6.3. It shows the mass balance, gas composition, hydrogen conversion and yield of CNTs and amorphous carbons. The TPO graph used to calculate the amounts of carbon deposition is also shown in figure 6.18.

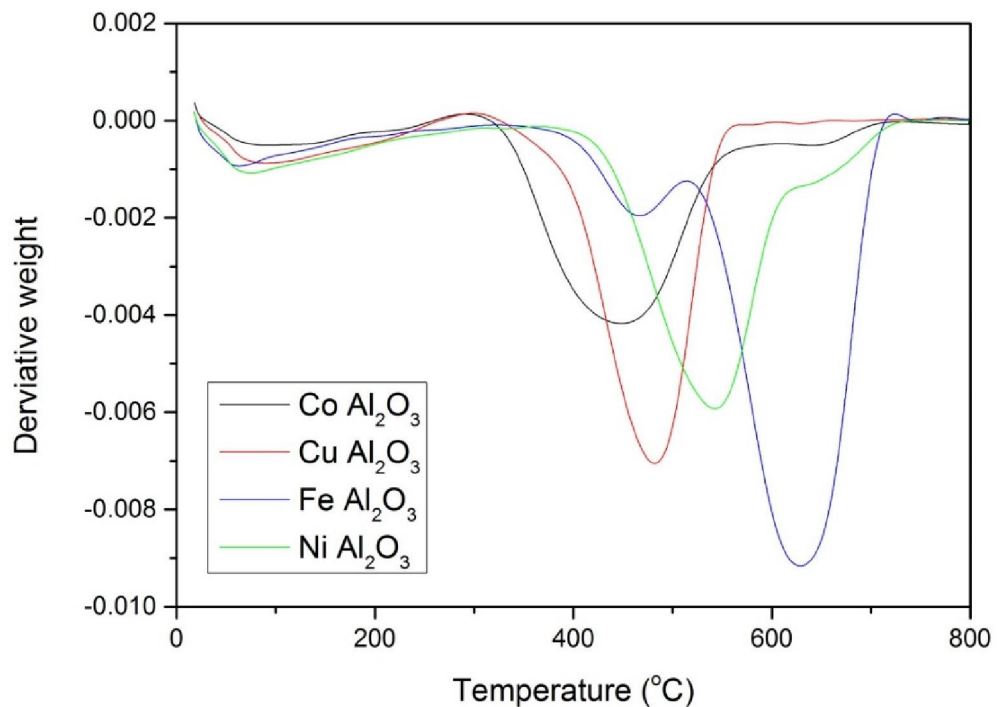


Figure 6.18 Derivative TPO plot for 5 wt% metal catalysts used for the two stage pyrolysis of LDPE

In terms of the effect of metal loading, there is a clear distinction between iron and nickel catalysts when compared with the cobalt and copper

catalysts. As seen in table 6.3, increasing the metal loading on the catalyst from 5 wt% to 10 wt% increases the proportion of gases produced from the two stage pyrolysis of LDPE, from 51.0 to 55.2 vol% for the nickel catalyst and from 48.1 to 51.5 vol% for the iron catalyst. The corresponding concentration of oils reduce for both catalysts, indicating that there is an increase in the breakdown of larger oil molecules into gases with increased metal loading. This indicates that the nickel and iron catalysts are catalytically active in the cracking of larger hydrocarbon chains, as increasing the amount of metal led to a reduction in oils. Similar reductions in the yield of oils from the steam reforming of hydrocarbon species were observed by Srinakruang et al and Bimbela et al when increasing the metal loading on nickel catalysts [29, 30]. The proportion of solids produced using the nickel and iron catalysts also increase when the metal loading is increased from 5 wt% to 10 wt%. The solids increase from 10.2 to 12.2 wt% for the nickel catalyst and 23.3 to 26.0 wt% for the iron catalyst. As the change in the amount of waxes produced was negligible, the increase was attributed to an increase in the production of solid carbons on the catalyst surface. In contrast, the proportions of gases, liquids and solids produced remain almost entirely unchanged for the cobalt catalyst when the metal loading is changed from 5 wt% to 10 wt%. This suggests that cobalt is not as catalytically active. This could be attributed to the strong catalyst support interaction observed for the cobalt catalyst in the TPR analysis, as shown in figure 6.8, preventing cobalt metal particles of a catalytically active size being formed. The copper catalyst actually produces a reduction in gases in favour of oil yields when the loading is increased from 5 wt% to 10 wt%. Solid yields also reduce, suggesting less carbon deposition has occurred.

In terms of the composition of the gases, the nickel, iron and cobalt catalysts all show an increase in the proportion of hydrogen, and a reduction in the proportions of methane and C₂-C₄ hydrocarbons. Hydrogen increases from 31.5 up to 36.6 vol% for the nickel catalyst, from 44.4 up to 50.6 vol% for the iron catalyst, and from 28.1 up to 31.3 vol% for the cobalt catalyst. This leads to an increase in the hydrogen yields and conversions obtained when the metal loading is increased. Meanwhile the yields of, methane and C₂-C₄ hydrocarbons reduce when the metal loading is increased from 5 wt% to 10 wt%.

Table 6.3 Effect of metal loading on the production of hydrogen and CNTs from the two stage pyrolysis of LDPE

Catalyst	Ni Al ₂ O ₃		Fe Al ₂ O ₃		Co Al ₂ O ₃		Cu Al ₂ O ₃	
Metal (wt%)	5%	10%	5%	10%	5%	10%	5%	10%
Gas (wt%)	51.0	55.2	48.1	51.5	54.2	54.6	56.2	55.0
Oils (wt%)	28.0	24.0	21.0	17.0	27.0	27.0	24.0	29.0
Solid (wt%)	9.0	11.0	21.0	24.0	9.0	9.0	9.0	7.0
H ₂ (vol%)	31.5	36.6	44.4	50.6	28.1	31.3	28.1	26.0
CH ₄ (vol%)	24.8	23.6	22.0	19.8	27.3	24.9	27.3	26.6
C ₂ -C ₄ (vol %)	43.7	39.8	33.6	29.6	44.7	43.8	44.7	47.4
Hydrogen production (g/100g sample)	1.7	2.3	2.7	3.7	1.6	1.8	1.6	1.4
Hydrogen conversion (%)	12.1	16.5	19.8	26.8	11.7	12.8	11.7	10.1
Mass amorphous carbons (mg)	65	50	23	8	66	68	57	47
Mass CNTs (mg)	8	46	140	179	5	6	0	0

Methane and C₂-C₄ hydrocarbons reduce from 24.8 and 43.7 vol% to 23.6 and 39.8 vol% for the nickel catalyst, from 22.0 and 33.6 vol% to 19.8 and 29.6 vol% for the iron catalyst and from 27.3 and 44.7 vol% down to 24.9 and 43.8 vol% for the cobalt catalyst. These reductions were reproducible and greater than the experimental error for the reactor. Coupled with the increase in solids observed, this suggests that as the metal loading is increased more hydrocarbons are deposited on the catalyst to form

hydrogen and carbon as the metal loading is increased. At 5 wt% metal loading, the nickel, cobalt and copper catalysts show a similar hydrogen yield, with 1.7 g/100g sample for the nickel catalyst and 1.6 g/100g sample for the cobalt and copper catalysts. This shows that increasing the metal loading has a much more significant effect for the nickel catalyst. As was observed for the 10 wt% loading, at 5 wt% loading the iron catalyst produces a larger hydrogen yield than the other catalysts, with 2.7 g/100g sample, again likely as a result of the large solid yield obtained with this catalyst. This suggests that a large amount of hydrogen is produced during the deposition of solid carbons on the iron catalysts. Conversely, the copper catalyst shows a reduction in the proportion of hydrogen, and increase in hydrocarbons once the metal loading is increased.

With regards to carbon nanotube production a similar pattern emerges, with increased metal loading resulting in higher yields on iron and nickel catalysts, but no effect on the cobalt and copper catalysts. At 5 wt% metal loading, the amount of CNTs produced are 8, 140 and 6 mg g⁻¹ sample for the nickel, iron and cobalt catalysts respectively. This confirms that the iron catalyst produced a great deal more carbon deposition at this metal loading than the other catalysts, leading to the higher hydrogen yield obtained. Increasing the metal loading led to an increase in the yield of CNTs. This is in agreement with studies by Govindaraj et al, Takenaka et al and Tian et al, who found similar results, with an increase in carbon deposition with increased metal loading, particularly at low metal loadings [20, 23, 31, 32]. The increase was attributed to the availability of more metal particles where carbon deposits can accumulate. As such, in this study the same conclusion can be applied to the increase in CNT deposition, since it is accompanied by a reduction in hydrocarbons and oils, and an increase in hydrogen production. The copper catalyst however fails to produce CNTs, irrespective of metal loading. This strengthens the conclusion that the copper catalyst is unsuitable for CNT production.

6.4 Conclusions

Carbon nanotubes and hydrogen gas were successfully produced simultaneously on nickel, iron and cobalt catalysts using a plastic feedstock. Copper catalysts however produced almost no CNTs. It is suggested that the interaction between the catalyst metal and alumina support played a strong part in governing the yield of CNTs, with a too weak an interaction

allowing sintering of metals to produce particles too large for CNT growth, and too strong an interaction hindering production. The nickel and iron catalysts proved to have an interaction which was neither too weak, like the copper catalyst, nor too strong, like the cobalt catalyst, resulting in significant CNT yields. CNT yields were as follows: Fe>Ni>Co>Cu, with the iron catalyst giving the largest yield with a value of 179 mg g⁻¹ sample. This work also shows that the iron-based catalyst giving the largest yield of hydrogen as opposed to the nickel catalyst which is traditionally used for hydrogen production.

Investigating the interaction between catalyst and support has been further carried out by developing Ni-based catalyst at different calcination temperatures. Results showed that the weaker interaction resulted in production of larger metal particles during the reaction, and hence a lower yield of carbon nanotubes was obtained.

Changing the metal loading on the catalysts showed that at higher loadings, more CNTs and hydrogen were produced. This was accompanied by reductions in hydrocarbons, and so it is concluded that at higher metal loadings more metal particles become available for the deposition of carbon.

References

1. Chen, Y.-g. and J. Ren, *Conversion of methane and carbon dioxide into synthesis gas over alumina-supported nickel catalysts. Effect of Ni-Al₂O₃ interactions*. Catalysis Letters, 1994. **29**: p. 39-48.
2. Zieliński, J., *Morphology of nickel/alumina catalysts*. Journal of Catalysis, 1982. **76**(1): p. 157-163.
3. Garcia, L., et al., *Influence of Calcination and Reduction Conditions on the Catalyst Performance in the Pyrolysis Process of Biomass*. Energy & Fuels, 1998. **12**: p. 139-143.
4. Heracleous, E., et al., *Investigation of Ni-based alumina-supported catalysts for the oxidative dehydrogenation of ethane to ethylene: structural characterization and reactivity studies*. Journal of Catalysis, 2005. **231**(1): p. 159-171.
5. Li, G., L. Hu, and J.M. Hill, *Comparison of reducibility and stability of alumina-supported Ni catalysts prepared by impregnation and co-precipitation*. Applied Catalysis A: General, 2006. **301**(1): p. 16-24.
6. Bolt, P.H., F.H.P.M. Habraken, and J.W. Geus, *Formation of Nickel, Cobalt, Copper, and Iron Aluminates from α- and γ-Alumina Supported Oxides: A Comparative Study*. Journal of Solid State Chemistry, 1998. **135**: p. 59-69.
7. Gao, X., et al., *Reduction of Supported Iron Oxide studied by Temperature-programmed Reduction combined with Mossbauer Spectroscopy and X-Ray Diffraction* Journal of the Chemical Society, Faraday Transactions, 1993. **89**(7): p. 1079-1084.

8. Griboval-Constant, A., et al., *Cobalt and iron species in alumina supported bimetallic catalysts for Fischer–Tropsch reaction*. Applied Catalysis A: General, 2014. **481**: p. 116-126.
9. Park, J.-Y., et al., *Alumina-supported iron oxide nanoparticles as Fischer–Tropsch catalysts: Effect of particle size of iron oxide*. Journal of Molecular Catalysis A: Chemical, 2010. **323**(1-2): p. 84-90.
10. Ren-Yuan, T., et al., *An in situ combined temperature-programmed reduction-Mössbauer spectroscopy of alumina-supported iron catalysts*. Journal of Catalysis, 1987. **106**(2): p. 440-448.
11. Schanke, D., et al., *Study of Pt-Promoted Cobalt CO Hydrogenation Catalysts*. Journal of Catalysis, 1995. **156**: p. 85-95.
12. Luo, M.-F., et al., *In situ XRD, Raman, and TPR studies of CuO/Al₂O₃ catalysts for CO oxidation*. Journal of Molecular Catalysis A: Chemical, 2005. **239**(1-2): p. 243-248.
13. Marino, F.J., et al., *Hydrogen from steam reforming of ethanol. Characterization and performance of copper-nickel supported catalysts*. International Journal of Hydrogen Energy, 1998. **23**(12): p. 1095-1101.
14. Nessim, G.D., *Properties, synthesis, and growth mechanisms of carbon nanotubes with special focus on thermal chemical vapor deposition*. Nanoscale, 2010. **2**(8): p. 1306-23.
15. Cheung, C.L., et al., *Diameter-Controlled Synthesis of Carbon Nanotubes*. Journal of Physical Chemistry B, 2002. **106**: p. 2429-2433.
16. Jourdain, V. and C. Bichara, *Current understanding of the growth of carbon nanotubes in catalytic chemical vapour deposition*. Carbon, 2013. **58**: p. 2-39.
17. Nasibulin, A., et al., *Correlation between catalyst particle and single-walled carbon nanotube diameters*. Carbon, 2005. **43**(11): p. 2251-2257.
18. Wang, P., et al., *Filamentous carbon prepared by the catalytic pyrolysis of CH₄ on Ni/SiO₂*. Applied Catalysis A: General, 2002. **231**: p. 34-44.
19. Acomb, J.C., C. Wu, and P.T. Williams, *Control of steam input to the pyrolysis-gasification of waste plastics for improved production of hydrogen or carbon nanotubes*. Applied Catalysis B: Environmental, 2014. **147**: p. 571-584.
20. Govindaraj, A., et al., *An investigation of carbon nanotubes obtained from the decomposition of methane over reduced Mg_{1-x}M_xAl₂O₄ spinel catalysts*. Journal of Materials Research, 1999. **14**(6): p. 2567-2576.
21. Kong, J., A.M. Cassell, and H. Dai, *Chemical vapor deposition of methane for single-walled carbon nanotubes*. Chemical Physics Letters, 1998. **292**: p. 567-574.
22. Liu, W.-W., et al., *Synthesis of Single-Walled Carbon Nanotubes: Effects of Active Metals, Catalyst Supports, and Metal Loading Percentage*. Journal of Nanomaterials, 2013. **2013**: p. 1-8.
23. Tan, S.-M., et al., *Effects of FeO_x, CoO_x, and NiO catalysts and calcination temperatures on the synthesis of single-walled carbon nanotubes through chemical vapor deposition of methane*. Journal of Alloys and Compounds, 2009. **477**(1-2): p. 785-788.

24. Chai, S.-P., S.H. Sharif Zein, and A.R. Mohamed, *The effect of catalyst calcination temperature on the diameter of carbon nanotubes synthesized by the decomposition of methane*. Carbon, 2007. **45**(7): p. 1535-1541.
25. Jiang, Z.W., et al., *Polypropylene as a carbon source for the synthesis of multi-walled carbon nanotubes via catalytic combustion*. Carbon, 2007. **45**(2): p. 449-458.
26. Das, N., et al., *The effect of feedstock and process conditions on the synthesis of high purity CNTs from aromatic hydrocarbons*. Carbon, 2006. **44**(11): p. 2236-2245.
27. Rostrup-Nielsen, J.R., *Steam Reforming Catalysts* 1975, Copenhagen: Danish Technical Press.
28. Moiala, A., A.G. Nasibulin, and E.I. Kauppinen, *The role of metal nanoparticles in the catalytic production of single-walled carbon nanotubes—a review*. Journal of Physics: Condensed matter, 2003. **15**: p. S3011-S3035.
29. Bimbela, F., et al., *Catalytic steam reforming of model compounds of biomass pyrolysis liquids in fixed bed: Acetol and n-butanol*. Journal of Analytical and Applied Pyrolysis, 2009. **85**(1-2): p. 204-213.
30. Srinakruang, J., et al., *A highly efficient catalyst for tar gasification with steam*. Catalysis Communications, 2005. **6**(6): p. 437-440.
31. Takenaka, S., *Structural Change of Ni Species in Ni/SiO₂ Catalyst during Decomposition of Methane*. Journal of Catalysis, 2002. **208**(1): p. 54-63.
32. Takenaka, S., *Ni/SiO₂ catalyst effective for methane decomposition into hydrogen and carbon nanofiber*. Journal of Catalysis, 2003.

7 Effect of temperature and sample:catalyst ratio on production of hydrogen and carbon nanotubes

In addition to the type of catalyst used, other factors also have a strong influence on the production of hydrogen and CNTs. This chapter will look at the influence of the temperature that the catalyst is held at (growth temperature), and the amount of feedstock used compared to the amount of catalyst. The same iron catalyst prepared by impregnation as used in chapter 6 will be used, with an iron loading of 10 wt%. The temperature of the second stage, where the catalyst is held, will be varied between 700 and 900 °C, whilst the amount of the LDPE sample will be varied between 0.5 and 1.25 g. The amount of catalyst will be kept at 0.5 g, and the first reactor where pyrolysis occurs will continue to be heated up to 600 °C, from ambient temperature. No steam is injected into the reactor.

7.1 Effect of temperature

7.1.1 Mass balance and hydrogen production

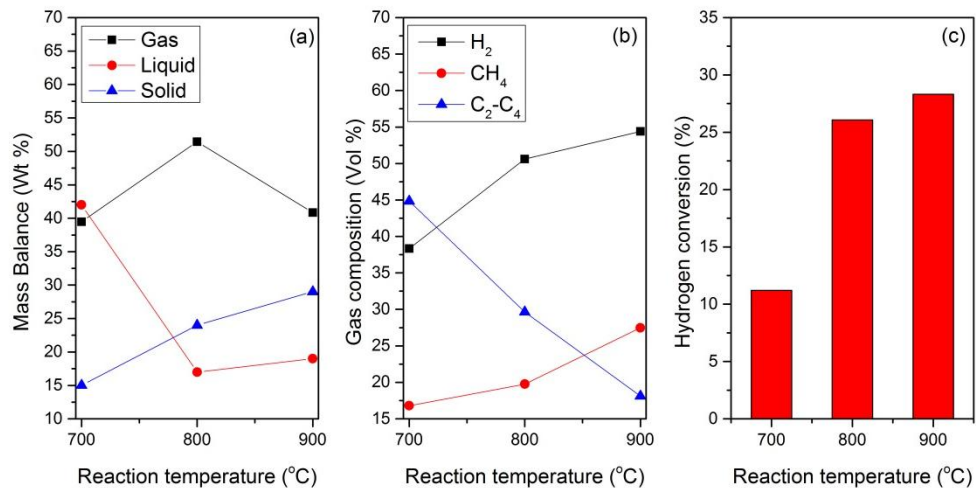


Figure 7.1 Effect of growth temperature on (a) mass balance, (b) gas composition and (c) hydrogen conversion from two stage pyrolysis of LDPE

Figures 7.1 (a) and (b) show the mass balances and gas compositions of the experiments at 700, 800 and 900 °C. Mass balances are given in terms of solids, liquids and gases produced, where the solids account for the carbon deposition on the catalyst surface. All mass balances obtained were above 89 wt%. As the reaction temperature is raised, the amount of solids produced rises, from 15.0 to 29.0 wt%, showing that more carbon deposition occurs. This is consistent with a number of studies, which see an increase in carbon deposition at higher temperatures [1-4]. The yield of gases initially increases with temperature, from 39.5 wt% at 700 °C up to 51.5 wt% at 800 °C, as the larger hydrocarbons are broken down into gases, consistent with the reduction in liquids observed. At 900 °C however a reduction in the yield of gases occurs, down to a value of 40.9 wt%. At this temperature more of the gases are converted into solid carbons on the surface of the catalyst, via reaction 7.1, accounting for the increase in solids seen at this temperature.



In terms of the gas composition it can be seen from figure 7.1 (b) that with increasing temperature the amount of hydrogen increases, from 38.4 to 54.4 vol%. This is also shown in figure 7.1(c) which shows the amount of hydrogen produced as a percentage of the maximum theoretical yield obtainable. The maximum theoretical yield was calculated based on the total amount of hydrogen in the plastic as obtained from elemental analysis (table 3.1). As the amount of solid carbons produced increases, the amount of hydrogen produced increases with it, since both are produced during the decomposition of hydrocarbons via reaction 7.1. Values of hydrogen conversion increase from 11.2% at 700 °C up to 26.1% at 800 °C and 28.3% at 900 °C. This is consistent with other studies investigating the production of hydrogen and carbon nanotubes [5, 6]. Figure 2 (b) shows that the composition of C₂-C₄ hydrocarbons reduce as the temperature is raised, falling from a value of 44.9 vol% at 700 °C to 29.6 vol% at 800 °C and 18.1 vol% at 900 °C. This is because they are either broken down to form methane, or deposited on the catalyst to form solid carbons.

7.1.2 Carbon nanotube production

Scanning and transmission electron microscopy were undertaken on the carbon deposition on the catalyst surface, with the images obtained shown in figures 7.2 (a-f).

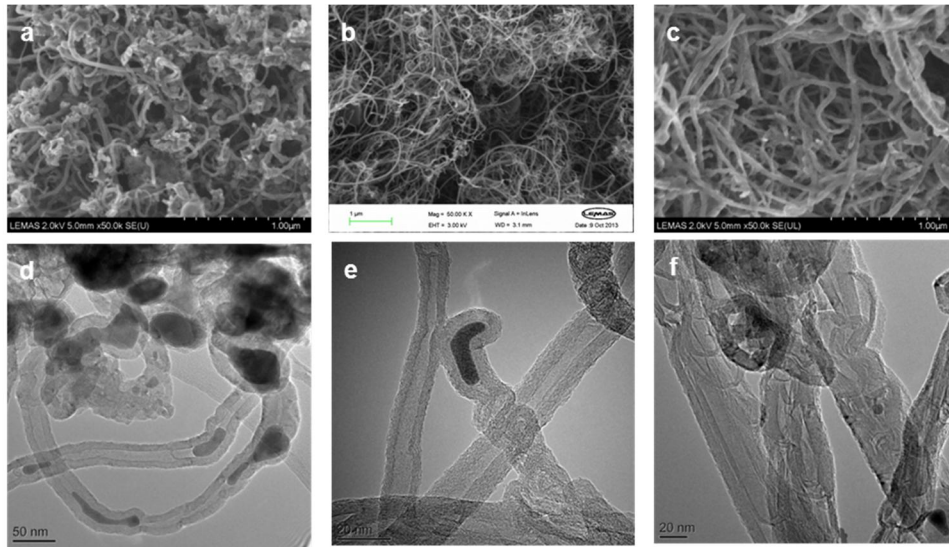


Figure 7.2 Scanning electron microscopy and transmission electron microscopy images of carbon deposition on catalyst at experimental temperature of 700 °C (a) and (d), 800 °C (b) and (e) and 900 °C (c) and (f)

The SEM image of the catalyst obtained from the experiments carried out at 700 °C, figure 7.2(a) shows the presence of filamentous carbons, as well as bobbles of more amorphous and encapsulating carbon. The corresponding TEM image figure 7.2(d) confirmed that the filamentous carbons were multiwalled carbon nanotubes, which had diameters of around 20-30 nm and were up to a number of μm in length. The amorphous and encapsulating carbons observed in SEM are also seen, and could contribute to the low yield of hydrogen at this temperature by deactivation of the catalyst. The deposits on the surface of the catalyst obtained at a catalyst temperature of 800 °C also show the presence of filamentous carbons on their SEM image in figure 7.2(b), however in this case they are far more densely packed and show no visible amorphous carbons. This is in accordance with a study by Mishra et al [7] who likewise saw a reduction of amorphous type carbon deposition with an increase in temperature up to 800 °C, when compared

with 600 and 700 °C. The corresponding TEM image for the carbon deposits obtained at 800 °C in figure 7.2(e) confirms that the filamentous carbons are multi walled carbon nanotubes, with dimensions similar to those seen at 700 °C, with diameters of around 20-30 nm and lengths of up to a number of μm . Thick deposits of filamentous carbons are also seen on the SEM image for the carbon deposition on the catalyst obtained at 900 °C in figure 7.2(c), however the TEM image in figure 7.2(f) shows that the quality of the carbon nanotubes has deteriorated. The filamentous carbons no longer show continuous and even walls, with some showing no hollow inner channel at all. The diameters of the filamentous carbons also increased to widths of 30-60 nm, with the lengths similar to those produced at other temperatures, being a number of μm .

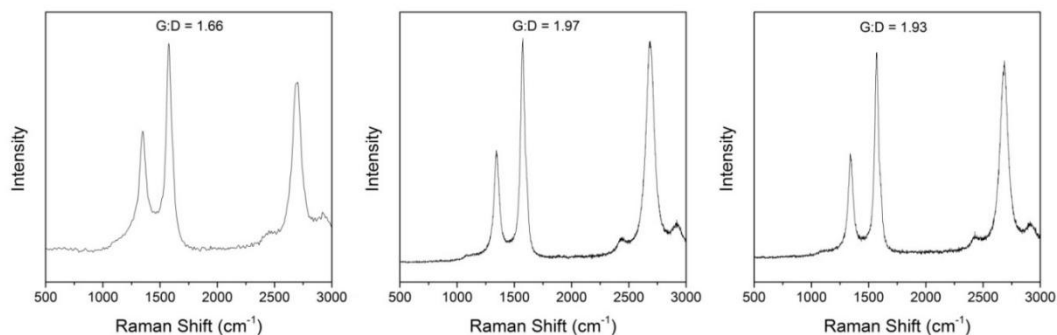


Figure 7.3 Raman spectra of carbon deposits obtained from experimental temperatures of (a) 700 °C, (b) 800 °C and (c) 900 °C

Raman spectroscopy is often used to characterise CNTs [8-12], and was undertaken to characterise the carbon deposits produced, with the spectrums for the catalysts from experiments carried out at 700, 800 and 900 °C shown in figure 7.3. Peaks are seen at 1589 and 1348 cm^{-1} for each of the samples. The peak at 1589 cm^{-1} corresponds to the G peak associated with graphitic carbon within the sample, the peak at 1348 cm^{-1} corresponds with the D peak and is associated with defects within the graphitic lattice; while the G' peak at the Raman shift around 2709 cm^{-1} indicates the two photon elastic scattering process, indicating the purity of CNTs. The ratio between the size of the G peak and D peak is a useful way of comparing the quality of the carbon nanotubes obtained in terms of how ordered and graphitic they are [5, 13-15]. This will enable the purity of the deposits in terms of CNTs produced to be evaluated, with a larger G/D ratio

indicating a higher purity. Raman spectrums in figure 7.3 show that the G/D ratio is significantly lower for the carbon deposits produced at 700 °C, with a value of 1.66, than for 800 and 900 °C with values of 1.97 and 1.93 respectively. This indicates that the carbon deposition at this lower temperature has a lower purity in terms of carbon nanotubes, as seen in electron microscopy. In addition, the CNTs produced at 700 °C also show the lowest intensity ratio of G'/G, compared to the CNTs produced at other temperatures; this further supports the contention that CNTs produced at such low temperature (700 °C) have the lowest purity. Mishra et al [7] likewise obtained a higher G/D ratio for carbon deposits obtained from higher reaction temperatures, indicating a higher quality of carbon nanotubes. A slight reduction in the G/D ratio is seen at 900 °C, and is most likely due to the fact that despite seeing more carbon deposition, the quality of the filamentous carbon is lower, with less ordered carbon walls, as observed from TEM.

In order to better determine the amount of carbon deposition and the relative amounts of carbon types on the catalyst surface, temperature programmed oxidation was carried out on the used catalyst samples. The derivative TPO plots in figure 7.4(a) show two distinct peaks, one between 350 °C and 450 °C, and another between 500 °C and 700 °C. Amorphous carbons are reported to show a peak at lower temperatures than filamentous carbons, due to being more reactive [16]. As such the low temperature peak is associated with the oxidation of amorphous carbons whilst the high temperature peak is associated with the oxidation of filamentous carbons such as carbon nanotubes.

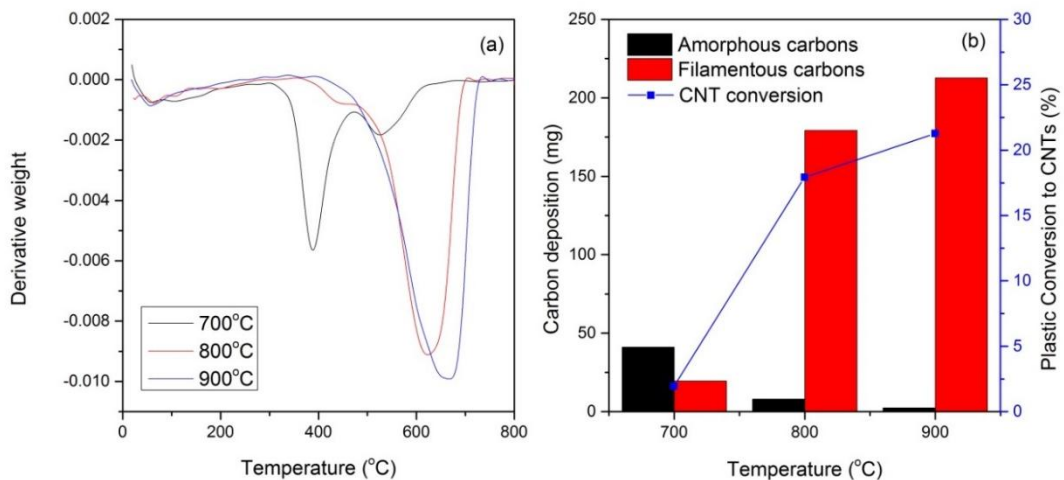


Figure 7.4 Temperature oxidation results showing effect of temperature; (a) derivative plot and (b) amount of carbon deposition and conversion of plastic to CNTs

Using the derivative TPO plot the total amount of each carbon type was calculated and displayed in figure 7.4(b). As the temperature is raised, the amount of filamentous carbons produced increases, with 213 mg g⁻¹ sample produced at 900 °C compared with 20 mg g⁻¹ sample and 179 mg g⁻¹ sample at 700 °C and 800 °C respectively. The percentage of plastic converted into CNTs was calculated based on the weight of carbon nanotubes produced as a percentage of the weight of LDPE used. These results show that more of the plastic is converted into carbon nanotubes as the temperature is increased, from 2.0 wt% at 700 °C to 17.9 wt% at 800 °C and 21.3 wt% at 900 °C, as shown in figure 7.4 (b). This is in accordance with other studies [1-4], and is likely due to the increase in the diffusion rate of carbon through the catalyst particle as a result of the higher temperature, an important step in the formation of carbon nanotubes. The amount of amorphous carbon produced at 700 °C, 41 mg g⁻¹ sample, is also significantly more than that produced at the other temperatures, with a further reduction also seen between 800 °C, 8 mg g⁻¹ sample, and 900 °C, 2 mg g⁻¹ sample. This shows that an increase in temperature also favours the production of CNTs over amorphous carbons.

Whilst more carbon deposition was produced at 900 °C, the TEM images and Raman spectroscopy showed that the quality of the carbon nanotubes in terms of the crystallinity and order of the walls produced at 800 °C was higher. CNTs produced at 800 °C showed similar dimensions to those produced from more standard means such as chemical vapour deposition,

with comparable Raman results in terms of G:D ratio also obtained [5, 17, 18]. This opens up the possibility of using the CNTs obtained in commercial applications. Multiwalled CNTs find current uses in a range of applications ranging from high strength composites, coatings, water treatment and energy technologies [19-26]. In order to be used in these applications however, a purification process would need to be undertaken on the CNTs to remove amorphous carbons and other contaminants.

7.2 Effect of feedstock:catalyst ratio

7.2.1 Mass balance and hydrogen production

Figure 7.5 shows the results for the mass balance and gas composition for experiments where the feedstock:catalyst ratio was varied, by changing the amount of LDPE used. From figure 7.5(a) it can be seen that as the amount of plastic used is increased, the percentage converted into solids reduces, from 32.0 wt% at 0.5 g to 16.0 wt% at 1.25 g. Simultaneously the percentage of gases and liquids increases from 42.8 wt% and 18.0 wt% at 0.5 g to 45.0 wt% and 28.8 wt% 1.25 g. This is because when more of the feedstock is used, the catalyst starts to get overloaded. The result is that not all the pyrolysis gases can gain access to the catalyst surface to deposit into carbon, yielding fewer solids. This also leads to a larger amount of longer hydrocarbons since they are left unreacted. When 1.25 g of LDPE is used, a reduction in the yield of gases is observed in favour of oils. This is result of larger hydrocarbon chains remaining from the pyrolysis stage, as the catalyst becomes overloaded and these long molecules can no longer gain access to the catalyst. This is mirrored in the gas composition shown in figure 7.5(b), as the amount of C₂-C₄ hydrocarbons rises as the amount of LDPE used increases from 18.9 vol% at 0.5 g up to 34.9 vol% at 1.25 g. This is consistent with other studies based on hydrocarbon gasification which show that the catalytic activity of a catalyst reduces as the feedstock:catalyst ratio increases [27-29].

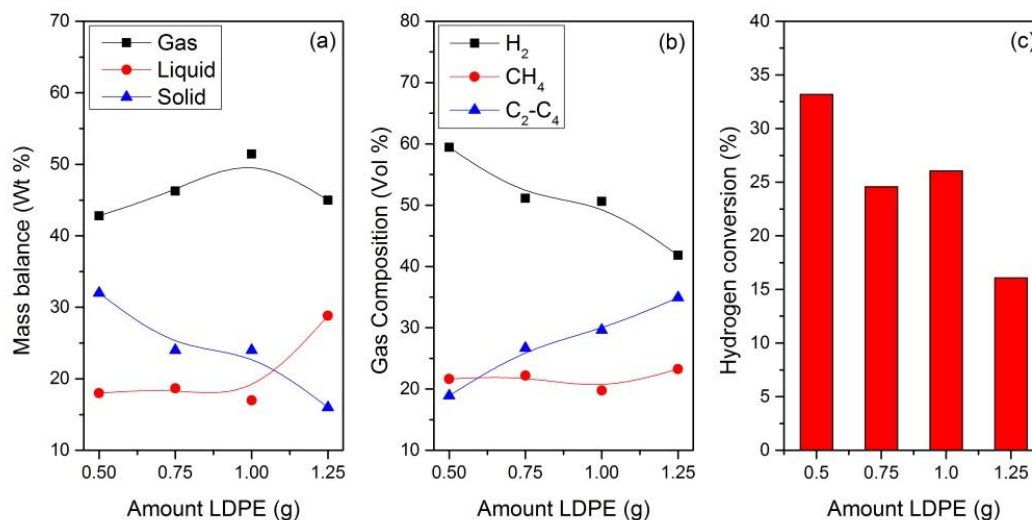


Figure 7.5 Effect of sample:catalyst ratio on (a) mass balance, (b) gas composition and (c) hydrogen conversion from the two stage pyrolysis of LDPE at 800 °C

The percentage of hydrogen produced in the gases also reduces with more feedstock used, from 59.4 vol% at 0.5 g to 41.8 vol% at 1.25 g, since a smaller proportion of the feedstock is converted into hydrogen and carbon via reaction 7.1 as a result of reduced catalytic activity. This is also shown in figure 7.5(c) where a reduction is observed in the hydrogen conversion, from 33.2% at 0.5 g to 16.1% at 1.25 g. Other studies on hydrogen production from hydrocarbon sources have also found similar results, with hydrogen production reducing as the amount of catalyst relative to the feedstock is lowered [27-30].

7.2.2 Carbon nanotube production

The carbon deposits produced from different amounts of LDPE were analysed by SEM and TEM, as seen in figures 7.6 and 7.7. There is little variation in the deposits shown, with all SEM images showing a thick covering of filamentous carbons on the surface of the catalyst. TEM images confirmed that the filamentous carbons were CNTs, with all catalyst:sample ratios showing multi walled CNTs with diameters between 20 – 30 nm.

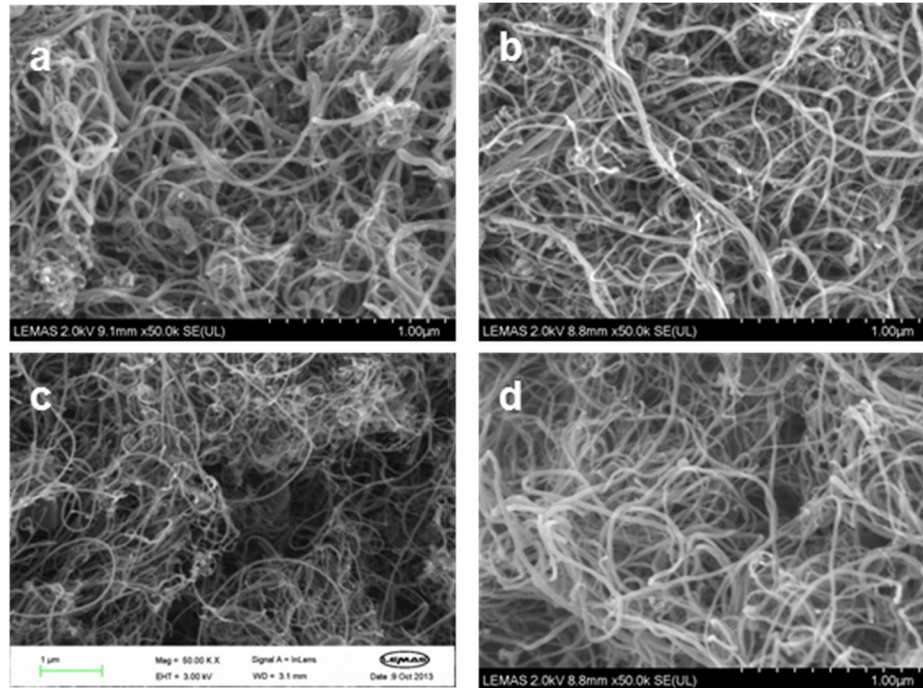


Figure 7.6 SEM images showing effect of amount of LDPE used at 800 °C. (a) 0.5g, (b) 0.75g, (c) 1.0g and (d) 1.25g

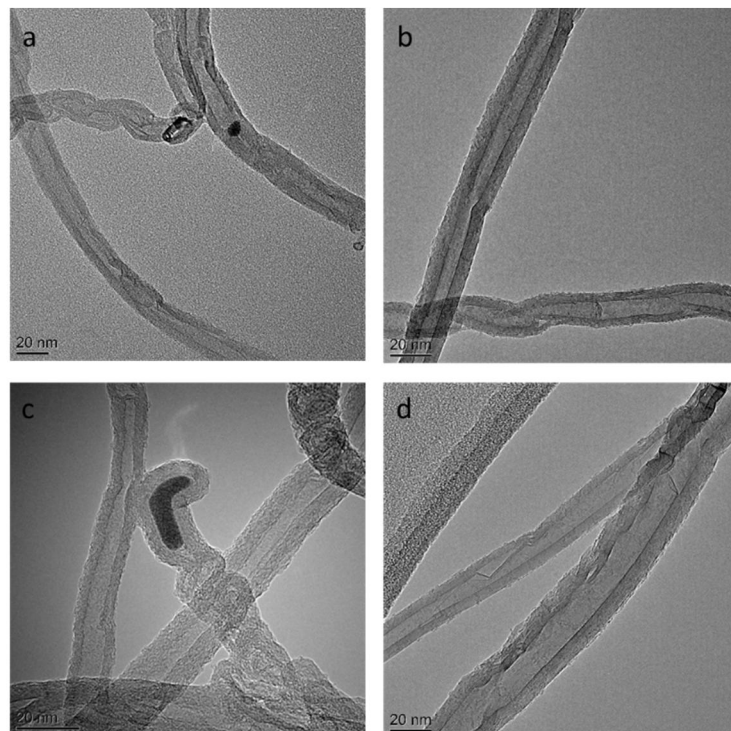


Figure 7.7 TEM images showing effect of amount of LDPE used at 800 °C. (a) 0.5g, (b) 0.75g, (c) 1.0g and (d) 1.25g

TPO of the carbon on the used catalyst was undertaken to determine the amount of different types of carbon deposition. Figure 7.8(a) shows the derivative plots obtained, and like the TPO results in figure 7.4(a) also shows the two distinct peaks associated with amorphous carbons, 350 – 450 °C, and filamentous carbons 500 – 700 °C.

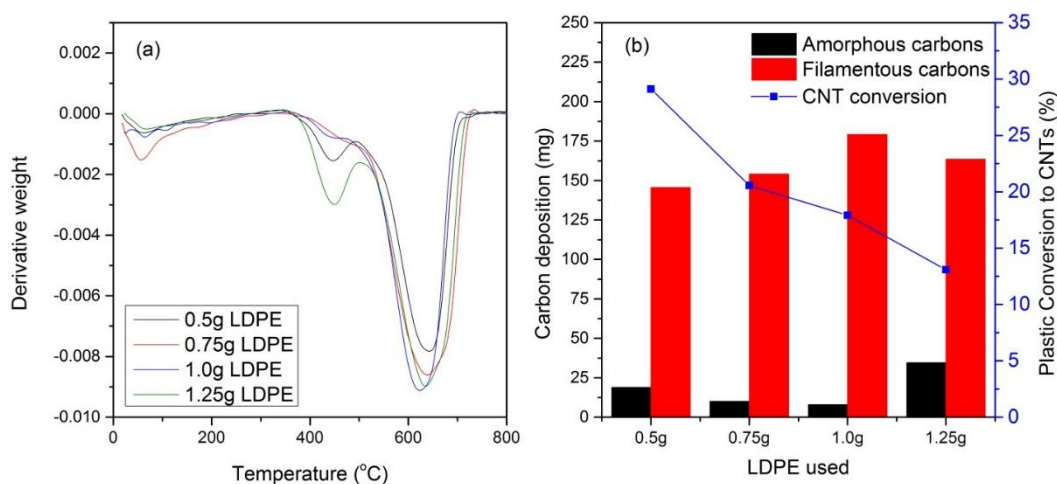


Figure 7.8 Temperature oxidation results showing effect of amount of LDPE used at 800 °C; (a) derivative plot and (b) amount of carbon deposition and conversion of plastic to CNTs

The higher temperature filamentous peak is significantly bigger for all the experiments, as expected based on the results obtained for 800 °C. From the derivative plot the amounts of amorphous and filamentous carbons produced were calculated and are shown in figure 7.8(b). As the amount of feedstock used increases, the amount of carbon nanotubes obtained on the catalyst increases from 146 mg / 0.5 g catalyst at 0.5 g LDPE up to 179 mg/ 0.5 g catalyst at 1.0 g LDPE. This is expected as there is a larger source of carbon when more LDPE is used. Das et al [2] found similar results when producing carbon nanotubes from liquid hydrocarbons. A higher yield of wt CNT/wt catalyst, was obtained at low catalyst:carbon ratios, when more feedstock is used relative to the amount of catalyst. The increase in CNT yield is true up to 1.25 g of LDPE, where a slight reduction (164 mg/ 0.5 g catalyst) in the amount of CNTs is observed. At the amount of 1.25 g LDPE a larger amount of amorphous carbons were produced. Unlike filamentous carbons such as carbon nanotubes, amorphous carbons are known to deactivate the catalyst by encapsulating catalyst particles [31], preventing

the production of CNTs and hydrogen. Though more CNTs are produced with larger amounts of LDPE, the percentage conversion of the plastic into carbon nanotubes, seen in figure 7.8(b), reduces. When 0.5 g of LDPE is used 29.1 wt% of the plastic is converted into carbon nanotubes, but when 1.25 g of sample is used, only 13.1 wt% of the plastic is converted. This is in accordance with mass balance results, as access to the catalyst gets overloaded and pyrolysis gases are left unreacted, producing a lower catalyst activity. Further work could be done to investigate the effect of the heating rate in the pyrolysis reactor, or flow rate through the reactor as varying these this would vary the residence time of the pyrolysis gases over the catalyst and could help to prevent the catalyst becoming overloaded with a large amount of hydrocarbons at the same time. When the feedstock:catalyst ratio is low, i.e. a small amount of plastic is used, the conversion of the plastics is high, however the amount of CNTs compared to the amount of catalyst used is low. The opposite is true of higher feedstock:catalyst ratios, with lower plastic to CNT conversions, but a larger amount CNT compared to the amount of catalyst. This sets up an interesting economic payoff between achieving high plastic conversions and the amount of catalyst used per g of CNTs produced. In order for the process to become economic however, the current batch method would need to be modified to a continuous process. This could be done by using similar conditions and materials in a two stage process using, for example a screw kiln for the first stage and where the second stage is replaced by a moving bed or screw kiln reactor where the catalyst could be collected after use to extract the CNTs.

7.3 Conclusion

Carbon nanotubes are formed through decomposition of hydrocarbons on the catalyst surface, producing solid carbons as well as hydrogen gas. Carbon deposition increased with reaction temperature, with a larger amount of CNTs produced at higher temperatures. This was because the growth rate of CNTs increases with reaction temperature as a result of faster carbon diffusion through the catalyst particle. This is thought to be the rate determining step in CNT formation, and so its increase leads to a larger CNT yield. Hydrogen production increases with the increase in CNTs production, since the two are both produced simultaneously by the decomposition of hydrocarbons. The highest quality CNTs were produced at 800 °C, with 700

°C producing more amorphous carbons and 900 °C producing less uniform CNTs.

Increasing the amount of LPDE used increased the yield of CNTs per 0.5 g catalyst up to a point. At 1.25 g LDPE loading, the yield of CNTs on the catalyst reduces due to the production of amorphous carbons. Whilst more carbon nanotubes were produced per 0.5 g catalyst at higher LDPE loading, the percent conversion from plastics to CNTs reduced since the catalyst became overloaded and a large amount of pyrolysis gases were left unable to deposit on the catalyst surface. This gives an economic payoff between large conversion of plastics into CNTs and large yields of CNTs per g of catalyst used.

References

1. Alves, J.O., et al., *Catalytic conversion of wastes from the bioethanol production into carbon nanomaterials*. Applied Catalysis B: Environmental, 2011. **106**(3-4): p. 433-444.
2. Das, N., et al., *The effect of feedstock and process conditions on the synthesis of high purity CNTs from aromatic hydrocarbons*. Carbon, 2006. **44**(11): p. 2236-2245.
3. Juang, Z., *On the kinetics of carbon nanotube growth by thermal CVD method*. Diamond and Related Materials, 2004. **13**(11-12): p. 2140-2146.
4. Lee, C.J., et al., *Temperature effect on the growth of carbon nanotubes using thermal chemical vapor deposition*. Chemical Physics Letters, 2001. **343**: p. 33-38.
5. Gallego, G.S., et al., *Production of hydrogen and MWCNTs by methane decomposition over catalysts originated from LaNiO₃ perovskite*. Catalysis Today, 2010. **149**(3-4): p. 365-371.
6. Liu, J., et al., *Catalytic pyrolysis of polypropylene to synthesize carbon nanotubes and hydrogen through a two-stage process*. Polymer Degradation and Stability, 2011. **96**(10): p. 1711-1719.
7. Mishra, N., et al., *Pyrolysis of waste polypropylene for the synthesis of carbon nanotubes*. Journal of Analytical and Applied Pyrolysis, 2012. **94**: p. 91-98.
8. Arena, U., et al., *An innovative process for mass production of multi-wall carbon nanotubes by means of low-cost pyrolysis of polyolefins*. Polymer Degradation and Stability, 2006. **91**(4): p. 763-768.
9. Jiang, Z.W., et al., *Polypropylene as a carbon source for the synthesis of multi-walled carbon nanotubes via catalytic combustion*. Carbon, 2007. **45**(2): p. 449-458.
10. Kong, Q.H. and J.H. Zhang, *Synthesis of straight and helical carbon nanotubes from catalytic pyrolysis of polyethylene*. Polymer Degradation and Stability, 2007. **92**(11): p. 2005-2010.

11. Tang, T., et al., *Synthesis of multiwalled carbon nanotubes by catalytic combustion of polypropylene*. *Angew Chem Int Ed Engl*, 2005. **44**(10): p. 1517-20.
12. Zhuo, C., et al., *Synthesis of carbon nanotubes by sequential pyrolysis and combustion of polyethylene*. *Carbon*, 2010. **48**(14): p. 4024-4034.
13. Arnaiz, N., et al., *Production of Carbon Nanotubes from Polyethylene Pyrolysis Gas and Effect of Temperature*. *Industrial & Engineering Chemistry Research*, 2013. **52**(42): p. 14847-14854.
14. Yang, Z., et al., *Coupled process of plastics pyrolysis and chemical vapor deposition for controllable synthesis of vertically aligned carbon nanotube arrays*. *Applied Physics A*, 2010. **100**(2): p. 533-540.
15. Yen, Y.W., M.D. Huang, and F.J. Lin, *Synthesize carbon nanotubes by a novel method using chemical vapor deposition-fluidized bed reactor from solid-stated polymers*. *Diamond and Related Materials*, 2008. **17**(4-5): p. 567-570.
16. Wang, P., et al., *Filamentous carbon prepared by the catalytic pyrolysis of CH₄ on Ni/SiO₂*. *Applied Catalysis A: General*, 2002. **231**: p. 34-44.
17. Sengupta, J., et al., *Effect of growth temperature on the CVD grown Fe filled multi-walled carbon nanotubes using a modified photoresist*. *Materials Research Bulletin*, 2010. **45**(9): p. 1189-1193.
18. Malek Abbaslou, R.M., J. Soltan, and A.K. Dalai, *The effects of carbon concentration in the precursor gas on the quality and quantity of carbon nanotubes synthesized by CVD method*. *Applied Catalysis A: General*, 2010. **372**(2): p. 147-152.
19. Volder, M.F.L.D., et al., *Carbon Nanotubes: Present and Future Commercial Applications*. *Science*, 2013. **339**(6119): p. 535-539.
20. Allaouia, A., et al., *Mechanical and electrical properties of a MWNT/epoxy composite*. *Composites Science and Technology*, 2002. **62**: p. 1993-1998.
21. Montazeri, A., et al., *Mechanical properties of multi-walled carbon nanotube/epoxy composites*. *Materials & Design*, 2010. **31**(9): p. 4202-4208.
22. Rahaman, M.S., C.D. Vecitis, and M. Elimelech, *Electrochemical carbon-nanotube filter performance toward virus removal and inactivation in the presence of natural organic matter*. *Environ Sci Technol*, 2012. **46**(3): p. 1556-64.
23. Gao, G. and C.D. Vecitis, *Electrochemical carbon nanotube filter oxidative performance as a function of surface chemistry*. *Environ Sci Technol*, 2011. **45**(22): p. 9726-34.
24. Sotowa, C., et al., *The reinforcing effect of combined carbon nanotubes and acetylene blacks on the positive electrode of lithium-ion batteries*. *ChemSusChem*, 2008. **1**(11): p. 911-5.
25. Beigbeder, A., et al., *Preparation and characterisation of silicone-based coatings filled with carbon nanotubes and natural sepiolite and their application as marine fouling-release coatings*. *Biofouling*, 2008. **24**(4): p. 291-302.
26. Coleman, J.N., et al., *High-Performace Nanotube-Reinforced Plastics: Understanding the Mechanism of Strength Increase*. *Advanced Functional Materials*, 2004. **14**(8): p. 791-798.

27. Bimbela, F., et al., *Catalytic steam reforming of model compounds of biomass pyrolysis liquids in fixed bed: Acetol and n-butanol*. Journal of Analytical and Applied Pyrolysis, 2009. **85**(1-2): p. 204-213.
28. Furusawa, T., et al., *The evaluation of the stability of Ni/MgO catalysts for the gasification of lignin in supercritical water*. Applied Catalysis A: General, 2007. **327**(2): p. 300-310.
29. Garcia, L., et al., *Hydrogen Production by Steam Gasification of Biomass Using Ni-Al Coprecipitated Catalysts Promoted with Magnesium*. Energy and Fuels, 2002. **16**: p. 1222-1230.
30. Mohanty, P., M. Patel, and K.K. Pant, *Hydrogen production from steam reforming of acetic acid over Cu-Zn supported calcium aluminate*. Bioresour Technol, 2012. **123**: p. 558-65.
31. Rostrup-Nielsen, J.R., *Steam Reforming Catalysts*1975, Copenhagen: Danish Technical Press.

8 Conclusions and future work

In this work simultaneous production of hydrogen gas and carbon nanotubes from a two stage thermal treatment process has been investigated. Various types of plastics as well as different transition metal catalysts were all investigated as well as other process conditions such as temperature and the injection of steam into the reactor.

8.1 Conclusions

The following conclusions were drawn from this work.

8.1.1 Pyrolysis-gasification of WEEE plastics

- Hydrogen was successfully yielded from a WEEE plastic sample using a two stage pyrolysis gasification process. The addition of a nickel catalyst increased the yield of hydrogen obtained, as a result of increased cracking. Gas yields increased, in particular hydrogen and carbon monoxide, at the expense of oils and C₂-C₄ hydrocarbons which were broken down with the aid of the catalyst. Increasing the loading of nickel on the catalyst from 5 wt% to 10 wt% further increased the yields of gas, hydrogen and carbon monoxide, indicating that the nickel catalyst plays a crucial role in hydrogen production. Hydrogen yields were highest from HIPS, with a conversion rate of 73%, compared with 33% for the ABS sample. The WEEE plastic produced a hydrogen conversion of 28%.
- Oil analysis showed that the nickel catalyst contributed to the breakdown of larger hydrocarbon species into smaller ones, and that this process increases when the metal loading was increased.
- Gas and oils analysis showed that the WEEE plastic was composed of a mixture of ABS and HIPS plastics.
- Carbon deposition on the surface of the catalyst was comprised of filamentous carbons. Only a very small number of carbon nanotubes

were seen from the HIPS and WEEE samples, whilst none were produced from ABS. Filamentous carbons were produced from all the samples, with WEEE producing less than the other plastics. The filaments from ABS were distinctly different and more irregular in their nature. The deposition of carbon was not a key parameter in determining the hydrogen yield.

- Overall it was found that hydrogen can be successfully yielded from WEEE plastics via a two stage pyrolysis-gasification process, with larger yields obtained with use of a Ni/Al₂O₃ catalyst. HIPS and ABS plastics likewise yielded hydrogen, with the HIPS sample producing the largest hydrogen conversion. This shows that WEEE plastics comprising HIPS would be most suitable for hydrogen production.

8.1.2 **Effect of steam injection rate and plastic type on production of carbon nanotubes and hydrogen**

- CNTs and hydrogen were successfully produced simultaneously from LDPE, PP and PS plastics using a nickel catalyst in a two stage pyrolysis gasification process.
- For each of the plastics, increasing the steam injection rate led to an increase in production of hydrogen. This was due to increased steam reforming and gasification of carbon deposits. The maximum hydrogen yields for the plastics were obtained at 4.74 g h⁻¹ steam injection and were as follows: LDPE>PS>PP. Pyrolysis gases from the first stage from LDPE contained more methane and small hydrocarbons, which are easier to steam reform in the second stage, leading to the highest hydrogen yields. The maximum yield obtained was 9.2 g/100g of sample, a hydrogen conversion of 64.6%. PS produced higher yields of hydrogen than PP as more was produced during the deposition of filamentous carbons. PS produced a larger amount of these filamentous carbons, which do not deactivate the catalyst.

- For LDPE, increasing the steam injection rate resulted in a reduction in the yield of CNTs, as carbon is gasified by steam. The largest CNT yield for LDPE was obtained without steam injection, with a value of 188 mg/ g sample.
- Without the injection of steam, PP and PS produced a smaller amount of CNTs than LDPE, as a result of a larger production of amorphous carbons which deactivate the catalyst. PP and PS produced their maximum yield of CNTs at 0.25 g/h steam injection. PS gave a yield of 324 mg/ g sample, whilst PP gave a yield of 104 mg/ g sample. The effect of increased catalytic activity by the destruction of amorphous carbons is larger than the effect of the destruction of CNTs by gasification. This was the case for PP and PS as when there are less amorphous carbons, more filamentous carbons are produced. For PP this is because it produces larger hydrocarbons in its pyrolysis gases, whilst the aromatic nature of PS also leads to more filamentous carbon production.
- At the higher steam injection rates of 1.90 and 4.74 g/h, the gasification of carbon increased and more carbon nanotubes were destroyed by gasification than enabled by the destruction of amorphous carbons. As a result the yield of CNTs reduced for PP and PS. Filamentous carbons were produced in favour of CNTs at high steam injection rates as gasification slows the rate of carbon deposition compared with carbon diffusion.
- Overall large yields of CNTs were produced from the plastics samples, suggesting a viable industrial process could be created. The largest CNT yields were obtained either with no steam injection or at low steam injection rates, whereas the largest hydrogen yields were obtained at the highest steam injection rates. As such, there is potential for a process with good flexibility over production, where by changing the steam injection rate the major product can be shifted from CNTs to hydrogen.

8.1.3 Effect of the catalyst on the production of carbon nanotubes and hydrogen

- CNTs and hydrogen were successfully synthesised from the pyrolysis of LDPE using iron, nickel and cobalt catalysts with an alumina support. Copper catalysts proved unsuccessful for the production of CNTs.
- The largest yield of hydrogen was produced from the iron catalyst, with a LDPE conversion of 26.8%. The yield of hydrogen from the catalysts was as follows Fe>Ni>Co>Cu. The iron catalyst gave the largest hydrogen yield as more was produced during the large amounts of hydrocarbon deposition which occurred on the catalyst surface.
- No CNTs were produced using the copper catalyst as its metal support interaction was too weak, leading to sintering of the metal until particle sizes were too large to produce CNTs. Copper also has a significantly lower carbon solubility than the other metals, which hindered CNT growth. Only a small yield of CNTs was produced using the cobalt catalyst as the metal support interaction was too strong, and prevented metal particles of the correct size for CNT production forming. The nickel and iron catalysts produced significant yields of carbon nanotubes, as the metal support interactions were neither too weak nor too strong, and led to the production of metal particles of the correct size for CNT growth. Iron produced a larger yield than nickel as a result of a higher carbon solubility.
- When the calcination temperature used to prepare the nickel catalyst was reduced, the yield of CNTs from the pyrolysis of LDPE fell. This was because the metal support interaction became weaker, and led to the production of larger metal particles, some of which were too large for CNT growth. Hydrogen yields also fell, as less was produced during deposition of hydrocarbons.

- When the metal loading of the catalysts was lowered, a significant decrease in the yields of hydrogen and CNTs were observed on the catalytically active iron and nickel catalysts. The effect of metal loading had less of an effect on the cobalt and copper catalysts.

8.1.4 Effect of temperature and feedstock:catalyst ratio

- As the temperature of the catalytic stage in the two stage catalytic pyrolysis of LDPE was raised, the hydrogen yield increased. This was because more was produced with an increase in deposition of carbon onto the catalyst. The largest yield was obtained at 900 °C, with a hydrogen conversion of 28%.
- The amount of carbon deposited onto the iron catalyst increases with increased catalyst temperature. This was shown by the amount of solids in the mass balance increasing, and by temperature programmed oxidation. With an increase in temperature of the catalytic stage, more carbon nanotubes were produced. At the lowest temperature of 700 °C a larger amount of amorphous carbons were produced, whilst at 800 and 900 °C, not only were significantly larger amounts of carbon deposited overall, but the vast majority of the deposits were now CNTs. CNT production also increased between 800 and 900 °C. The increase in CNT production was attributed to faster carbon diffusion through catalyst particles, a key step in CNT growth. Whilst more carbon deposition occurs at 900 °C, the CNTs produced at 800 °C were of the highest quality.
- Increasing the amount LDPE sample used increased the yield of CNTs per 0.5 g of catalyst. This was because a larger source of carbon is present for CNT production. The increase was seen between LDPE amount of 0.5 and 1.0 g. When 1.25 g of LDPE is used however, the yield of CNTs per 0.5 g of catalyst reduced. This is thought to be due to an increase in the amount of amorphous carbons produced.

- As the amount of LDPE used is increased, the percentage of gases in the mass balance increases. This was due to an increase in large hydrocarbons in the gas stream as the pyrolysis gases from the first stage are left unreacted as a result of the catalyst becoming overloaded. Increasing the amount of LDPE led to a decrease in the percentage of plastic converted into CNTs and hydrogen. This too is because the catalyst became overloaded, and so a significant percentage of the pyrolysis gases cannot gain access to the catalyst to decompose in CNTs and hydrogen.

8.2 Future work

8.2.1 Production of carbon nanotubes

Whilst a large number of factors have been considered in the production of CNTs, there are a number of possibilities for further investigation.

- Different methods of preparing the catalysts could be investigated, such as sol-gel or co-precipitation methods. These could have an impact on the surface area, metal surface loading or other factors related to the catalyst.
- Using alternative catalyst supports to alumina could also be investigated, for example studies have shown SiO₂ to produce large carbon yields [1, 2]. Different supports would have an effect on the metal support interaction, which proved to be an important factor in CNT growth.
- The flow rate and heating rate could also be investigated. Varying these could affect the rate at which the pyrolysis gases arrive at the catalyst, and therefore affect CNT growth.

Further work should make use of more real world waste as a feedstock.

- Real world plastic wastes such as PP, PS and LDPE could be used to demonstrate the potential to produce CNTs and hydrogen from waste rather than virgin plastics. Making use of WEEE plastics again with catalysts and conditions more favourable to CNT growth could also be investigated.

- Other plastics such as polyvinyl chloride and polyethylene terephthalate could also be tested for their potential to produce CNTs and hydrogen. Different mixtures of plastics could then be investigated.
- The effect of different contaminants such as chlorine, bromine could be investigated further to see if they interrupt the production of CNTs or deactivate the catalyst.

A batch process is currently used, however large scale industrial production would benefit from a continuous process.

- Work on a more continuous process could be developed such as using moving bed or screw kiln reactors.

8.2.2 Purification

In order to utilise the CNTs produced in commercial or industrial applications, they have to be purified and separated from the catalyst and other types of carbon deposition. In order to do this purification techniques could be investigated.

- Treatments using acids to dissolve amorphous carbons and metal catalyst particles have proved successful in other studies [3-6] and could be investigated for the CNTs produced in this work.
- Thermal treatments using air to combust more reactive types of carbon than CNTs have likewise proven successful in other studies [3, 4, 7, 8] and could be investigated for the CNTs produced in this work.

8.2.3 Uses for carbon nanotubes produced

Once the most suitable purification techniques have been identified, the CNTs produced can then be tested in a number of applications, to compare their properties to those produced by current production techniques such as chemical vapour deposition. Based on the multi wall nature of the CNTs produced, possible uses could include:

- Filtration or separation of pollutants from water [9-12].

- Reinforcement of plastics to increase their strength [13-15].
- Energy applications such as catalyst supports for fuel cells or use in batteries [16, 17].

References

1. Ermakova, M., et al., *Decomposition of Methane over Iron Catalysts at the Range of Moderate Temperatures: The Influence of Structure of the Catalytic Systems and the Reaction Conditions on the Yield of Carbon and Morphology of Carbon Filaments*. Journal of Catalysis, 2001. **201**(2): p. 183-197.
2. Takenaka, S., et al., *Decomposition of methane over supported-Ni catalysts: effects of the supports on the catalytic lifetime*. Applied Catalysis A: General, 2001. **217**: p. 101-110.
3. Moon, J.-M., K.H. An, and Y.H. Lee, *High-Yield Purification Process of Singlewalled Carbon Nanotubes*. Journal of Physical Chemistry B, 2001. **105**: p. 5677-5681.
4. Park, T.-J., et al., *Purification strategies and purity visualization techniques for single-walled carbon nanotubes*. Journal of Materials Chemistry, 2006. **16**(2): p. 141.
5. Shi, Z., et al., *Purification of single-wall carbon nanotubes*. Solid State Communications, 1999. **112**: p. 35-37.
6. Xu, Y.-Q., et al., *Controlled Multistep Purification of Single-Walled Carbon Nanotubes*. Nano Letters, 2004. **5**(1): p. 163-168.
7. Chattopadhyay, D., I. Galeska, and F. Papadimitrakopoulos, *Complete elimination of metal catalysts from single wall carbon nanotubes*. Carbon, 2002. **40**: p. 985-988.
8. Yang, C.-M., et al., *Effect of Purification on Pore Structure of HiPco Single-Walled Carbon Nanotube Aggregates*. Nano Letters, 2002. **2**(4): p. 385-388.
9. Gao, G. and C.D. Vecitis, *Electrochemical carbon nanotube filter oxidative performance as a function of surface chemistry*. Environ Sci Technol, 2011. **45**(22): p. 9726-34.
10. Rahaman, M.S., C.D. Vecitis, and M. Elimelech, *Electrochemical carbon-nanotube filter performance toward virus removal and inactivation in the presence of natural organic matter*. Environ Sci Technol, 2012. **46**(3): p. 1556-64.
11. Sae-Khow, O. and S. Mitra, *Carbon Nanotube Immobilized Composite Hollow Fiber Membranes for Pervaporative Removal of Volatile Organics from Water*. Journal of Physical Chemistry C, 2010. **114**: p. 16351–16356.
12. Sears, K., et al., *Recent Developments in Carbon Nanotube Membranes for Water Purification and Gas Separation*. Materials, 2010. **3**(1): p. 127-149.

13. Allaouia, A., et al., *Mechanical and electrical properties of a MWNT/epoxy composite*. Composites Science and Technology, 2002. **62**: p. 1993-1998.
14. Coleman, J.N., et al., *High-Performance Nanotube-Reinforced Plastics: Understanding the Mechanism of Strength Increase*. Advanced Functional Materials, 2004. **14**(8): p. 791-798.
15. Montazeri, A., et al., *Mechanical properties of multi-walled carbon nanotube/epoxy composites*. Materials & Design, 2010. **31**(9): p. 4202-4208.
16. Li, W., et al., *Carbon nanotubes as support for cathode catalyst of a direct methanol fuel cell*. Carbon, 2002. **40**: p. 787-803.
17. Sotowa, C., et al., *The reinforcing effect of combined carbon nanotubes and acetylene blacks on the positive electrode of lithium-ion batteries*. ChemSusChem, 2008. **1**(11): p. 911-5.